DYNAMIC RELAXATION ANALYSIS OF PRETENSIONED NETWORKS SUPPORTED BY COMPRESSION ARCHES

A thesis submitted to The City University

by David Simon Wakefield for the

degree of Doctor of Philosophy

Department of Civil Engineering

The City University

May, 1980

To my mother

DYNAMIC RELAXATION ANALYSIS OF PRETENSIONED NETWORKS SUPPORTED BY COMPRESSION ARCHES

ABSTRACT

This thesis is concerned with the application of direct integration methods, particularly Dynamic Relaxation, to the non-linear formfinding and analysis of pretensioned networks supported by compression arches. The development and application of such methods is reviewed in Chapter 2.

The automated control of Dynamic Relaxation is considered in Chapter 3, and a modified kinetic damping procedure shown to be an efficient and simple alternative to viscous nodal damping that does not require prior determination of a damping constant. It is shown that Dynamic Relaxation may be interpreted as a dynamic implementation of a first order gradient method.

A modification of Buchholdt's implementation of the Scaled Conjugate Gradient method to permit arbitrary cable strains is presented in Chapter 4. The efficiency of this method and Dynamic Relaxation is compared in Chapter 5 for a generalised test problem having variable design parameters. Dynamic Relaxation is shown to be more efficient in all cases.

In Chapter 6 Dynamic Relaxation is applied to the non-linear analysis of plane and space frames. The effects of finite displacements, bowing and axial force on the moment-curvature relations are included in the analysis. The method presented is compared successfully with published solutions to planar and spatial problems exhibiting snap-through buckling and subsequent post-buckling response.

The development of numerical methods for formfinding is reviewed at the start of Chapter 7. The suitability of kinetic damping for controlling Dynamic Relaxation formfinding is demonstrated and the generation of moment-free compression arches illustrated.

In Chapter 8 the cable and spatial flexural elements are combined for unified Dynamic Relaxation of the complete structure. This method, with full non-linear idealisation of the boundary structure, has demonstrated convergence at least twice as rapidly as the Scaled Conjugate Gradient method with linear boundary response.

Dynamic Relaxation has been shown to be a simple and efficient analysis technique, retaining a clear physical analogy that facilitates the understanding, implementation and execution of non-linear response investigations. For the particular problem of pretensioned networks supported by compression arches it is a straightforward procedure to investigate the stabilising effect of the tension network on the boundary structure, thus enabling the use of lighter, more economic, compression members.

ACKNOWLEDGEMENTS

I would like to thank Dr. Michael Barnes for enthusiastic encouragement and guidance throughout his supervision of this thesis. Thanks are also due to Professor P.O. Wolf and Professor J.E. Gibson for their continuing support and interest during my studies at The City University.

The financial support of this work by the Science Research Council in the form of a Research Studentship is gratefully acknowledged.

I am indebted to Janet Prange for her excellent typing of this manuscript and for her cheerful friendship throughout its preparation. The friendship of my fellow researchers, Manolis Papadrakakis and Barry Topping is also gratefully acknowledged.

Finally I would like to thank my wife Catherine and my father for their continual encouragement, understanding and patience.

CHAPTER 1

INTRODUCTION - DYNAMIC RELAXATION ANALYSIS OF PRETENSIONED NETWORKS SUPPORTED BY COMPRESSION ARCHES

Recent years have seen rapid developments in the field of cable and membrane tensile surface structures, encouraged both by the natural aesthetics of their equilibrium of form and function and by their ability to provide an economic solution to the problems of achieving long, clear, spans. As loads are transmitted to the bearing structure by purely tensile forces, there are no problems of stability and the maximum use of the cross-sectional area of high tensile steel cable is possible. This efficient utilisation of structural elements becomes progressively more economical as spans are increased.

The support system utilised to equilibriate the tension member forces forms a major component of the cost of this type of structure. The support may comprise tension anchors, compression masts, or flexural internal or external compression contours subject to both axial and bending forces. The latter, with which this thesis is principally concerned, may be either planar or spatially curved arches or ring beams. These boundary elements have traditionally been very stiff in comparison with the net surface, and permisssible deflections have been minimised in an attempt to recreate the fixed boundary condition. At the design stage this adoption of stiff boundary contours leads into the viscious circle of stiff members attracting bending moments, requiring additional stiffening to support these moments and thus attracting further moments.

It is likely that future developments of such structures will concentrate upon the use of increasingly flexible boundary contours having significant permitted displacements and utilising the stabilising effect of the tension network.

Analysis techniques in structural mechanics have developed in parallel with the availability of computing power. The displacement approach to finite element analysis was developed for linear structural problems and subsequently extended into non-linear applications involving multiple implicit solutions of sets of simultaneous equations and ever increasing program complexity and size.

The present generation of computers have made substantial analysis potential available to the engineer, with linear analysis readily achieved on such systems. For non-linear techniques to be equally readily available it is important that the method used be easily understood as successful user control may be an essential feature in path-dependent problems. In particular, for the analysis of tension systems, the necessary finite elements are simple and alternatives to conventional implicit methods may be considered in order to achieve efficiency of computer time, coding and core space together with ease of understanding and control.

Both Dynamic Relaxation and the Scaled Conjugate Gradient method are explicit non-linear techniques that have been established as suitable for the analysis of cable structures. Dynamic Relaxation (DR) in particular has proved highly suited to shape-finding investigations, coping naturally with structural mechanisms, cable slackening and gross out-of-balance forces. Difficulty in selection of the parameters controlling the viscously damped integration steps of DR may, however, have tended to preclude its wider application. The Scaled Conjugate Gradient (SCG) method has previously been extended to the analysis of the complete structure by the inclusion of spatial flexural elements for idealisation of the boundary system, for which

a linear load/deflection response was assumed.

The aim of this thesis is the presentation of extended and fully automated explicit integration techniques for the full non-linear formfinding and analysis requirements of pretensioned networks supported by compression arches. Such analyses will permit the numerical investigation of relatively flexible boundary contours, with full account being taken of the influence of the tension network upon the stability of the support structure.

In Chapter 2 the development, formulation and applications to date of Dynamic Relaxation and the Scaled Conjugate Gradient method are reviewed.

The efficient control and implementation of DR is examined in Chapter 3. Kinetic damping and optimised fictitious mass components are presented as automatically assigned controls on the numerical integration. The efficiency of nodal residual calculations is examined for arbitrary finite element types. DR is shown to be a dynamic implementation of a first order gradient method.

The convergence of the gradient minimisation methods is considered in Chapter 4. A modification of Buchholdt's method is presented that enables an exact analysis for cable members subject to arbitrary strains.

In Chapter 5 a general test problem is presented for the comparative analysis of pretensioned networks which enables the ready adjustment of network curvature, pretension, idealisation and loading pattern. DR and SCG are compared for variations of the above parameters and also for the problem modified to include the

on-off non-linearities of cable slackening under load.

In Chapter 6 rotational degrees of freedom are introduced into the DR analysis scheme to permit the inclusion of planar and spatial flexural elements. Finite displacements are treated directly, with full non-linear effects incorporated in the member natural stiffness relations. The proposed method is applied to the analysis of published non-linear frame problems.

Formfinding is an integral and essential part of numerical investigations of network structures with compression boundary contours. Chapter 7 presents a brief review of the development of numerical formfinding techniques, followed by examples of the utilisation of kinetic damping and the derivation of moment-free compression contours by Dynamic Relaxation.

In Chapter 8 the DR analyses for networks and rigid-jointed structures presented in preceding chapters are combined for the unified analysis of the complete structure. Previous approaches to this problem are reviewed, and a generalisation of the gradient method to include non-linear boundary structures is outlined. The explicit DR and SCG methods are then applied to published planar and saddle-shaped network problems.

CHAPTER 2

REVIEW OF EXPLICIT METHODS OF STRUCTURAL ANALYSIS

An explicit solution technique is one that does not require the direct solution of an associated set of simultaneous equations. Two principal methods of this type have been employed for the analysis of linear and nonlinear structures, in particular to network structures and their support systems. In this chapter the development, formulation and applications of these methods, Dynamic Relaxation and Scaled Conjugate Gradients, are reviewed.

2.1 *Dynamic Relaxation*

The static solution of both linear and nonlinear structures subjected to either externally or internally applied loading may be regarded as the limiting equilibrium state of damped structural vibrations excited by that loading. The physical basis of Dynamic Relaxation as initially perceived by Day (60) is that of a step by step solution, for small time increments Δt, of Newton's second law of motion applied to a loaded structure subjected to an imposed viscous damping. This explicit solution technique originated from an anology with tidal flow computations previously reported by Day and Otter (180).

The structure under consideration may be idealised by either finite element or finite difference discretisations. Since the equations of equilibrium and compatibility are separated, only 'natural' finite element stiffnesses are required for the former idealisation, rather than transformed stiffnesses assembled into an overall matrix. To date, however, published applications of Dynamic Relaxation have predominantly centred on finite difference approaches.

The trace of nodal displacements in DR is achieved by central difference numerical integration. Newmark (128) had previously suggested the possibility of obtaining static solutions from damped dynamic analyses, but had proposed the use of a relatively inefficient implicit integration scheme.

2.1.1 *Recurrence Relations*

The formulation of Dynamic Relaxation is based solely upon Newton's second law of motion and the stress-strain relations of the structural components under consideration. The former may be written, for motion in direction x at node i:

$$F_{ix} = M_i \cdot \dot{v}_{ix} \tag{2.1}$$

At any time t the total force acting on the node in this direction, F_{ix}, comprises two parts, the current residual R^t_{ix} of applied and member loads acting on the node, and an imposed viscous damping force acting in the opposite sense to the nodal velocity v^t_{ix}:

$$R^t_{ix} - \dot{C}_i v^t_{ix} = M_i \cdot \dot{v}^t_{ix} \tag{2.2}$$

where C is the viscous damping constant at node i. For a small time interval, Δt, this equation may be rewritten in central finite difference form:

$$R^t_{ix} = \frac{M_i}{\Delta t}(v^{t+\Delta t/2}_{ix} - v^{t-\Delta t/2}_{ix}) + \frac{\dot{C}_i}{2}(v^{t+\Delta t/2}_{ix} + v^{t-\Delta t/2}_{ix}) \tag{2.3}$$

Re-arranging equation (2.3), the recurrence relation for the nodal velocity is then:

$$v_{ix}^{t+\Delta t/2} = v_{ix}^{t-\Delta t/2} \left\{ \frac{M_i/\Delta t - \dot{C}_i/2}{M_i/\Delta t + \dot{C}_i/2} \right\} + R_{ix}^{t} \left\{ \frac{1}{M_i/\Delta t + \dot{C}_i/2} \right\} \quad (2.4)$$

The damping factor $\dot{C}_i$ may be defined as constant for the whole structure or, conveniently, the damping per unit mass may be assumed constant:

$$\dot{C}_i = M_i \cdot (C/\Delta t) \quad (2.5)$$

Then:

$$v_{ix}^{t+\Delta t/2} = A \cdot v_{ix}^{t-\Delta t/2} + B_i \cdot R_{ix}^{t} \quad (2.6)$$

where $A = \left\{ \frac{1 - C/2}{1 + C/2} \right\}$, constant for the structure

and $B = \frac{\Delta t}{M_i} \left\{ \frac{1}{1 + C/2} \right\}$, constant for node i.

Nodal coordinates may then be updated for the structure:

$$x_{ix}^{t+\Delta t} = x_{ix}^{t} + \Delta t \cdot v_{ix}^{t+\Delta t/2} \quad (2.7)$$

The current nodal residuals $R^{t+\Delta t}$ may now be calculated and the next stage of the analysis recommenced at equation (2.6).

No assumptions have been made as to the residual calculations, and either constant, linear,or updated, non-linear, force displacement relations may be employed. These iterations proceed until the required degree of convergence, as indicated by the magnitude of the current residuals, has been achieved.

For the first iteration of the analysis it is assumed that $v_{ix}^{-\Delta t/2} = -v_{ix}^{\Delta t/2}$ (i.e. $v_{ix}^{o} = 0$) and consequently:

$$v_{ix}^{\Delta t/2} = \frac{B_i}{(1 + A)} \cdot R_{ix}^{o} \qquad (2.8)$$

If the structure is initially in equilibrium then $R_{ix}^{o} = P_{ix}$, the applied nodal loading.

2.1.2 Stability and Optimisation of the Numerical Integration

Instability of the numerical integration process outlined above will occur when the time interval, Δt, exceeds a certain critical value.

The calculations may be regarded as a wave which must outrun the wave corresponding to the physical problem, and consequently Δt must be less than the minimum time taken by either pressure, shear or flexural waves to travel between any pair of adjacent nodes.

For finite difference idealisations with orthogonal grids Otter, Cassel and Hobbs (135) refer to the expression due to Forsythe and Wasow (70) for a system having m cartesian coordinate directions:

$$\Delta t < \frac{1}{C_v} \left\{ \left(\frac{1}{\Delta X_1}\right)^2 + \ldots + \left(\frac{1}{\Delta X_m}\right)^2 \right\}^{-1/2} \qquad (2.9)$$

where $\Delta X_1 \ldots \Delta X_m$ are the respective mesh lengths and C_v is the maximum wave velocity. Cassel, Kinsey and Sefton (48) quote expressions for the pressure and flexural wave velocities in beams and plates. These expressions relate to orthogonal finite difference meshes, and a more general approach is necessary when complex meshes or finite element idealisations are employed.

If the basic DR recurrence relation (eqn. 2.6) is multiplied through by Δt, then:

$$\Delta x_t^{t+\Delta t} = \Delta t . v_{ix}^{t+\Delta t/2} = \frac{\Delta t^2}{M(1+\frac{C}{2})} . R^t + \frac{(1-\frac{C}{2})}{(1+\frac{C}{2})} \Delta x_{t-\Delta t}^t \qquad (2.10)$$

where $\Delta x_t^{t+\Delta t}$ is the displacement increment between time points t and $t + \Delta t$. This equation has been termed dynamic iteration by Otter et al (135), who noted its similarity to the recursion formula proposed by Frankel (181) and named the second-order Richardson process by him. The optimal form of Frankel's method (181) is:

$$\Delta x_n^{n+1} = \left\{ \frac{2}{\sqrt{a} + \sqrt{b}} \right\}^2 . R^n + \left\{ \frac{\sqrt{a} - \sqrt{b}}{\sqrt{a} + \sqrt{b}} \right\} . \Delta x_{n-1}^n \qquad (2.11)$$

Comparison of equations (2.10) and (2.11) yields:

$$\frac{\Delta t^2}{M} = \frac{4}{a + b} \quad \text{and} \quad C = \frac{4\sqrt{ab}}{a + b} \qquad (2.12)$$

where a and b are the smallest and largest eigenvalues respectively of the stiffness matrix associated with the structural assembly under consideration. Cassel and Hobbs (49) have suggested that

an upper bound for b may be found from Gershgörin's theorem:

$$|b| \leqslant b_G = \max_i \sum_{j=1}^{n} |S_{ij}| \qquad (2.13)$$

where S_{ij} are the elements of the stiffness matrix, and the maximum value of the sum for each row i is taken. If the structure is such that $a \ll b$, and consequently $|a + b| \leqslant b_G$, which is frequently the case, then

$$\frac{\Delta t^2}{M_i \min} = \frac{4}{b_G} \qquad (2.14)$$

and a safe estimate for Δt may be obtained.

Barnes (13,21) has directly derived criteria for stability of the numerical integration by considering the relative motion of adjacent nodes, and that derivation is reproduced here.

Consider the x-axis components of vibration of node i having structural connections to adjacent nodes k, and from equation (2.6):

$$v_{ix}^{t+\Delta t/2} = A \cdot v_{ix}^{t-\Delta t/2} + B_i \cdot R_{ix}^{t} \qquad (2.15)$$

Then, assuming that the motions of nodes k and i are parallel to the x-axis, for the next time interval:

$$v_{ix}^{t+3\Delta t/2} = A \cdot v_{ix}^{t+\Delta t/2} + B_i \left\{ R_{ix}^{t} - \sum S_{ikx}^{t+\Delta t} \cdot \Delta\delta_{ikx}^{t+\Delta t} \right\} \qquad (2.16)$$

where, $S^{t+\Delta t}_{ikx}$ is the x-axis direct stiffness of node i relative to adjacent nodes k due to the structural elements connecting nodes i and k.

$\Delta\delta^{t+\Delta t}_{ikx}$ is the increment of x-deflection of node i relative to adjacent nodes k during the time interval $t \rightarrow t+\Delta t$.

If the time interval is large when the stiffness/mass ratio (S_{ikx}/M) is large, instability in the form of successive reversal and buildup in the amplitude of velocities and deflections may occur.

Bounds to Δt may be obtained by considering adjacent nodes I and K of a part of a structure at which the S/M ratio of the nodes, or of one of the nodes, is highest. The most critical structural configuration and state of motion will be such that all nodes k adjacent to I are different from all nodes i adjacent to K, with the relative vibrations of nodes i and k exactly out of phase.

Substituting R^{t}_{ix} from (2.15) into (2.16), for node I, one obtains:

$$v^{t+3\Delta t/2}_{Ix} - (A+1)v^{t+\Delta t/2}_{Ix} + Av^{t-\Delta t/2}_{Ix} = -B_I\left[\left[S_{Ikx}.(\Delta\delta_{Ix} - \Delta\delta_{kx})\right]\right]^{t+\Delta t} \quad (2.16)$$

and similarly for node K:

$$v^{t+3\Delta t/2}_{Kx} - (A+1)v^{t+\Delta t/2}_{Kx} + Av^{t-\Delta t/2}_{Kx} = -B_K\left[\left[S_{Kix}.(\Delta\delta_{Kx} - \Delta\delta_{ix})\right]\right]^{t+\Delta t} \quad (2.17)$$

For the most critical condition assume that the direct stiffness/mass ratios of all nodes i and k are equal, and for oscillations which are just stable : All $\Delta\delta_{ix} = \Delta\delta_{Ix}$ and all $\Delta\delta_{kx} = \Delta\delta_{Kx}$.

Thus subtracting (2.18) from (2.17)

$$v^{t+3\Delta t/2}_{IKx} - (A+1)v^{t+\Delta t/2}_{IKx} + Av^{t-\Delta t/2}_{IKx} = -B_i(S_{Ix} \cdot 2\Delta\delta^{t+\Delta t}_{IKx}) \qquad (2.19)$$

where v_{IKx} is the velocity of I relative to K

S_{Ix} is the direct stiffness of node I relative to all adjacent nodes (assumed highest in the x-direction)

The limiting case of stability is when v_{xIK} during one time increment produces relative deflection changes $\Delta\delta_{IKx}$ such that v_{xIK} in the next time increment is equal and opposite to the previous value. Hence:

$$-2(A+1)v^{t+\Delta t/2}_{IKx} = -B_I \cdot S_{Ix} \cdot 2\Delta\delta^{t+\Delta t}_{IKx}$$

$$(A+1)/B_I = S_{Ix}\cdot\Delta t$$

$$\Delta t_{crit.} = \sqrt{\frac{2M_I}{S_{Ix}}} \qquad (2.20)$$

Alternatively, assuming $S_{Kx}/M_K << S_{Ix}/M_I$ when subtracting (2.18) from (2.17):

$$\Delta t_{crit.} = \sqrt{\frac{4M_I}{S_{Ix}}} \qquad (2.21)$$

When calculating the permissible value for Δt, constant throughout the analysis for the whole structure, the highest ratio of S/M at any node in any co-ordinate direction must be considered. Barnes (21) has stated that the true critical time interval has always been found to lie within the above limits whilst analysing cable and space structures.

In the preceding review of the stability criteria for the numerical integration it has been assumed that the true, lumped, mass has been specified for each node. As a consequence the resultant iteration bears some resemblance to the true dynamic behaviour of the structure, and engineering judgement may be used when estimating the critical viscous damping constant. However, as only the eventual static equilibrium solution is required, there is no reason why real masses should be employed.

If a 'fictitious' mass is to be used for each degree of freedom of the structure, then equations (2.14) or (2.20) may be rearranged and utilised to ensure that the chosen time interval is the optimum for each of those degrees of freedom:

$$M_i = \frac{\Delta t^2}{4} \sum_{j=1}^{n} \left| S_{ij} \right| \qquad \text{for degree of freedom } i$$

$$\text{or} \qquad M_i = \frac{\Delta t^2}{2} \cdot S_i \qquad (2.22)$$

A unit time interval may then be conveniently chosen in order to reduce computational effort, and the number of iterations to convergence has been minimised by this use of fictitious masses.

Fictitious masses in Dynamic Relaxation were first suggested by Welch (135) and King (135), and the first published results using this technique presented by Rushton (145) and subsequently Cassel (47). It is now standard practice in DR analysis.

For non-linear problems Cassel and Hobbs (50) have updated the fictitious mass components at discrete intervals as the analysis proceeds. The Gershgörin bounds were used for calculating these masses, and separation of the linear and non-linear components ensured that only the latter need be updated. This technique has been applied by Turvey (167) and Frieze, Hobbs and Dowling (71), in both cases for large deflection analysis of plates. Subsequently Frieze (72), applying DR to the elastic-plastic buckling of thin walled rectangular sections, has shown that fictitious masses calculated on the basis of elastic rigidities alone provided satisfactory convergence even when deformations were well into the plastic region. It was concluded that the additional computation required for inclusion of the updated non-linear components of the fictitious masses more than offset any gains in reduced time to convergence.

As an alternative the possibility of continually updating iteration parameters has been investigated by Lynch, Kelsey and Saxe (116) for linear structures, although no comparisons of relative computational effort were given.

For non-linear structures, with significant changes in stiffness, Barnes (21) has proposed that the above technique be

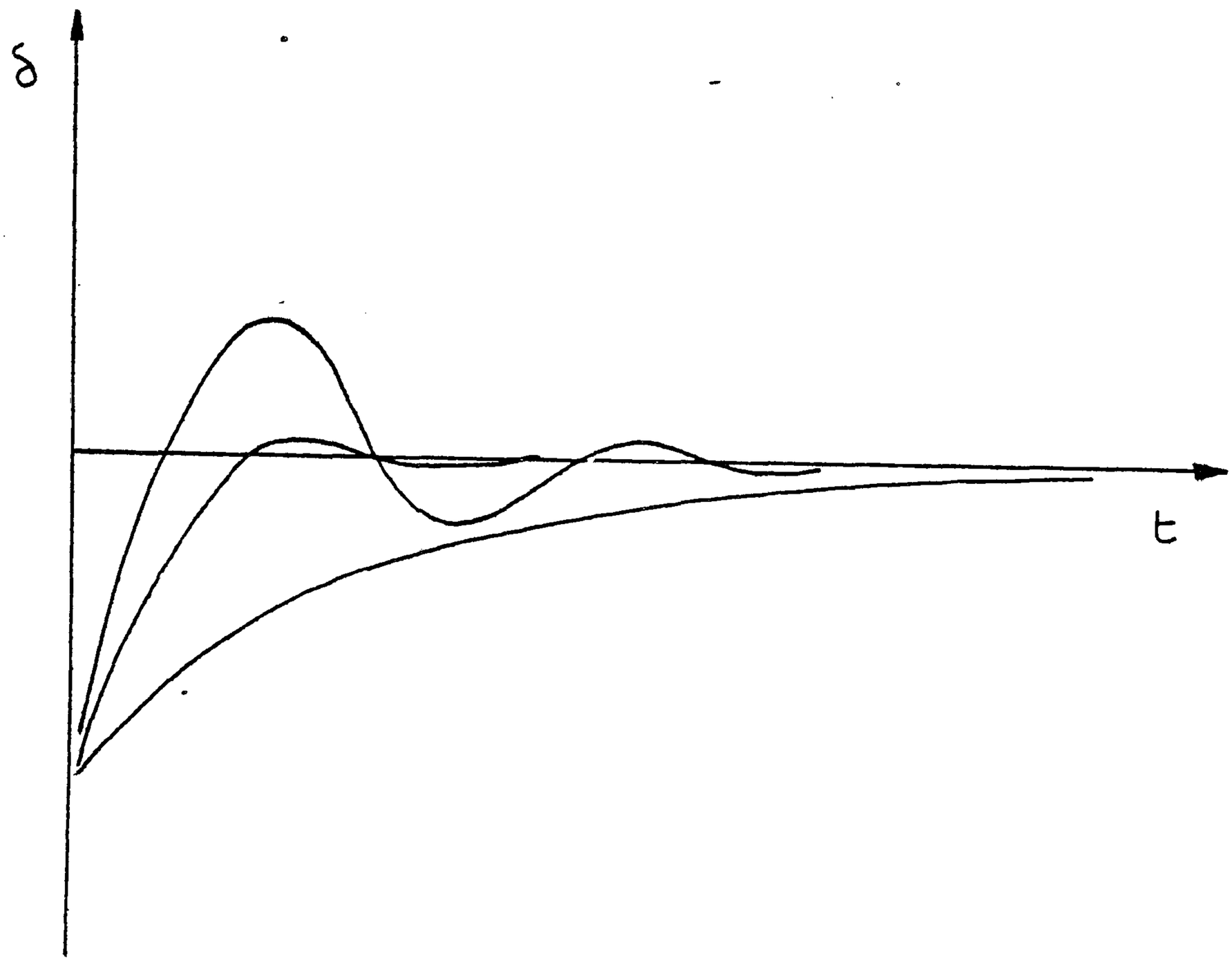

Figure 2.1

combined with an update of the associated fictitious mass components. This approach to the control of viscously damped Dynamic Relaxation has been examined in detail by Papadrakakis (183).

2.1.3 Viscous Damping

For an ideal one degree of freedom system, the critical damping factor, $C'_{crit.}$, may be expressed in terms of the stiffness and mass of that degree of freedom (30):

$$C'_{crit.} = 2\sqrt{S.M} \tag{2.23}$$

and the frequency, f, of free vibrations is:

$$f = \frac{1}{2\Pi}\sqrt{\frac{S}{M}} \tag{2.24}$$

thus:

$$C'_{crit.} = 4\Pi fM \tag{2.25}$$

and, for $C_{crit.}$, the critical damping factor per unit mass, as defined by equation (2.5), is then given by:

$$C_{crit.} = 4\Pi f\ \Delta t \tag{2.26}$$

Figure 2.1 shows the displacement/time trace for the one degree of freedom case with varying degrees of damping. The use of critical damping ensures monotonic convergence to the static equilibrium state. However, slightly sub-critical damping will

enable more rapid convergence, and the oscillatory behaviour about the true displacement gives an indication of the current error bounds of the solution.

For structural systems with many degrees of freedom the assessment of the viscous damping constant may be based upon the fundamental frequency of the system. Otter (132) takes the damping constant to be 0.8 of the value determined from the fundamental frequency. When a regular structure is under consideration, and real masses are employed, then engineering experience may be used in the estimate of this frequency. Otherwise it may be assessed from the deflection traces of selected nodes from a trial undamped Dynamic Relaxation analysis. Separate damping factors may be applied to the principal components of displacement (71, 124). For parametric studies of structural components this trial analysis need only be performed once, and Barnes (21) has suggested that it provides useful information for the preliminary design of tension structures.

Rushton (144) has proposed that a trace be made of the total kinetic energy of the undamped system, with the first energy peak occuring at approximately 1/4 of the fundamental period, as opposed to the 1/2 of that period when deflection peaks are examined. In addition to this reduction in trial analysis time, Rushton suggests that this approach gives a clearer indication of the fundamental frequency.

Chaplin (51, 52) has outlined a scheme, termed metadynamic relaxation by him, wherein damping close to the critical

value is maintained at every node throughout the analysis, with local eigenvalues used to smooth control. The method has been applied to soil-structure interaction problems, but has not, however, been generalised for arbitrary structures.

2.1.4 Applications

The majority of applications of Dynamic Relaxation reported to date have utilised finite difference idealisations of the problem. The initial impetus for the development of the method was provided by the need to analyse the prestressed concrete pressure vessels for nuclear reactors. Day's original paper (60) included an example of a thick cylinder subjected to pressure loading, and Otter (132), Welch (184) and Orr and Holland (185) have subsequently reported on the same problem. Holland (89) has also performed local analyses of the stress distribution in anchorage zones and nozzle/shell intersections for pressure vessels.

Day (1, 4) also described the finite difference analysis of elastic plates with varying boundary conditions, and Rushton (144, 145) has considered grooved flat plates and interaction with elastic foundations. Soil-structure interaction has also been considered by Galletly and Tuma (73) and Chaplin (51). Basu and Dawson have analysed rectangular isotropic and orthotropic sandwich plates (23). Malvick and Pearson (186) analysed a solid quartz circular mirror of 4m diameter, considering the deformation of the optical surface for varying support systems.

Malvick subsequently investigated a parabolic mirror of similar dimensions (187).

Cassel (47), together with Kinsey and Sefton (48), describes the elastic analysis of cylindrical shells and shells of revolution, and Dowling and Bawa (67) have prepared influence surfaces for stiffened steel bridge decks using DR and finite differences.

Rushton (146) introduced geometric non-linearity, investigating large deflection behaviour of variable thickness plates, and subsequently extended his plate analyses to include specified boundary stresses (147) and the post-buckling response of tapered plates (148). Turvey and Wittrick (166) extended the investigation of post-buckling behaviour to laminated plates. Large deflection plate analyses by DR have also been reported by Aalami (1), Alwar and Ramachandra Rao (3, 4), Murthy and Sherbourne (124) and Turvey (167).

Extending the finite difference idealisation to cover combined material and geometric non-linearity, Lowe and Flint (115) studied the collapse behaviour of single-span composite bridge decks. Rushton and Hook (149) analysed the creep of beams and rectangular plates obeying non-linear stress-strain laws. Cundall (58) included the effects of particle contact when modelling granular material in geomechanics problems. Harding, Hobbs and Neal (81) and Frieze, Hobbs and Dowling (71) have investigated the large deflection elasto-plastic behaviour of plates with initial

imperfections, whilst Frieze (72) has considered the buckling of short thin-walled beams and columns.

Finite element structural idealisations in conjunction with DR have been utilised less frequently, even though Day (60) gave an example for a portal frame in his original paper. In a discussion on Dynamic Relaxation (135), both Zienkiewicz and King commented on the possibilities of combining the advantages of the two methods.

Brew and Brotton (32, 33) analysed the nonlinear behaviour of structural plane frames, accounting for the effects of bowing and stability within the individual element stiffnesses. Bunce and Brown (45) performed a similar large deflection analysis, but used large numbers of simple bending elements rather than include stability functions.

Plane stress triangular finite elements were employed by Lynch, Kelsey and Saxe (116) for the analysis of stress concentrations around circular, elliptical and square holes.

Day and Bunce (62, 63) first used pin-jointed elements with DR for the analysis of cable structures, and demonstrated its application to structural mechanisms by means of a simple pendulum problem. Barnes (13→19, 21) has subsequently used DR for the formfinding and analysis of a wide range of network, membrane and pneumatic structures, including the effects of cable slackening, membrane buckling and non-linear material properties.

Iwegbue and Brotton (92), using numerical integration (Newmark's method) for flutter investigations of suspension bridges, have also incorporated viscous damping in order to obtain the static solution.

Barnes (21) has proposed the use of Dynamic Relaxation for optimisation of the form of space trusses subject to a single, dominant, load case. Using a modular ground structure, with generally defined external boundaries containing all possible alternative structures compatible with the modular grid, member sizes are continuously modified during the process until the structure complies with criteria for a least weight optimum. Physically the process of modification is such that, as loads are taken up and transmitted to supports, members which do most work are increased in size and those that do least are decreased. In the limit, the majority of members have reduced to zero area whilst the remainder, forming the optimum, are stable in size and configuration.

Topping (188) has investigated this design procedure further, giving details of the stability and control of the method, extending it to the sizing of modular space structures of fixed topology (including deflection constraints), and comparing solutions and computation times with non-linear programming techniques. Multiple loading cases have also been considered for formfinding and sizing.

2.2 *Gradient Minimisation Methods*

The determination of the equilibrium state for any structural assembly, subject to either internally or externally applied loading, may be regarded as the process of minimising the total potential energy of that assembly with respect to all possible displacements.

The objective function of this minimisation, the total potential energy W, may be expressed as:

$$W = U + V \tag{2.27}$$

where U is the strain energy of the deformed assembly, and V the potential energy of the applied loading $\{P\}$. An arbitrarily defined initial configuration provides a zero-energy reference state. For an assembly of M elements, subject to loading $\{P\}$ which remains constant in both magnitude and direction, and having finite displacements $\{\delta\}$, equation (2.27) may be written:

$$W = \sum_{m=1}^{M} U_m - \{P\}^T\{\delta\} \tag{2.28}$$

where U_m is the strain energy of the mth component. The equilibrium state is then that which satisfies the condition:

$$\left\{\frac{\partial W}{\partial \delta}\right\} = 0 \tag{2.29}$$

which is necessary for the minimisation of the objective function. This first derivative is the gradient vector, denoted by $\{g\}$.

Although direct minimisation techniques, such as random search or Monte-Carlo methods, which only make use of the objective function have been applied to non-linear structural analysis (189), it is the gradient techniques that have been employed most generally and successfully.

For a system having n degrees of freedom the objective function may be regarded as a surface in n-dimensional space. Provided that this surface is convex, and the initial state lies on the surface, a solution may be sought be following a specified descent direction, $\{dv\}$, in n-dimensional space until a local minimum of the objective function is located. The descent direction is then reset and the process repeated until the global minimum is reached. The displacement vector has thus been updated iteratively

$$\{\delta\}^{k+1} = \{\delta\}^{k} + S^{k} . \{dv\}^{k} \qquad (2.30)$$

where S^{k} is a scalar factor, termed the steplength, applied to the descent direction vector to locate the function local minimum. Normalisation of the descent vector is not necessary, as it merely has the effect of scaling the steplength S^{k}.

The determination of the descent direction dv may be achieved by either first or second order gradient methods. First order methods, requiring the gradient vector $\{g\}$, have been successfully applied by Buchholdt (34) to the analysis of pre-tensioned networks, and have the advantage of being explicit.

As a consequence computer storage requirements are reduced as there is no need for the formation of an overall system of linear equations. The Newton-Raphson matrix method for non-linear structural analysis, an implicit technique, can be shown to be a second order gradient method, requiring the second derivative of the objective function, and has been used as such with a steplength control by Buchholdt (40).

It has been shown that the energy surface of a pin-jointed assembly is convex when all members of that assembly remain in tension (36). This is not, however, a necessary condition, and some members may go temporarily into compression during the descent process.

2.2.1 The Gradient Vector

As a precursor to any of the gradient methods the first derivative $\left\{\partial W/\partial \delta\right\} = \left\{g\right\}$ must be obtained. For any node i of the assembly, to which there are J members connected (having node numbers i,j) it can be shown (section 4.2) that:

$$\left\{ \frac{\partial W}{\partial \delta_i} \right\} = - \sum_{m=1}^{J} \frac{T_{ij}}{L_{ij}} . \left\{ \Delta X_{ij} \right\} - \left\{ P_i \right\} = \left\{ g_i \right\} \qquad (2.31)$$

where the coordinate differences, $\left\{ \Delta X_{ij} \right\} = \left\{ X_j \right\} - \left\{ X_i \right\}$, length L_{ij}, and tension T_{ij} for the connecting members are all related to the

current deformed configuration of the assembly. Thus the gradient vector represents exactly the vector of out of balance forces in the global coordinate system for a displacement vector $\{\delta\}$, where $\{\delta\} = \{X\} - \{X^o\}$, and has the direction of greatest increase of the total potential. Clearly at any stage:

$$\{g\}^k = -\{R\}^k \tag{2.32}$$

where $\{R\}^k$ is the current vector of out of balance forces acting on the joints of the assembly.

This exact expression for the gradient vector was derived by Buchholdt and published in his earlier papers (36). More recent publications (37, 42) have, however, presented an approximate expression:

$$\left\{\frac{\partial W}{\partial \delta_i}\right\} = -\sum_{m=1}^{J} \frac{T_{ij}}{L^o_{ij}} \{\Delta X_{ij}\} - \{P_i\} \tag{2.33}$$

wherein the current member length L_{ij} has been replaced by the length at the initial state L^o_{ij} on the assumption of small member strain. The reasons for the introduction of this approximation are discussed in chapter 4, where an extension of Buchholdt's method accounting for arbitrary member strains is presented.

2.2.2 The Descent Direction

Having obtained the gradient vector, the descent direction must then be chosen. Buchholdt and McMillan (39) have reviewed

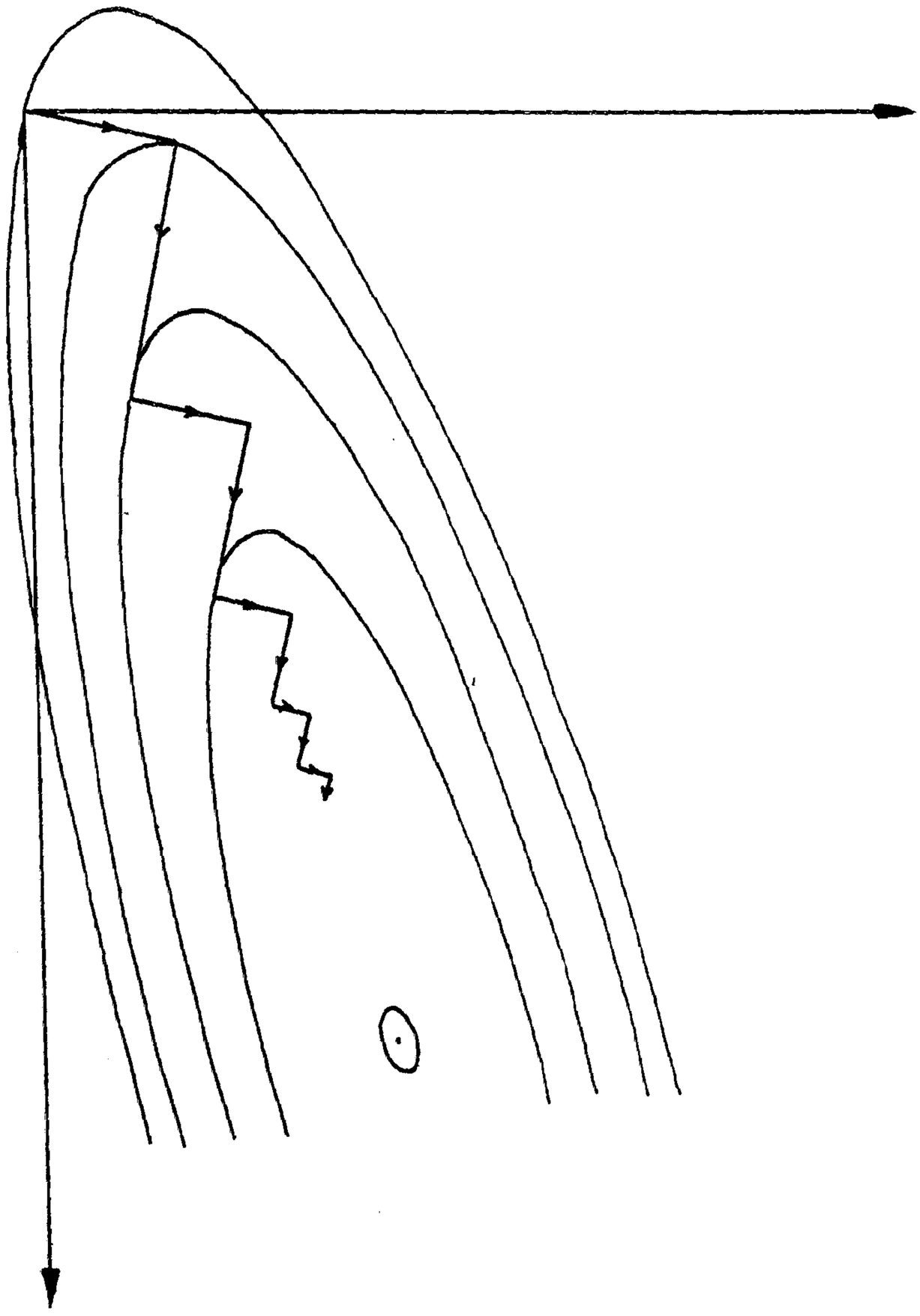

Figure 2.2

several suitable gradient minimisation methods.

Initial investigations were based on the method of steepest descent:

$$\{dv\}^k = -\{g\}^k = \{R\}^k \qquad (2.34)$$

and thus:

$$\{\delta\}^{k+1} = \{\delta\}^k + S^k \{R\}^k \qquad (2.35)$$

Only the initial direction of each step is in the direction of steepest descent, and since the descent direction is followed until W is minimised locally then each successive step is orthogonal to the preceeding one. This zig-zag path of the steepest descent method (figure 2.2) results in very slow convergence, which may be improved by the adoption of a relaxed steplength:

$$\{\delta\}^{k+1} = \{\delta\}^k + \lambda . S^k \{R\}^k \qquad (2.36)$$

with a relaxation factor $1.<\lambda<0$. As λ becomes smaller, the computed path follows the true steepest descent more closely, but this advantage must be traded off against the reduction in progress along that path to solution. It was therefore suggested that λ be applied for 3 steps out of 4, with the full steplength being used every fourth step. For a small cable network analysis the use of relaxed steepest descent, with $0.05<\lambda<0.95$, reduced the number of iterations to between 5% and 25% of those required when using the full steplength throughout. Optimum selection of λ has not, however, proved possible.

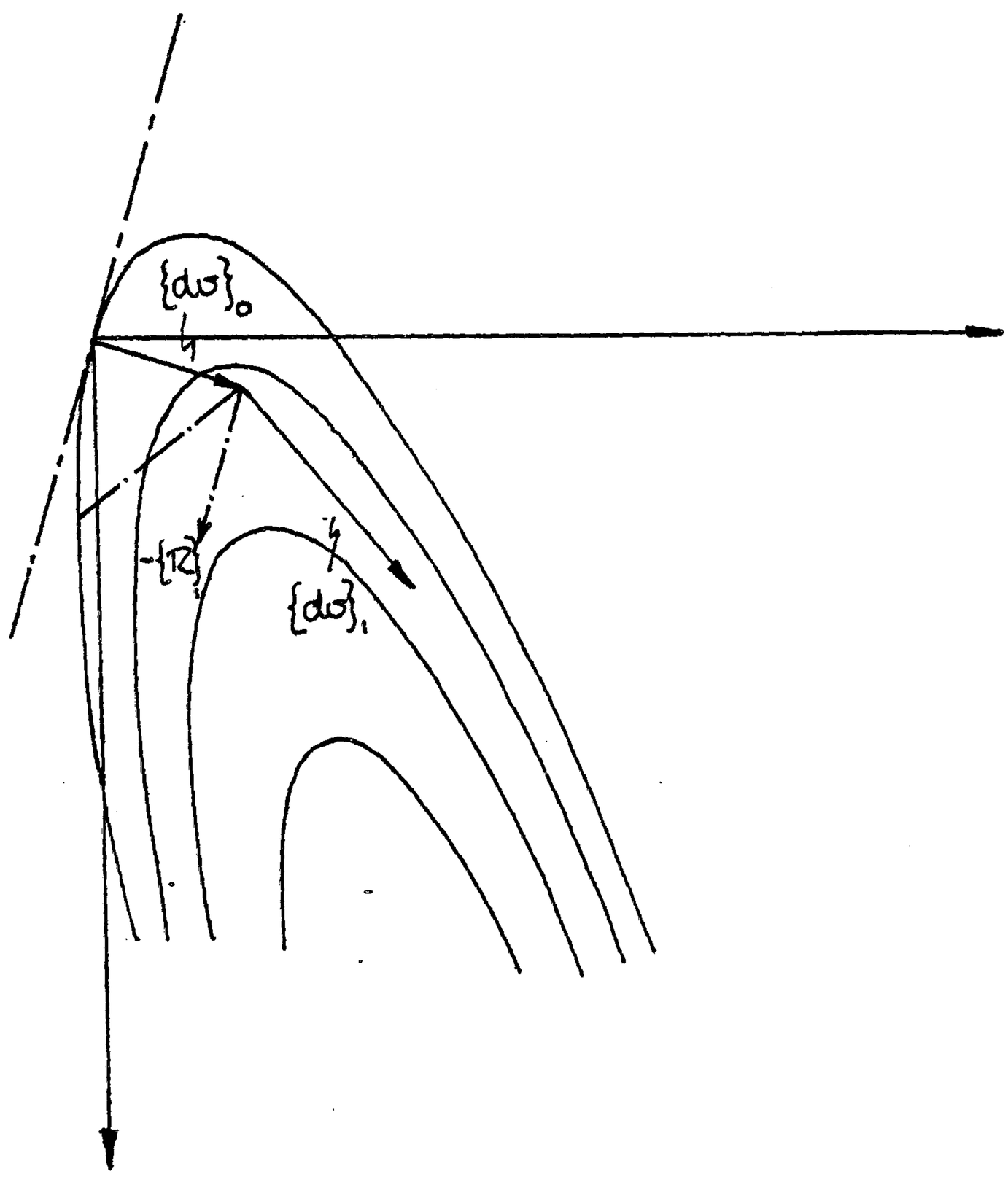

Figure 2.3

The most efficient first order method proved to be that of conjugate gradients, as developed by Hestenes and Stiefel (86) for the solution of sets of linear equations. Convergence is improved as the conjugate gradient method enables accumulated knowledge of the local behaviour of the objective function to be taken into account (figure 2.3).

A pair of vectors are said to be conjugate provided that:

$$\{dv\}_i^T [K] \{dv\}_j = 0 \quad (i \neq j) \tag{2.37}$$

and Fletcher and Reeves (69) have shown that, for $[K]$ constant:

$$\beta^{k} = \frac{\{R\}^{T}_{k+1} \cdot \{R\}^{k+1}}{\{R\}^{T}_{k} \cdot \{R\}^{k}} \tag{2.38}$$

when the conjugate gradient incrementation of the descent direction is:

$$\{dv\}^{k+1} = \{R\}^{k+1} + \beta^{k} \cdot \{dv\}^{k} \tag{2.39}$$

Conjugate descent directions have been set without direct reference to the system matrix $[K]$. For a linear problem, exact convergence will be obtained within n steps (69), where n equals the number of degrees of freedom. For nonlinear problems, however, where $[K]$ is no longer constant, convergence may take longer as the directions are now only approximately conjugate. The process may

be restarted by returning to the steepest descent direction at regular intervals for highly non-linear problems.

2.2.3 *The Linear Search*

Several methods have been suggested for the linear search for the stationary condition of the objective function in the descent direction. Fletcher and Reeves (69) outlined one technique, based on that of Davidon (190), wherein a bracketing process is used to locate bounds to the minimum which are then used in a cubic interpolation refinement. Papadrakakis (183) has compared the relative efficiencies of this and other linear search methods in conjunction with the conjugate gradient algorithm for tension structure analysis. Buchholdt (34) has derived an expression for the total potential in terms of the descent direction steplength which is then used to locate the stationary condition. This approach is reviewed here, and forms the basis of the revised method presented in chapter 4.

For any member m, having connecting nodes i and j, the current tension is given by:

$$T_{ij} = T^{\circ}_{ij} + \frac{\grave{EA}}{L^{\circ}_{ij}} \cdot e_{ij} \qquad (2.40)$$

where e_{ij} is the current extension from the length L°_{ij} associated with the pretension T°_{ij}, and $\grave{EA} = EA_{ij} + T^{\circ}_{ij}$. The member strain energy, based on the pretension reference state, can then

be expressed:

$$U_m = \int_0^{\ell_{ij}} T_{ij} \, de = T^{\circ}_{ij} \cdot e_{ij} + \frac{EA`}{2L^{\circ}_{ij}} \cdot e^2_{ij} \qquad (2.41)$$

Then if the member strain e_{ij} is associated with the assembly displacement state, $\{\delta`\}$ at any point along the current descent direction:

$$\{\delta`\} = \{\delta\} + S\{dv\} \qquad (2.42)$$

it can be seen that:

$$(L^{\circ} + e)^2_{ij} = \left\{\{\Delta X^{\circ}\} + \{\Delta\delta\} + S\{\Delta dv\}\right\}^T \left\{\{\Delta X^{\circ}\} + \{\Delta\delta\} + S\{\Delta dv\}\right\} \qquad (2.43)$$

where
$$\{\Delta X^{\circ}\} = \{X^{\circ}_j\} - \{X^{\circ}_i\}$$
$$\{\Delta\delta\} = \{\delta_j\} - \{\delta_i\}$$
$$\{\Delta dv\} = \{dv_j\} - \{dv_i\}$$

Expanding equation (2.43), and neglecting e^2_{ij} on the assumption that $e_{ij} << L_{ij}\ e_{ij}$, one obtains:

$$e_{ij} = \frac{1}{L^{\circ}_{ij}}\Big[\left(\{\Delta X^{\circ}\}^T\{\Delta\delta\} + \{\Delta\delta\}^T\{\Delta\delta\}/2\right) + S.\left(\{\Delta X^{\circ}\}^T\{\Delta dv\} + \{\Delta dv\}^T\{\Delta\delta\}\right) + S^2.\left(\{\Delta dv\}^T\{\Delta dv\}/2\right) \Big] \qquad (2.44)$$

or:

$$e_{ij} = (a_1 + a_2.S + a_3.S^2)/L^{\circ}_{ij} \qquad (2.45)$$

Backsubstituting this equation into the expression for member strain energy, Buchholdt obtained a quartic polynomial, in the steplength S, for the total potential:

$$W = C_1 S^4 + C_2 S^3 + C_3 S^2 + C_4 S + C_5 \qquad (2.46)$$

The total potential at any projected displacement state along the descent direction may be written:

$$W = U - \{P\}^T\{\delta\} - S\{P\}^T\{dv\} \qquad (2.47)$$

For an assembly of pinjointed bar elements, the coefficients $C_1, \ldots C_5$ of the potential polynomial are:

$$C_1 = \sum EA\, a_3^2 / 2L^{o3} \qquad C_2 = \sum EA\, a_2 a_3 / L^{o3}$$

$$C_3 = \sum \left[\frac{T^o}{L^o} a_3 + \frac{EA}{2L^{o3}} (a_2^2 + 2a_1 a_3) \right]$$

$$C_4 = \sum \left[\frac{T^o}{L^o} a_2 + \frac{EA}{L^{o3}} a_1 a_2 \right] - \{P\}^T\{dv\}$$

$$C_5 = \sum \left[\frac{T^o}{L^o} a_1 + \frac{EA}{2L^{o3}} a_1^2 \right] - \{P\}^T\{\delta\}$$

where the summation is for each member of the assembly.

The stationary position in the descent direction may then be found by differentiating the polynomial with respect to S, and solving the resultant cubic equation for the smallest positive root:

$$\frac{\partial W}{\partial S} = 4C_1 S^3 + 3C_2 S^2 + 2C_3 S + C_4 = 0 \qquad (2.49)$$

The displacement vector may then be incremented:

$$\{\delta\}^{k+1} = \{\delta\}^{k} + S^{k} . \{dv\}^{k} \qquad (2.50)$$

and the minimistation process continued.

2.2.4 Rigid Jointed Boundary Structures

The analysis of tension structures by the conjugate gradient method was extended by Buchholdt, Das and Al-Hilli (42) to include rigid jointed boundary structures. The behaviour of these support structures was assumed to be linear, and for such a system the total potential energy may be written:

$$W_B = \frac{1}{2} \{\delta\}^T [K] \{\delta\} - \{P\}^T \{\delta\} \qquad (2.51)$$

where the displacement vector $\{\delta\}$ now comprises both translational and rotational components. Differentiation with respect to these displacements yields the gradient vector:

$$\left\{\frac{\partial W_B}{\partial \delta}\right\} = [K] \{\delta\} - \{P\} \qquad (2.52)$$

The coefficients, B_1 .....B_5, for the contribution of the boundary structure to the total potential energy polynomial must now be assessed:

$$W = (C_1 + B_1)S^4 + (C_2 + B_2)S^3 + (C_3 + B_3)S^2 + (C_4 + B_4)S + (C_5 + B_5) \qquad (2.53)$$

Equation (2.51) may be rewritten in member summation form for any projected displacement state on the descent direction:

$$W_B = \frac{1}{2}\left\{\{\delta\} + S\{dv\}\right\}^T [K_m] \left\{\{\delta\} + S\{dv\}\right\} - \{P\}^T \left\{\{\delta\} + S\{dv\}\right\} \qquad (2.54)$$

where $[K_m]$ is the boundary member m's elemental stiffness matrix. On expansion of this equation and comparison with equation (2.53), the following polynomial coefficients are obtained:

$$B_1 = B_2 = 0$$

$$B = \frac{1}{2}\int \{dv\}^T [K_m] \{dv\}$$

$$B = \int \{\delta\}^T [K_m] \{dv\} - \{P\}^T \{dv\}$$

$$B = \frac{1}{2}\int \{\delta\}^T [K_m] \{\delta\} - \{P\}^T \{\delta\} \qquad (2.55)$$

The introduction of boundary structures into the analysis, however, highlighted convergence difficulties with the application of the conjugate gradient method to problems with a large condition number.

2.2.5 The Scaled Conjugate Gradient Method

The convergence rate of the method is dependent on the condition number of the associated stiffness matrix, defined as the

ratio of the maximum and minimum eigenvalues of that matrix. These eigenvalues are inversely proportional to the squares of the lengths of the axes forming the total potential contours for a quadratic surface. When the condition number is large, the potential ellipses are long and narrow and the conjugate gradient method converges slowly. This convergence rate increases as the condition number approaches unity and the total potential contours approach circularity.

In an attempt to overcome these convergence problems, the concept of transformation of the total potential energy surface was introduced (42). In the minimisation process the true displacement vector is replaced by a scaled vector $\{u\}$, such that:

$$\{\delta\} = [H]\{u\} \tag{2.56}$$

where $[H]$ is a square scaling matrix. Substituting this relation into the expression for the total potential of a nonlinear problem characterised by the current system of equations $[K_T]$, it can be seen that the effect is the transformation:

$$[\grave{K}_T] = [H]^T[K][H] \tag{2.57}$$

and similarly for the gradient vector:

$$\left\{\frac{\partial W}{\partial u}\right\} = [H]\left\{\frac{\partial W}{\partial \delta}\right\} = \{d\} \tag{2.58}$$

Thus the introduction of scaling may be interpreted as either the transformation of the gradient vector into another

direction, or as an overall transformation of the total potential surface.

The condition number of the transformed problem would be reduced to unity if $\left[H \right]$ could be established such that $\left[\grave{K}_T \right]$ was equivalent to the identity matrix, but in practice such optimal scaling has proved very difficult to achieve.

Buchholdt et al (42) have adopted a diagonal form for $\left[H \right]$, with non-zero terms:

$$H_{ii} = (1/K_{ii})^{1/2} \qquad (2.59)$$

With this formulation the leading diagonal of the transformed system matrix $\left[\grave{K}_T \right]$ is unity, and convergence is then improved as the off-diagonal terms tend towards zero. In addition, the choice of a diagonal scaling matrix minimises the additional computer storage required, and is well suited to the explicit nature of the analysis. The individual scaling terms can be established on an element by element basis without the need to formulate the overall stiffness matrix of the assembly. Then, if:

$$\left\{ \delta \right\} = \left\{ hu \right\} \quad \text{and} \quad \left\{ dv \right\} = \left\{ hd \right\} \qquad (2.60)$$

where the individual coefficients of the scaled gradient, $\left\{ u \right\}$, and descent, $\left\{ d \right\}$, vectors have been multiplied by their associated scaling factors, the modified coefficients for the total potential polynomial can be obtained by direct substitution.

This scaled conjugate gradient method was initally applied to the boundary structure only by Al-Hilli (2), whilst the pretensioned network was left unscaled, and these two segments were analysed alternately as substructures. This 'shuttling technique' was found to diverge in its basic form as relatively small changes in edge cable forces produced significant displacements in the boundary structure, which were then reflected back as excessive cable force changes and a form of oscillatory instability developed. To ensure convergence an overall, optimised, reduction factor was proposed for the boundary structure displacements, this factor being established by total potential minimisation for the descent direction indicated by these current boundary displacements.

Das (191), however, showed that the complete structure could be efficiently analysed simultaneously by application of scaling to both the boundary structure and the cable network. These initial investigations were confined to flat nets, but Buchholdt (43) has used scaled conjugate gradient analysis for design studies of saddle-shaped nets, circular in plan, supported by spatially curved reinforced concrete boundary arches.

McMillan and Buchholdt (41) have shown that the total potential energy of a cable assembly subjected to uniformly distributed loading along the cables may be expressed as an eight order polynomial. Das (191) showed that convergence could be significantly increased for this class of problem by use of the scaled conjugate gradient method. In order to estimate the

scaling terms, use was made of the element stiffness matrix derived by Mollmann (119) on the assumption of parabolic cable deformation between joints.

CHAPTER 3

EFFICIENT DYNAMIC RELAXATION CONTROL AND IMPLEMENTATION

The efficient use of dynamic relaxation requires that optimised fictitious mass components be employed that ensure stability of the numerical integration and permit rapid convergence to the static solution through a suitable damping function. The automatic assessment of these fundamental controls on the iterative process is considered in this chapter. Overall efficiency is also highly dependent on the nodal residual calculations, which are examined here for arbitrary finite element types. Finally, the basis of the proposed analysis scheme is compared with that of the other commonly used explicit analyses, the direct gradient minimisation methods.

3.1 *Kinetic Damping*

Viscous damping coefficients are generally determined from initial undamped or lightly damped trial analyses. The fundamental frequency is then estimated by tracing displacements, or, more efficiently, by tracing the kinetic energy which varies at twice the fundamental frequency and should also enable a clearer indication of that frequency. The same approach may be followed when separate damping constants are applied to individual displacement components, with separate trial analyses for each of these components (71).

When dynamic relaxation is used for parametric studies of structural components, as is frequently the case with the finite difference formulations (71, 72), the viscous damping constants do not generally change significantly as the investigations proceed. Initial trial analyses do not then represent a significant proportion of the overall computations. Barnes (21) has suggested that trial analyses provide useful design information for tension structures, and should not, therefore, be considered disadvantageous.

For some cases, however, the optimum viscous damping factor may prove difficult to estimate, such as the formfinding of funicular lattice shells (20) where the initial configuration is that of an unconfined mechanism. In the presence of gross geometric deformation and significant out of balance forces varying damping constants and fictitious member stiffnesses must be employed as the analysis proceeds in stages. Frieze et al (71)

reported the need for similar varying controls during buckling analyses of plates, where significantly different levels of damping were required for varying levels of applied loading.

If dynamic relaxation is to be generally, and readily, used for nonlinear structural analysis a method of iteration control is ideally required that does not incorporate trial analyses for parameters and copes naturally with gross deformation and residual forces, whilst retaining the essential simplicity of the method.

Lynch, Kelsey and Saxe (116) suggested an automatic on-going adjustment of iteration parameters based on iterative determination of the minimum eigenvalue of the equivalent system matrix. Barnes has outlined a similar treatment based on updated estimates of the asymptotic convergence rate from the incremental displacement vectors (21).

A more radical alternative is to dispense with viscous damping. When an oscillating body passes through its static equilibrium position, the plot of total kinetic energy against time passes through a local maximum. Cundall, examining the application of explicit integration methods to problems in geomechanics (58), suggested that the total kinetic energy be traced as the undamped oscillations proceed, and that all current nodal velocities be reset to zero whenever an energy peak is detected. For a linear elastic system oscillating in one mode the first peak achieved would represent the static equilibrium position, the displacement accuracy of which would depend on the

current nodal velocities and the integration time step. For practical problems, however, the process must be continued through further peaks, eliminating the kinetic energy from other modes, until the required degree of convergence is obtained. This process, termed kinetic damping, requires no trial runs to determine iteration controls, of which only the fictitious mass components need to be established at the start of the analysis. The simplicity and readily understood physical analogy of the method remain.

The iterative equations may be obtained directly from Newton's Second Law:

$$\left\{ R^{t} \right\} = \left[M \right] \left\{ \dot{v}^{t} \right\} \tag{3.1}$$

which is expressed in central difference form:

$$\left\{ R^{t} \right\} = \left[M \right] \cdot \frac{1}{\Delta t} \left\{ v^{t+\Delta t/2} - v^{t-\Delta t/2} \right\} \tag{3.2}$$

On rearranging:

$$\left\{ v^{t+\Delta t/2} \right\} = \left\{ v^{t-\Delta t/2} \right\} + \left[B \right] \left\{ R^{t} \right\} \tag{3.3}$$

and:

$$2 \cdot KE^{t+\Delta t/2} = \left\{ v^{t+\Delta t/2} \right\}^{T} \left[M \right] \left\{ v^{t+\Delta t/2} \right\} \tag{3.4}$$

$$\left\{ x^{t+\Delta t} \right\} = \left\{ x^{t} \right\} + \Delta t \cdot \left\{ v^{t+\Delta t/2} \right\} \tag{3.5}$$

where KE denotes the current kinetic energy of the system.

The initial application of this method to the formfinding of funicular structures was reported in reference (20). For an energy peak detected at time $t+\Delta t/2$, (i.e. $KE^{t+\frac{\Delta t}{2}} < KE^{t-\frac{\Delta t}{2}}$), the analysis was then restarted from the current nodal coordinates in store, $\left\{x^t\right\}$, with velocities such that the linearly interpolated values at time t would be zero:

$$\left\{v^{t+\Delta t/2}\right\} = \frac{1}{2}\left[B\right]\left\{R^t\right\} \qquad (3.6)$$

For this implementation, with time interval $\Delta t = \alpha.\Delta t_{crit}$, a lower bound to the peak kinetic energy value was found before the required convergence level had been attained when $\alpha \geqslant .9$. At this limiting situation an energy peak was detected at each successive time step, with the structure effectively oscillating about the equilibrium state. Full convergence was obtained by reducing the time interval, with the effect of refining the displacement increments. For the example of reference (20), the use of $\alpha < .9$ ensured convergence, with the most efficient solution given by $\alpha = .7$, but subsequent problems indicated that this does not represent a global optimum reduction factor. Investigating the form of a large funicular structure, Barnes (21) has reported slow final convergence of this formulation. The mass components used by Cundall (58) were not established critically, and this conservative assessment ensured eventual convergence for the same reasons as above.

One way of overcoming this problem is to initiate the analysis using the critical time interval, which is then

automatically reduced when the number of steps between peaks is too few, indicating possible limited convergence. The full time interval is then restored when the peak has been satisfactorily located. Optimum values for this localised reduction factor and the minimum number of steps between peaks are problem dependent, although use of standardised values (say, $\Delta t = 0.5\ \Delta t$, > 3 steps between peaks) have ensured convergence whilst enabling the full time interval to be used for the majority of increments.

A simple alternative procedure that ensures full convergence without adjustment of the time interval is proposed here. For a kinetic energy peak at time $t-\Delta t/2$, the analysis is restarted from the nodal coordinates at that time. These are established by linear interpolation between the coordinates at times $t-\Delta t$ and t, a 'bracketing' technique that permits convergence to any required level consistent with the accuracy of the initial data.

If both velocities and coordinates are incremented within the same loop in the program, then $\left\{x^{t}\right\}$, $\left\{v^{t+\frac{\Delta t}{2}}\right\}$ and $\left\{R^{t}\right\}$ are the variables currently in store when a peak is located, and the reinitialisation coordinates $\left\{x^{i}\right\} = \left\{x^{t-\frac{\Delta t}{2}}\right\}$ are then sought:

$$\left\{x^{i}\right\} = \frac{1}{2}\left\{x^{t-\Delta t} + x^{t}\right\} \tag{3.7}$$

On readjustment of the iteration equations (3.3) and (3.5) it can be shown that:

$$\left\{x^{i}\right\} = \left\{x^{t+\Delta t}\right\} - \frac{\Delta t}{2}\left\{3.\left\{v^{t+\frac{\Delta t}{2}}\right\} - [B]\left\{R^{t}\right\}\right\} \tag{3.8}$$

These reinitialisation coordinates may thus be obtained directly from variables currently in store when a peak is detected.

In the central difference approximation to the dynamic analogy, nodal velocities are assumed to vary linearly between times $t-\Delta t/2$. and $t+\Delta t/2$. Consequently the variation of displacement increments is quadratic within that interval. An alternative expression for the reinitialisation coordinates may then be determined. At time $t-\frac{\Delta t}{2}+t^*$:

$$\left\{ v^{t-\frac{\Delta t}{2}+t^*} \right\} = \frac{t^*}{\Delta t} \left\{ v^{t+\frac{\Delta t}{2}} - v^{t-\frac{\Delta t}{2}} \right\} + \left\{ v^{t-\frac{\Delta t}{2}} \right\} \qquad (3.9)$$

and the required displacement increment $\{\delta\}$ is given by:

$$\{\delta\} = \int_0^{\frac{\Delta t}{2}} \left\{ v^{t-\frac{\Delta t}{2}+t^*} \right\} .dt^* + \Delta t. \left\{ v^{t+\frac{\Delta t}{2}} \right\} \qquad (3.10)$$

where:

$$\{\delta\} = \left\{ x^{t+\Delta t} \right\} - \left\{ x^{t-\frac{\Delta t}{2}} \right\} = \left\{ x^{t+\Delta t} \right\} - \left\{ x^{i} \right\} \qquad (3.11)$$

Substituting equation (3.9) into (3.10), evaluating the integral and rearranging one obtains:

$$\left\{ x^{i} \right\} = \left\{ x^{t+\Delta t} \right\} - \frac{3\Delta t}{8} \left\{ 4 \left\{ v^{t+\frac{\Delta t}{2}} \right\} - \left[B \right] \left\{ R^{t} \right\} \right\} \qquad (3.12)$$

Both equations (3.8) and (3.12) have been implemented in kinetic damping schemes, with no clear advantage in terms of

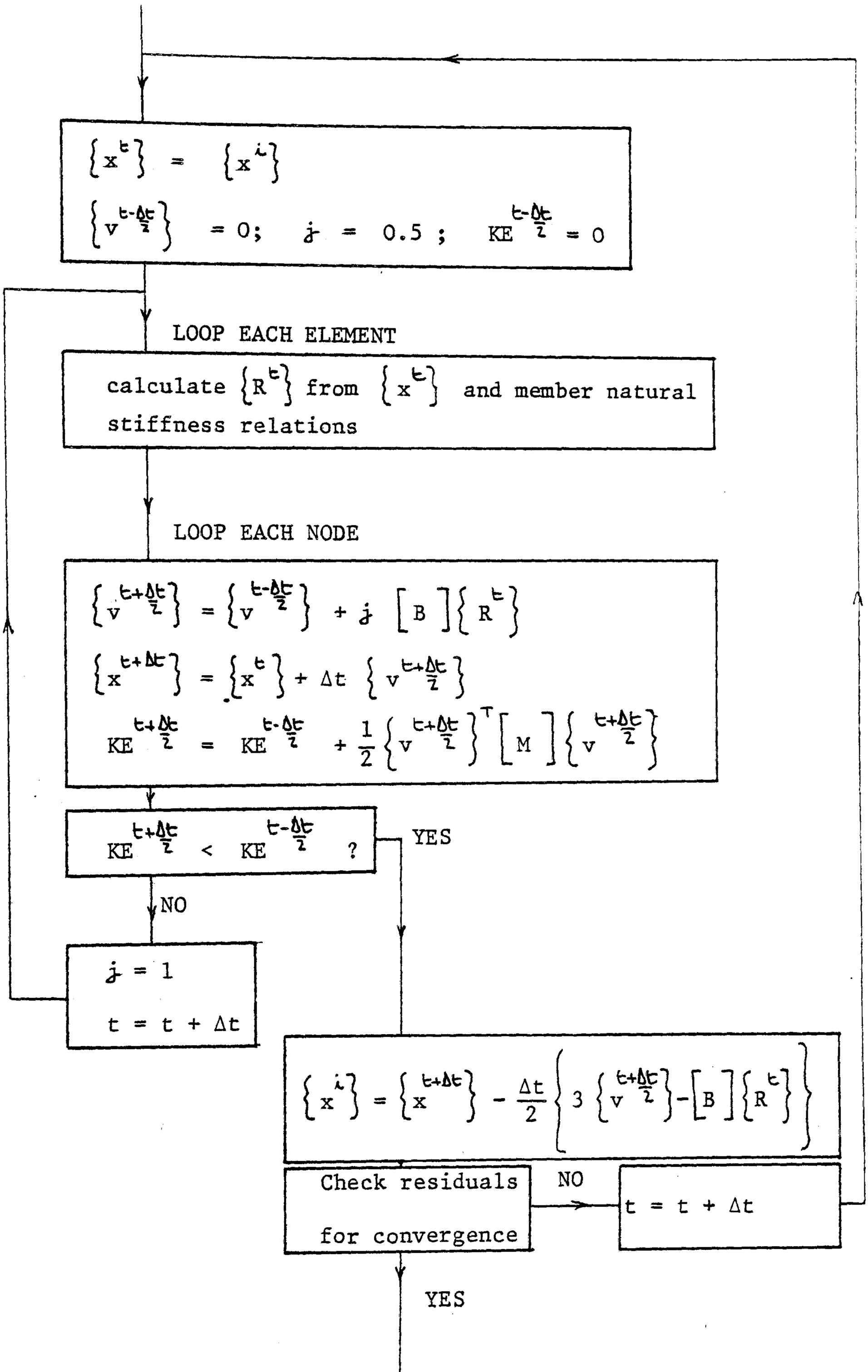
$\{x^t\} = \{x^i\}$
$\{v^{t-\frac{\Delta t}{2}}\} = 0$; $j = 0.5$; $KE^{t-\frac{\Delta t}{2}} = 0$
LOOP EACH ELEMENT
calculate $\{R^t\}$ from $\{x^t\}$ and member natural stiffness relations
LOOP EACH NODE
$\{v^{t+\frac{\Delta t}{2}}\} = \{v^{t-\frac{\Delta t}{2}}\} + j [B]\{R^t\}$
$\{x^{t+\Delta t}\} = \{x^t\} + \Delta t \{v^{t+\frac{\Delta t}{2}}\}$
$KE^{t+\frac{\Delta t}{2}} = KE^{t-\frac{\Delta t}{2}} + \frac{1}{2}\{v^{t+\frac{\Delta t}{2}}\}^T [M] \{v^{t+\frac{\Delta t}{2}}\}$
$KE^{t+\frac{\Delta t}{2}} < KE^{t-\frac{\Delta t}{2}}$?
YES
NO
$j = 1$
$t = t + \Delta t$
$\{x^i\} = \{x^{t+\Delta t}\} - \frac{\Delta t}{2}\{3\{v^{t+\frac{\Delta t}{2}}\} - [B]\{R^t\}\}$
Check residuals for convergence
NO
$t = t + \Delta t$
YES

Figure 3.1

convergence for one or the other. The results presented in this thesis have all been obtained using the linear coordinate interpolation of equation (3.8), and a general flowchart for the iterative process is shown in figure 3.1.

An attempt was also made to locate the peak more accurately by fitting a quadratic polynomial through the kinetic energy values at, and either side of, the detected maximum. However the difference of several orders of magnitude between subsequent kinetic energies resulted in peaks being effectively located at the same time as nodal coordinates, with consequent limited convergence as previously found.

3.2 Optimised Ficticious Mass Components

The only iteration control to be established for dynamic relaxation with kinetic damping is that of the ficitious mass components, which must be sufficient to ensure stability of the numerical integration.

As only the eventual static equilibrium solution is required, the form of the nodal mass matrix $\left[M_i\right]$ is arbitrary, and is initially assumed here to be square. The recurrence relation for the undamped velocities of node i is:

$$\left\{ v_i^{t+\frac{\Delta t}{2}} \right\} = \left\{ v_i^{t-\frac{\Delta t}{2}} \right\} + \left[B_i \right] \left\{ R_i^{t} \right\} \qquad (3.13)$$

where $\left[B_i\right] = \Delta t . \left[M_i\right]^{-1}$, as shown in the preceeding section.

Barnes (13, 21) has presented a direct derivation of the critical nodal mass components, in which it was assumed that the principal nodal direct stiffness components coincided with the global coordinate system. A vector treatment of that derivation is presented here that is indèpendent of any assumptions regarding the direct stiffness components.

Consider the spatial vibrations of a node i with structural connections to adjacent nodes k:

$$\left\{ V_i^{t+\frac{\Delta t}{2}} \right\} = \left\{ V_i^{t-\frac{\Delta t}{2}} \right\} + \left[B_i \right] \left\{ R_i^{t} \right\} \tag{3.14}$$

and for the next time interval

$$\left\{ V_i^{t+3\frac{\Delta t}{2}} \right\} = \left\{ V_i^{t+\frac{\Delta t}{2}} \right\} + \left[B_i \right] \left\{ \left\{ R_i^{t} \right\} - \sum \left[S_{ik} \right] \left\{ \delta\Delta_{ik}^{t+\frac{\Delta t}{2}} \right\} \right\} \tag{3.15}$$

where

$\left[S_{ik} \right]$ = direct stiffness of node i relative to adjacent node k due to the structural element connecting nodes i and k

$\left\{ \delta\Delta_{ik}^{t+\frac{\Delta t}{2}} \right\} = \Delta t \left\{ V_{ik}^{t+\frac{\Delta t}{2}} \right\}$ = increment of node i deflection relative to node k during interval $t \rightarrow t + \Delta t$.

Instability in the form of successive reversal and build-up in the amplitude of velocities and displacements may occur when the time interval and stiffness/mass ratios are large. For an optimised analysis the stiffness/mass ratios will be approximately equal throughout the structure, and the critical time interval may be obtained by considering adjacent nodes I and K. The most critical structural configuration and state of motion will be such that all nodes k adjacent to I are different from all nodes i adjacent to K, with the relative vibrations of nodes I and K exactly out of phase.

Substituting $\left\{R_{\lambda}^{t}\right\}$ from (3.14) into (3.15) for both I and K:

$$\left\{v_{I}^{t+3\frac{\Delta t}{2}}\right\} - 2\left\{v_{I}^{t+\frac{\Delta t}{2}}\right\} + \left\{v_{I}^{t-\frac{\Delta t}{2}}\right\} = -\left[B_{I}\right]\left\{\sum\left[S_{Ik}\right]\left\{\delta\Delta_{I}^{t+\frac{\Delta t}{2}} - \delta\Delta_{k}\right\}\right\} \quad (3.16)$$

$$\left\{v_{K}^{t+3\frac{\Delta t}{2}}\right\} - 2\left\{v_{K}^{t+\frac{\Delta t}{2}}\right\} + \left\{v_{K}^{t-\frac{\Delta t}{2}}\right\} = -\left[B_{K}\right]\left\{\sum\left[S_{Ki}\right]\left\{\delta\Delta_{K}^{t+\frac{\Delta t}{2}} - \delta\Delta_{i}\right\}\right\} \quad (3.17)$$

Then for the optimised analysis and oscillations which are just stable, all $\left\{\delta\Delta_{i}\right\} = \left\{\delta\Delta_{I}\right\}$ and $\left\{\delta\Delta_{k}\right\} = \left\{\delta\Delta_{K}\right\}$, and subracting (3.17) from (3.16):

$$\left\{v_{IK}^{t+3\frac{\Delta t}{2}}\right\} - 2\left\{v_{IK}^{t+\frac{\Delta t}{2}}\right\} + \left\{v_{IK}^{t-\frac{\Delta t}{2}}\right\} = -2\left[B_{I}\right]\left[S_{I}\right]\left\{\delta\Delta_{IK}^{t+\frac{\Delta t}{2}}\right\} \quad (3.18)$$

where $\left\{v_{IK}\right\}$ = velocity of node I relative to node K

$\left[S_{I}\right]$ = direct stiffness of I relative to all adjacent nodes.

The limiting case for stability of the integration is when $\left\{v_{IK}\right\}$ during one time increment produces relative deflection changes $\left\{\delta\Delta_{IK}\right\}$ such that $\left\{v_{IK}\right\}$ in the next increment is equal and opposite to the previous value. Thus:

$$-4\left\{v_{IK}^{t+\Delta t/2}\right\} = -2\left[B_I\right]\left[S_I\right]\left\{v_{IK}^{t+\Delta t/2}\right\}\Delta t \qquad (3.19)$$

and for stability:

$$\left[B_I\right] = \frac{2}{\Delta t}\left[S_I\right]^{-1}$$

$$\left[M_I\right] = \frac{\Delta t^2}{2}\left[S_I\right] \qquad (3.20)$$

For the particular case when the integration axes associated with the global coordinate system coincide with the nodal principal stiffness directions then $\left[S_I\right]$, and consequently $\left[M_I\right]$ and $\left[B_I\right]$ are diagonal matrices. Equations (3.20) are then identical to those obtained by Barnes (13, 21). In general these axes will not coincide, so consider, therefore, a modified analysis scheme with a localised integration coordinate system for each node.

At any node i, the local coordinate system $\left\{\grave{X}_i\right\}$ that coincides with the principal direct stiffness directions is related to the global system $\left\{X\right\}$ by the transformation matrix $\left[\lambda_i\right]$:

$$\left\{\grave{X}_i\right\} = \left[\lambda_i\right]\left\{X\right\} \qquad (3.21)$$

The incremental relation for the integration is then:

$$\left\{\grave{v}_i^{t+\frac{\Delta t}{2}}\right\} = \left\{\grave{v}_i^{t-\frac{\Delta t}{2}}\right\} + \left[\grave{B}_i\right]\left\{\grave{R}_i^{t}\right\} \qquad (3.22)$$

where $\left[\grave{B}_i\right]$ is diagonal, with non-zero coefficients $B_{jj} = 2/\grave{S}j.\Delta t$ for stability, and $\grave{S}j$ is the associated principal direct stiffness.

Introducting the transformation matrix:

$$\left[\lambda_i\right]\left\{v_i^{t+\frac{\Delta t}{2}}\right\} = \left[\lambda_i\right]\left\{v_i^{t-\frac{\Delta t}{2}}\right\} + \left[\grave{B}_i\right]\left[\lambda_i\right]\left\{R_i^{t}\right\} \qquad (3.23)$$

and on premultiplication by its transpose:

$$\left\{v_i^{t+\frac{\Delta t}{2}}\right\} = \left\{v_i^{t-\frac{\Delta t}{2}}\right\} + \left[\lambda_i\right]^T\left[\grave{B}_i\right]\left[\lambda_i\right]\left\{R_i^{t}\right\} \qquad (3.24)$$

the equivalent process in global coordinates is found, where:

$$\left[B_i\right] = \left[\lambda_i\right]^T\left[\grave{B}_i\right]\left[\lambda_i\right] \qquad (3.25)$$

Then:

$$\left[B_i\right] = \frac{2}{\Delta t}\left[\lambda_i\right]\left[\grave{S}_i\right]\left[\lambda_i\right] = \frac{2}{\Delta t}\left[S_i\right] \qquad (3.26)$$

The adoption of a square mass matrix, based on the square nodal direct stiffness matrix, can be seen to be directly equivalent to the use of local nodal integration coordinates chosen so as to optimise analysis with diagonal mass matrices. In this case the effect of coupling of movement between the several degrees of freedom at each node is minimised, and a close to optimum time interval may be employed for efficient analysis.

The physical significance of square nodal fictitious mass matrices may thus be readily visualised. However, although their usage will minimise the number of steps required to solution, the additional computation involved may mean that a diagonal mass

matrix, suitably factored to account for coupling effects, will prove more efficient. Limitations on available computer storage will certainly favour diagonal operations.

If $\left\{ \grave{M}_i \right\}$ is the vector of diagonal mass components associated with node i, then, from equation (3.20):

$$\left\{ \grave{M}_i \right\} = \frac{\Delta t^2}{2} \left\{ S^*_i \right\} \quad . \tag{3.27}$$

where the equivalent direct stiffness components $\left\{ S^*_i \right\}$ must be determined from the nodal direct stiffness matrix $\left[S_i \right]$.

One such determination is based purely on the diagonal terms of $\left[S_i \right]$, such that for the jth degree of freedom at the node:

$$S^*_j = \alpha_m S_{jj} \tag{3.28}$$

When the nodal principal stiffnesses coincide with the global coordinate system, this will yield stable integration with factor $\alpha_m = 1.0$. In general, however, this will not be the case and an increased value of α_m is necessary to ensure stability.

Consider, for example, two unstressed pin-jointed truss elements inclined to the two global axes in the planar case, with intermediate node i as shown in figure 3.2.

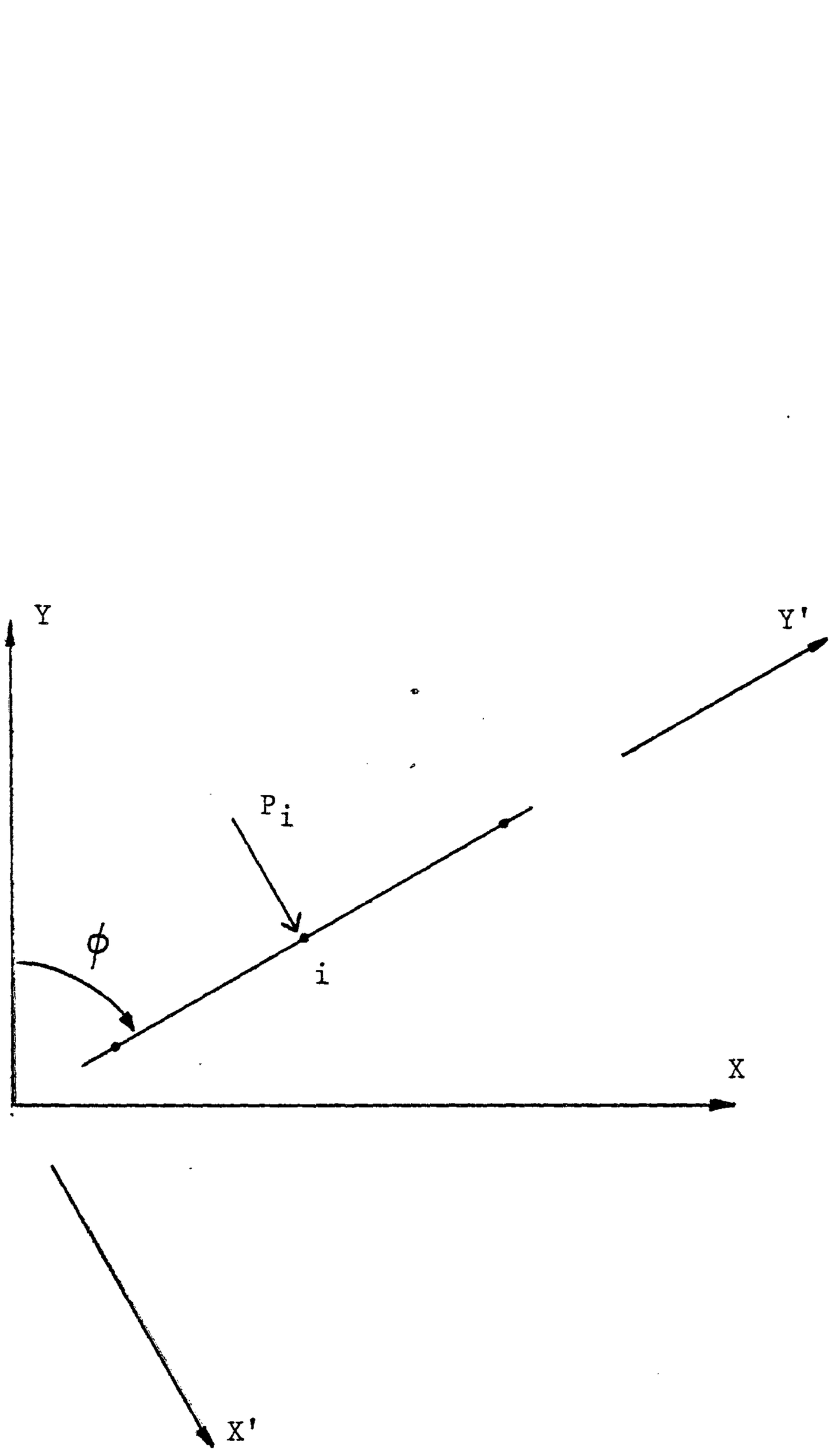

Figure 3.2

Nodal loading P_i is applied normal to the elements, and the principal direct stiffness is in the Y direction, with zero X component. For the most critical case, when $\phi = \Pi/4$, then all of the components of $\left[S_i\right]$ have the same magnitude and a factor $\alpha_m = 2$ is necessary to ensure stability if a diagonal mass matrix based on (3.28) is employed. For a node on such a series of elements equally inclined to the axes of the three dimensional case, a value of $\alpha_m = 3$ is theoretically required.

In practice, however, this latter case is extreme as cable elements are generally pretensioned, with transverse direct stiffness components as a consequence. Similarly flexural elements exhibit transverse stiffness components. A value of $\alpha_m = 2$ has proved satisfactory when this formulation has been applied to a wide range of pin and rigid jointed planar and spatial structures. The mass components so determined are, however, considerably overestimated when the principal direct stiffnesses lie close to the global coordinate system, as is the case for shallow networks and reticulated shells. This effect may be overcome by an alternative approach.

Diagonal mass components may be assessed from equation (3.27), where the equivalent diagonal stiffness components $\left\{S^*\right\}$ are the row sum of the absolute values of the corresponding row of the $\left[S\right]$ matrix.

$$S_j^* = \alpha_m \cdot \sum_{k=1}^{f} \left| S_{jk} \right| \qquad (3.29)$$

where f is the number of displacement components. Coupling effects

are then accounted for on the assumption of equal residual forces for each degree of freedom. For cable elements, equation (3.29) yields identical mass components to those of the Gershgörin bound assessment as reviewed in Chapter 2. The scaling factor α_m may be set to unity here, although in practice a slightly higher value may be chosen to ensure continued stability of the integration as deformation occurs under load.

This problem of changing parameters under the effects of loading is especially critical in, for example, a flat region of a pretensioned network with low normal direct stiffness compared with the in-plane components. Although the mass components may be updated as the analysis proceeds using the above relations, it is generally preferable to make allowance for this problem prior to the analysis. This is most readily achieved by the addition of an 'added mass component', ΔM, equally to each of the nodal mass components calculated as above.

The added mass component might be calculated as the difference between the maximum calculated component at a node and that based on the maximum principal direct stiffness. Alternatively, and more conveniently for simplified automatic mass calculations, a minimum value for the coefficients of $\{S^*_i\}$ is set as a specified fraction, β_m, of the maximum coefficient:

$$S^*_j \geqslant \beta_m . S^*_{max} \qquad (3.30)$$

The same factor may be applied to the square mass matrix, where the absolute row sum values are compared and matrix coefficient

rows are scaled up proportionally as required.

For the examples considered in this thesis, values of β_m between 0.05 and 0.1 have proved satisfactory for the analysis of both pin and rigid jointed structures. For formfinding applications, with gross deformations such as encountered when using a plane mesh as initial data, β_m may be increased up to 1.0, say, and a unified method of control is used for all situations.

The three methods of control summarised below have been applied to a range of problems, and their efficiencies in terms of iterations and solution times to convergence are compared in subsequent chapters:

(a) diagonal mass matrices, with coefficients based on leading diagonal direct stiffness terms (equation (3.28)).

(b) diagonal mass matrices, with coefficients based on the row sums of the direct stiffness matric (equation (3.29)).

(c) square mass matrices, defined by equation (3.20).

For the diagonal mass formulation, the corresponding terms of the diagonal $[B]$ matrices may be obtained directly:

$$B_{jj} = \Delta t/\hat{M}_j \tag{3.31}$$

When the mass matrix is square, the determination of B for node i involves the inversion of at most a (3x3) matrix for the

spatial case, as translation and rotation effects are considered uncoupled (see Chapter 6):

$$\left[B_i \right] = \Delta t. \left[M_i \right]^{-1} \tag{3.32}$$

This inversion may be readily achieved directly by, for example, Cholesky's method, or by transformation of the mass, or stiffness, matrix into diagonal form followed by application of equation (3.31) and retransformation back to global coordinates. The former process is the most efficient for static analyses, whilst the latter, though apparently long winded, may have an application in transient dynamic analysis of lightweight structures by central difference numerical integration.

Consider, for example, the transient dynamic response of a spatially curved pneumatic structure. Interest may primarily be confined to the displacements normal to the structure surface, whilst the stability of the numerical integration is governed by the higher stiffness in the plane of the structure. The effective local integration coordinates of the square mass matrix enable in-plane motion to be 'damped' by the specification of artificially high principal mass components in that plane. The integration of the out of plane motion, with real mass values, may then be optimised without significantly disturbing that motion.

In and out of plane motions have been decoupled by the normalised local coordinate scheme associated with a square nodal mass matrix. The integration time step is optimised for the out of plane motion with real mass components, whilst the stability of integration for the in plane motion is assured by the use of

fictitious principal mass components in that plane. The surface plane of the structure need not coincide with any of the global coordinate planes, but, for this application, the principal stiffness components and their associated coordinate transformations must be obtained explicitly to enable correct scaling of the principal mass components. These are then transformed back into square mass matrices for the global coordinate integration. With separated translation and rotations at general nodes with six degrees of freedom, these operations involve only (3x3) matrices at most. The derivation of principal direct stiffness directions and values is given for 2 and 3 degrees of freedom in Appendix A.

3.3 Natural Stiffness Relations for Residual Force Calculations

At each stage of the iteration, the current vector $\{R\}$ of nodal out of balance, or residual, forces must be determined. The equivalent nodal forces associated with the current element strain state must be established for each finite element type employed. For both transient dynamic analyses, and static analyses based on the damped dynamic analogy, the efficiency of this force calculation reflects critically upon their overall efficiency, in terms of both computer storage requirements and time to achieve a solution.

Belyschko et al (26) utilised the concept of local, or convected, coordinates for efficient derivation of nodal forces for

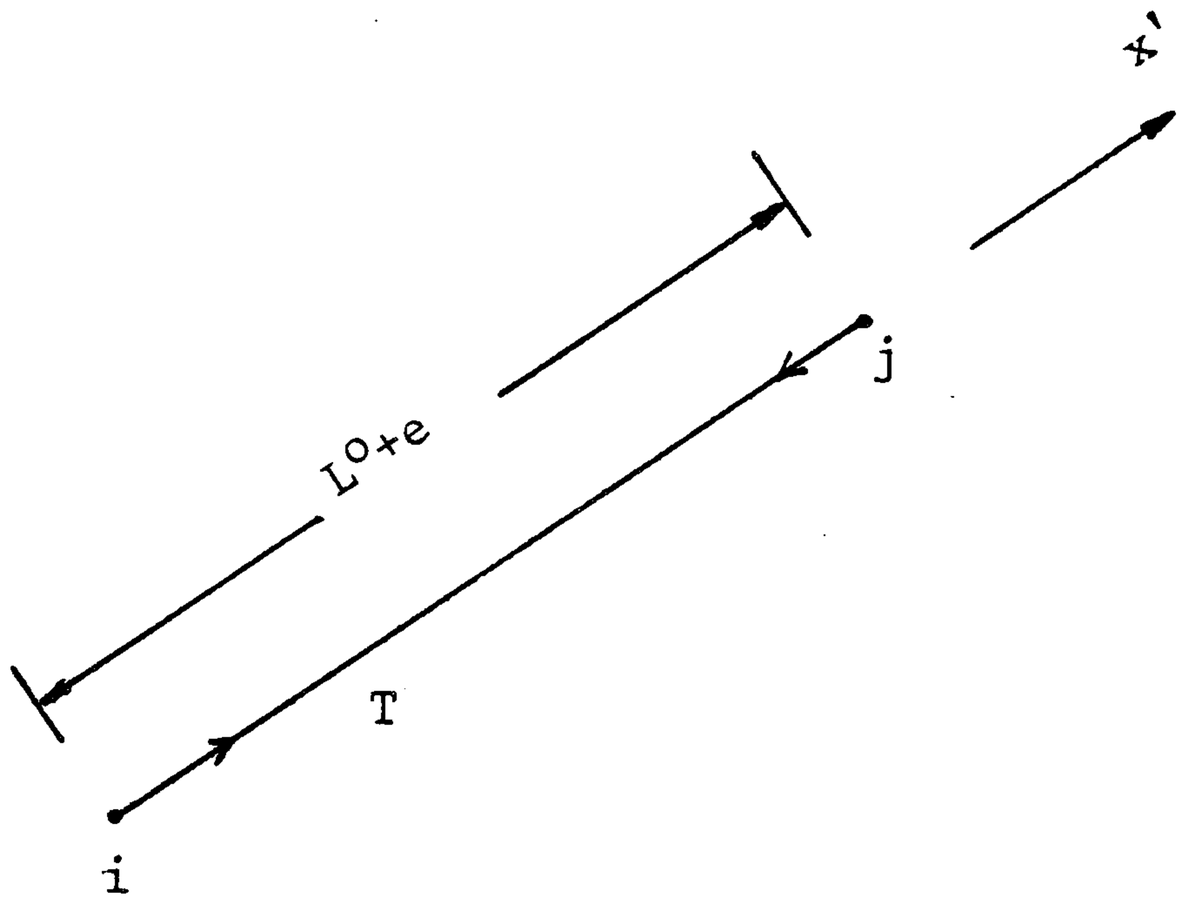

Figure 3.3

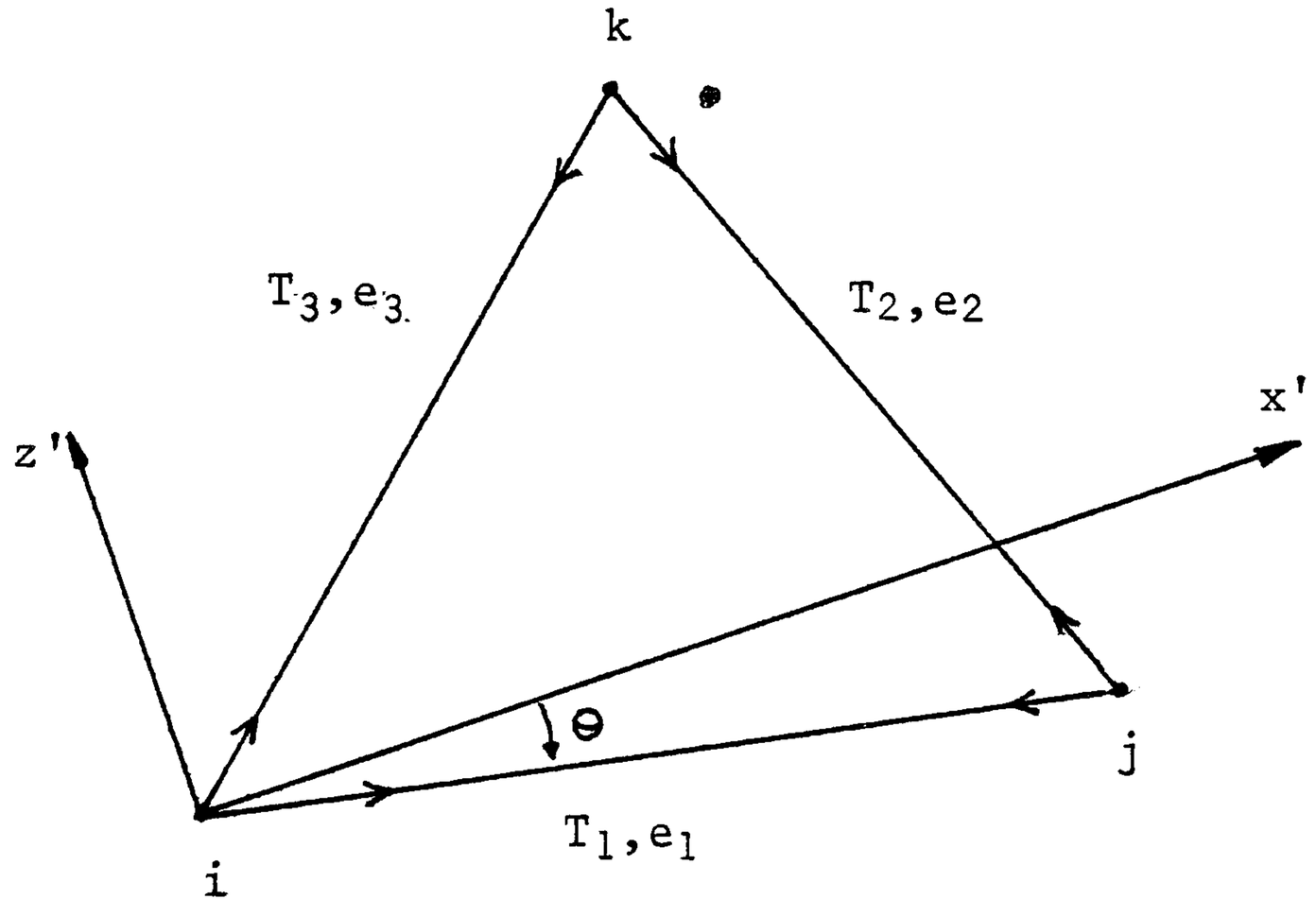

Figure 3.4

nonlinear transient analysis. The origin of these local member coordinates being specified by one node of the element, with another used to define the axis directions. The local coordinates are thus free to translate and rotate with the element as the structure undergoes deformation.

This approach had been adopted by Argyris (6), Mollmann (122) and as the basis for the derivation of stiffness matrices for geometrically nonlinear finite element analysis. Argyris has termed this the 'natural mode' technique, after the (q-b) natural modes which describe the independent pure deformations of an arbitrary element with q total degrees of freedom and b permissible rigid body motions. These basic displacements, or strain measures (122), are the smallest number of geometric quantities necessary to completely determine the deformed configuration of an element, independent of rigid body motion. A set of basic, or natural, member forces are associated with these displacements, these two quantities being related by the element natural stiffness.

The pin jointed strut/cable element of figure 3.3 has one basic displacement, the axial extension e. The constant strain triangular membrane element with natural modes defined by the three side extensions (figure 3.4) was first proposed by Argyris (6) as an intermediate stage in a direct stiffness element derivation. Barnes (13, 21) has applied this element in its natural form, with a (3x3) natural stiffness matrix, to the dynamic relaxation formfinding and analysis of prestressed membrane structures.

The angle Θ is generally specified as zero except for the case of anisotropic material properties. Belytschko et al (28) derived the same element in terms of the three independent relative nodal basic displacements for $\Theta = 0$.

In general the derivation of natural stiffness relations for any element takes three distinct stages:

(i) define the element local coordinates, basic displacements and associated natural forces.

(ii) express the natural forces in terms of the basic displacements/strains.

(iii) establish the transformation matrix relating local and global coordinate systems, thus enabling calculation of basic displacements from nodal coordinates and transformation of natural forces back into the global system.

For most elements, except complex higher order isoparametric varieties, this will result in the most efficient calculation of nodal residuals and minimise computer storage requirements (28). This residual calculation process may then be summarised for each element at every time step:

(i) establish the coordinate transformation matrix.

(ii) calculate basic displacements from the global nodal coordinates.

(iii) calculate natural forces from the basic displacements

using either linear or nonlinear natural stiffness relations.

(iv) sum transformed natural forces into the nodal residual vector.

Detailed applications of these sequences are given for planar and spatial linear and nonlinear flexural elements in Chapter 7.

3.4 The Gradient Minimisation Analogy

The idea of kinetic damping was conceived by Cundall (58) from the physical process of structural vibration, as the original concept of static solution from dynamic analysis by the method of dynamic relaxation was perceived by Day (60).

An alternative derivation may, however, be obtained by reconsidering the first order gradient methods for minimising the total potential energy of a system. The operation of these methods, such as steepest descent and conjugate gradients, may, as reviewed in Chapter 2, be most readily visualised for a problem with two degrees of freedom. In this case the total potential energy can be represented as a three dimensional surface, with the displacement components as the two horizontal axes. The equilibrium, minimum potential, position is then the lowest point on this surface. Starting from a higher, out of balance, position on the energy

surface, the standard gradient methods then seek a solution by successive steps in chosen directions, seeking always to minimise further the objective function, until the equilibrium position is attained.

Rather than a series of linear searches, a dynamic descent of the energy surface might be proposed. The problem may then be visualised as that of a marble, say, released from a point on the energy surface and descending towards the minimum potential point at the bottom of the valley. This marble represents the undamped motion of the structure through displacement space, which may be traced by central finite difference integration with fictitious nodal masses chosen to ensure numerical stability for a given time step.

As with conventional gradient methods, any descent path should only be followed until the total potential is locally minimised along that path. The illustrative marble should, therefore, be halted as soon as its path stops descending, and allowed to restart from rest at that point until the sequence is repeated again. For this 'dynamic minimisation' the minimum total potential position along the descent path may conveniently be interpreted as the maximum kinetic energy position, since the total energy of a vibrating, undamped, system remains constant.

The descent takes place in small increments governed by the stability of the numerical integration, and the current kinetic energy is traced until a peak is detected. The current descent direction is fixed by the current nodal velocities, and the

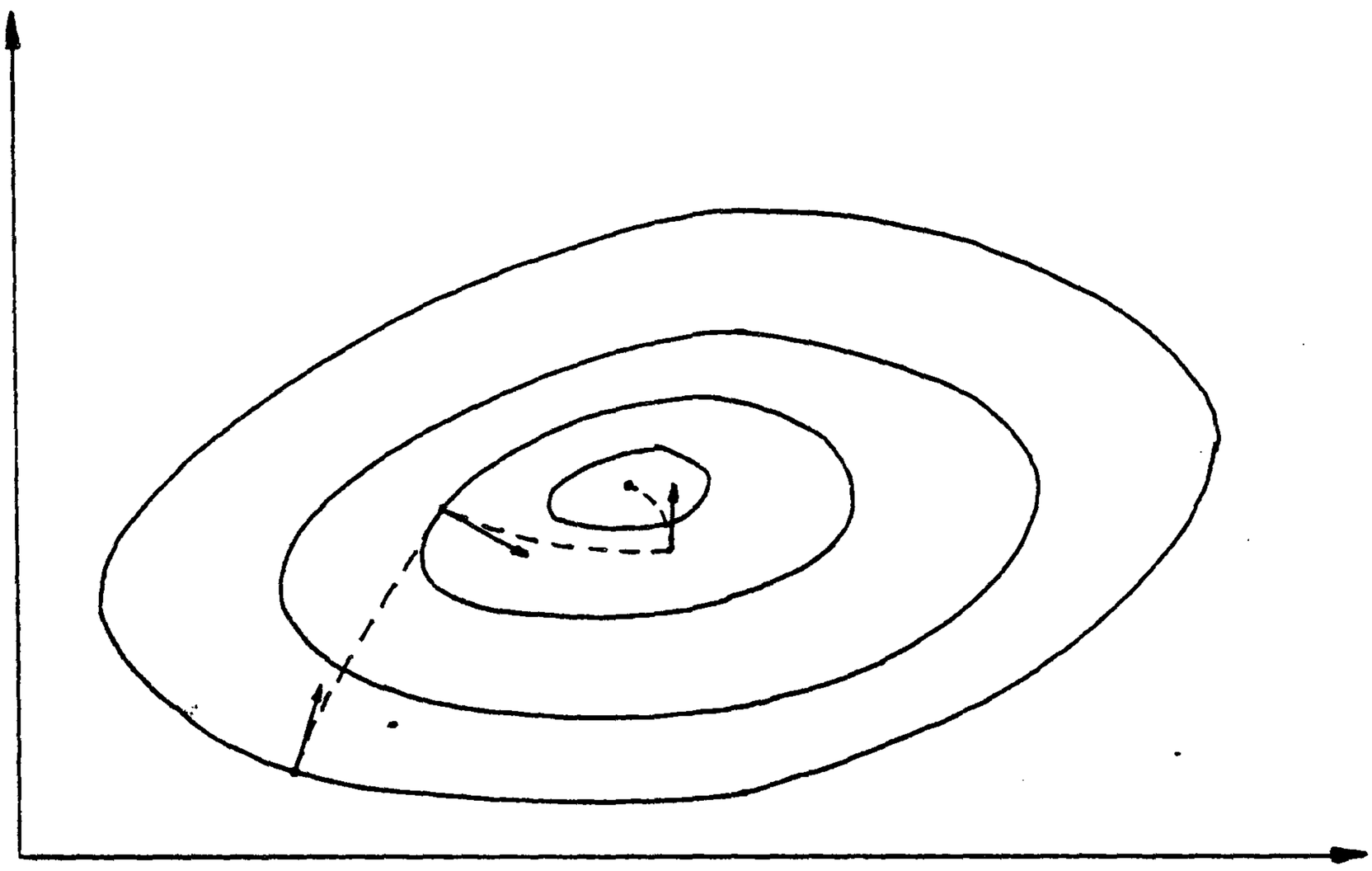

Figure 3.5

similarity between the incremental equation for these velocities, and that in the conjugate gradient method, may be seen. In both cases experience gained in preceding steps is considered when updating the descent direction. For the dynamic minimisation this permits a curved descent path between reset stages, as shown in figure 3.5. The first step after each reinitialisation, as defined by equation (3.6), is in the direction of steepest descent.

From the above it is clear that dynamic relaxation with kinetic damping may be interpreted as a dynamic implementation of a first order gradient minimisation method. The use of optimised fictitious mass components is analogous to the scaling of the conjugate gradient method.

The introduction of the time variable might seen an unnecessary complication of the gradient method, but for general nonlinear structural analysis it has several advantages, and no apparent disadvantages.

The 'exact' steplength calculation by local potential energy minimisation employed by Buchholdt (42) becomes more involved and time consuming as the complexity of the finite element increases. In contrast, the kinetic energy trace of the dynamic minimisation is independent of the structural components, with geometric and material nonlinearity automatically accounted for. The number of small displacement increments between energy resets is such that the bracketing techniques for locating the reinitialisation point described in section 3.1 are sufficiently accurate to ensure rapid convergence. Although the scaled conjugate gradient

method will probably converge in fewer steps than dynamic relaxation, this advantage is offset by the relative complexities of the 'steplength' calculations.

Dynamic relaxation will, however, exhibit fewer energy peak reset stages, as the curved descent path between these stages follows more closely the optimum descent path. In addition, the small displacement increments should enable DR to cope more readily with gross out of balance forces and the highly disturbed energy surfaces of significantly nonlinear problems. The occasional automatic recourse to the steepest descent direction enhances this control, and should permit natural treatment of on-off nonlinearities such as cable slackening.

3.5 Summary

In this chapter the automated control of dynamic relaxation has been considered, together with the implementation of arbitrary element types within the analysis and relationship of that analysis to the first order gradient minimisation methods.

As an alternative to viscous nodal damping, the kinetic damping process suggested by Cundall (58), which does not require prior determination of a damping constant, has been examined. Initial problems with limited convergence of the method when near optimum mass components are employed have been overcome by a simple

modification that enables convergence to any required level.

The fictitious nodal mass components must still be established prior to the analysis, to ensure the stability of the numerical integration, and the direct derivation of critical components proposed by Barnes (13) has been generalised to include the effects of coupled motion at the nodes. These relations provide the basis for the proposed automatic establishment of either diagonal or square nodal mass matrices. The adoption of the latter has been shown equivalent to the use of diagonal mass components in an optimised integration scheme with local integration coordinates that coincide with the nodal principal direct stiffness directions.

The efficient calculation of nodal residual forces through the use of natural finite element stiffness relations has been considered, and general schemes outlined for their derivation and implementation.

In the final section a comparison has been made between the dynamic relaxation method, with kinetic damping, and gradient minimisation techniques. The former has been shown to be a dynamic implementation of a first order gradient method, in which the inherent simplicity of dynamic relaxation nonlinear analysis has been coupled with the automatic control characteristic of the gradient method to provide an effective analysis procedure that retains a clear physical interpretation.

CHAPTER 4

CONVERGENCE OF THE GRADIENT MINIMISATION METHODS

An essential feature of all gradient minimisation methods is the linear search in the descent direction to determine the optimum distance to descent in that direction. Several approaches to this problem have been considered, as reviewed in Chapter 2. Direct solution of the total energy polynomial along the descent direction in order to optimise the steplength has been proposed by Buchholdt, and applied to a wide range of cable network problems.

It is, therefore, the convergence of this widely published method that is examined in this chapter. As a consequence, a modification of Buchholdt's method is presented that enables an exact analysis for cable members subject to arbitrary strains.

4.1 *Convergence of Buchholdt's Method*

The convergence to the correct solution by any gradient method is assured once the gradient vector is effectively zero, and the overall minimum total potential position has been located on the n-dimensional energy surface.

In order to facilitate the calculation of the optimum steplength S in the descent direction at any stage of the iteration, Buchholdt has shown that the total potential energy of the system may be expressed as a fourth order polynomial:

$$W = C_1 S^4 + C_2 S^3 + C_3 S^2 + C_4 S + C_5 \qquad (4.1)$$

The distance S along the descent direction to a minimum potential value is then obtained by differentiation, and solution of the consequent cubic equation:

$$\frac{\partial W}{\partial S} = 4C_1 S^3 + 3C_2 S^2 + 2C_3 S + C_4 \qquad (4.2)$$

The 'steplength' S so calculated should strictly be regarded as a scaling factor applied to the descent direction vector, which has not necessarily been normalised.

As the minimisation process approaches the global minimum, then the steplength S must tend towards zero and, from equation (4.2), the polynomial coefficient C_4 must likewise approach zero for this to be possible. This coefficient, C_4, is the component of the gradient vector in the descent direction:

$$C_4 = g \left\{dv\right\} = - \left\{R\right\}^T \left\{dv\right\} \qquad (4.3)$$

For successful convergence of any gradient method using this approach to the linear search in the descent direction, the derivation of both gradient vector and steplength polynomial coefficients must include identical approximations, if any should need to be made. Otherwise the minimum sought by solution of the cubic equation will not also satisfy the overall minimisation requirements for the objective function.

This requirement explains the use of an approximate expression for the gradient vector (equation 2.33) by Buchholdt in his more recent publications (37, 42) as opposed to the exact relationship applied previously (36). This was necessary to ensure convergence of the method, as the polynomial coefficients derived for cable elements were based on the assumption of small strain ($e^2 \ll L^o.e$) as reviewed in Chapter 2. Investigations have shown that the use of Buchholdt's coefficients in conjunction with an exact determination of the gradient vector may result either in unsatisfactorily high residual forces at 'convergence', or complete divergence, especially when the analyses include flexible boundary structures.

One alternative approach would be to calculate a modified C_4 coefficient from equation (4.3), with exact values for the gradient vector, whilst the remaining coefficients were as established by Buchholdt for small member strains. This should enable convergence to the correct solution, but, especially in

highly nonlinear cases, the only approximate compatibility of the polynomial coefficients may cause a reduction in the rate of convergence, and possibly even divergence through calculation of a negative steplength.

To ensure convergence, and enable a realistic comparison with dynamic relaxation, Buchholdt's approach to the control of gradient minimisation methods has been extended to cater for arbitrary member strains. For completeness a derivation of the exact gradient vector, which is fully compatible with this arbitrary strain formulation, is also included in the following section. As the scaled gradient method has been shown to be the most efficient first order gradient technique, the notation used is directly compatible with that method, but the results are equally applicable to any alternative algorithm.

4.2 Exact Gradient Minimisation for Arbitrary Cable Strains

The total potential, W, of a structural assembly of M members, subject to applied loading $\{P\}$, may be written:

$$W = \sum_{m=1}^{M} U_m - \{P\}^T \{\delta\} \qquad (4.4)$$

where U_m is the strain energy of member m, and $\{\delta\}$ the true displacement vector.

Then for any node i the equilibrium state at the minimum total potential position is given by:

$$\left\{\frac{\partial W}{\partial \delta_i}\right\} = \left\{0\right\} \tag{4.5}$$

and, from equation 4.4 , the nodal gradient vector is:

$$\left\{\frac{\partial W}{\partial \delta_i}\right\} = \sum_{j=1}^{J} \left\{\frac{\partial U_{ij}}{\partial \delta_i}\right\} - \left\{P_i\right\} \tag{4.6}$$

where the summation is for the J members connected directly to node i, having connecting nodes i and j. If the member tensile force is T_{ij} , and its associated extension e_{ij} , then:

$$\partial U_{ij} = T_{ij} \cdot \partial e \tag{4.7}$$

and:

$$\left\{\frac{\partial U_{ij}}{\partial \delta_i}\right\} = \frac{\partial U_{ij}}{\partial e_{ij}} \cdot \left\{\frac{\partial e_{ij}}{\partial \delta_i}\right\}$$

$$= T_{ij} \cdot \left\{\frac{\partial e_{ij}}{\partial \delta_i}\right\} \tag{4.8}$$

Defining the differences in initial nodal coordinates and in displacements by:

$$\left\{\Delta X^{\circ}_{ij}\right\} = \left\{X^{\circ}_{j}\right\} - \left\{X^{\circ}_{i}\right\}$$

$$\left\{\Delta \delta_{ij}\right\} = \left\{\delta_j\right\} - \left\{\delta_i\right\} \tag{4.9}$$

and, if the initial member length is L°_{ij} , then:

$$L^{\circ 2}_{ij} = \left\{\Delta X^{\circ}_{ij}\right\}^{T} \left\{\Delta X^{\circ}_{ij}\right\} \tag{4.10}$$

$$(L^{o}_{ij} + e_{ij})^2 = \left\{\Delta X^{o}_{ij} + \Delta\delta_{ij}\right\}^T \left\{\Delta X^{o}_{ij} + \Delta\delta_{ij}\right\} \qquad (4.11)$$

therefore, on expansion and subtraction:

$$2L^{o}_{ij} \cdot e_{ij} + e^2_{ij} = 2. \left\{\Delta\delta_{ij}\right\}^T \left\{\Delta X^{o}_{ij}\right\} + \left\{\Delta\delta_{ij}\right\}^T \left\{\Delta\delta_{ij}\right\} \qquad (4.12)$$

Differentiation with respect to $\left\{\Delta\delta_{ij}\right\}$ gives:

$$2L^{o}_{ij} \cdot \left\{\frac{\partial e_{ij}}{\partial\Delta\delta_{ij}}\right\} + 2e_{ij} \cdot \left\{\frac{\partial e_{ij}}{\partial\Delta\delta_{ij}}\right\} = 2. \left\{\Delta X^{o}_{ij}\right\} + 2. \left\{\Delta\delta_{ij}\right\} \qquad (4.13)$$

Thus: $$\left\{\frac{\partial e_{ij}}{\partial\Delta\delta_{ij}}\right\} = \frac{1}{(L^{o}_{ij} + e_{ij})} \left\{\Delta X^{o}_{ij} + \Delta\delta_{ij}\right\} \qquad (4.14)$$

Now:

$$\left\{\frac{\partial e_{ij}}{\partial\delta_i}\right\} = \left\{\frac{\partial e_{ij}}{\partial\Delta\delta_{ij}}\right\} \cdot \left\{\frac{\partial\Delta\delta_{ij}}{\partial\delta_i}\right\} \qquad (4.15)$$

therefore from the above definition of $\left\{\Delta\delta_{ij}\right\}$:

$$\left\{\frac{\partial e_{ij}}{\partial\delta_i}\right\} = -\left\{\frac{\partial e_{ij}}{\partial\Delta\delta_{ij}}\right\} \qquad (4.16)$$

and:

$$\left\{\frac{\partial U_{ij}}{\partial\delta_i}\right\} = -\frac{T_{ij}}{(L^{o}_{ij} + e_{ij})} \cdot \left\{\Delta X^{o}_{ij} + \Delta\delta_{ij}\right\} \qquad (4.17)$$

Thus at node i:

$$\left\{\frac{\partial W}{\partial\delta_i}\right\} = -\sum_{j=1}^{J} \frac{T_{ij}}{(L^{o}_{ij} + e_{ij})} \cdot \left\{\Delta X^{o}_{ij} + \Delta\delta_{ij}\right\} - \left\{P_i\right\} \qquad (4.18)$$

and this gradient vector represents exactly the nodal out of balance

forces in the global coordinate system for a displacement vector $\{\delta\}$, and has the direction of greatest increase of the total potential.

At any stage of the analysis, therefore:

$$\left\{\frac{\partial W}{\partial \delta}\right\} = -\{R\} \qquad (4.19)$$

where $\{R\}$ is the vector of residual forces acting on the nodes of the assembly.

The scaled gradient vector may then be established:

$$\left\{\frac{\partial W}{\partial u}\right\} = [H]\left\{\frac{\partial W}{\partial \delta}\right\} \qquad (4.20)$$

with the diagonal scaling matrix $[H]$ as described in section 2.2.5 and the scaled descent direction incremented:

$$\{hd\}^{k+1} = -\left\{\frac{\partial W}{\partial u}\right\}^{k+1} + \beta^{k}.\{hd\}^{k} \qquad (4.21)$$

The optimum steplength S along this descent vector must then be determined before the scaled displacement vector $\{u\}$ may be updated and the next complete iteration commenced.

Consider the member projected extension e_{ij} which is associated with a projected coordinate vector $\{X^{s}\}$ for the nodes of the assembly:

$$\{X^{s}\} = \{X^{o}\} + \{hu\} + S\{hd\} \qquad (4.22)$$

The smallest positive value of S that minimises the total potential energy of the system is sought.

Let

$$e'_{ij} = e_{ij} + e'_{ij} \tag{4.23}$$

where e_{ij} is the member extension associated with the current length L_{ij} and coordinates $\left\{X^{\circ} + hu\right\}$:

$$e_{ij} = L_{ij} - L^{\circ}_{ij} \tag{4.24}$$

and e'_{ij} is the change in extension due to movement along the descent direction. The current length L_{ij} has been calculated exactly by a square root operation whilst forming the gradient vector, and is assumed to be retained in the computer program.

Then, using the Δ notation as before to denote the difference between values at nodes j and i:

$$L^2_{ij} = \left\{\Delta X^{\circ}_{ij} + \Delta hu_{ij}\right\}^T \left\{\Delta X^{\circ}_{ij} + \Delta hu_{ij}\right\} \tag{4.25}$$

$$(L_{ij} + e'_{ij})^2 = \left\{\Delta X^{\circ}_{ij} + \Delta hu_{ij} + S\Delta hd_{ij}\right\}^T \left\{\Delta X^{\circ}_{ij} + \Delta hu_{ij} + S\Delta hd_{ij}\right\} \tag{4.26}$$

Expansion and subtraction yields:

$$2L_{ij}\, e'_{ij} + e'^2_{ij} = 2S \left\{\Delta hd_{ij}\right\}^T \left\{\Delta X^{\circ}_{ij} + \Delta hu_{ij}\right\} + S^2 \left\{\Delta hd_{ij}\right\}^T \left\{\Delta hd_{ij}\right\} \tag{4.27}$$

Then, neglecting e'^2_{ij} as very small compared to $L_{ij}.\, e'_{ij}$, one obtains:

$$e'_{ij} = \frac{S}{L_{ij}} \left\{\Delta hd_{ij}\right\}^T \left\{\Delta X^o_{ij} + \Delta hu_{ij}\right\} + \frac{S^2}{2L_{ij}} \left\{\Delta hd_{ij}\right\}^T \left\{\Delta hd_{ij}\right\} \quad (4.28)$$

$$= a'_2 S + a'_3 S^2 \quad (4.29)$$

or:

$$e^s_{ij} = a'_1 + a'_2 . S + a'_3 . S^2 \quad (4.30)$$

where $a'_1 = e_{ij}$

Note that, unlike that made by Buchholdt, the approximation made in neglecting e'^2_{ij} has no effect on the eventual accuracy of the solution obtained since $e^s \rightarrow e$ and $e' \rightarrow 0$ as convergence is reached.

Equation (4.30) may then be substituted into the expression for member strain energy:

$$U_m = T^o_{ij} (a'_1 + a'_2 S + a'_3 S^2) + \frac{EA}{2L^o_{ij}} (a'_1 + a'_2 S + a'_3 S^2)^2 \quad (4.31)$$

The total potential energy of the system may again be expressed as a fourth order polynomial in S:

$$W = C'_1 S^4 + C'_2 S^3 + C'_3 S + C'_4 S + C'_5 \quad (4.32)$$

On expansion of equation (4.31), and summing for all the members, the following polynomial coefficients are obtained for cable elements subject to arbitrary straining:

$$C_1' = \sum \alpha\, a_3'^2 \qquad C_2' = \sum \alpha\, 2a_2'\, a_3'$$

$$C_3' = \sum \beta\, a_3' + \alpha\,(a_2'^2 + 2a_1'\, a_3')$$

$$C_4' = \sum (\beta a_2' + \alpha\, 2a_1'\, a_2') - \{P\}^T \{hd\}$$

$$C_5' = \sum (\beta a_1' + \alpha\, a_1'^2) - \{P\}^T \{hu\} \qquad (4.33)$$

where: $\alpha = \dfrac{EA}{2L^\circ_{ij}} = \dfrac{(EA + T^\circ_{ij})}{2L^\circ_{ij}}$; $\beta = T^\circ_{ij}$

In the limit, as the true equilibrium state is approached, no approximations have been made in calculating either the gradient vector or the polynomial coefficients. Expanding C_4' in full:

$$C_4' = \sum \left[\frac{T^\circ_{ij}}{L_{ij}} \left\{ \Delta X^\circ_{ij} + \Delta hu_{ij} \right\}^T \left\{ \Delta hd_{ij} \right\} + \frac{EA}{L^\circ_{ij}} \frac{e_{ij}}{L_{ij}} \left\{ \Delta X^\circ_{ij} + \Delta hu_{ij} \right\}^T \left\{ \Delta hd_{ij} \right\} \right]$$

$$- \{P\}^T \{hd\} \qquad (4.34)$$

or:

$$C_4' = \left\{ \frac{\partial W}{\partial u} \right\}^T \{hd\} \qquad (4.35)$$

Consequently convergence to the true equilibrium state is ensured for arbitrary member strains. The only additional computer storage required compared with Buchholdt's small strain formulation is that of member current lengths, and in critical situations even these could be calculated afresh as required rather than stored.

For the analysis of linear boundary structures, referring back to equations 2.51 and 2.55 , it can be seen that:

$$B_4 = \left\{ \frac{\partial W_B}{\partial u} \right\}^T \left\{ hd \right\} \qquad (4.36)$$

and convergence to the correct solution is assured within the accuracy of the assumption of linear behaviour, an assumption that has been applied to the calculation of both gradient vector and polynomial coefficients. Consequently the B and $\grave{C}$ coefficients have been combined for the analysis of pretensioned networks within rigid-jointed flexible boundary structures as considered in Chapter 8.

4.3 Numerical Example

The simple pretensioned cable example shown in figure 4.1 has been chosen to clearly illustrate the comments of the preceding sections and demonstrate the convergence of the arbitrary strain formulation to the exact solution.

Initially the test problem has been subjected to a range of vertically applied loads, thus producing varying degrees of nonlinearity for a problem that has effectively one degree of freedom. Scaling of the energy surface would have no effect on the convergence of this problem, and has not been applied.

The performance of Buchholdt's coefficients, coupled with both exact and approximate (but compatible) calculation of nodal residuals, is compared with those proposed in the

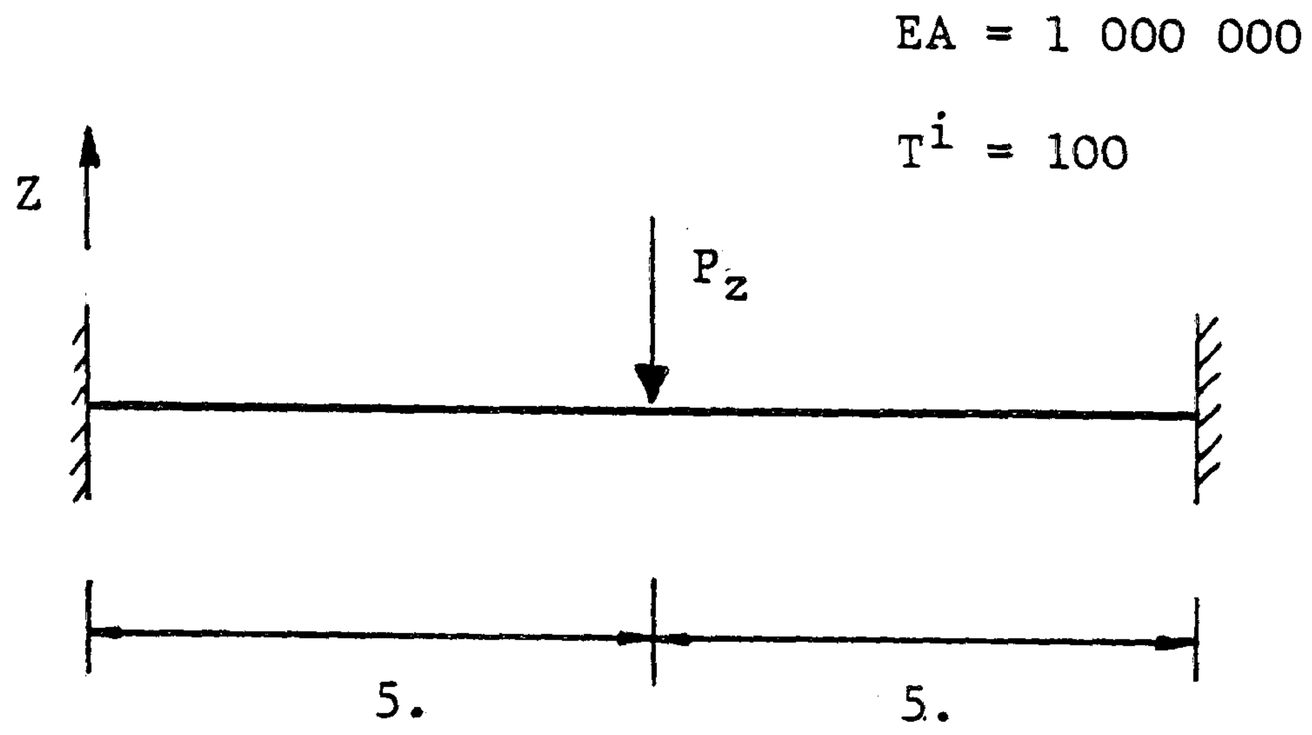

Figure 4.1

ANALYSIS METHOD		APPLIED LOAD P_z		
		10.	100.	1000.
BUCHHOLDT COEFFICIENTS AND EXACT RESIDUALS	δ_z	-.0923684	-.224893	-.496650
	n_α	1	1	1
	R_z	-.2244 E-02	-.1469	- 7.2910
BUCHHOLDT COEFFICIENTS AND APPROX. RESIDUALS	δ_z	-.0923684	-.224893	-.496650
	n_α	1	1	1
	R_z	.5821 E-10	.4191 E-08	.3353 E-07
EXACT ARBITRARY STRAIN FORMULATION	δ_z	-.923775	-.225011	-.497886
	n_α	2	3	3
	R_z	0.	.4796 E-07	.7860 E-06

Table 4.1

arbitrary strain formulation. The results are presented in table 4.1, which gives the deflection, δ_z, in the direction of the applied load, the number of iterations, n_d, to achieve that value to a 6 significant figure accuracy, and the limiting residual force, R_z.

Both applications utilising Buchholdt's coefficients can be seen to converge to the same displacement values, in one step, for each of the load cases. The relatively high limiting out of balance forces for the analyses with exact residual calculations clearly illustrate the need for compatibility of derivation. Here the C_4 coefficient has been minimised, and the analysis proceeds no further even though the overall minimisation requirement of $\left\{\frac{\partial W}{\partial x}\right\} \rightarrow 0$ has not been satisfied.

Application of the proposed arbitrary strain coefficients has resulted in successful overall minimisation of the exact nodal residuals, although the zero out of balance force obtained in one case is probably fortuitous. The number of steps to the specified degree of convergence has been increased. For this problem the modified coefficients are such that the Buchholdt solution is obtained at the first iteration, and subsequently corrected.

When the problem is extended to three degrees of freedom, by introducting loads $P_x = P_y = .1\ P_z$, this discrepancy in convergence rates is proportionally less critical. The results for these unscaled analyses are given in table 4.2

ANALYSIS METHOD		APPLIED LOAD P_z		
		10.	100.	1000.
BUCHHOLDT COEFFICIENTS AND EXACT RESIDUALS	δ_z	-.0921123	-.224198	-.495350
	n_d	28	29	59
	R_z	-.2269 E-02	-.1155	-.5348 E-01
BUCHHOLDT COEFFICIENTS AND APPROX. RESIDUALS	δ_z	-.0921123	-.224172	-.495017
	n_d	15	41	93
	R_z	.5821 E-06	.9659 E-04	.2010 E-02
EXACT ARBITRARY STRAIN FORMULATION	δ_z	-.0921215	-.224290	-.496252
	n_d	15	48	99
	R_z	.6550 E-04	.1035 E-04	.1801 E-02

Table 4.2

4.4 *Summary*

The convergence of Buchholdt's version of the conjugate gradient method has been examined, and it has been shown that, for the required minimisation to succeed, the derivation of energy polynomial coefficients and the gradient vector must be based on identical theoretical treatment. The coefficients proposed by Buchholdt are limited to cable elements exhibiting small strains, and consequently approximations must also be made in the calculations of the gradient vector, or nodal residuals.

Buchholdt's method has been extended to enable compatibility with exactly determined nodal residuals and to permit arbitrary member strains. This modification is achieved without the need for any additional computer storage. A simple numerical example has been used to illustrate the comments on convergence and the successful application of the proposed formulation.

This extended version of Buchholdt's method has been used for all the subsequent comparisons with dynamic relaxation in this thesis. For pretensioned cable networks it ensures that both methods converge to identical solutions, where no approximations have been made in residual determinations, and comparisons may be made on an equal footing.

The proposed method may be confidently applied in situations where significant strains may develop, such as ultimate load analyses.

CHAPTER 5

COMPARATIVE ANALYSIS OF PRETENSIONED NETWORKS

A general test problem is presented for the comparative analysis of pretensioned networks which enables the ready adjustment of network curvature, pretension, idealisation and loading pattern.

The performance of the dynamic relaxation and scaled conjugate gradient methods are then compared for variations of the above parameters. Comparisons are also made for the problem modified to induce the on-off nonlinearities of cable slackening.

The test problem is also used to examine the relative efficiencies of the automatic mass component assessments proposed for dynamic relaxation in Chapter 3.

5.1 *The Test Problem*

A generalised test problem, which admits simple adjustment of salient parameters without recourse to significant data re-preparation, is best suited to the comparison of analysis methods. Such a problem is proposed here for the comparitive analysis of pretensioned cable networks with rigid boundaries which allows for ready adjustment of network curvature, pretension and idealisation.

The test problem, as shown in figure 5.1, is square in plan with an orthogonal projected network and equal horizontal cable spacing throughout. The fixed boundary nodes lie on the surface of a hyperbolic parabaloid with high (H) and low (L) points as indicated in the figure. Various degrees of network curvature may then be obtained by adjustment of the rise/span ratio (h/d).

By specifying a constant horizontal component of pre-tension throughout the structure, which is assumed to have negligible dead load, the orthogonal plan format of the network is retained at the pretension state. This assumption also has the effect of defining the vertical equilibrium coordinates such that all the nodes lie on the same hypar surface as the boundary points. The vertical coordinate z_i of any node having plan coordinates x_i , y_i is then given by the expression:

$$z_i = \frac{h}{2} + \frac{2h}{d^2}\left\{(y_i - \frac{d}{2})^2 - (x_i - \frac{d}{2})^2\right\} \qquad (5.1)$$

for the dimensions and coordinate system of figure 5.1.

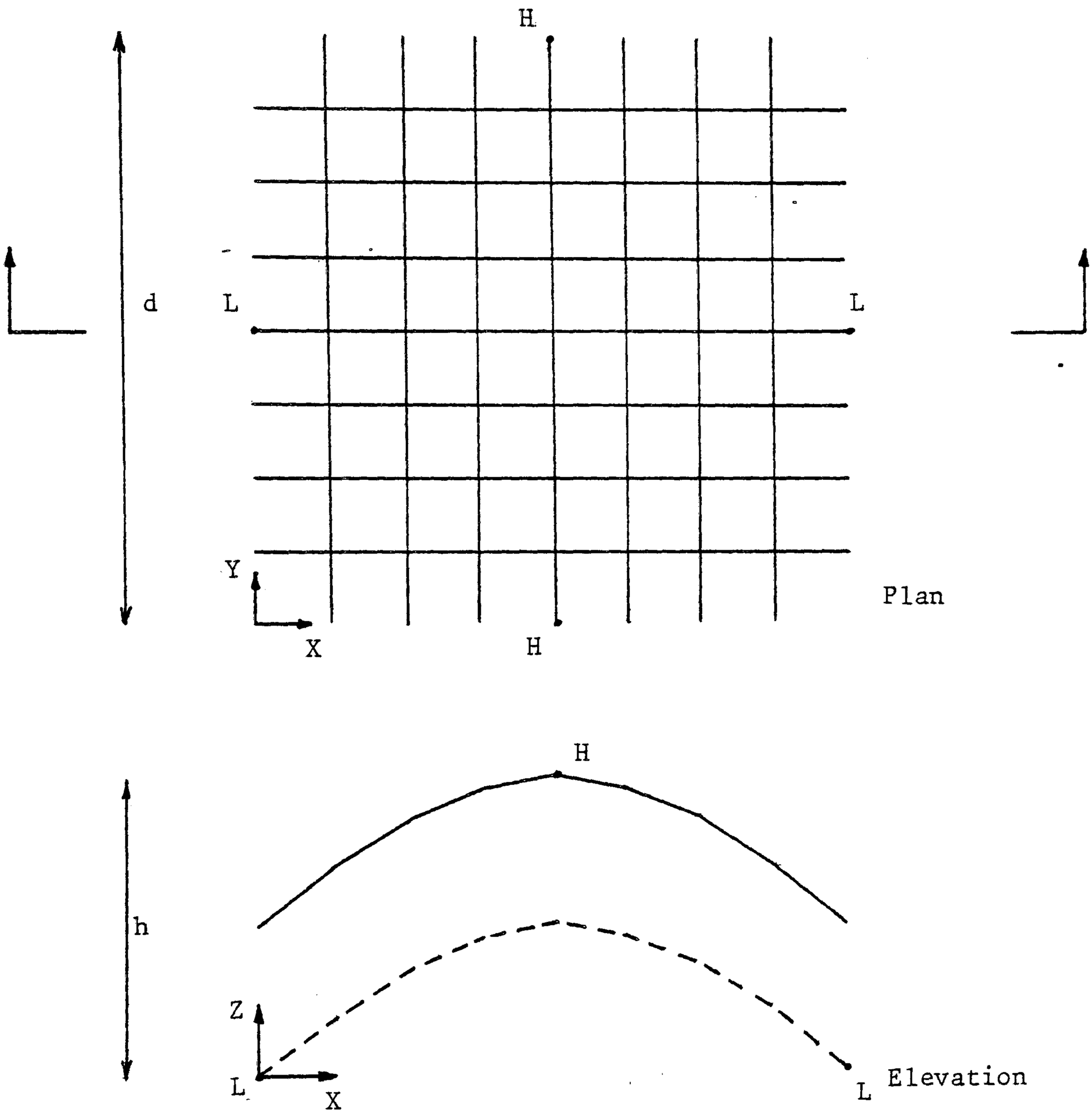

Figure 5.1

Thus no separate formfinding analysis is required for the pretension state, and the regular nature enables fully automatic definition of all nodal coordinates and of the node and element numbering systems and connectivity details. If the number of cables in each direction is a variable for this process, then varying mesh sizes are rapidly obtainable for any specified rise/span ratio.

Although cable lengths vary through the structure, the hypar surface ensures a smooth distribution of cable forces, which are readily established from their geometry and specified horizontal force component.

For the subsequent comparisons, the following dimensions and member properties have been assumed (unless specifically stated otherwise):

Side dimension (d) = 10.0 m

Horizontal pretension component (T_H) = 50 kN/m

Live load (P_L) = 1.5 kN/m^2 plan area.

If the number of cables in each direction is k_c, then the individual cable horizontal pretension component (t_H) is given by:

$$t_H = T_H \times d/(k_c + 1) \qquad (5.2)$$

The cable EA value, constant throughout the structure, is based on the assumption of a strain of .005 for loading equal to the horizontal force component:

$$EA = t_H /.005 \qquad (5.3)$$

Two loading patterns have been specified, one symmetric and the other asymmetric. For the first, (case LF), the vertical live load is applied to all the active nodes of the structure. All these nodal components are equal, having been determined automatically according to the mesh size and specified load per unit plan area. For the second case, (LQ), these same individual loads are applied to all the nodes within one quadrant of the structure as defined by:

$$x_i , y_i \leqslant d/2 \qquad (5.4)$$

Six combinations of loading pattern and rise/span ratio have been investigated in the following sections, and for convenience they have been assigned designatory letters, A to F, as shown in table 5.1.

The smaller h/d ratio is typical of many roofing structure applications, whilst the two larger values have been selected for investigation of the effects of increasing curvature on the performance of the analysis methods.

Similarly three mesh sizes have been selected for investigation. Mesh I is sufficiently fine to provide a basis for comparisons of the effects of load and pretension level, and also of cable slackening. Meshes II and III enable the analysis to be tested on problems having in excess of 1000 and 2500 degrees of freedom respectively. Table 5.2 gives full details of the three chosen idealisations, which have been applied to each of the six load/curvature configurations.

		RISE/SPAN RATIO		
		.1	.5	1.
LOAD PATTERN	LF	A	B	C
	LQ	D	E	F

Table 5.1

IDEALISATION	I	II	III
NO. OF CABLES IN EACH DIRECTION	9	19	29
NO. OF ELEMENTS	220	840	1860
TOTAL NO. OF NODES	117	437	957
NO. OF ACTIVE NODES	81	361	841
NO. OF DEGREES OF FREEDOM	243	1083	2523

Table 5.2

In order to enable a fair comparison to be made both dynamic relaxation and scaled conjugate gradient programs utilised identical data preparation and output segments and were written to perform as efficiently as possible.

For all cases convergence has been defined as that state when the residuals of all active degrees of freedom are less than .1% of the value of the applied nodal live load. For the DR method this criterion has been checked at every energy peak. Rather than recalculate the residuals for the peak coordinates as reset by equation 3.8 , the residuals currently in store, which refer to the configuration at time $\Delta t/2$ after the peak, have been checked. Thus in some cases the convergence times quoted for DR may be slightly conservative.

As the scaled conjugate gradient method has significantly more steps than DR has energy peaks, this full residual check has only been implemented every step once the current Euclidean norm of the residuals is less than .1% of its initial value. These latter values having been obtained as an essential part of the conjugate gradient process.

Thus the time taken by residual checks has been made as close as possible for each method, though tests have shown these times to be negligible in comparison with the overall solution times. Similarly the automatic data preparation segment required only .015 seconds CDC 7600 execution time for the largest mesh used.

5.2 *The Influence of Load and Pretension on Convergence*

Using idealisation I, both dynamic relaxation and scaled conjugate gradient methods have been applied to problem configurations A to F for the following load and pretension values:

load (P_L) - .15, 1.5 and 15. kN/m^2 plan area

pretension component (T_H) - 10., 50. and 100. kN/m

For each of the nine possible combinations of P_L and T_H the cable EA value has been held constant at 10000., the value associated with a strain of .005 for P_L = 1.5 kN/m^2 and T_H = 50. kN/m for this idealisation.

Member slackening has not been permitted, and consequently compressive forces are present in some of the solutions.

The results of the analyses are presented in tables 5.3, 5.4 and 5.5, where, at convergence:

n_c - no. of iterations

k_c - no. of energy peaks (for DR only)

t_c - CDC 7600 execution time (secs.).

The fictitious mass components for the DR analysis are based on the leading diagonal direct stiffness terms, with controlling factors α_m = 2. and β_m = .1, as described in section 3.2.

For dynamic relaxation, referring to the results tables,

RISE/SPAN = .1 : PROBLEMS A(LF) , D(LQ)

METHOD	LOAD		PRETENSION (kN/m)					
	(kN/m^2)		10.		50.		100.	
			n_c (k_c)	t_c	n_c (k_c)	t_c	n_c (k_c)	t_c
DR	LF	.15	105(11)	.918	95(11)	.845	74(11)	.698
		1.5	217(12)	1.713*	91(12)	.829	76(12)	.721
		15.	391(12)	2.931*	75(10)	.695	70(9)	.651
	LQ	.15	229(12)	1.812	105(11)	.922	89(13)	.826
		1.5	229(12)	1.808	105(11)	.924	89(13)	.826
		15.	269(12)	2.092*	177(10)	1.425	131(11)	1.112
SCG	LF	.15	60	1.254	35	.772	31	.694
		1.5	244	4.846*	37	.809	33	.734
		15.	174	3.479*	66	1.380	41	.890
	LQ	.15	110	2.250	54	1.143	46	.988
		1.5	149	3.021	61	1.274	46	.987
		15.	440	8.748*	102	2.087	59	1.244

* - indicates compression members in the solution

Table 5.3

RISE/SPAN = .5 : PROBLEMS B(LF) , E(LQ)

METHOD	LOAD (kn/m²)		PRETENSION (kN/m)					
			10.		50.		100.	
			n_c (k_c)	t_c	n_c (k_c)	t_c	n_c (k_c)	t_c
DR	LF	.15	96(9)	.834	86(10)	.772	63(10)	.611
		1.5	115(10)	.975	86(10)	.777	63(10)	.611
		15.	321(15)	2.468*	91(11)	.817	68(10)	.647
	LQ	.15	414(12)	3.120	184(10)	1.491	114(10)	.989
		1.5	335(11)	2.551	184(10)	1.485	114(10)	.988
		15.	248(13)	1.550*	171(11)	1.407	131(11)	1.121
SCG	LF	.15	70	1.457	53	1.122	36	.788
		1.5	86	1.771	55	1.151	40	.866
		15.	N/C		65	1.354	51	1.083
	LQ	.15	224	4.471	106	2.145	87	1.778
		1.5	285	5.663	114	2.340	87	1.776
		15.	251	5.002*	140	2.808	91	1.855

* - indicates compression members in the solution

N/C - no convergence obtained

Table 5.4

RISE/SPAN = 1. : PROBLEMS C(LF) , F(LQ)

METHOD	LOAD (kN/m^2)		PRETENSION (kN/m)					
			10.		50.		100.	
			n_c (k_c)	t_c	n_c (k_c)	t_c	n_c (k_c)	t_c
DR	LF	.15	134(10)	1.110	67(9)	.629	57(8)	.550
		1.5	134(10)	1.108	83(10)	.752	57(8)	.551
		15.	391(12)	2.931*	75(10)	.695	70(9)	.651
	LQ	.15	363(11)	2.751	171(10)	1.381	116(10)	.991
		1.5	370(11)	2.797	171(10)	1.395	116(10)	.991
		15.	269(12)	2.092*	177(10)	1.425	131(11)	1.107
SCG	LF	.15	62	1.291	45	.967	34	.751
		1.5	70	1.448	46	.983	34	.750
		15.	N/C		51	1.083	38	.831
	LQ	.15	174	3.503	99	2.025	80	1.652
		1.5	199	3.993	101	2.049	80	1.651
		15.	236	4.719*	107	2.179	83	1.710

* - indicates compression members in the solution

N/C - no convergence obtained

Table 5.5

it can be seen that the increase of pretension for any given load has improved convergence in all cases. This improvement is most marked for the more steeply curved networks, where the definition of pretension results in higher individual cable forces, and for the asymmetric loading case. Varying net curvature has little effect on the convergence rate for the symmetric loading pattern, but this is possibly due to the conservative assessment of mass components for the flattest net.

The changes in loading magnitude for a given pretension have not had a significant effect on the dynamic relaxation convergence, but the load range was chosen to lie within realistic values and as such is only limited.

Excepting problems B and C, when half of the members are in compression for P_L = 15. kN/m and T_H = 10. kN/m, the DR solution times have not been adversely effected by the presence of compressive forces.

As with dynamic relaxation, increase of pretension for a given load improves the scaled conjugate gradient solution times. The increase of load from .15 to 1.5 kN/m has little effect, but the further increase to 15. kN/m has reduced the convergence rate in all cases. Increasing nonlinearity appears to progressively reduce the convergence of the SCG method.

The presence of compression members in the solution produces an adverse effect on SCG solution times, this effect becoming more marked as the number of such members increases and

RATIOS OF SOLUTION TIMES (CDC 7600) : t_{DR}/t_{SCG}

PRE-TENSION (kN/m)	LOAD (kN/m^2)	PROBLEM CONFIGURATION					
		A	B	C	D	E	F
10.	.15	.73	.57	.86	.81	.70	.79
	1.5	.35*	.55	.77	.60	.45	.70
	15.	.18*	NS	NS	.15*	.39*	.44
50.	.15	1.09	.69	.65	.81	.70	.68
	1.5	1.02	.68	.76	.73	.63	.68
	15.	.52	.60	.64	.44	.50	.65
100.	.15	1.01	.78	.73	.84	.56	.60
	1.5	.98	.71	.73	.84	.56	.60
	15.	.80	.60	.78	.64	.60	.65

* - solutions include compression members

NS - no solution obtained by conjugate gradients

Table 5.6

the convex nature of the energy surface is subject to increasing disturbance. For the problems B and C, where the DR solution indicated equal numbers of tensile and compressive members, no solution was obtained with the SCG method.

In order to compare the relative efficiencies of DR and SCG, table 5.6 gives the ratios of CDC 7600 execution times (t_{DR}/t_{SCG}) for the above comparisons. Except for three symmetric loading cases on the flattest net, DR has proved faster than SCG throughout. In these three cases SCG is only marginally faster than DR, which has been handicapped by a conservative estimate of fictitious mass components. Automatic assessments of mass components which alleviate this problem were described in Chapter 3, and their application to this test data are detailed in a subsequent section.

5.3 The Influence of Problem Size

In this section the two analysis methods are compared for problems with increasing numbers of degrees of freedom and elements. The three idealisations detailed in table 5.2 are applied to the six configurations of the standard problem as defined in section 5.1.

The numbers of iterations and computing times for convergence are given in table 5.7, and table 5.8 shows their

METHOD	PROBLEM CONFIG'N	IDEALISATION					
		I		II		III	
		n_c (k_c)	t_c	n_c (k_c)	t_c	n_c (k_c)	t_c
DR	A	91(12)	.829	166(11)	5.047	273(13)	17.550
	B	86(10)	.777	178(12)	5.483	264(12)	17.224
	C	83(10)	.752	179(13)	5.444	220(12)	14.331
	D	105(11)	.924	216(13)	6.529	312(14)	20.183
	E	184(10)	1.485	385(13)	10.938	600(14)	36.811
	F	171(10)	1.395	367(13)	10.606	556(14)	34.723
SCG	A	37	.809	84	6.473	137	22.886
	B	55	1.151	144	10.805	227	37.198
	C	46	.983	124	9.438	198	32.854
	D	61	1.274	137	10.315	215	35.322
	E	114	2.340	249	18.748	378	62.468
	F	101	2.049	235	17.456	363	59.169
DEGREES OF FREEDOM		243		1083		2523	
CABLE ELEMENTS		220		840		1860	

Table 5.7

RATIOS OF SOLUTION TIMES : t_{DR}/t_{SCG}

MESH SIZE	PROBLEM CONFIGURATION					
	A	B	C	D	E	F
I	1.02	.68	.76	.73	.63	.68
II	.78	.51	.58	.63	.58	.61
III	.77	.46	.44	.57	.59	.59

Table 5.8

n_{sd}	PROBLEM					
	IID		IIE		IIF	
	n_c	t_c	n_c	t_c	n_c	t_c
25	213	15.946	851	62.743	779	57.448
50	156	11.754	530	39.205	452	33.464
100	138	10.434	342	25.410	338	25.108
∞	137	10.315	249	18.748	235	17.456

Table 5.9

associated ratios of solution times (t_{DR}/t_{SCG}).

The solution times for DR and SCG are effectively equal for problem IA, but DR shows to advantage for the more refined meshes of IIA and IIIA. Estimation of DR mass components on the row sum basis (with $\alpha_m = 1.$ and $\beta_m = .1$) produces time ratios of .76, .75 and .67 for problems IA, IIA and IIIA respectively.

Overall the relative efficiency of dynamic relaxation compared to scaled conjugate gradient analysis is increased as the number of variables in the problem increases. For flat networks DR solution times are between .6 and .7 of those for SCG, whilst the ratio lies between .45 and .6 for the more curved configurations. Both methods can, however, be seen to be capable of efficient analysis of large problems.

In order to try and improve SCG convergence, the effect of restarting from the steepest descent direction every n_{sd} steps was investigated. No improvement in the convergence rate was obtained for a variety of values of n_{sd}. For example, table 5.9 shows the effect on the analysis of problems IID, IIE and IIF.

This procedure is only theoretically recommended (69) for $n_{sd} = f + 1$, where f is the number of degrees of freedom, when the equivalent system matrix remains constant. In this case the change in the nonlinear system matrix for a pretensioned network will all members remaining in tension is not significant enough to warrant a more frequent return to the steepest descent direction.

5.4 *Analysis in the Presence of Cable Slackening*

Although in earlier designs for prestressed networks pretension values were usually sufficiently high to preclude cable slackening under working loads, recent trends favour more lightly prestressed nets with a consequent reduction in foundation costs. In these cases cable slackening may occur in practice under normal loading conditions, and will almost certainly happen in special circumstances such as ultimate load or construction stage analysis. In the latter case particularly the form and mode of action of the structure may change significantly as cables become slack and retensioned. Any analysis method used for tension structures should be able to cope with this type of situation.

To investigate the ability of dynamic relaxation and scaled conjugate gradients to cope with cable slackening, the general problem of this chapter has been subjected to increased loading and reduced pretension. Rather than provide realistic load and pretension levels, the aim here is to simulate cable slackening situations. For symmetric loading on the hypar structure the effect is to reduce tension in the 'tensioning' cables, whilst the 'hanging' cables carry the load. This pattern is less regular for the asymmetric loading case.

For both DR and SCG, cable tensions are checked within every iteration and reset to zero if found to be negative, this procedure being simpler than modifications to the member elastic

DYNAMIC RELAXATION			
T_H	n_c (k_c)	t_c	NO. OF SLACK CABLES
.01	174(13)	1.437	86
1.	202(15)	1.654	46
10.	145(16)	1.259	18

Table 5.10

SCALED CONJUGATE GRADIENTS						
n_{sd}	T_H = .01		T_H = 1.		T_H = 10.	
	n_c	t_c	n_c	t_c	n_c	t_c
1	267	5.364	403	8.072	368	7.381
5	184	3.737	254	5.145	128	2.629
10	305	6.162	286	5.779	142	2.192
25	216	4.373	252	5.090	153	3.116
50	206	4.176	173	3.513	184	3.735
100	215	4.337	218	4.397	218	4.404
∞	266	5.359	615	12.317	1216	24.253

Table 5.11

properties. For SCG the contribution of slack members to the steplength polynomial coefficients is also zero. As there are significant changes in the equivalent stiffness matrix when cables go slack, frequent recourse to the steepest descent direction is investigated as a means of improving, or ensuring, convergence of the scaled conjugate gradient method. This function is fulfilled automatically at the energy peak stages of the dynamic relaxation process with kinetic damping.

Consider, then, problem idealisation I with a rise/span ratio of .5, EA = 10000., and an initially symmetric load of 30 kN/m . Analysis of this problem was carried out for three levels of pretension. The results for the DR analyses, with mass components based on leading diagonal direct stiffnesses (α_m = 2., β_m = .1), are shown in table 5.10, which also indicates the number of slack elements detected.

The results of the SCG analyses, with reinitialisation in the steepest descent direction every n_{sd} steps, are given in table 5.11. Clearly there is an advantage to be gained by this reinitialisation, but, as this example shows, selection of the optimum reset frequency could prove difficult. However, in spite of this improvement, dynamic relaxation is at least twice as rapid as the optimum conjugate gradient solution for these examples.

The above analysis was repeated for the asymmetric load pattern, in which case only five cable members were found to go slack for a horizontal component of pretension of .01 kN/m. The results for both DR and SCG for this case are presented in table 5.12.

METHOD	n	n (k)	t
SCG	5	963	19.241
	10	679	13.578
	25	363	7.297
	50	319	6.428
	100	305	6.146
	250	390	7.839
	500	573	11.463
	∞	1099	21.922
DR	-	237(15)	1.905

Table 5.12

Here dynamic relaxation is more than three times faster than the best conjugate gradient solution, which is perhaps surprising in view of the small number of slack members.

The mass control factor $\alpha_m = 2.$ has proved satisfactory for the above DR analsyes in the presence of cable slackening. Investigations of structures undergoing more serious changes in their mode of action because of slackening have indicated that the time interval may require further reduction in order to obtain a solution. This effective reduction in 'steplength' ensures better control of the descent of a severely distorted energy surface.

When kinetic damping is employed it is possible to envisage a situation arising wherein the form alternates between two different, but not yet fully converged, states at consecutive energy peaks. A further reduction in time interval may be needed to escape this situation, or alternatively viscous over-damping might be introduced to provide an alternative path to a particular solution.

5.5 Nodal Mass Components for Dynamic Relaxation

For the test problem results presented in this chapter the direct stiffnesses for both DR mass optimisation and the scaling terms for the conjugate gradient method have been

established from the cable element tangent stiffness relations in the initial, pretension, state:

$$\left[K_T\right] = \frac{EA - T^\circ}{L^\circ}\begin{bmatrix} \ell^2 & \ell m & \ell n \\ m\ell & m^2 & mn \\ n\ell & nm & n^2 \end{bmatrix} + \frac{T}{L}\begin{bmatrix} 1 & 0 & 0 \\ 0 & 1 & 0 \\ 0 & 0 & 1 \end{bmatrix} \quad (5.5)$$

The stability of the numerical integration for a DR diagonal mass system based on leading diagonal direct stiffnesses subject to varying values of α_m (as defined in chapter 3) is illustrated in table 5.13. Considering mesh I only, stability is assured for all six load/structure configurations when $\alpha_m = 2$. On reduction of α_m to 1.5, and subsequently to 1.2, however, only the calculations for the flattest net (cases A and D) remain stable. In this case the principal direct stiffness axes are still sufficiently close to the global integration axes for continued numerical stability, but this is no longer the case for the more sharply curved arrangements.

The three approaches to the fictitious mass component calculation outlined in section 3.2 , namely:

(i) diagonal masses and leading diagonal direct stiffness

(ii) diagonal masses and nodal direct stiffness row sum

(iii) square nodal mass matrix and nodal direct stiffness matrix (3x3),

DYNAMIC RELAXATION ANALYSIS : IDEALISATION I		
LEADING DIAGONAL STIFFNESS MASS ESTIMATION		
	α_m=2. β_m=.1	α_m=1.5 β_m=.1	α_m=1.2 β_m=.1
	n_c (k_c)	n_c (k_c)	n_c (k_c)
A	91(12)	72(11)	80(11)
B	86(10)	NI	NI
C	83(10)	NI	NI
D	105(11)	90(12)	86(11)
E	184(10)	NI	NI
F	171(10)	NI	NI

NI - numerical instability

Table 5.13

have been applied to the six load/configuration combinations for each of the three problem idealisations. The number of iterations (n_c), energy peaks (k_c) and CDC 7600 execution seconds (t_c) to convergence are drawn in table 5.14.

As expected, the number of iterations to solution is least throughout when the block operations of the square nodal mass matrices are employed. Considering the diagonal mass matrices, the row sum approach is generally more efficient that the leading diagonal method for the flatter net and both loading conditions. For the more curved nets, the leading diagonal method is more efficient for symmetric loading, whilst the row sum method is more efficient for the asymmetric case. The extra computation required initially for the row sum approach is not significant when compared with that of the other diagonal mass method.

From table 5.14 it can be seen that the block operation technique frequently has the shortest computer time to solution, and is in no case the slowest of the three methods employed. The reduction in the number of iteration steps has been sufficient to offset the additional calculations, both initial and at each iteration. In this instance the required inversion of the (3x3) nodal mass matrices was performed directly by Choleski's method (142).

IDEALISATION	PROBLEM CONFIGURATION	DYNAMIC RELAXATION CONTROL : DIRECT STIFFNESS ESTIMATION FOR MASSES					
		LEADING DIAGONAL		ROW SUM DIAGONAL		BLOCK OPERATIONS	
		$\alpha_m = 2.$	$\beta_m = .1$	$\alpha_m = 1.$	$\beta_m = .1$	$\alpha_m = 1.1$	$\beta_m = .1$
		n_c (k_c)	t_c	n_c (k_c)	t_c	n_c (k_c)	t_c
I	A	91(12)	.829	66(8)	.621	32(11)	.628
	B	86(10)	.777	91(10)	.827	43(11)	.747
	C	83(10)	.752	84(9)	.757	43(11)	.752
	D	105(11)	.924	85(10)	.789	54(12)	.885
	E	184(10)	1.485	176(11)	1.432	92(12)	1.305
	F	171(10)	1.395	146(9)	1.214	88(12)	1.265
II	A	166(11)	5.047	156(12)	4.834	66(14)	3.895
	B	178(12)	5.483	193(13)	5.941	89(13)	4.774
	C	179(13)	5.444	165(12)	5.073	95(13)	5.058
	D	216(13)	6.529	194(13)	5.992	104(14)	5.439
	E	385(13)	10.938	344(13)	9.960	174(14)	8.349
	F	367(13)	10.606	345(12)	10.028	190(14)	9.046
III	A	273(13)	17.550	235(12)	15.285	107(14)	12.235
	B	264(12)	17.224	271(12)	17.662	119(14)	13.338
	C	220(12)	14.331	229(11)	14.853	132(14)	14.636
	D	312(14)	20.183	316(14)	20.579	141(14)	15.308
	E	600(14)	36.811	491(13)	30.569	302(15)	30.143
	F	554(14)	34.723	515(13)	32.346	300(15)	30.065

Table 5.14

5.6 *Summary*

A generalised test problem for the comparitive analysis of pretensioned networks with rigid boundaries has been proposed which permits ready adjustment of network curvature, pretension and idealisation. This problem has then been analysed by the scaled conjugate gradient method, with modified polynomial coefficients as presented in the last chapter, and by dynamic relaxation with kinetic damping.

Dynamic relaxation has been found to converge more quickly than scaled conjugate gradients for this problem with a range of network curvatures, pretension levels and loading cases. Both methods have been applied to increasingly large meshes, with up to 2523 degrees of freedom and 1860 elements. Dynamic relaxation has required between .4 and .8 of the time for SCG convergence, with an advantage increasing with problem size.

By a reduction in pretension and increase in applied load, the test problem has been used to compare the relative merits of DR and SCG in the presence of cable slackening. The SCG analysis was performed with occasional recourse to the steepest descent direction. The optimum steepest descent reset frequency is difficult to locate automatically, and even for that situation DR converged at least twice as quickly for the symmetric load patterns and over three times faster for the asymmetric case.

The three methods of automatic assessment of nodal fictitious mass components for dynamic relaxation, as outlined in

chapter 3, have been compared. In terms of time to convergence, the block operations involving square nodal mass matrices have proved most efficient. In practice, however, this advantage must be offset against the storage requirements of the additional mass components and the need for explicit retention of the square nodal $[B]$ matrices. The complexity of the program has been marginally increased, although the generality of application to arbitrary element types is not restricted. In general, then, a diagonal mass matrix scheme will probably be adopted, with the row sum variant of equation offering the most rational mass assessment for varied structural configurations.

CHAPTER 6

DYNAMIC RELAXATION NON-LINEAR ANALYSIS OF RIGID-JOINTED STRUCTURES

Prior to the investigation of complete lightweight structures, the method to be employed should be shown capable of the nonlinear analysis of the boundary structure to the same degree of accuracy as for the surface structure.

In this chapter rotational degrees of freedom are introduced into the dynamic relaxation analysis scheme to permit the inclusion of planar and spatial flexural elements. Finite displacements are treated directly, with full nonlinear effects readily incorporated into the natural stiffness relations of the members. A simplified flexural element is also proposed for planar problems, and the elements presented are applied to the analysis of published nonlinear frame analysis problems.

6.1 *Plane Frame Analysis by Dynamic Relaxation*

Rotational degrees of freedom must be introduced into the DR iterative scheme to enable the inclusion of cubic displacement line bending elements. This presents no difficulties, and the assessment of diagonal or square nodal ficititious mass matrices follows the general sequence outlined in chapter 3. However, whereas the current nodal translations are traced as the current global coordinates, $\{x\}$, the rotations $\{\theta\}$ are conveniently treated as displacements from an initially zero state at the start of the analysis. This section presents the implementation of planar flexural elements, following the general sequence proposed in chapter 3.

The bending element, with connecting nodes i and j, is shown in figure 6.1 with its associated basic displacements α_i, α_j and $\varepsilon = e/L_o$. Figure 6.2 shows the related natural forces acting on the element, with $\{\grave{S}\}$ translational and $\{\grave{M}\}$ rotational components, where:

$$\{\grave{M}\} = \begin{Bmatrix} \grave{M}_{ij} \\ \grave{M}_{ji} \end{Bmatrix} \qquad \{\grave{S}_i\} = \begin{Bmatrix} \grave{S}_i^x \\ \grave{S}_i^z \end{Bmatrix} \tag{6.1}$$

and, for equilibrium:

$$\{\grave{S}_i\} = -\{\grave{S}_j\} = \{\grave{S}\} \tag{6.2}$$

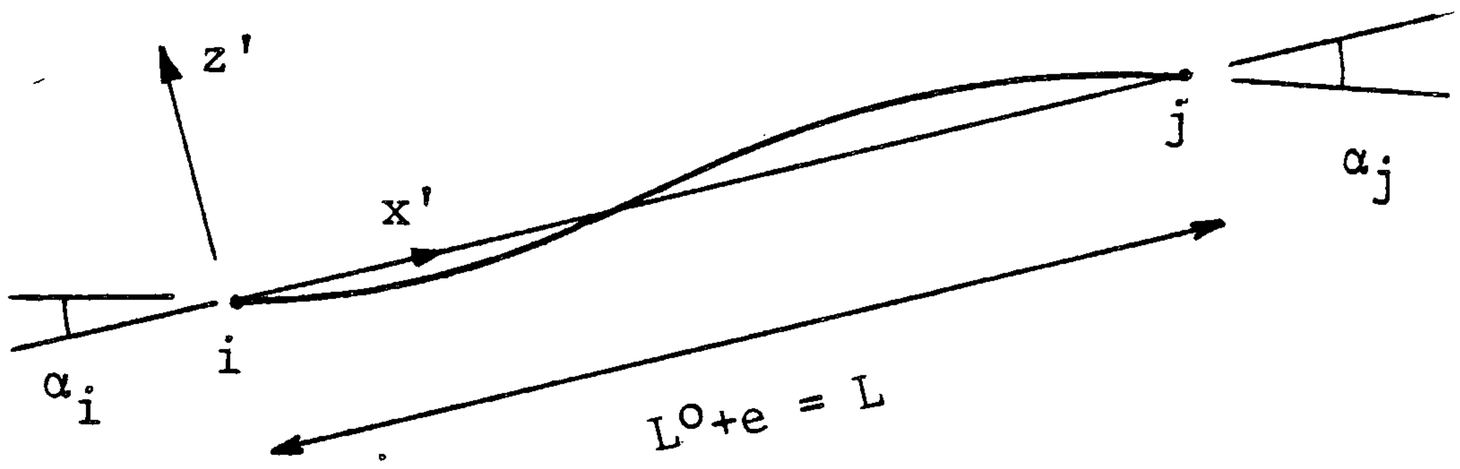

Figure 6.1

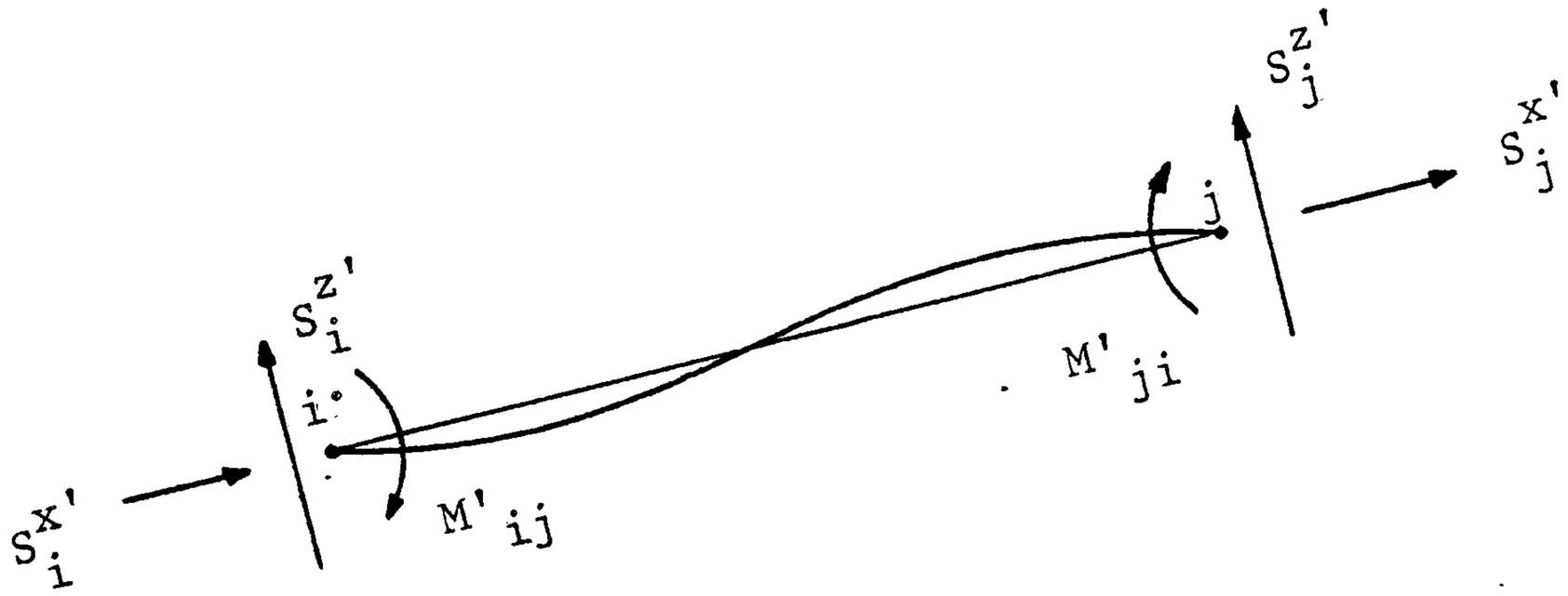

Figure 6.2

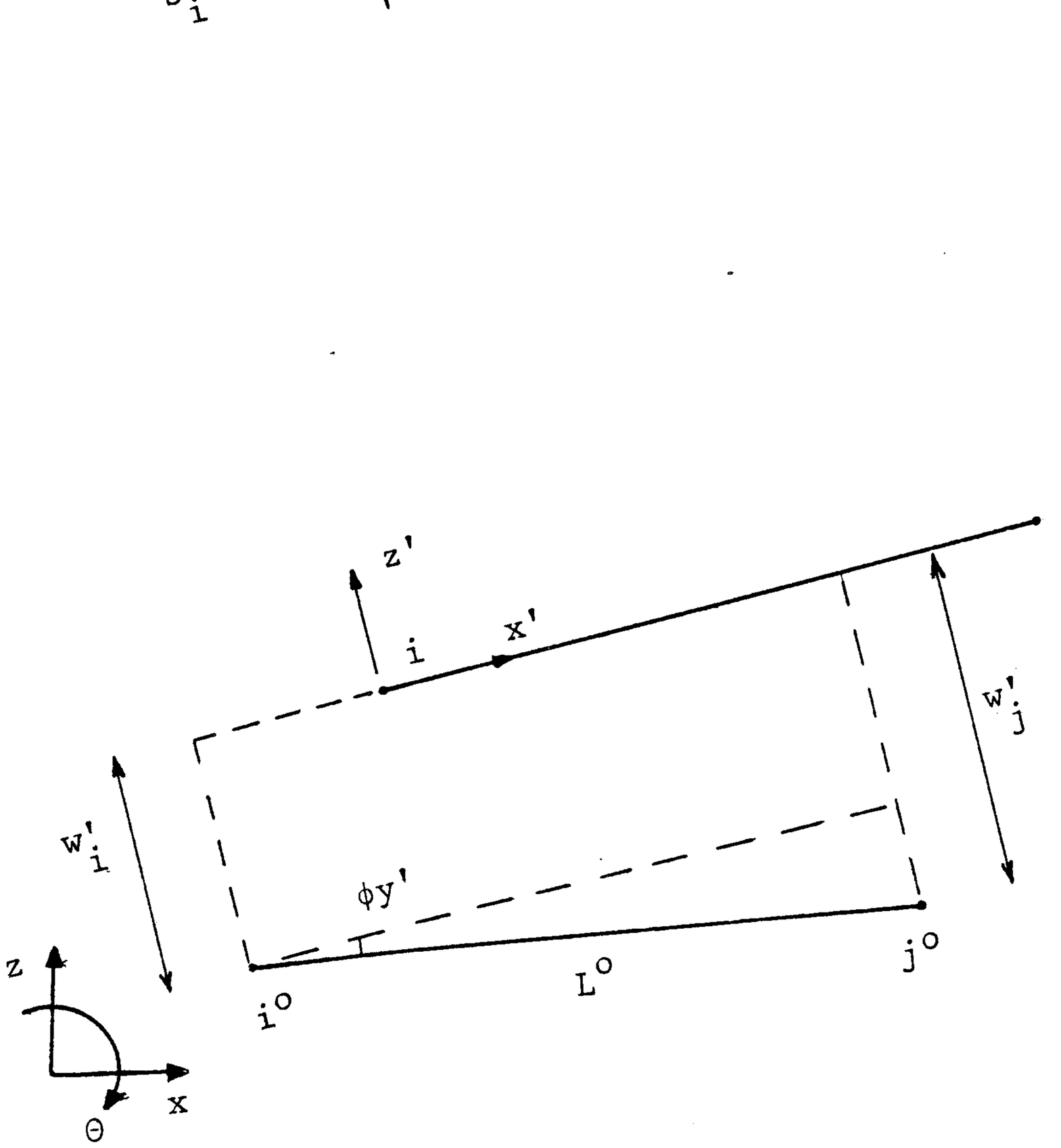

Figure 6.3

For linear moment curvature relations the member constitutive equations are then:

$$\begin{Bmatrix} M'_{ij} \\ M'_{ji} \end{Bmatrix} = \frac{EI}{L} \begin{bmatrix} 4 & 2 \\ 2 & 4 \end{bmatrix} \begin{Bmatrix} \alpha_i \\ \alpha_j \end{Bmatrix} \tag{6.3}$$

where $\{\alpha\}$ refers to the difference between member current and initial end slopes, and

$$S^{x'} = - \frac{EA}{L^o} \cdot e$$

$$S^{z'} = - (M'_{ij} + M'_{ji})/L \tag{6.4}$$

The transformation between current local coordinates $\{x'\}$, and global coordinates $\{x\}$ is given by:

$$\{x'\} = [\lambda]\{x\} = \begin{bmatrix} \ell & n \\ -n & \ell \end{bmatrix} \{x\} \tag{6.5}$$

where ℓ, n are the current x, z direction cosines respectively of the member ij.

The sway angle $\phi^{s'}$, shown in figure 6.3, must then be determined in order to allow for arbitrary member displacement in space when calculating the relative rotational displacements $\{\alpha\}$ from the overall nodal rotations θ_i and θ_j. The relative end displacement, $\delta w'$, in the z' direction is given by:

$$\delta w' = w'_j - w'_i = \begin{bmatrix} \ell & n \end{bmatrix} \begin{Bmatrix} x_{ij} - x^o_{ij} \\ z_{ij} - z^o_{ij} \end{Bmatrix} \tag{6.6}$$

where $\left\{x_{ij}\right\} = \left\{x_j - x_i\right\}$, etc., and it is necessary to retain the initial member position vector $\left\{x^o_{ij}\right\}$. The sway angle is then:

$$\phi^{\backprime} = \sin^{-1}\left[-\frac{\delta w^{\backprime}}{L^o}\right] \tag{6.7}$$

for a clockwise positive angle as shown.

The current relative rotations are then:

$$\alpha_i = \theta_i - \phi^{\backprime}\ ,\quad \alpha_j = \theta_j - \phi^{\backprime} \tag{6.8}$$

The member natural forces must then be summed into the nodal residual vector, taking account of the necessary change of sign. The moments $\left\{M^{\backprime}\right\}$ are subracted directly from the current rotational residuals at the connecting nodes, whilst the direct forces must first be transformed into the global coordinate system:

$$\left\{S\right\} = \left[\lambda\right]^T\left\{S^{\backprime}\right\} \tag{6.9}$$

The dynamic relaxation scheme treats finite nodal displacements automatically, and other nonlinear effects may readily be included. The stability functions s and c (114) may be directly included in equation 6.3 to account for the effect of axial force on the moment-curvature relations:

$$\begin{Bmatrix} M^{\backprime}_{ij} \\ M^{\backprime}_{ji} \end{Bmatrix} = \frac{EI}{L}\begin{bmatrix} s & sc \\ sc & s \end{bmatrix}\begin{Bmatrix} \alpha_i \\ \alpha_j \end{Bmatrix} \tag{6.10}$$

When kinetic damping is employed, it is convenient to reset the stability functions at the energy peak coordinate adjustment stage. This is efficiently achieved by utilising Livesley's power series (114):

$$s = 3\phi_2 + \phi_1$$

$$sc = 3\phi_2 - \phi_1$$

where:

$$\phi_1 = \frac{(64 - 60\rho + 5\rho^2)}{(16-\rho)(4-\rho)} - \sum_{n=1}^{n=7} \frac{a_n \rho^n}{2^{3n}}$$

$$\phi = \frac{\Pi^2 \rho}{12(1-\phi_1)}$$

ρ = P/P_E, the ratio of current and Euler compressive forces

and:

$a_1 = 1.57973627$ $\quad$ $a_2 = 0.15858587$

$a_3 = 0.02748899$ $\quad$ $a_4 = 0.00547540$

$a_5 = 0.00115281$ $\quad$ $a_6 = 0.00024908$

$a_7 = 0.00005452$

Alternatively, the nonlinear natural stiffness relations derived by Jennings (95) might be used. By assuming that the lateral deflection curve is cubic, these relations account for the nonlinearities due to axial force and to axial shortening through bowing. In this case the axial force is given by:

$$P = EA\left[\frac{e}{L^{o}} + \frac{1}{30}\left\{2\alpha_i^2 - \alpha_i\alpha_j + 2\alpha_j^2\right\}\right] \qquad (6.11)$$

and the nonlinear constitutive equation is:

$$\begin{Bmatrix} \dot{M}_i \\ \dot{M}_j \end{Bmatrix} = \begin{bmatrix} (4q + 4r) & (2q - r) \\ (2q - r) & (4q + 4r) \end{bmatrix} \begin{Bmatrix} \alpha_i \\ \alpha_j \end{Bmatrix}$$

where $q = \frac{EI}{L^{o}}$ and $r = \frac{PL^{o}}{30}$. Again it is convenient to reset the natural stiffness relations at energy peaks. Clearly the nature of dynamic relaxation enables simple inclusion of nonlinear effects into the analysis scheme.

On-off nonlinearities, such as the formation of plastic hinges might also be included. In this case, when the plastic moment is exceeded at the end of a member, a plastic hinge is imposed at that point and the member end moment held equal to the plastic moment as long as the hinge continues to rotate in the same direction. Elastic behaviour is restored if the sense of rotation is subsequently reversed, with some consequent permanent deformation of the member at the hinge position. In such an incrementally loaded, path dependent, process the use of crictical viscous damping might prove superior to that of kinetic damping. For the latter, plasticity checks should be made at each step to ensure stability. The smoother displacement pattern of viscous damping should permit less frequent plasticity checks and a better control on the solution.

The desired boundary conditions associated with beam elements must also be incorporated. Encastré joints are implemented by holding the nodal rotational displacement to zero throughout the analysis. For a pinned connection at a member end, the natural stiffness relations may be summarised:

$$\begin{Bmatrix} \grave{M}_i \\ \grave{M}_j \end{Bmatrix} = \begin{bmatrix} a & b \\ b & a \end{bmatrix} \begin{Bmatrix} \alpha_i \\ \alpha_j \end{Bmatrix}$$

where, for $\grave{M}_i = 0$, $\alpha_i = -\frac{b}{a}\alpha_j$,

and for $\grave{M}_j = 0$, $\alpha_j = -\frac{b}{a}\alpha_i$, (6.13)

and the ratio b/a must be updated every reset stage when nonlinear stiffness relations have been employed.

6.2 A Simplified Planar Bending Element

The separation of equilibrium and compatibility in dynamic relaxation makes it particularly suitable for the incorporation of a simplified bending element. The flexural member is idealised as a series of bar elements, which are permitted to deform axially but not in bending. The flexural stiffness is lumped at the nodes connecting these bar elements, and the associated rotation is established from the relative inclination of the adjacent elements. In this way only translational displacement variables are required, and the discretisation of the

flexural member ensures that both stability and bowing effects are automatically accounted for. Figure 6.4 shows a single bar element and the forces acting upon it, whilst two adjacent elements are shown in figure 6.5 together with the lumped rotation $\delta\phi_j$ at their interconnecting node j. This angle is shown greatly exaggerated, and in the subsequent derivation is assumed to be the difference between current and initial rotations.

This element was initially applied in finite difference form for the large displacement transient response analysis of beams and rings subject to impact loading (140, 172) by central difference time integration. By idealising a section as a layered series of such elements, plasticity effects have also been included (82, 176).

If the normals to the element mid-points are constructed as in figure 6.5, then for the small angle $\delta\phi_j$:

$$R_j \cdot \delta\phi_j = (L_a + L_b)/2 \qquad (6.14)$$

Then, if it is assumed that R_j is the mean radius of curvature of deformation of the flexural member at node j, the bending moment, M_j, at that point may be expressed:

$$M_j = EI \cdot \frac{1}{R_j} = EI \cdot \frac{2\delta\phi_j}{(L_a + L_b)} \qquad (6.15)$$

For M_j taken as a positive hogging moment, with $\delta\phi_j$ positive as shown, then:

$$\grave{M}_{ji} = M_j = -\grave{M}_{jk} \qquad (6.16)$$

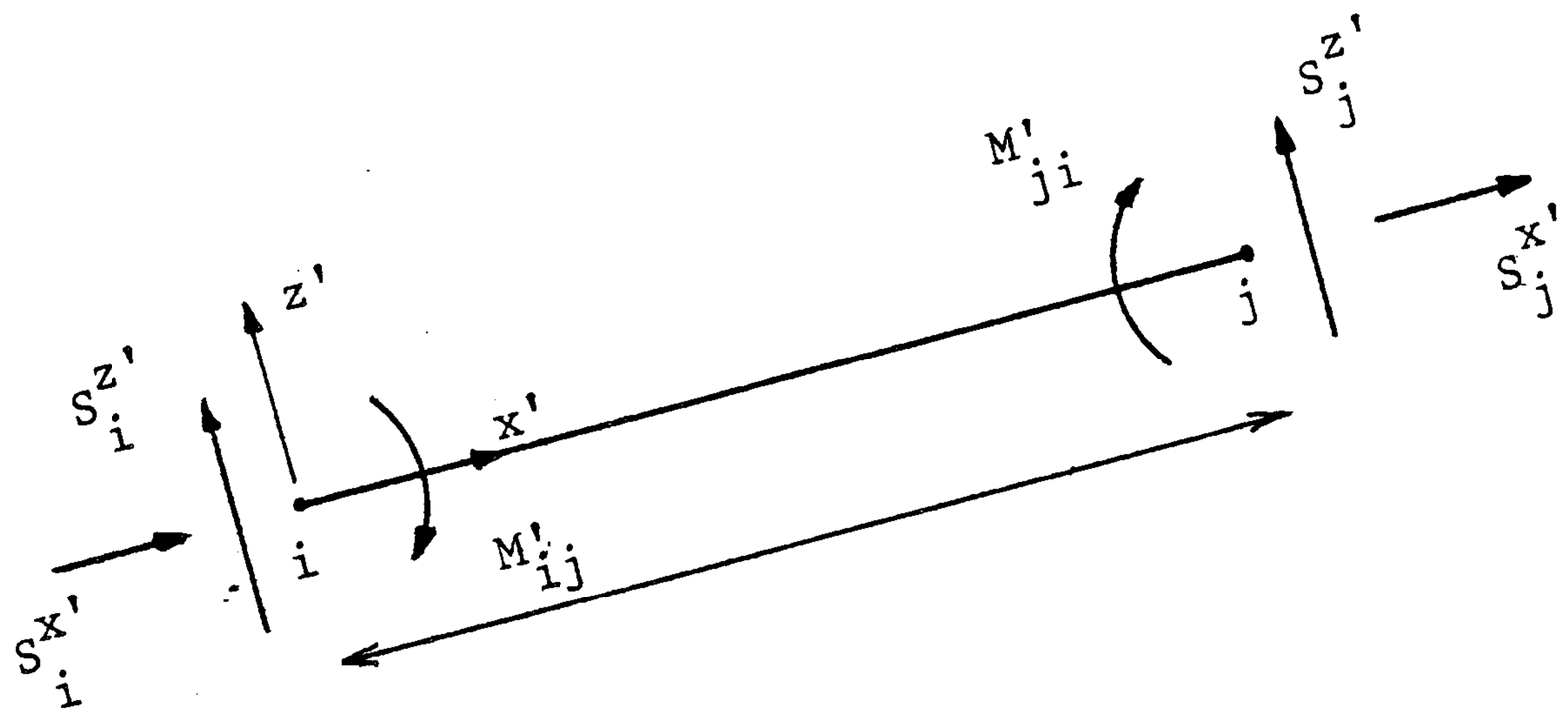

Figure 6.4

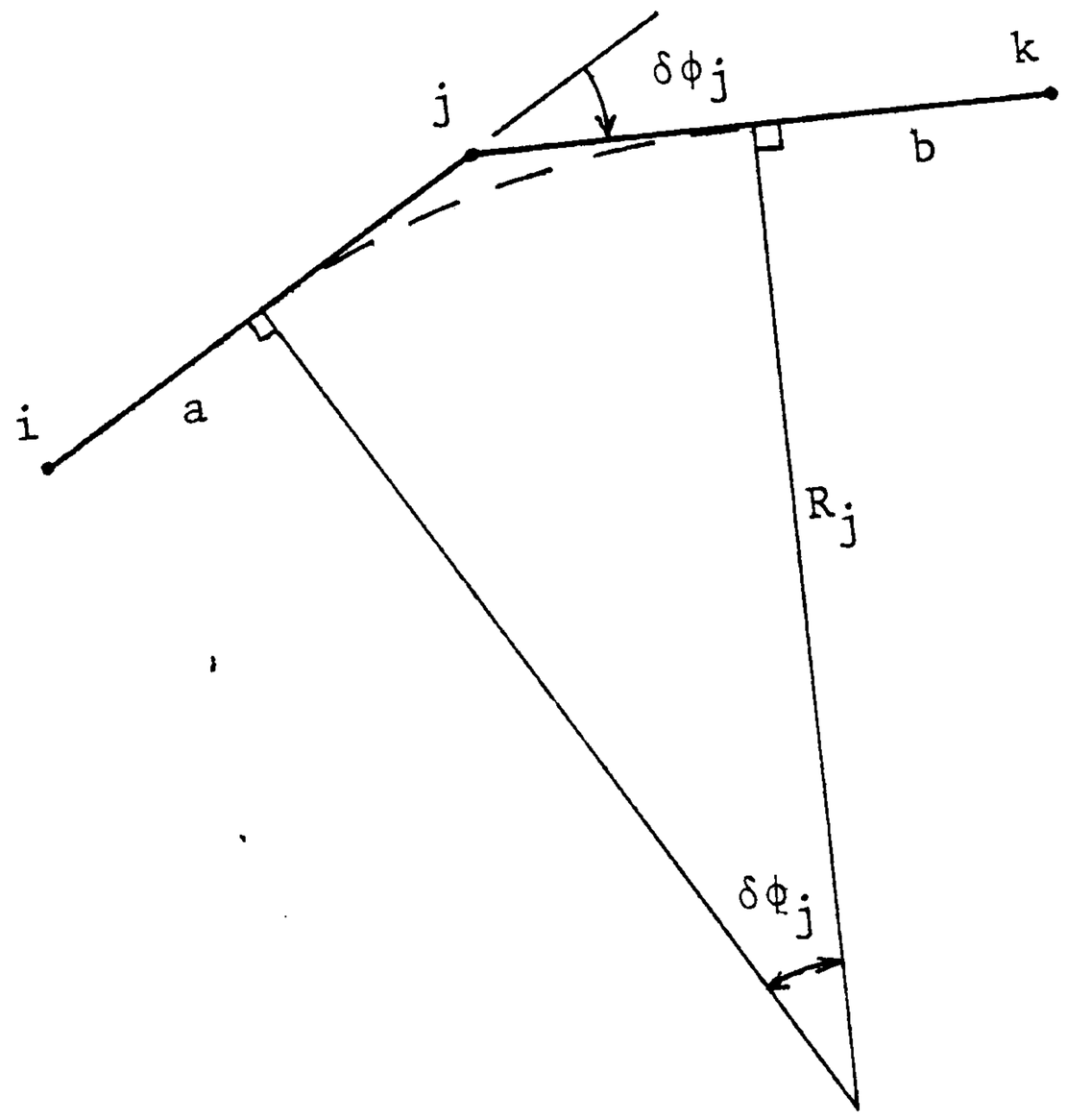

Figure 6.5

The bending action has been effectively idealised as a series of constant moments between element mid-points. Axial and transverse forces must then also be obtained, the former from the elastic extension and the latter by resolution of the bending equilibrium of the element:

$$S_i^{\grave{e}} = (M_{ij}^{\grave{}} + M_{ji}^{\grave{}})/(L^{\circ} + e) \qquad (6.17)$$

The direct and transverse forces acting on the element are then resolved into the global coordinate system and added into the nodal residuals as usual. A full bending analysis has thus been obtained in terms of translational degrees of freedom only, as $\delta\phi_j$ is found directly from the element vectors.

Before a solution is obtained, however, the boundary conditions to the problem must be imposed. Both pinned footings and free ends may be treated by holding the relevant nodal rotations at zero, with the consequent imposition of zero bending moment at those nodes. For an encastré footing the tangent to the flexural member at the fixed point remains constant, as shown in figure 6.6 Considering, then, the fictitious adjacent element shown that enables satisfaction of this condition, it can be seen that the total rotation at the node e is $2\delta\phi_e$, thus:

$$\frac{1}{R_e} = \frac{2.\delta\phi e}{L_a} \quad , \quad M_e = EI \cdot \frac{2\delta\phi e}{L_a} \qquad (6.18)$$

For such cases the initial inclination of the member must be stored in order to obtain $\delta\phi_e$.

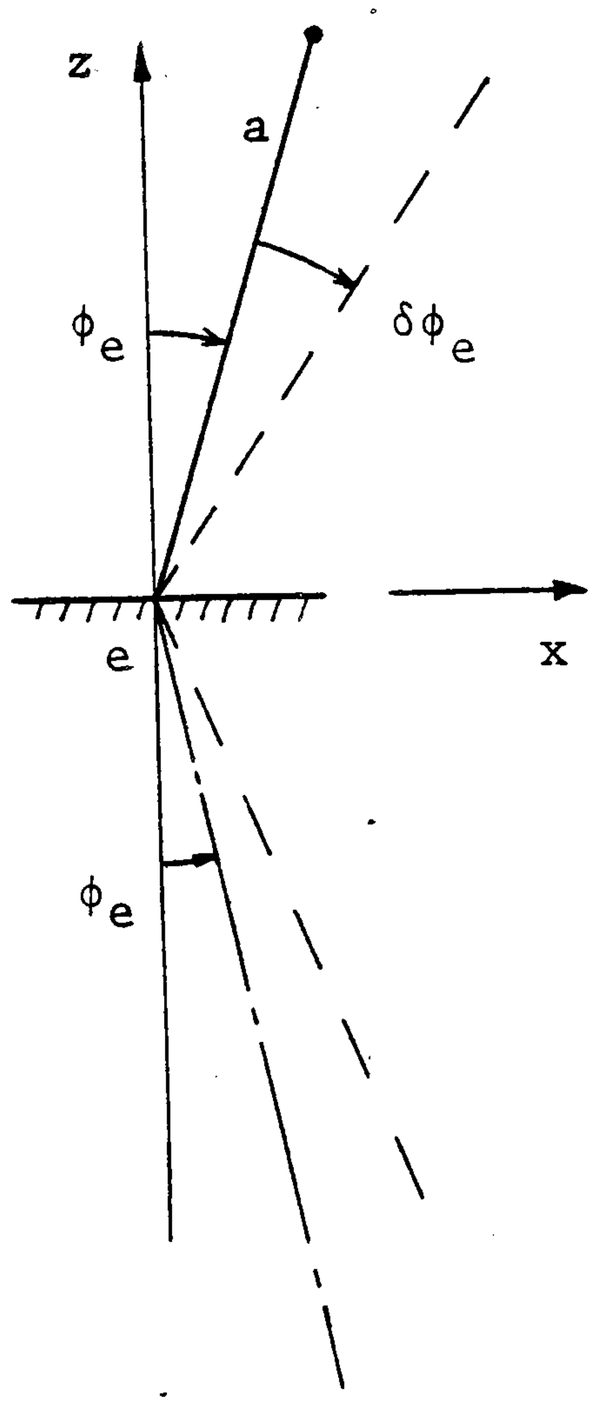

Figure 6.6

For the nonlinear impact analysis of plane frames, Ni (129) has also used the above formulation with two degrees of freedom at each node, except at framework joints where a rotational degree of freedom was additionally introduced. These joints were then regarded as moving boundaries during the dynamic deformation process of the structural members.

This introduction of an extra degree of freedom at the joints is not necessary, however, and an alternative is presented here for incorporation in a dynamic relaxation scheme. Consider a joint J connected to a number of elements with initial inclinations ϕ^{i} to the z-axis, as shown in figure 6.7. The joint is assumed to remain rigid at all stages of the analysis. The current end moments are initially calculated assuming fixity against rotation at J (figure 6.8); for example:

$$\delta\phi_\alpha = \phi_\alpha - \phi_\alpha^i \text{ and (using 6.18) } M_\alpha = -2\frac{EI}{L_\alpha}\delta\phi_\alpha \qquad (6.19)$$

where both moment and rotation are clockwise positive.

Then the current clockwise out of balance moment at joint J is given by:

$$\Delta M_J = -2\sum \frac{EI}{L}\delta\phi \qquad (6.20)$$

with summation for all the connected members. If δM_J is defined as the out of balance moment due to a unit rotation of the joint:

$$\delta M_J = -2\sum \frac{EI}{L} \qquad (6.21)$$

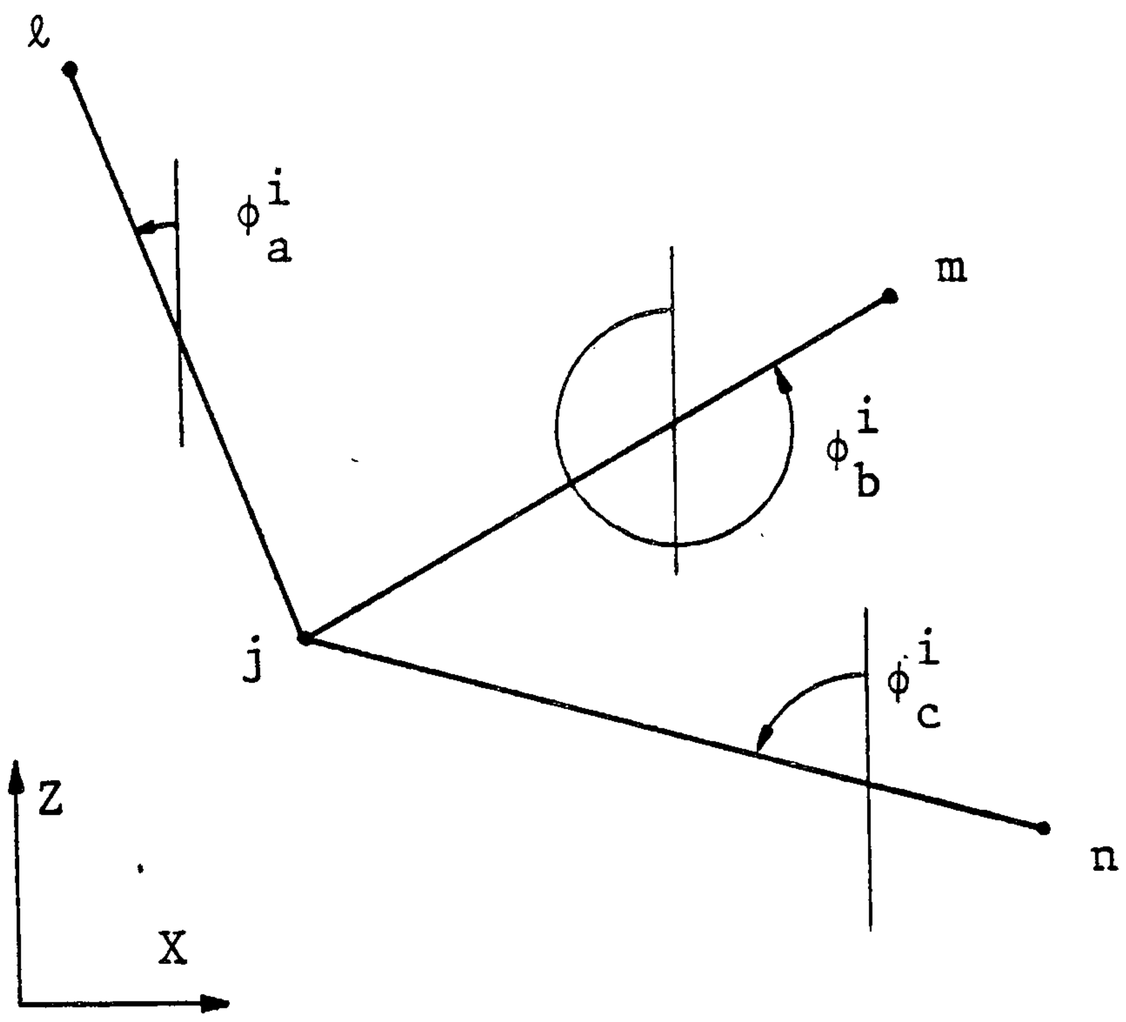

Figure 6.7

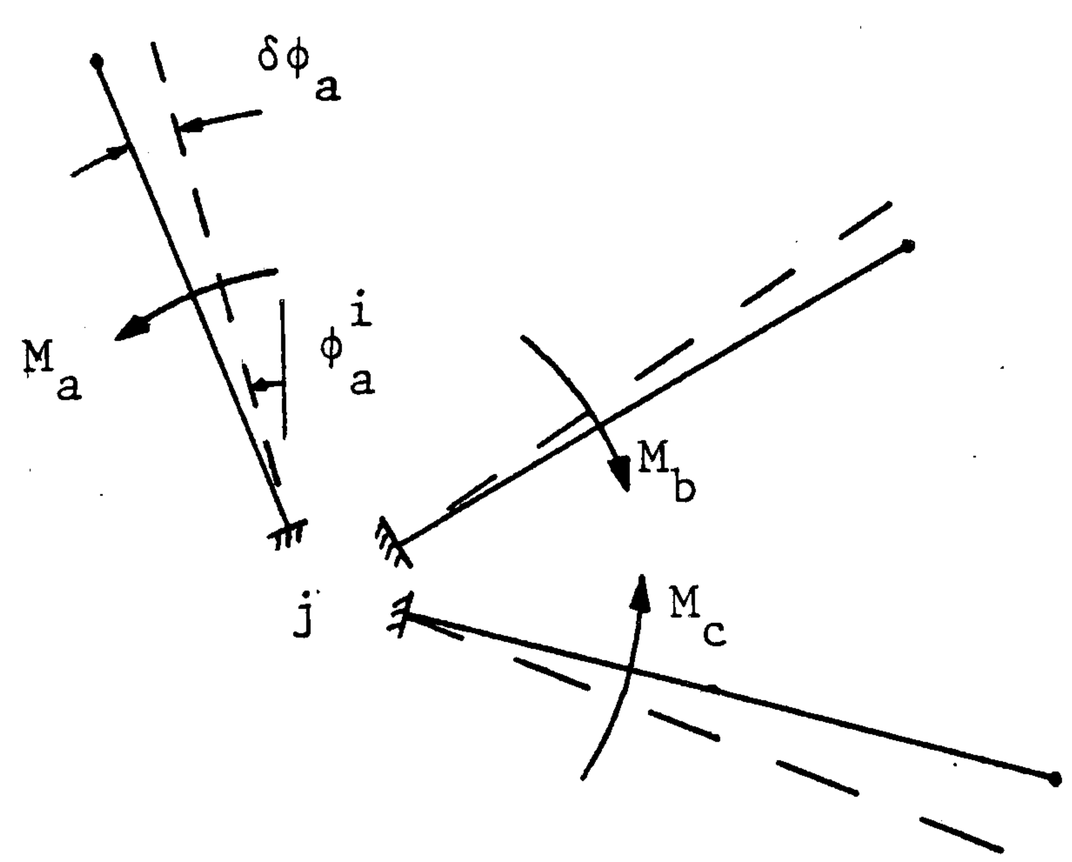

Figure 6.8

and the equivalent joint rotation $\Delta\theta_J$ for the current out of balance moment is given by:

$$\Delta\theta_J = \Delta M_J / \delta M_J \qquad (6.22)$$

Thus in order to maintain moment equilibrium the joint is allowed to rotate by $-\Delta\theta_J$, this being achieved by updating the 'initial' inclinations of the adjacent elements:

$$\phi_r^i \Rightarrow \phi_r^i + \Delta\phi_J \qquad (6.23)$$

and the analysis then proceeds with the force determination stage.

As these joint nodes may have any number of adjoining elements, then the standard boundary conditions may be considered as special cases of the above formulation. An encastré footing may be treated as a joint with only one connecting member and ΔM_J held at zero so that no rotation occurs. Pinned member ends may be specified by resetting the member 'initial' inclination to always coincide with the current value, thus ensuring zero end moments. Combination pinned and rigid joints are therefore possible.

In addition, moments may be applied at any point in the frame structure by specifying a joint node at that point, and adding the applied moment $\grave{M}$ to the current out of balance value:

$$\Delta M_J = -2 \sum \frac{EI\delta\phi_a}{L_a} + \grave{M} \qquad (6.24)$$

6.3 *Space Frame Analysis by Dynamic Relaxation*

The nonlinear plane frame analysis presented in section 6.1 may readily by extended to spatial analysis. Consider an initially straight beam element, arbitrarily orientated in space, as shown in figure 6.9 with the local element coordinate system, $\{X'\}$, defined by the member chord and section principal axes. This spatial bending element has six basic displacement components, which are shown in figure 6.10, together with the associated natural forces acting on the element. These forces may be summarised:

$$\left\{ M_i' \right\} = \begin{Bmatrix} M_i^{x'} \\ M_i^{y'} \\ M_i^{z'} \end{Bmatrix}$$

$$\left\{ S' \right\} = \left\{ S_i' \right\} = \begin{Bmatrix} S_i^{x'} \\ S_i^{y'} \\ S_i^{z'} \end{Bmatrix} = - \left\{ S_j' \right\} \qquad (6.25)$$

The member constitutive relations are then:

$$\begin{Bmatrix} M_i^{y'} \\ M_j^{y'} \end{Bmatrix} = \frac{EI^{y'}}{L} \begin{bmatrix} 4 & 2 \\ 2 & 4 \end{bmatrix} \begin{Bmatrix} \alpha_i^{y'} \\ \alpha_j^{y'} \end{Bmatrix}$$

$$\begin{Bmatrix} M_i^{z'} \\ M_j^{z'} \end{Bmatrix} = \frac{EI^{z'}}{L} \begin{bmatrix} 4 & 2 \\ 2 & 4 \end{bmatrix} \begin{Bmatrix} \alpha_i^{z'} \\ \alpha_j^{z'} \end{Bmatrix}$$

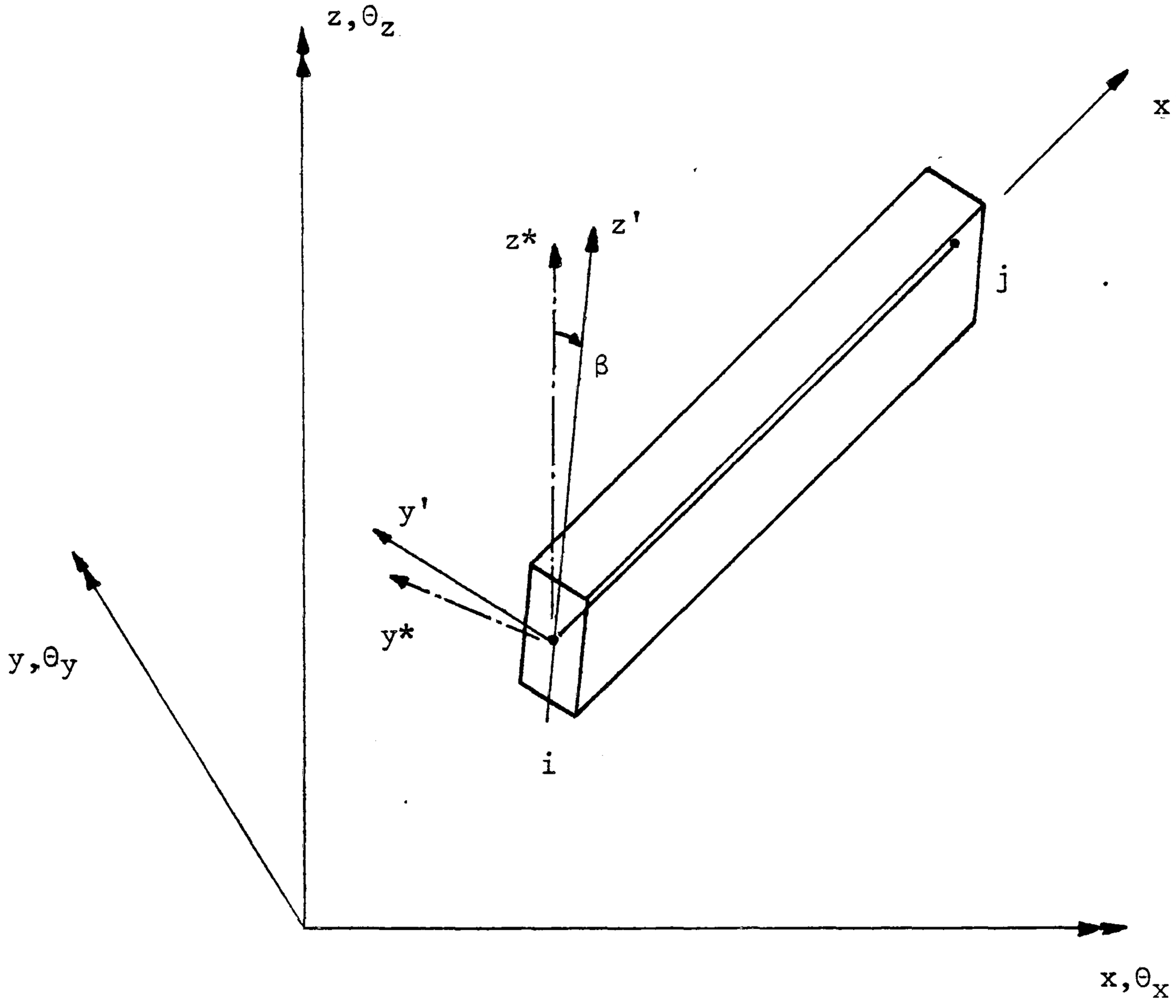

Figure 6.9

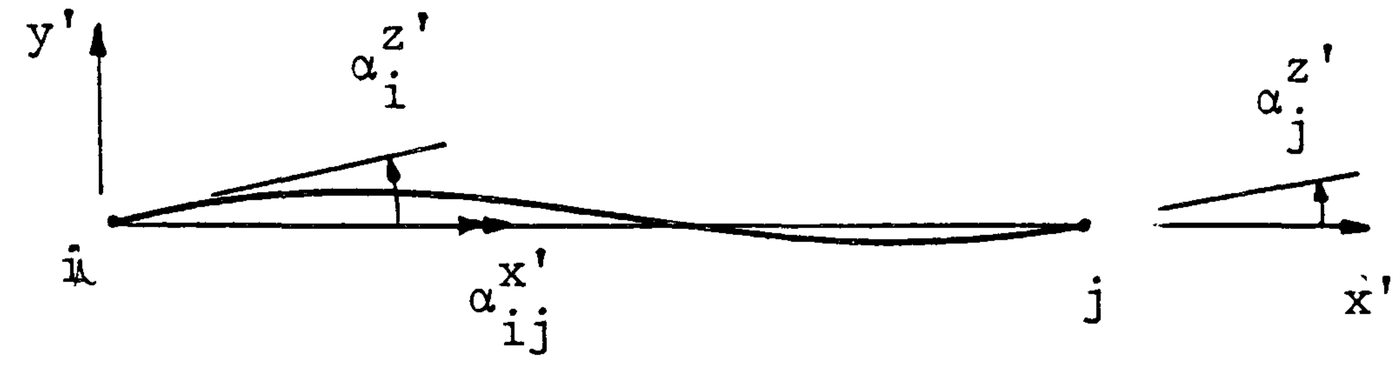

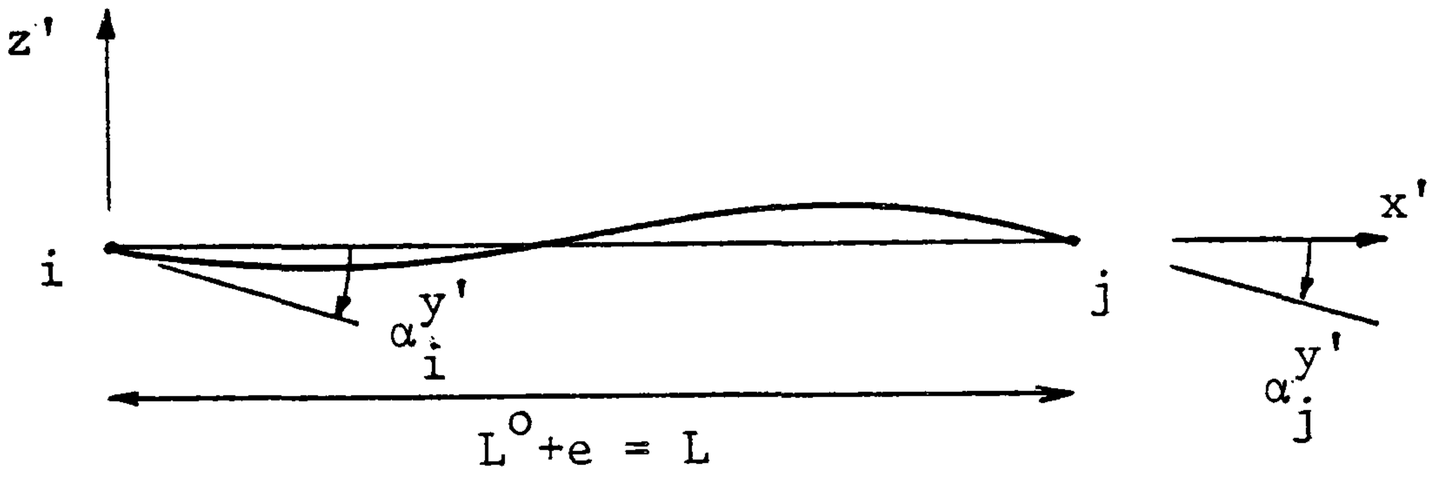

Basic Displacements

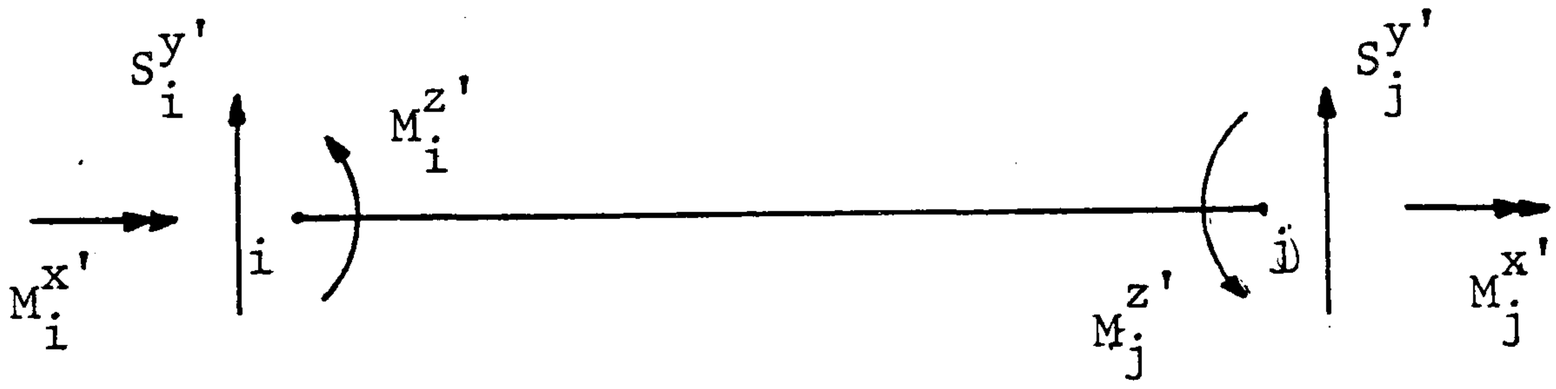

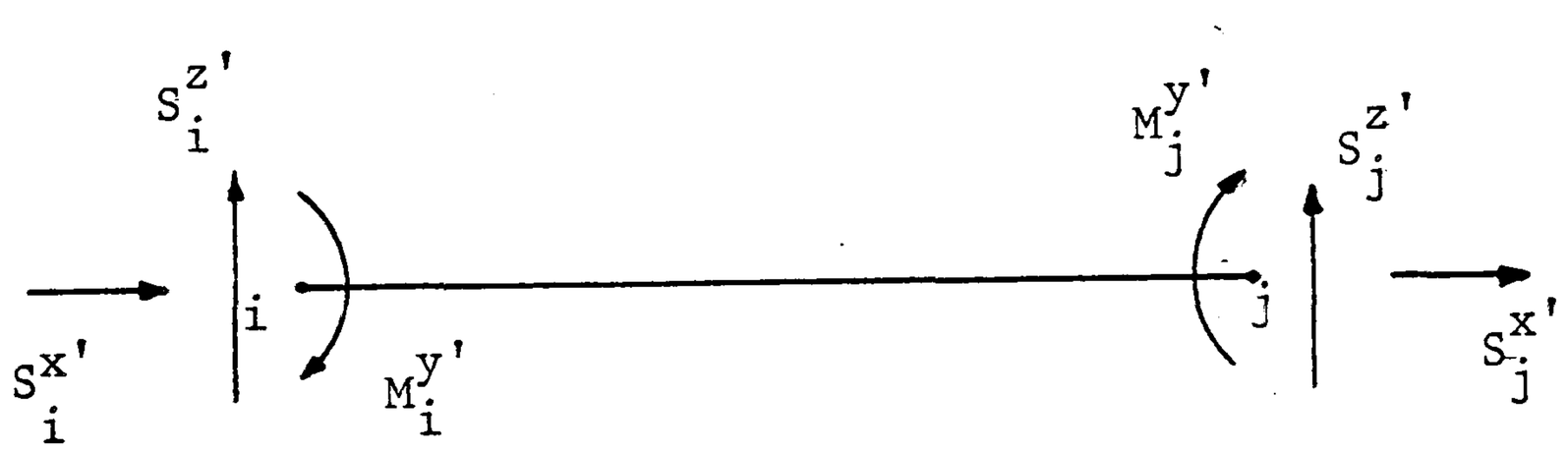

Natural Forces

Figure 6.10

$$M_i^{x'} = -M_j^{x'} = -\frac{GJ}{L} \cdot \alpha_{ij}^{x'}$$

$$S_i^{x'} = -S^{x'} = -\frac{EA}{L} \cdot e$$

$$S_i^{y'} = -S_j^{y'} = (M_i^{z'} + M_j^{z'})/L$$

$$S_i^{z'} = -S_j^{z'} = -(M_i^{y'} + M_j^{y'})/L$$

$$L = L^{\circ} + e \qquad (6.26)$$

The transformation between local $\{x'\}$ and global $\{x\}$ axes is performed in two stages through the intermediate $\{x^*\}$ system (figure 6.9) used to define the angle of rotation β in space. The z^*-axis is perpendicular to the x-axis and parallel to the zx plane.

The member is assumed to twist linearly along its axis, and the current rotation β is assumed to be the sum of the initial value β° and the mean axial rotation in the local coordinate system.

$$\beta = \beta^{\circ} + (\theta_i^{x'} + \theta_j^{x'})/2 \qquad (6.27)$$

where

$$\theta_i^{x'} = \left[\ell \; m \; n \right] \left\{ \theta_i \right\}$$

and $\left\{\theta_i\right\}$ are the nodal rotational displacements, ℓ, m, n the direction cosines of the member chord ij.

With β thus established, the full orthogonal transformation $\left[\lambda\right]$ is given by:

$$\left\{x'\right\} = \left[\lambda\right]\left\{x\right\} \qquad (6.28)$$

where $[\lambda]$ may be conveniently subdivided:

$$[\lambda] = \begin{bmatrix} \ell & m & n \\ [& \lambda_s &] \end{bmatrix}$$

$$[\lambda_s] = \begin{bmatrix} \cos\beta & \sin\beta \\ -\sin\beta & \cos\beta \end{bmatrix} \begin{bmatrix} -m/a & \ell/a & 0 \\ -n\ell/a & -nm/a & a \end{bmatrix}$$

$$a = \sqrt{1 - n^2} \qquad (6.29)$$

For the particular case where the x and z axes are coincident, then:

$$[\lambda_s] = \begin{bmatrix} -n\sin\beta & \cos\beta \\ -n\cos\beta & -\sin\beta \end{bmatrix} \qquad (6.30)$$

The full derivation of these transformations is given in Appendix C .

As in the case of the planar finite displacement analysis, member sway angles must be otained prior to calculation of the rotational basic displacements. These are again obtained from the initial and current geometry by considering relative deflections, transformed into the current coordinate system, as given by Johnson and Brotton (98). The two sway angles, $\phi^{y'}$ and $\phi^{z'}$, are defined in figures 6.11 and 6.12, and the required relative deflections are:

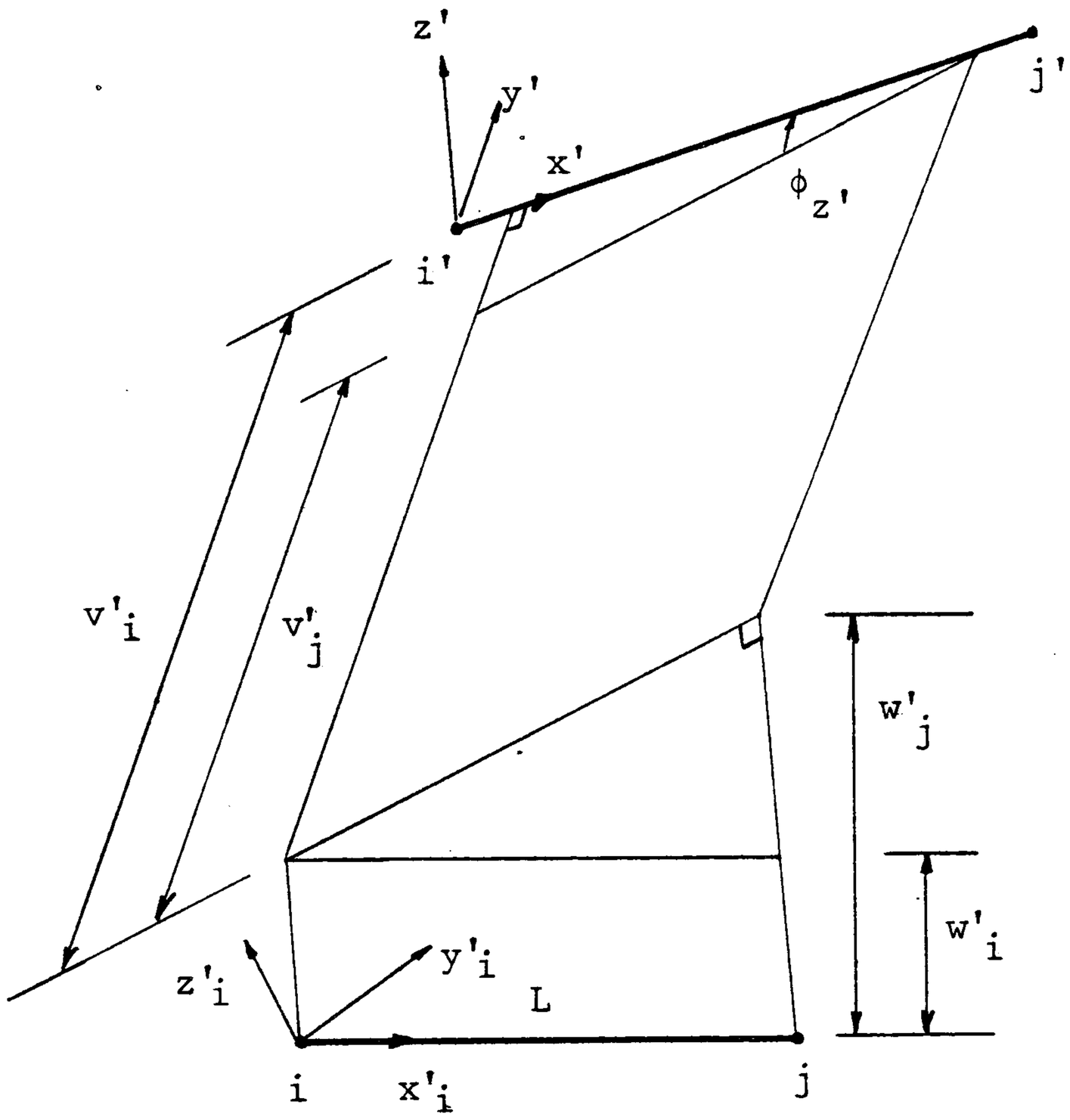

Figure 6.11

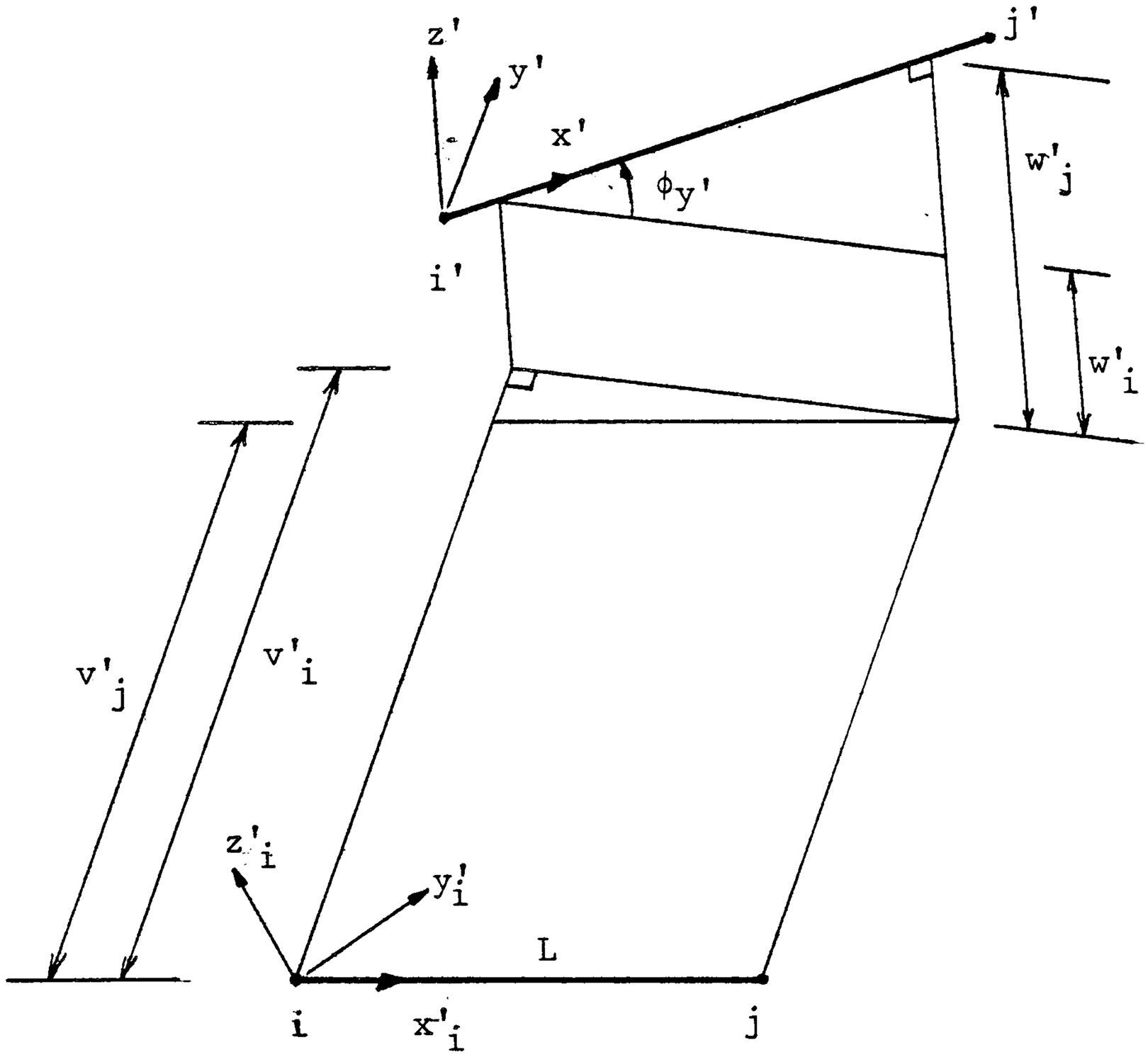

Figure 6.12

$$\begin{Bmatrix} \delta v' \\ \delta w' \end{Bmatrix} = \begin{Bmatrix} v'_j - v'_i \\ w'_j - w'_i \end{Bmatrix} = \begin{bmatrix} \lambda_s \end{bmatrix} \begin{Bmatrix} x_{ij} - x^{\circ}_{ij} \\ y_{ij} - y^{\circ}_{ij} \\ z_{ij} - z^{\circ}_{ij} \end{Bmatrix} \qquad (6.31)$$

where $x_{ij} = x_j - x_i$, etc.

The angles shown in the figures are both negative, thus:

$$\phi^{y'} = \sin^{-1} \left\{ -\delta w' / \sqrt{L^2 - \delta v'^2} \right\}$$

$$\phi^{z'} = \sin^{-1} \left\{ \delta v' / \sqrt{L^2 - \delta w'^2} \right\} \qquad (6.32)$$

The basic, or natural, displacements are then given by:

$$\begin{aligned} \alpha^{y'}_i &= \theta^{y'}_i - \phi^{y'} \\ \alpha^{z'}_i &= \theta^{z'}_i - \phi^{z'} \end{aligned} \qquad (6.33)$$

where:

$$\begin{Bmatrix} \theta^{x'}_i \\ \theta^{y'}_i \\ \theta^{z'}_i \end{Bmatrix} = \begin{bmatrix} \lambda_s \end{bmatrix} \begin{Bmatrix} \theta^{x}_i \\ \theta^{y}_i \\ \theta^{z}_i \end{Bmatrix}$$

The member twist is then obtained:

$$\alpha^{x'}_{ij} = (\theta^{x'}_j - \theta^{x'}_i) \qquad (6.34)$$

and these values are then substituted into the constitutive equations to calculate the member natural forces. These forces must then be transformed into the global coordinate system, and

subtracted from the current nodal residual vector. For example, for moments at node i, for the element ij:

$$\left\{ M_i \right\} = \left[\lambda \right]^T \left\{ \grave{M}_i \right\}$$

$$\text{and} \qquad \left\{ R_i \right\} \Rightarrow \left\{ R_i \right\} - \left[\lambda \right]^T \left[\grave{M}_i \right] \qquad (6.35)$$

with identical treatment for node j, and for the direct natural forces.

As in the planar case, nonlinear effects may be readily incorporated. The s and c stability functions may be included in the constitutive relations, with separate functions and critical loads for each of the two bending planes. The corrections for planar bowing due to Saafan (151) may be extended into the spatial case (Appendix B). As an alternative, the Jennings nonlinear element discussed above has been generalised for space frame analysis by Dickie and Broughton (66). In this case the moment-curvature relations are:

$$M_i^{\grave{y}} = \alpha_i^{\grave{y}} \left\{ \frac{4EI_{\grave{y}}}{L^\circ} + \frac{4PL^\circ}{30} \right\} + \alpha_j^{\grave{y}} \left\{ \frac{2EI_{\grave{y}}}{L^\circ} - \frac{PL^\circ}{30} \right\} + \frac{EI_{\grave{z}\grave{y}}}{L^\circ} \left\{ 4\alpha_i^{\grave{z}} + 2\alpha_j^{\grave{z}} \right\}$$

$$M_j^{\grave{y}} = \alpha_j^{\grave{y}} \left\{ \frac{2EI_{\grave{y}}}{L^\circ} - \frac{PL^\circ}{30} \right\} + \alpha_j^{\grave{y}} \left\{ \frac{4EI_{\grave{y}}}{L^\circ} + \frac{4PL^\circ}{30} \right\} + \frac{EI_{\grave{z}\grave{y}}}{L^\circ} \left\{ 2\alpha_i^{\grave{z}} + 4\alpha_j^{\grave{z}} \right\} \qquad (6.36)$$

and similarly for $M_i^{\grave{z}}$ and $M_j^{\grave{z}}$, where:

$$P = \frac{EA}{L^o} \left\{ L - L^o + q \right\}$$

$$q = L^o \left\{ \left[2(\alpha_i^{y'^2} + \alpha_j^{y'^2} + \alpha_i^{z'^2} + \alpha_j^{z'^2}) - \alpha_i^{y'} \cdot \alpha_j^{y'} - \alpha_i^{z'} \cdot \alpha_j^{z'} \right] \frac{1}{30} \right.$$

$$\left. + (I_{z'} + I_{y'}) \alpha_{ij}^{x'^2} / 2AL^{o2} \right\}$$

and:

$$M_i^{x'} = -M_j^{x'} = -\left\{ \frac{GJ}{L^o} + \frac{P}{AL^o} (I_{z'} + I_{y'}) \right\} \qquad (6.37)$$

For sections with symmetry about either the y' or z' axes, the $I_{z'y'}$ term will be zero, and the above relations can therefore be simplified accordinly for most cases.

The boundary conditions may then be imposed in the same way as for the planar case.

6.4 Control of Dynamic Relaxation Analysis of Rigid Jointed Structures

The automatic procedure presented in chapter 3 for the assessment of fictitious nodal mass components may be applied to rigid jointed structures.

For the spatial framework analysis, with six degrees of freedom per node, a (6x6) square matrix of mass components is theoretically necessary for the optimised integration at each node.

As this would prove very inefficient, in terms of both computational effort and storage, the translational and rotational components are considered here to be uncoupled, resulting in two (3x3) mass matrices for each node.

The elemental contributions to the nodal direct stiffness matrices are then:

$$\begin{aligned} \left[S_T \right] &= \left[\lambda \right]^T \left[\grave{S}_T \right] \left[\lambda \right] \\ \left[S_R \right] &= \left[\lambda \right]^T \left[\grave{S}_R \right] \left[\lambda \right] \end{aligned} \qquad (6.38)$$

for the translational and rotational stiffnesses respectively,

where:

$$\grave{S}_T = \begin{bmatrix} EA/L & 0 & 0 \\ 0 & 12EI_{\grave{z}}/L^3 & 0 \\ 0 & 0 & 12EI_{\grave{y}}/L^3 \end{bmatrix}$$

$$\grave{S}_R = \begin{bmatrix} GJ/L & 0 & 0 \\ 0 & 4EI_{\grave{y}}/L & 0 \\ 0 & 0 & 4EI_{\grave{z}}/L \end{bmatrix} \qquad (6.39)$$

and the member coordinate transformation $\left[\lambda \right]$ is as defined earlier in this chapter.

Mass components for flexural elements have been assigned purely on the basis of elastic stiffness, even for the prestressed boundary structures of tension networks. As these rigid jointed structures have a softening response curve under load, this is a reasonable assumption that has proved satisfactory in practice.

Row sum and leading diagonal mass components are assessed as before from the $[S_T]$ and $[S_R]$ matrices. For planar analyses, the relevant stiffness terms for the $\grave{x}$, $\grave{z}$ and θ components are:

$$\grave{S}_P = \begin{bmatrix} EA/L & 0 & 0 \\ 0 & 12EI/L^3 & 0 \\ 0 & 0 & 4EI/L \end{bmatrix} \qquad (6.40)$$

where the rotational component is unchanged in the transformation into the global coordinate system, and not required for the implementation of the simplified, 'constant moment' bending element.

6.5 Numerical Examples: Planar Problems

The rigid jointed toggle problems shown in figure 6.13 were initially proposed by Williams (170) for the investigation of nonlinear plane frame analyses accounting for finite deformations. This toggle was investigated with two sets of rise values δ, both of which result in highly nonlinear load-deflection characteristics, the latter exhibiting the phenomenon of snap-through buckling for the given loading condition. Williams included the effects of axial forces and flexural shortening on the moment curvature relations, and compared the answers with experimental results for the two cases. The problems have subsequently been analysed by

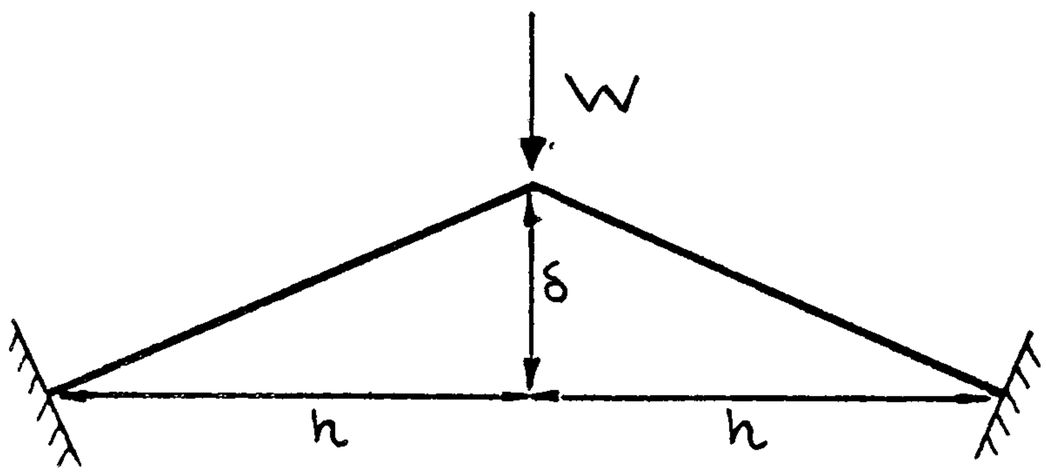

EI = 9.27 x 10

EA = 1.855 x 10

case	δ	h	ℓ
(i)	0.320	12.9360	12.94
(ii)	0.3863	12.9360	12.9418

Figure 6.13 Williams' Toggle

Jennings (95) using nonlinear stiffness relations and a matrix iteration process, achieving identical results of those of Williams' analytic technique.

These two toggles have both been reanalysed using dynamic relaxation with kinetic damping as described in the preceeding sections. The following idealisations have been employed:

(a) cubic displacement linear flexural element
(3 degrees of freedom per node)

(b) Jennings nonlinear flexural element
(3 degrees of freedom per node)

(c) constant moment bending element
(2 degrees of freedom per node)

with varying number of equal length elements per toggle member. The load-displacement curves for these analyses are given in figures 6.14 to 6.19 inclusive. The curves for toggle (i) were obtained by successive load incrementation, with fictitious mass components updated prior to the application of each increment. In order to trace the snap-through behaviour of toggle (ii), the displacement δ was specified, with the apex node restrained against vertical movement. The value of the nodal residual for this restrained degree of freedom at convergence was then the equivalent loading associated with the specified displacement.

WILLIAMS TOGGLE I PROBLEM

DYNAMIC RELAXATION ANALYSIS - 3 D.O.F./NODE

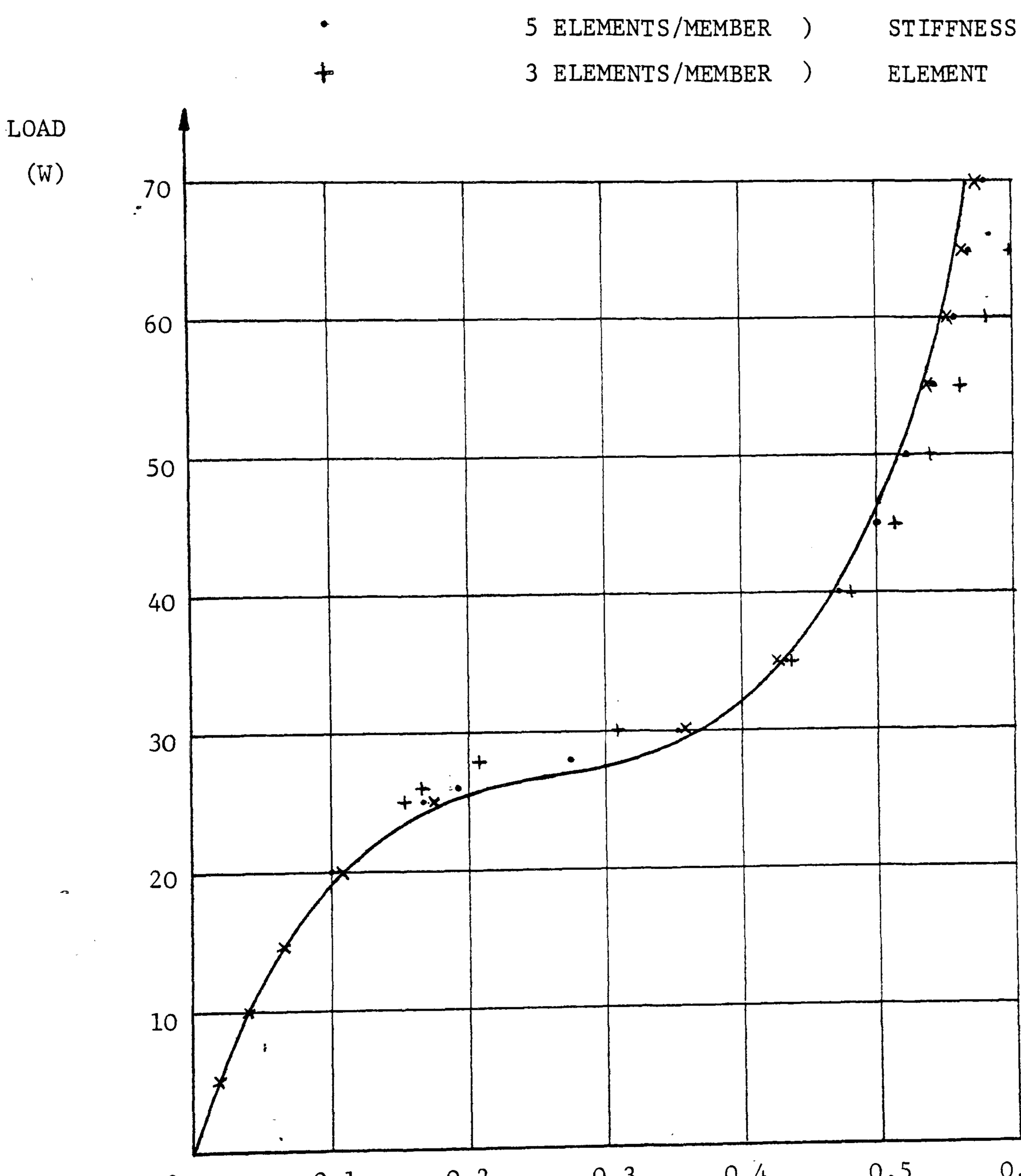

Figure 6.14

WILLIAMS TOGGLE I PROBLEM

DYNAMIC RELAXATION ANALYSIS - 3 D.O.F./NODE

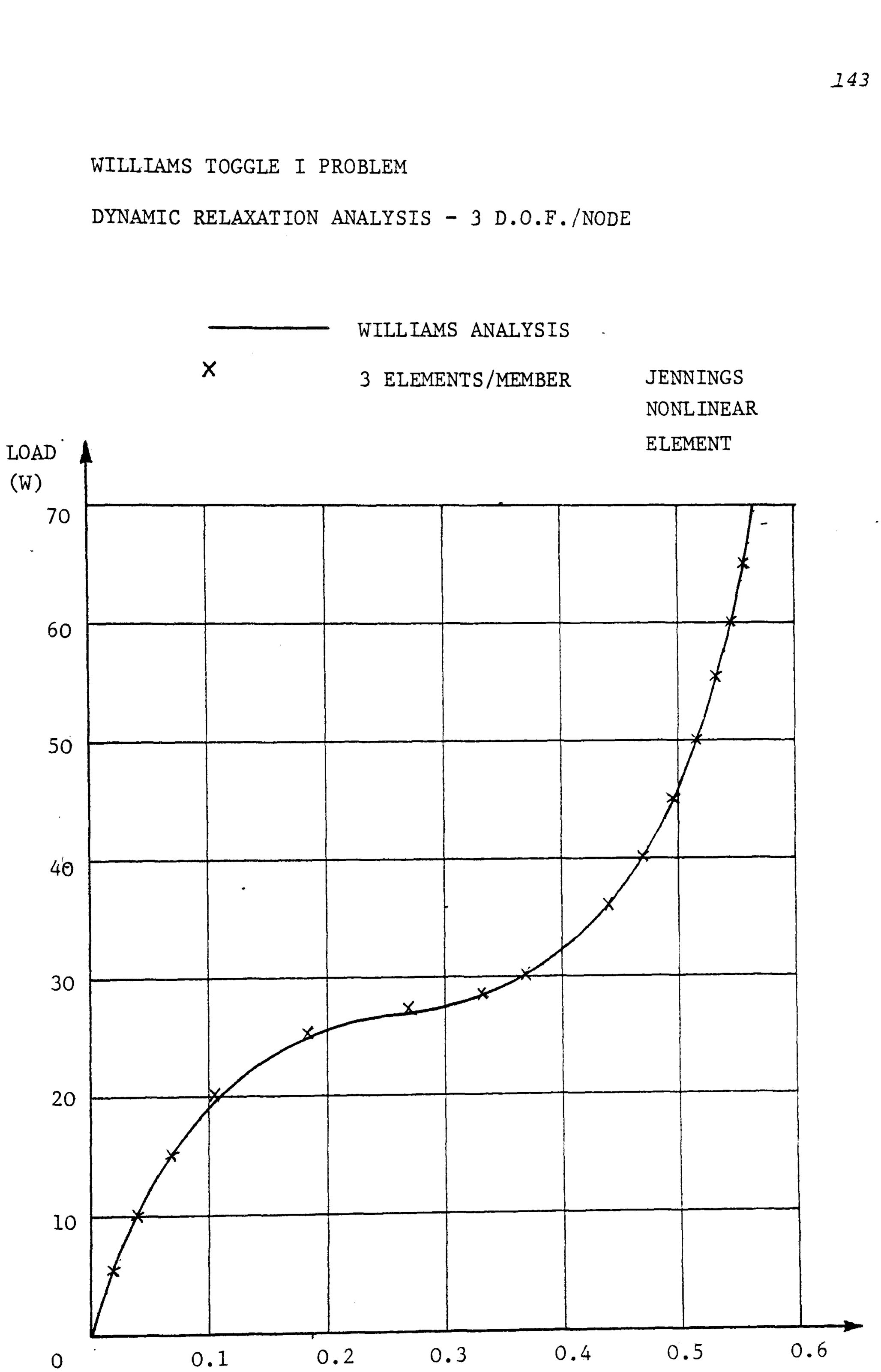

Figure 6.15

WILLIAMS TOGGLE I PROBLEM

DYNAMIC RELAXATION ANALYSIS - 2 D.O.F./NODE

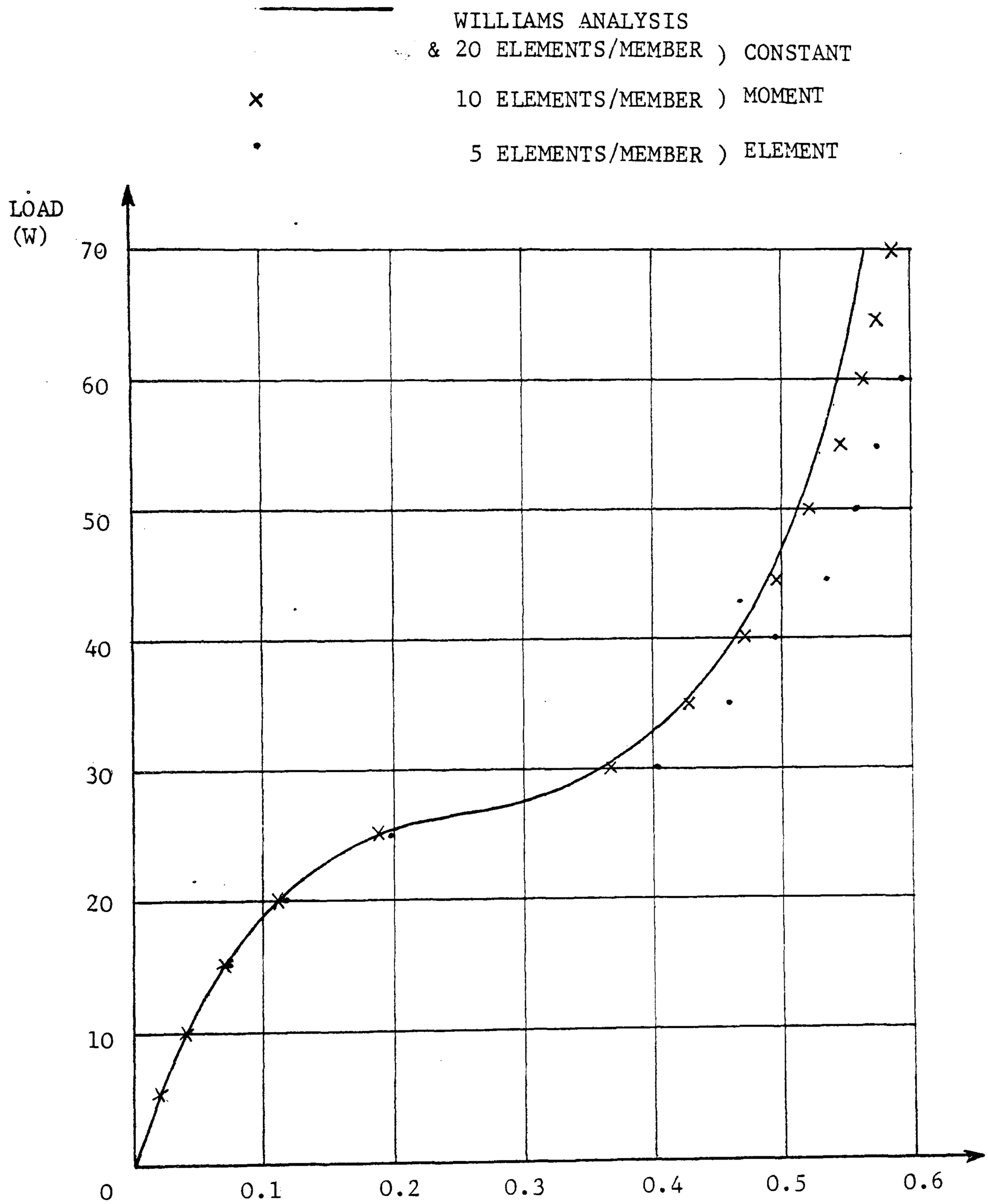

Figure 6.16

WILLIAMS TOGGLE II PROBLEM

DYNAMIC RELAXATION ANALYSIS - 3 D.O.F./NODE

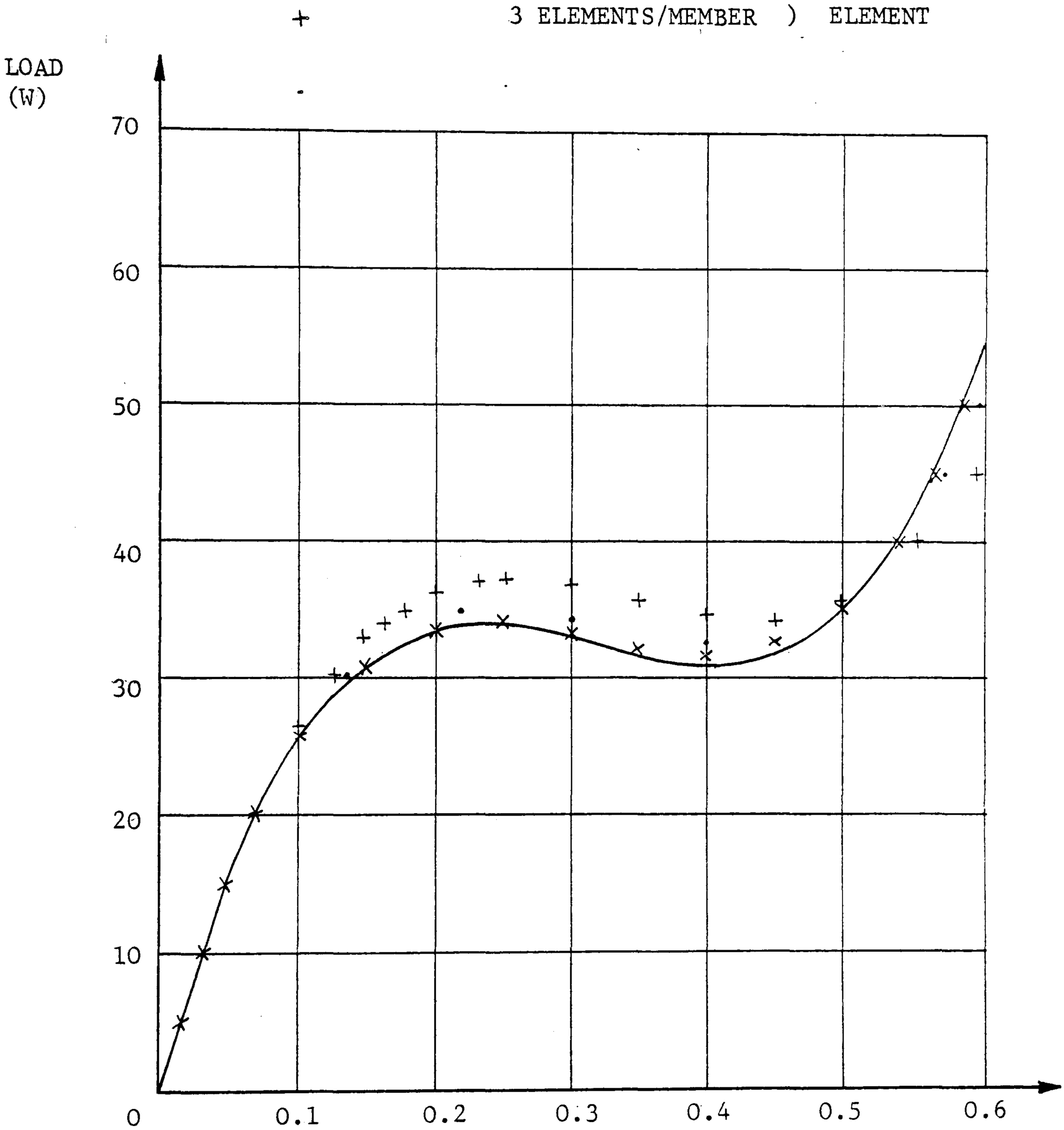

Figure 6.17

WILLIAMS TOGGLE II PROBLEM

DYNAMIC RELAXATION ANALYSIS - 3 D.O.F./NODE

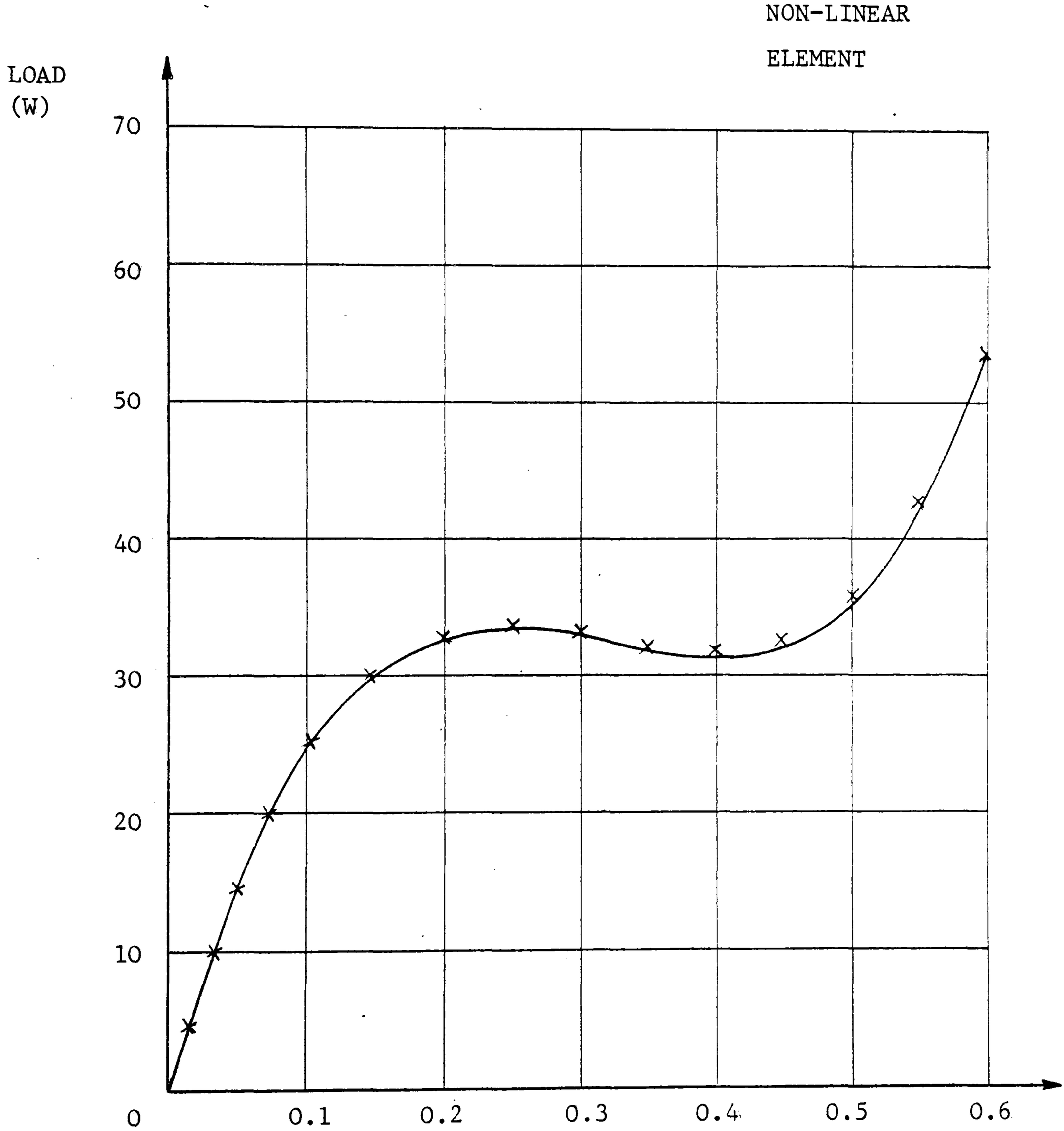

Figure 6.18

WILLIAMS TOGGLE II PROBLEM

DYNAMIC RELAXATION ANALYSIS - 2 D.O.F./NODE

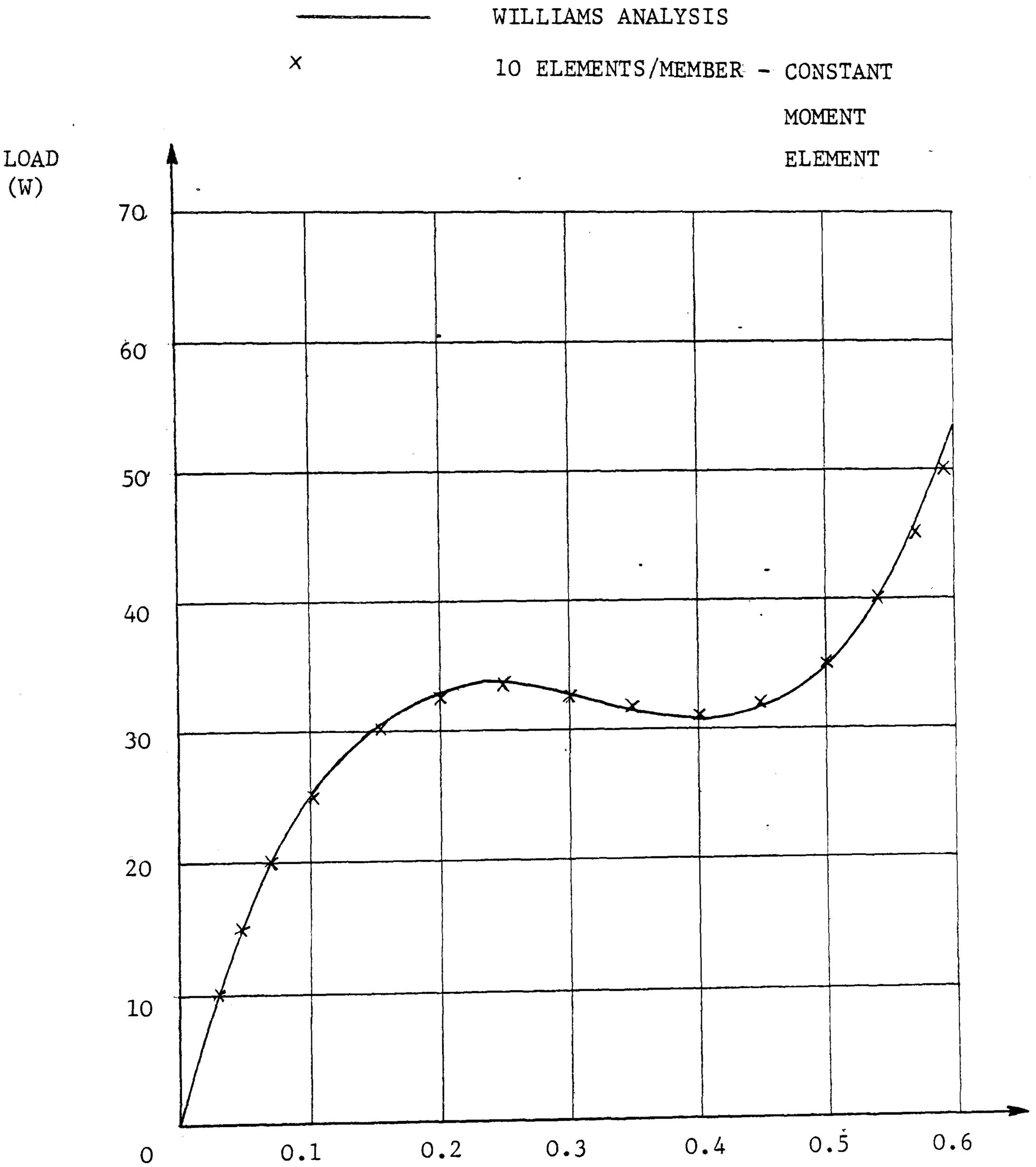

Figure 6.19

For the linear element of idealisation (a), up to 10 elements/toggle member are required to closely reproduce Williams' solution, with no effective displacement change upon a further doubling of the number of elements employed. Inclusion of the nonlinear terms of idealisation (b) enables a satisfactory solution to be obtained with 3 elements/member, with no improvement on increase to 5 elements/member.

The ability of the constant moment element ot trace the nonlinear and snap-through buckling behaviour is demonstrated by figures 6.16 and 6.19 . Here displacement results identical to those achieved by idealisation (b) are achieved by 20 elements/ member, although the behaviour under load has been closely represented by 10 elements/member. The nodal bending moments for the latter case are all within 2% of those obtained from the same number of cubic displacement linear flexural elements.

The semi-circular arch problem of figure 6.20 was used by Broughton (80) to illustrate the discussion of the paper by Happold and Liddell on the timber lattice roof for the Mannheim Bundesgartenschau (79). Broughton obtained a buckling load of 1820 lb for the problem as idealised by 18 nonlinear flexural elements.

This problem has been reanalysed by dynamic relaxation, with figure 6.21 showing the load-displacement curve of the apex node for the three element types used in the toggle reanalysis and an 18 element idealisation.

SEMICIRCULAR ARCH PROBLEM

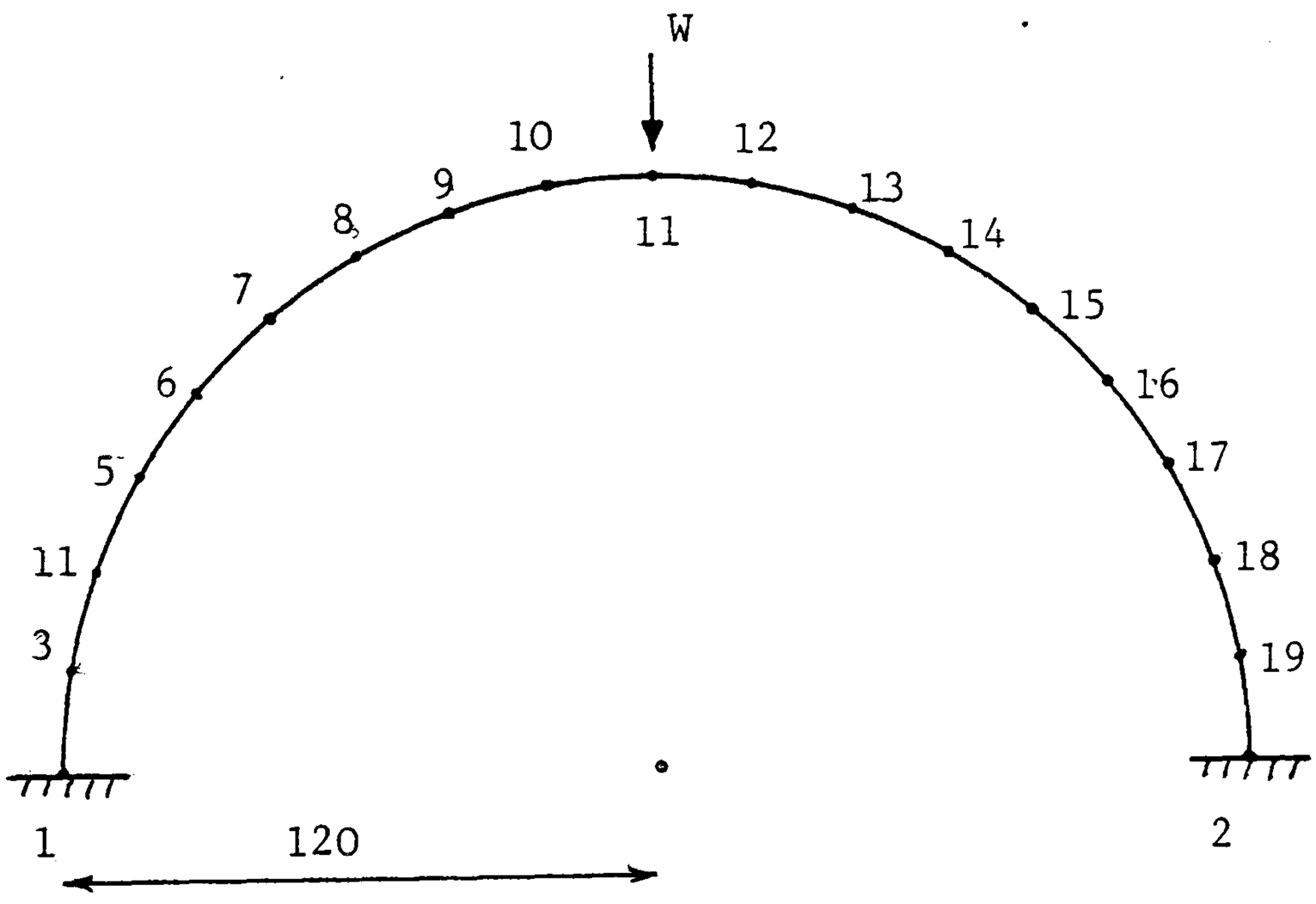

$EI = 2.5 \times 10^6$

$EA = 3.0 \times 10^6$

Figure 6.20

SEMICIRCULAR ARCH PROBLEM

DYNAMIC RELAXATION ANALYSIS

———— JENNINGS ELEMENT

× LINEAR ELEMENT

• CONSTANT MOMENT ELEMENT

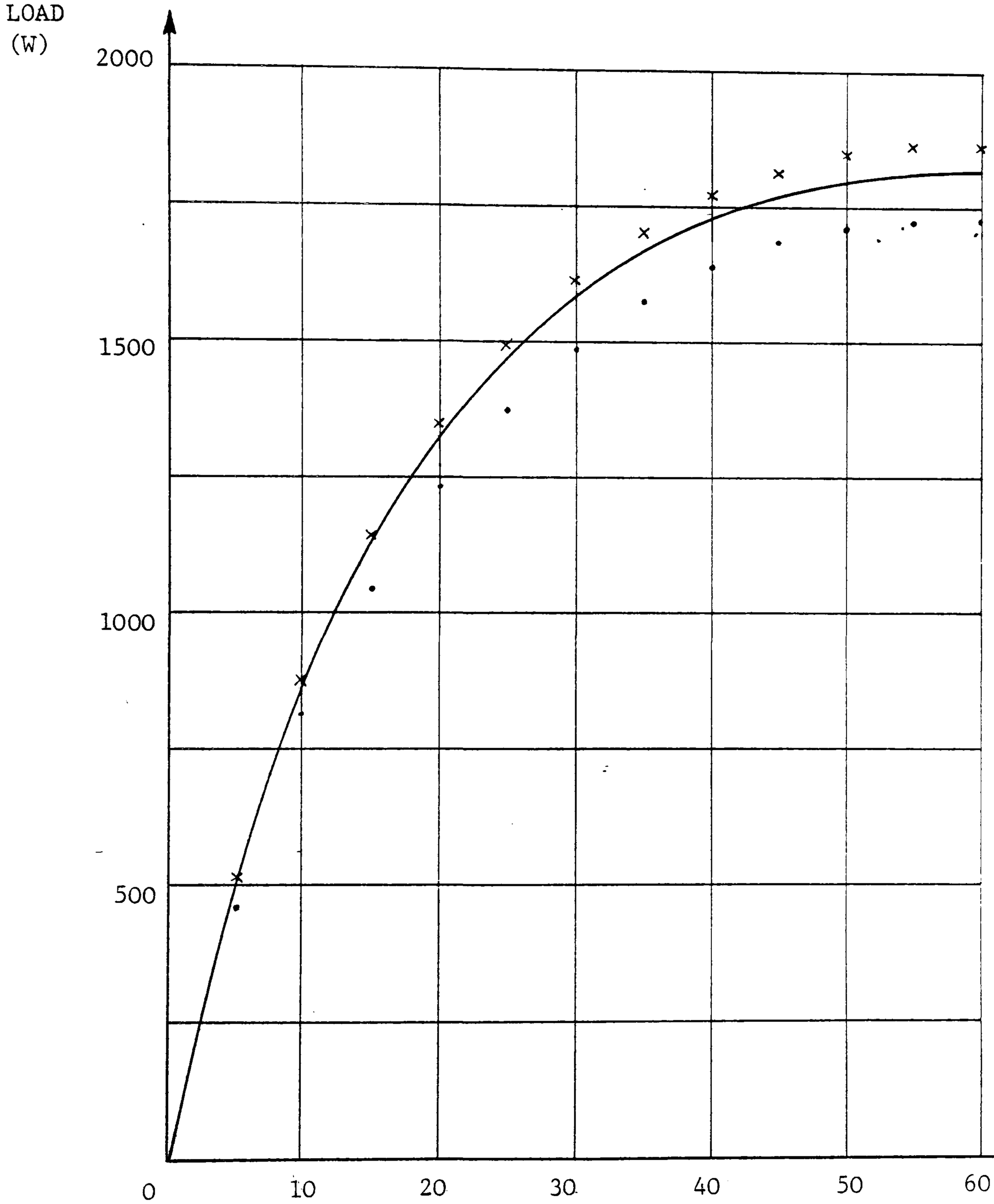

Figure 6.21

NODE	ELEMENT		
	LINEAR 3 dof/node	JENNINGS 3 dof/node	CONSTANT MOMENT 2 dof/node
1	39.68	38.55	35.36
2	13.21	12.75	10.97
3	-12.07	-11.87	-11.96
4	-31.23	-30.44	-29.03
5	-38.23	-37.17	-34.90
6	-30.17	-29.28	-27.17
7	-10.35	- 9.93	- 8.93
8	15.17	15.02	14.45
9	41.57	40.75	38.75
10	64.53	63.04	60.30

Semicircular Arch Bending Moments x 10^{-3} ((+)ve hogging)

for specified apex displacement, δ = 50.

Table 6.1

The identical buckling load was obtained for the application of the Jennings nonlinear element with DR, and the linear three degree of freedom and constant moment idealisations are within +2% and -4% of this value respectively. The nodal bending moments for a specified apex displacement of 50 ins are given in table 6.1. Again the constant moment elements have yielded a satisfactory moment distribution considering the gross deformation and rapidly changing moment pattern. These values would have been improved by further refinement of the idealisation, and post-buckling behaviour traced by the use of specified displacement increments.

6.6 Numerical Examples: Spatial Problems

Many papers have been written that refer to the nonlinear analysis of plane frame problems, as reviewed by Baron and Venkatesan (22), but relatively few refer to the general, three dimensional, case. Consequently there are few results available for physical or numerical investigations of spatial rigidly jointed frameworks subject to gross deformation.

Johnson and Brotton (98) have analysed a shallow dome with a single vertical load applied at the apex, as shown in figure 6.22. A linear flexural element was utilised, in conjunction with a Newton Raphson iteration scheme, with subdivision of critical

SHALLOW DOME PROBLEM

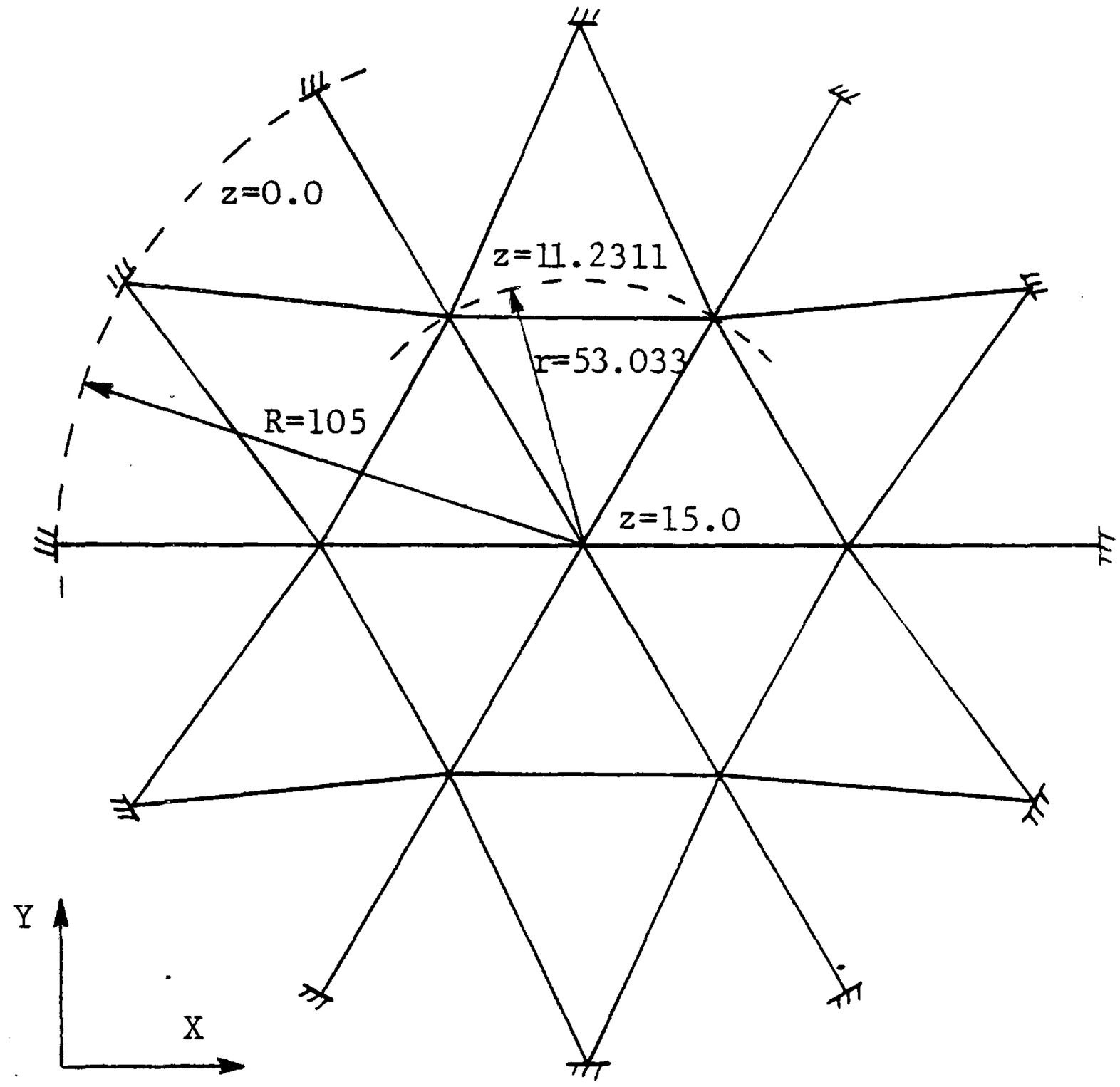

ALL NODES LIE ON A SPHERE OF RADIUS 375.0

MEMBER PROPERTIES: EA = 106080

$EI_{y'} = EI_{z'} = 917800$

GJ = 724356

$\beta = 0$

Figure 6.22

members to account for bowing effects. This problem has subsequently been reanalysed by Dickie and Broughton (66), using a spatial derivation of Jenning's nonlinear element, who obtained effectively the same results.

This shallow dome problem has been reanalysed by dynamic relaxation, using the following elements in the idealisations:

(a) spatial flexural element with s and c stability functions

(b) as for (a), with the addition of Saafaris bowing terms

(c) with Dickie and Broughton's spatial extension of Jennings' nonlinear bending element.

All joints of the dome lie on the surface of a sphere of 750 ft diameter, with an apex rise of 15 ft above the boundary joints.

Each of the three idealisations above produced almost identical results, the apex load/deflection curve being shown in figure 6.23. These results agree closely with those obtained previously by Johnson and Brotton (98) and by Dickie and Broughton (66). The lack of any significant difference in results for idealisations (a) and (b) suggests that the effect of axial shortening due to member bowing is not significant for this problem.

An inclined portal framework subjected to asymmetric loading and exhibiting a high degree of nonlinearity was proposed by Tezcan and Mahapatra (162) to illustrate nonlinear space frame

SHALLOW DOME PROBLEM

DYNAMIC RELAXAION ANALYSIS

——— NONLINEAR ELEMENT

× NONLINEAR ELEMENT + BOWING CORRECTION

• JENNINGS ELEMENT

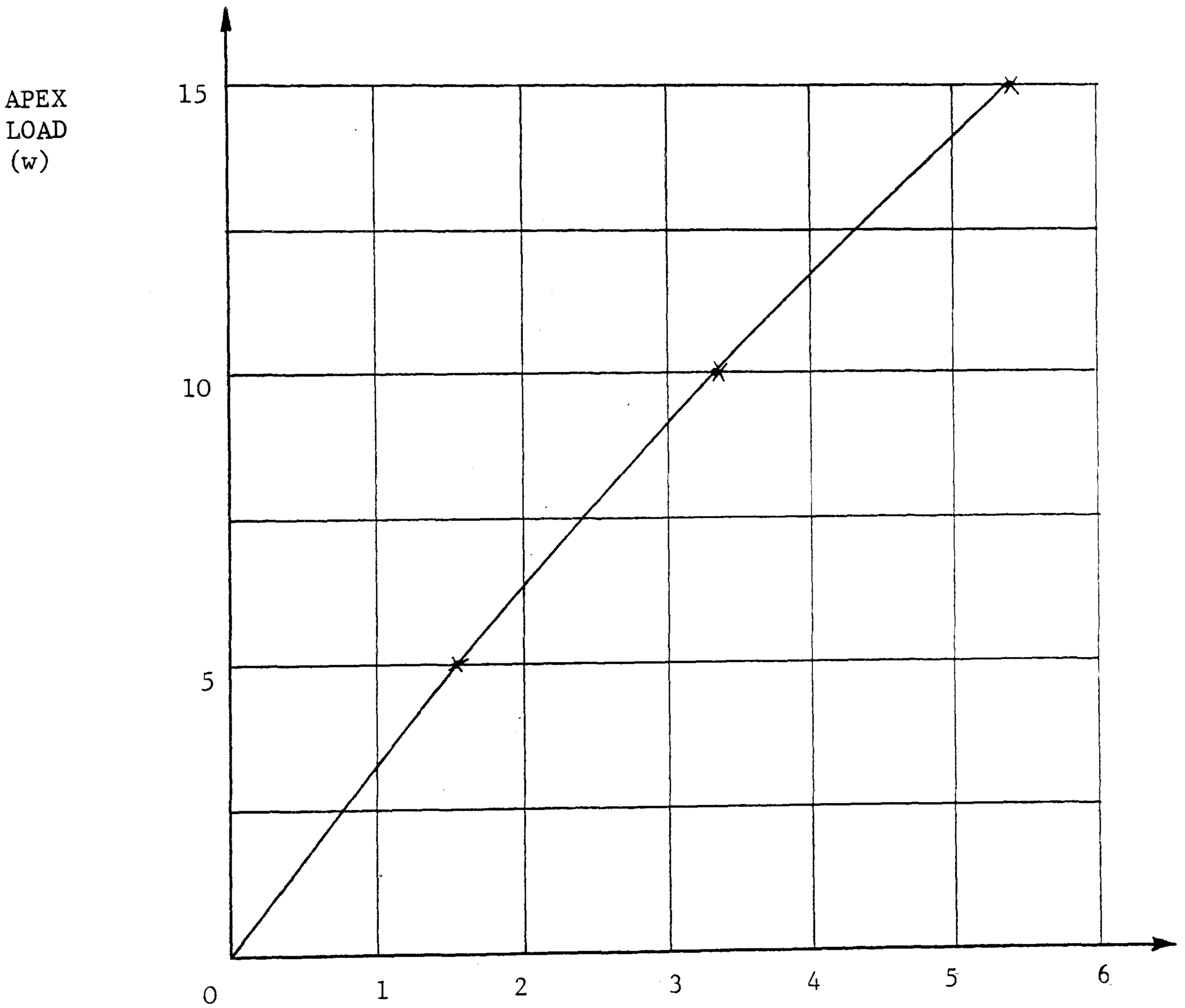

Figure 6.23

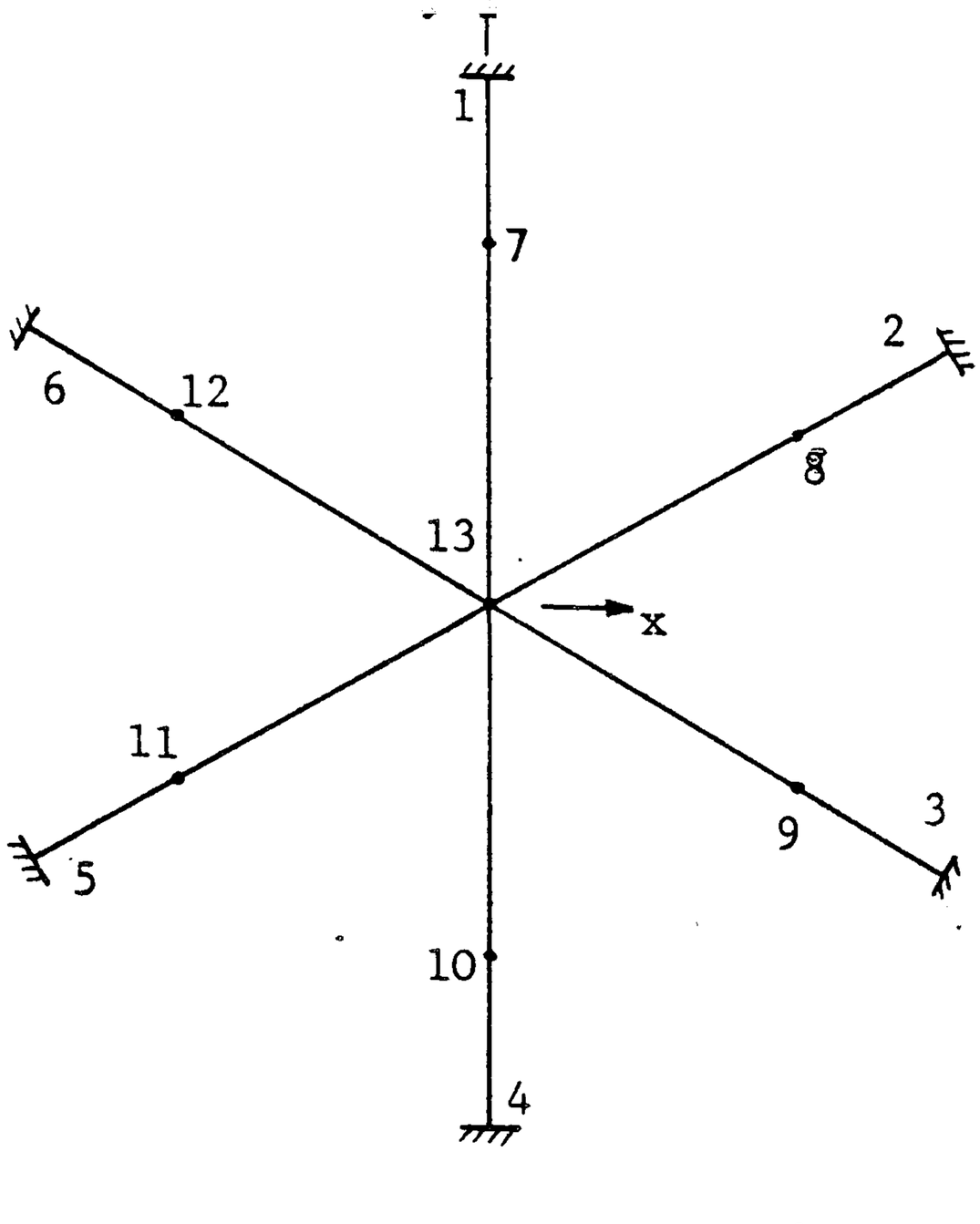

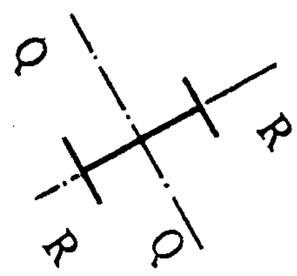

NODAL COORDINATES

NODE	x	y	z
1	0.	207.85	0.
2	180.	103.92	0.
3	180.	-103.92	0.
4	0.	-207.85	0.
5	-180.	-103.92	0.
6	-180.	103.92	0.
7	0.	138.56	240.
8	120.	-69.28	240.
9	120.	-69.28	240.
10	0.	-138.56	240.
11	-120.	-69.28	240.
12	-120.	-69.28	240.
13	0.	0.	300.

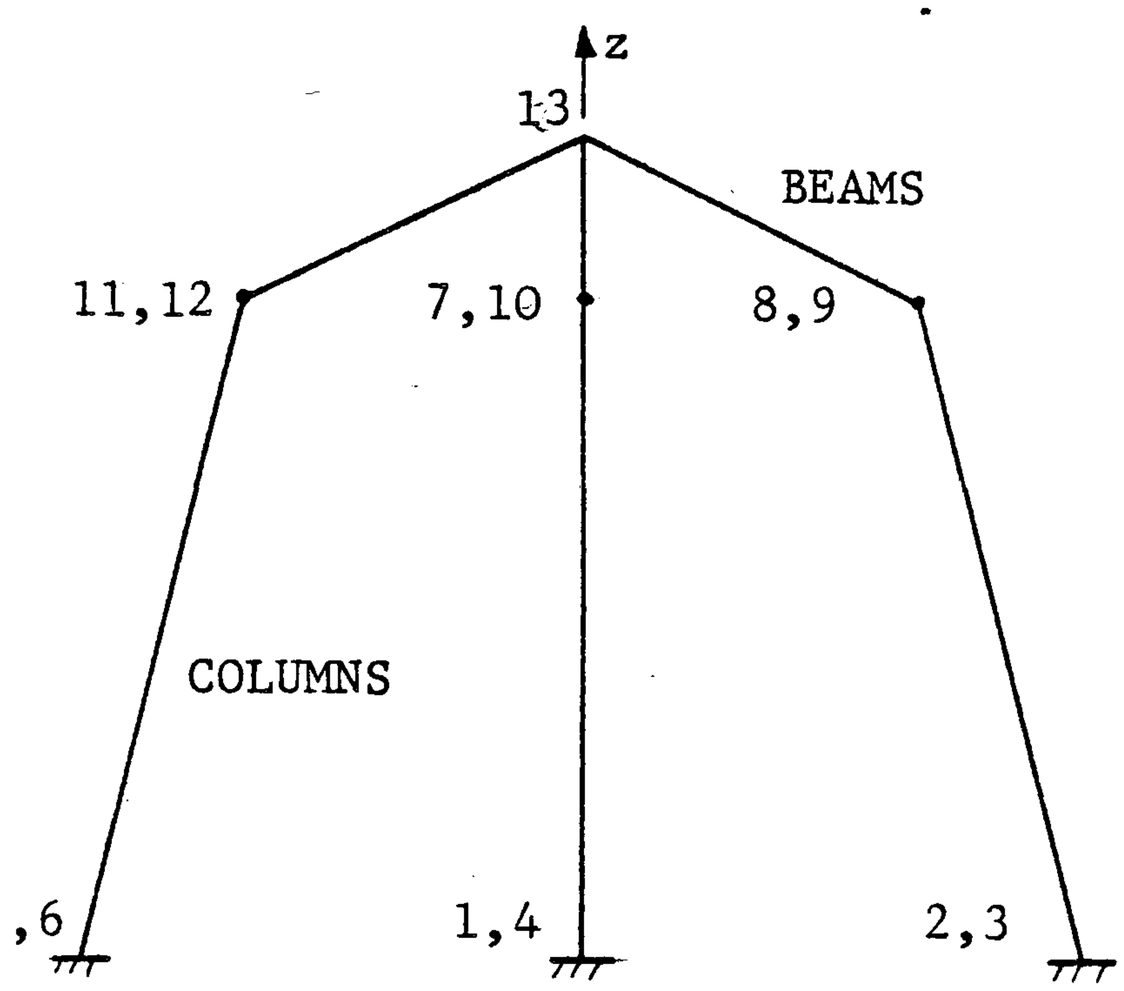

3D - INCLINED PORTAL FRAME

Figure 6.24

LOAD FACTORS

JOINT	P_x	P_y	P_z
11	w	0.	-1000w
12	w	0.	-1000w
13	0.	0.	-10w

MEMBER DATA

	A	I_Q	I_{TZ}	J
COLUMNS	35.31	1071.7	345.1	13.13
BEAMS	17.06	227.3	74.9	3.36

E = 30x10 $\quad \nu = 0.25$

G = 12x10

analysis. Reanalysis by Broughton (80) yielded differing results, and the current results obtained here by DR suggests that the Tezcan and Mahapatra solution refers to one half of the stated loading, with consequent apparently overstiff solutions. The problem data is given in figure 6.24.

The results of dynamic relaxation analysis, with linear and nonlinear flexural elements, are given in figure 6.25 for the translational displacement of node 12. The effect of the inclusion of nonlinear terms is clearly seen, but again the additional treatment of bowing had no significant effect on the displacements. The spatial Jennings' element produced identical results to the beam element with s and c functions when used in the DR formulation. However, the reasons for the differences between this result and those published for the Broughton (80) implementation of the Jennings' element are not clear.

In addition the x-displacement solution obtained by Tezcan and Mahapatra for twice the stated solution has been shown, agreeing closely with the dynamic relaxation solution.

Tables 6.2 and 6.3 indicate the number of steps to convergence and the corresponding computer execution time (CDC 7600) for the shallow dome and inclined portal frame problems. Each of the three methods for assessment of the fictitious nodal mass components summarised in section 6.4 have been utilised, namely those based on leading diagonal (LD), row sum (RS) and nodal square matrix (SM) direct stiffnesses.

3D - INCLINED PORTAL FRAME

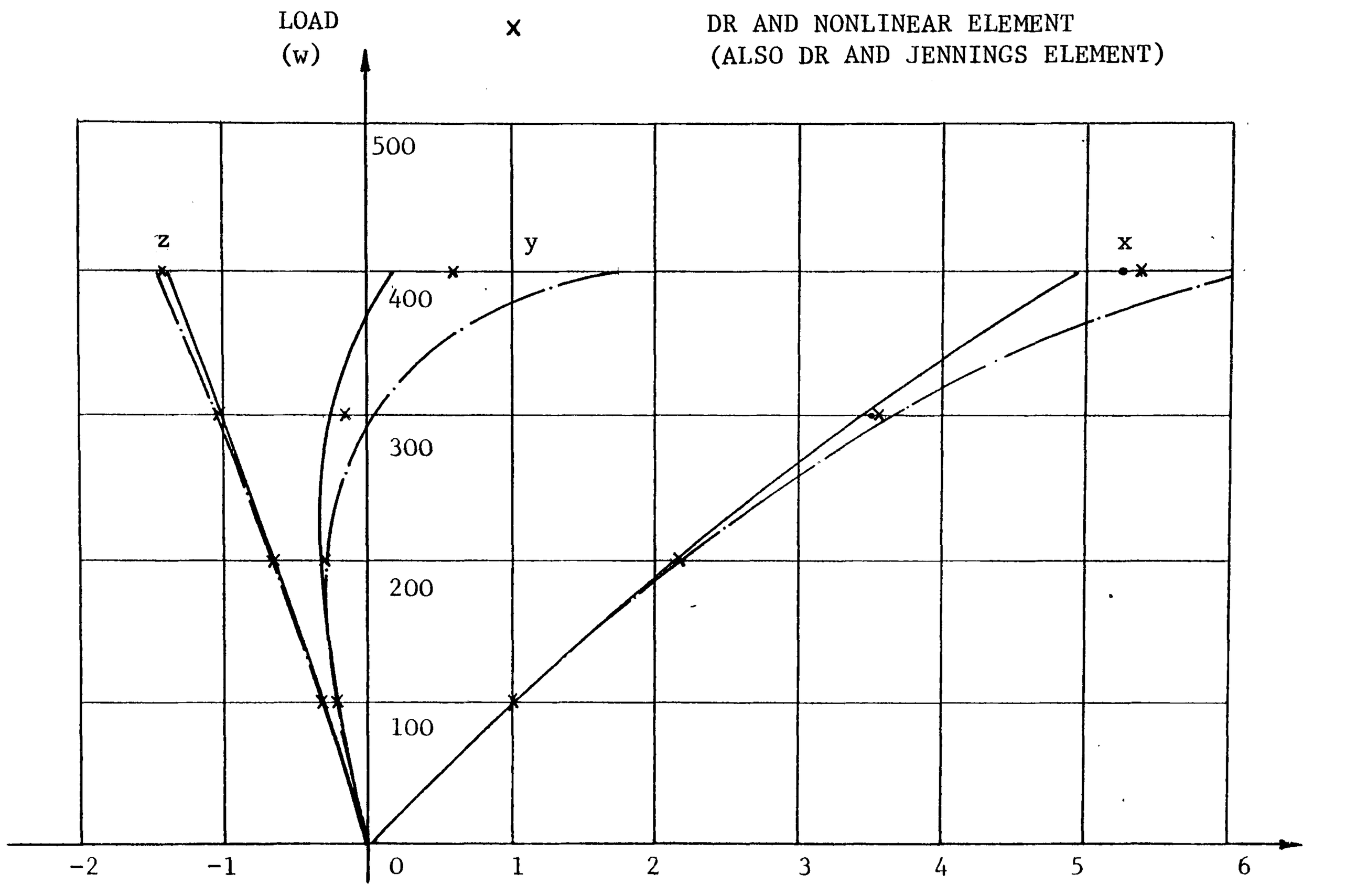

NODE 12 TRANSLATIONAL DISPLACEMENTS

Figure 6.25

SHALLOW DOME PROBLEM				
LOAD	MASS ASSESSMENT	α_m	CONVERGENCE	
			STEPS	EXEC'N TIME (CDC 7600 secs)
5.	RS	1.	39	.444
	LD	2.	28	.363
	SM	1.	21	.344
10.	RS	1.	37	.430
	LD	2.	30	.377
	SM	1.	22	.352
15.	RS	1.	47	.510
	LD	2.	37	.436
	SM	1.	25	.385

Table 6.2

RS - row-sum

LD - leading diagonal

SM - square matrix

INCLINED PORTAL FRAME PROBLEM				
			CONVERGENCE	
LOAD FACTOR	MASS ASSESSMENT	α_m	STEPS	EXEC'N TIME (CDC 7600 secs)
100.	RS	1.	274	.919
	LD	2.	214	.734
	SM	1.	143	.650
200.	RS	1.	318	1.037
	LD	2.	273	.914
	SM	1.	112	.539
300.	RS	1.	484	1.537
	LD	2.	348	1.135
	SM	1.	164	.733
400.	RS	1.	413	1.327
	LD	2.	391	1.266
	SM	1.	160	.724

Table 6.3

The optimised block operation scheme has proved most efficient in all cases, with the additional computation necessary being offset by the reduction in iteration steps to convergence. The leading diagonal direct stiffness assessment of the diagonal mass terms, with factor $\alpha_m = 2$ (chapter 3), has proved next most efficient for these problems, with the row sum technique the least efficient.

6.7 *Summary*

As a precursor to the analysis of pretensioned networks with external or internal boundary structures, the method of dynamic relaxation has been extended to the analysis of framed structures.

Rotational degrees of freedom have been introduced into the DR scheme and treated in the same way as the translational components, excepting that rotations are conveniently traced as displacements from the initial state rather than absolute values.

Section 6.1 describes the implementation of planar flexural elements. Rigid body motion is treated naturally by the method, and the natural member stiffness relations are employed for efficient calculation of residual forces. Livesley's s and c functions (114) are included to account for the effect of axial force on the moment curvature relations. These functions are updated at the energy peak reset stages. The alternative nonlinear

natural stiffness relations due to Jennings (95) may also be included.

A simplified, constant moment, bending element is presented in section 6.2 for planar analysis. The flexural member is idealised as a series of bar elements, which are permitted to deform axially, whilst the flexural stiffness is lumped at the nodes interconnecting those elements. As a consequence only the two translational variables are required at each node, with the lumped rotation obtained from the relative inclination of the adjacent elements. The treatment of boundary conditions and rigid joints is presented. Although a finer idealisation is necessary for a given accuracy by comparison with conventional cubic displacement elements, this element may still be useful for planar problems where such an idealisation is a geometric or topographic requirement.

In the following section the full nonlinear DR analysis has been extended to the spaceframe problem. The member force calculation procedure may be summarised (using the basic stages outlined in chapter 3):-

(i) establish the coordinate transformation matrix (eqn. 6.29)

(ii) calculate basic member displacements from global coordinates (eqns. 6.33 and 6.34)

(iii) calculate natural forces from basic displacements using either linear (eqn. 6.26) or nonlinear (eqns. 6.10 or 6.36) natural stiffness relations

(iv) sum transformed natural forces into the nodal residual vector (eqn. 6.35).

The control of dynamic relaxation analysis of rigid jointed structures is then detailed in section 6.4, with comparative computation times presented subsequently for the numerical examples considered. The use of square nodal mass matrices with the associated block operations has proved most efficient for the structures investigated.

The results of dynamic relaxation analyses are then compared with published solutions to nonlinear plane and spaceframe problems. The successful treatment of finite displacements, through to snapthrough and the post-buckling response, is demonstrated.

CHAPTER 7

FORMFINDING

Formfinding is an integral and essential part of numerical investigations of network structures supported by compression boundary structures. Dynamic Relaxation may be utilised at the conceptual stage for generating moment-free compression contours under dead loading, and subsequently for determination of the pretension geometry with the boundary idealised by rigid-jointed spatial flexural elements. The general topic of formfinding, and the application of Dynamic Relaxation, has been dealt with in detail elsewhere (20,21). This chapter is intended as a brief summary of the development of numerical formfinding techniques, followed by examples of the utilisation of kinetic damping and the treatment of moment-free compression contours in the Dynamic Relaxation method.

7.1 *Formfinding - A Review*

In 1959 Bandel (11) derived a set of linear algebraic equations for the shapefinding and analysis of hyperbolic parabaloidal pretressed nets with orthogonal cable arrangements. Vertical joint displacements only were considered for applied temperature changes and vertical loading. This method of shapefinding for orthogonal, or projected, nets was generalised for arbitrary boundary configurations by Siev and Eidelman (157), and has subsequently been applied by Møllman (121) and Thornton and Birnstiel (163). If T_{Hx} and T_{HY} are the specified horizontal force components for the two cable sets, then for equilibrium of any node i connected to adjacent nodes j by members M_x , M_Y :

$$\sum_{M_x} \frac{T_{Hx}}{\ell_{Hx}} (Z_i - Z_j)_{M_x} + \sum_{M_Y} \frac{T_{HY}}{\ell_{HY}} (Z_i - Z_j)_{M_Y} = P_{zi} \qquad (4.1)$$

where P_{zi} is the nodal vertical load and ℓ_{Hx}, ℓ_{HY} are the horizontal components of cable length in each direction. The full set of linear equilibrium equations may then be expressed in matrix form:

$$\left[H \right] \left\{ Z \right\} = \left\{ P_z^{`} \right\} \qquad (4.2)$$

where $\left[H \right]$ is square, $\left\{ Z \right\}$ is the vector of nodal vertical coordinates and $\left\{ P_z^{`} \right\}$ is the load vector modified by the transfer of known boundary conditions from the left hand side of the equations.

Iterative procedures for the shapefinding of geodesic nets

based on the above procedure have been proposed by Mollmann (121) and Siev (158).

Dean and Ugarte (64) derived closed form trigonometric series solutions for initially flat multiply threaded nets subject to vertical loading. This approach has been extended by Buchanan and Akin (34) for elevated and spatially curved boundaries, and by Buchholdt (35) for a variety of boundary and net patterns with the Fourier series solutions expressed as matrix products.

Schek (154) has extended the above method of Siev and Eidelman for three degrees of freedom at each node and thus obtained a general linear formfinding technique.

Consider a network with N free and N_δ fixed nodes, having coordinates $\{X\}$ and $\{X_\delta\}$, connected by M members in the pattern defined by the connection submatrices $[C]$ and $[C_\delta]$ for member j:

$$\begin{aligned} C_{ji} &= +1 \text{ for end 1} \equiv \text{node i} \\ &= -1 \text{ for end 2} \equiv \text{node i} \\ &= 0 \text{ otherwise} \end{aligned} \tag{4.3}$$

The vector of element coordinate differences, $\{dX\}$, is then:

$$\{dX\} = [C]\{X\} + [C_\delta]\{X_\delta\} \tag{4.4}$$

and for member forces $\{T\}$, equilibrium of the free nodes is satisfied provided:

$$\left[C\right]^{T}\left[DX\right]\left[L\right]^{-1}\left\{T\right\} = \left\{P\right\} \qquad (4.5)$$

where $\left[DX\right]$ is the diagonal matrix of $\left\{dX\right\}$ and $\left\{P\right\}$ is the vector of applied loads. If the member force densities, or tension coefficients, are defined by:

$$\left\{q\right\} = \left[L\right]^{-1}\left\{T\right\} \qquad (4.6)$$

then equation (4.5) may be rewritten:

$$\left[C\right]^{T}\left[DX\right]\left\{q\right\} = \left\{P\right\} \qquad (4.7)$$

or

$$\left[C\right]^{T}\left[Q\right]\left\{dX\right\} = \left\{P\right\} \qquad (4.8)$$

with diagonal matrices $\left[Q\right]$, $\left[L\right]$ for member tension coefficients and lengths respectively. Substituting equation (4.4) into (4.8) one obtains:

$$\left[C\right]^{T}\left[Q\right]\left[C\right]\left\{X\right\} + \left[C\right]^{T}\left[Q\right]\left[C_{f}\right]\left\{X_{f}\right\} = \left\{P\right\} \qquad (4.9)$$

or

$$\left[H\right]\left\{X\right\} = \left\{P\right\} - \left[H_{f}\right]\left\{X_{f}\right\} = \left\{\hat{P}\right\} \qquad (4.10)$$

The square matrix $\left[H\right]$ is positive definite for all $q > 0$, and solution of the linear equations (4.10) yields the free node coordinates $\left\{X\right\}$ for given load and boundary conditions, there being one equilibrium state for each prescribed set of tension coefficients.

Although the above linear method, termed force densities method, produces approximately regular nets when constant force densities are specified throughout (154), it still suffers from the same basic drawback of the earlier linear procedures. Their ability

to provide initial shapes rapidly and economically is tempered by the constructional impracticality of the solutions so found. Nonlinear methods must be employed for uniform mesh or geodesic networks, but the methods of this section are still highly suited to initial investigations of form and as starting points for subsequent nonlinear procedures, which are reviewed in the next section.

The implicit Newton Raphson (NR) iterative procedure has been applied to the formfinding of funicular networks by several researchers. Using sketches of the shape of the required structure as a starting point for the iteration, Haug and Powell (83) have demonstrated the shapefinding of a variety of structural types. Possible convergence problems with the NR method for strongly nonlinear problems were avoided by incremental loading and specification of a maximum permissible displacement increment for any degree of freedom, all increments being scaled down proportionally if this maximum was exceeded. Provided the intermediate convergence criteria are not too severe then a single iteration will suffice for the load step, resulting in an Euler type procedure, with updated tangent stiffness at each stage, until the final load increment when the full NR method provides the final required degree of convergence. By this stage the modified NR procedure with constant stiffness matrix may well be successfully employed. Constant force, or geodesic, members were introduced with purely geometric stiffness matrices. Formfinding of a

pretensioned net supported by a central mast took 15 iterations (83), whilst that of a hexagonal mesh suspended net required 33 iterations. In the later case fictitious pretensions were introduced for the first iteration only to avoid singularity of the stiffness matrix for the initially plane net. Cable slack lengths were modified during the formfinding of an adaptable net to simulate the effect of turnbuckles. The gross out of balance forces thus generated were successfully controlled by the above procedures, and an average of 30 NR iterations was required for each of the structure modifications. For this problem convergence was improved by allowing compressive forces in some of the cables during iteration.

Argyris and Scharpf (8) used similar controls on the NR iteration for formfinding of prestressed networks, with the addition of a specified maximum nodal out of balance force at any stage of the process. For the formfinding of the Munich Olympic stadia an initial net was generated iteratively on the mathematical surface of the structure, which had been determined as a series of localised fourth order polynomials from photogrammetric measurements of the architect's model. Prescribed stress conditions were approximated in the subsequent NR iteration for net equilibrium by holding the force constant in at least one end member of each cable. Additionally, reduced stiffnesses were assigned to boundary cables in order to increase the rate of convergence in edge regions.

As a consequence of large initial out of balance forces and compression in some members the convergence rate of NR formfinding based on initial data from sketches or models may be

very slow, or even divergent. Thus, as an alternative, Argyris, Angelopolous and Bichat (10) proposed a wholly mathematical model in which analytical shapefinding commenced from an initially flat net of linear elastic elements. A doubly curved equilibrium figure was then derived by incremental movement of specified nodal points, accompanied by iteration for equilibrium of the remaining free nodes. Again an Euler incremental procedure with tangent stiffness reset at every stage was initially suitable, with the full NR method then used for final convergence. The cable forces resulting from such an anlysis are generally excessively high and must then be modified by adjustment of member slack lengths, with equilibrium regained by further NR iteration. This process may be repeated as often as desired, with the end result representing the chosen compromise between geometric and force distribution requirements. A uniform mesh net will, however, not have been obtained and this must be generated on the model surface using the techniques of Argyris and Scharpf (8) or Knudson and Nagy (105).

Schek (154) has imposed additional constraints on the linear force densities method to effect control over member forces or lengths as required. The linear solution of the initial specified force densities $\{q_o\}$ acts as the starting point for the subsequent adjustments. Since member end coordinates, and hence lengths, are functions of the force densities of the assembly these t constraints may be expressed vectorially:

$$\{g\}\left(\{q\}\right) = 0 \qquad (4.11)$$

These equations are nonlinear, and a solution is then sought for:

$$\{q'\} = \{q_o\} + \{\Delta q\} \qquad (4.12)$$

such that:

$$\{g\}\left(\{q'\}\right) = 0$$

Then if the iterations to solution are linearised:

$$\{g_.\}\left(\{q_o\}\right) + \frac{\partial\{g\}\left(\{q_o\}\right)}{\partial\{q\}}\{\Delta q\} \qquad (4.13)$$

which can be expressed in matrix form:

$$[G]^T\{\Delta q\} = \{r\} \qquad (4.14)$$

where $[G]^T$ is a (t x M) matrix. Since the number of members M is frequently greater than the number of conditions t, these equations have (M - t) linearly independent solutions. A single solution may then be sought by a least squares minimisation. Schek suggests the solution of the (t x t) equation system:

$$[G]^T[G]\{k\} = \{r\} \qquad (4.15)$$

for $\{k\}$ and hence $\{\Delta q\}$, where:

$$\{\Delta q\} = [G]\{k\} \qquad (4.16)$$

This has the effect of minimising $\{\rho\}^T\{\rho\}$ for the equation system:

$$[G]\{k\} = \{r`\} + \{\rho\}$$

where $\{r\} = [G]^T\{r`\}$, which may be rewritten:

$$[G]^T\{\Delta q - \rho\} = \{r\} \qquad (4.17)$$

on premultiplication by $[G]^T$ and substitution for $\{\Delta q\}$ from equation (4.16). Schek has indicated that the solution of equation (4.15) has the effect of minimising $\{\Delta q\}^T\{\Delta q\}$, whilst the above analysis suggests that is the lack of fit of $\{\Delta q\}$ for the increment that is being minimised in order to optimise the path to $\{q`\}$.

The force densities may then be incremented (equation (4.12)) and the iteration repeated until satisfactory convergence has been achieved. Schek derives the submatrices of $[G]$ for geodesic, constant length, and elastically controlled members, and suggests several weighted least squares procedures with improved convergences over the basic method.

Barnes (21) has successfully applied Dynamic Relaxation with viscous damping to a wide range of tension structue formfinding problems. The rapid initial convergence of the method makes it suitable for both initial form and final convergence studies, with realistic constructional restraints applied at all stages. In addition the dynamic nature of DR enables ongoing adjustment of design parameters without the need to reinitialise the analysis,

which, coupled with its relatively small computer storage requirements, makes it a very suitable method for interactive computer aided design of tension structures.

No report has been made of the application of gradient minimisation techniques to the calculation of cable structure pretension geometry. Buchholdt has indicated verbally that convergence has only been obtained successfully when the initial geometry and tensions closely approximate the eventual equilibrium state. This may be a consequence of several factors. Convergence of the gradient methods depends on the true equilibrium state being located at the bottom of the 'valley' of the total potential energy surface on the side of which lies the starting point of the analysis. This is the case when a load analysis commences from the pretension state, but may well not be so for the initial data of a shape finding analysis and its associated lack of equilibrium. The implementation of geodesically controlled members requires continuously variable, fictitious, member stiffnesses for the assessment of strain energy. As a consequence the potential energy surface is itself continuously variable, and no advantage can be made of the conjugate gradient method as information from the previous descent direction is no longer relevant. A reversion to the steepest descent method is then necessary, an approach that has given either very slow or no convergence for conventional load analyses.

7.2 *Formfinding and Kinetic Damping*

The investigation of kinetic damping as a possible alternative to viscous nodal damping for the control of Dynamic Relaxation was first considered when investigating hanging chain models for the shapefinding of lattice shells. The form of these structural mechanisms being dependent solely upon the funicular equilibrium of member forces and deadweight loading. It had been noted that viscous damping proved less efficient for this problem than when applied to self-equilibriating tensile systems because of the sensitivity of the lattice structure to mechanical deformations and also because of gross initial out of balance forces (20).

Subsequent investigations reported in this thesis have established kinetic damping as an efficient and automatic control on Dynamic Relaxation for a wide range of problems. Of particular relevance to interactive numerical formfinding is the ability of kinetic damping to cope successfully with significant local modifications to the structure without violent propagation of this disturbance throughout the structure. Thus a structure may be readily updated during formfinding without the need to return to the initial problem data.

In reference (20) the shapefinding of a small star-shaped lattice shell was utilised as an example to illustrate the method. The initial configuration of the problem is shown in figure 7.1. The uniform net is initially flat, with member lengths of 1.0, except for those elements connected to boundary point nodes. Initial out of balance forces were set by specifying all member strain

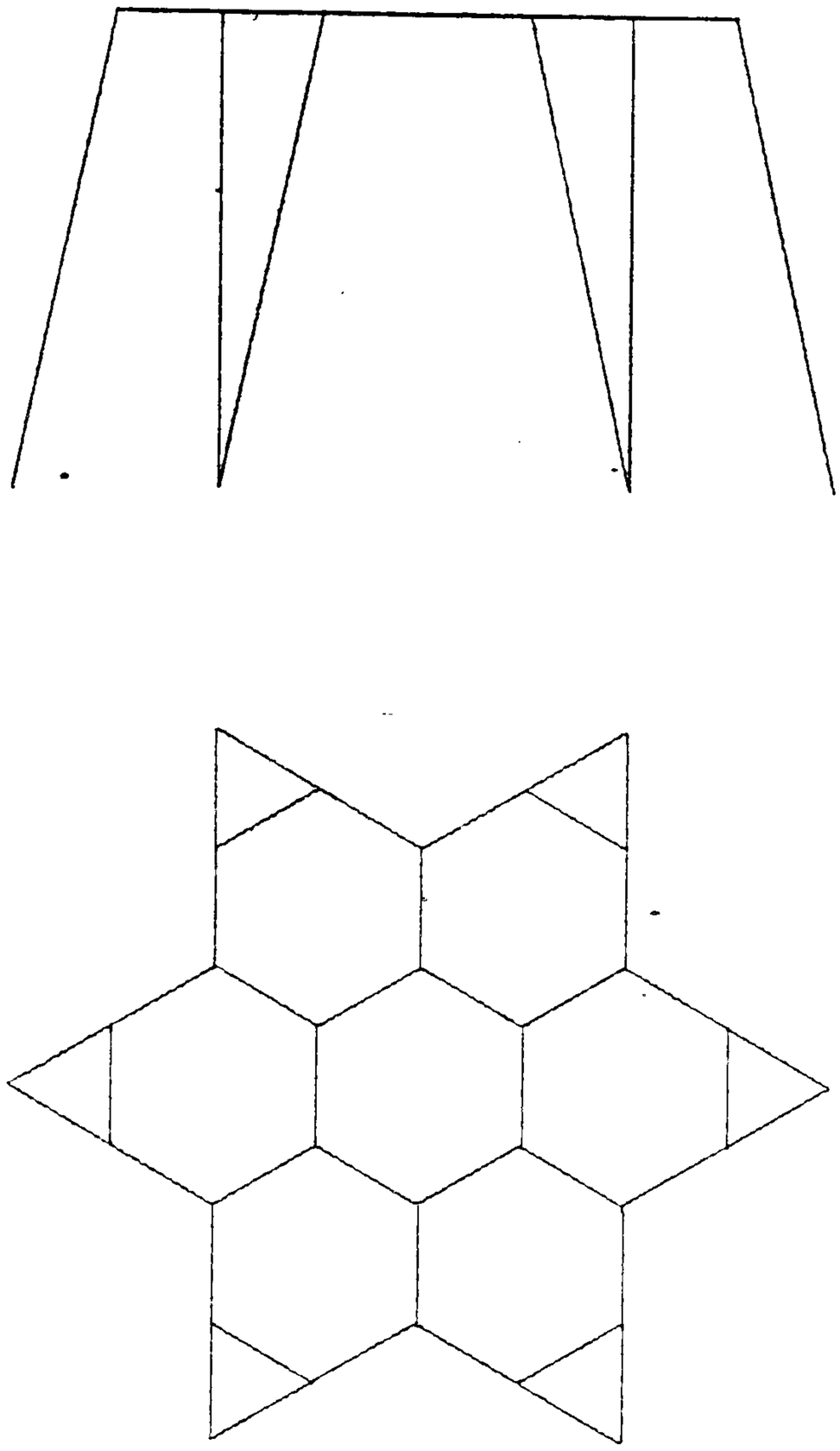

Figure 7.1

free lengths to be 1.2, thus inducing compressive forces in the surface members and tensile forces in the boundary links, whose initial length is approximately 3.4 times the slack length. An EA value of 10^6 was specified for all members, and vertical loads of 100 were applied at all surface nodes.

The progression of the analysis may be seen in figures 7.2a to 7.2e, showing the form at energy/coordinate reset stages 1, 2, 3, 5 respectively, and in the converged state. The numbers of iterations to each stage and the current kinetic energy value are tabulated in table 7.1. The figures illustrate how readily the form is obtained, with a close approximation to the final state being obtained after only a few reset stages. The smooth path to convergence presented here may be contrasted with that shown in reference (20). The revised method of kinetic damping achieves the desired form both more rapidly and more smoothly.

Results are also given in table 7.1 for a repeat of the analysis with the flat net initially 100.above the boundary points rather than 4.. The method is shown to be capable of controlling out of balance forces of the order of 10^5 times the converged member forces, with no apparent bounds upon any further increase of this factor.

7.3 Formfinding and Analysis with Rigid Members

In Dynamic Relaxation investigations, line elements are readily controlled by the specification of elastic properties or

ENERGY RESET NUMBER	ITERATION	KINETIC ENERGY	ITERATION	KINETIC ENERGY
1	2	.66e08	3	.65e11
2	5	.16e08	5	.20e11
3	10	.38e07	9	.64e10
4	12	.22e06	11	.14e09
5	16	.85e05	14	.30e08
10	41	.25e02	35	.37e04
20	537*	.20e-03	-	-
24	-	-	655*	.86e-06
INITIAL CONFIG'N	$Z_i = 4.$		$Z_i = 100.$	

* convergence to max. residual force = 0.1

Table 7.1 : Analysis Profile for Formfinding of Star-shaped Lattice Shell

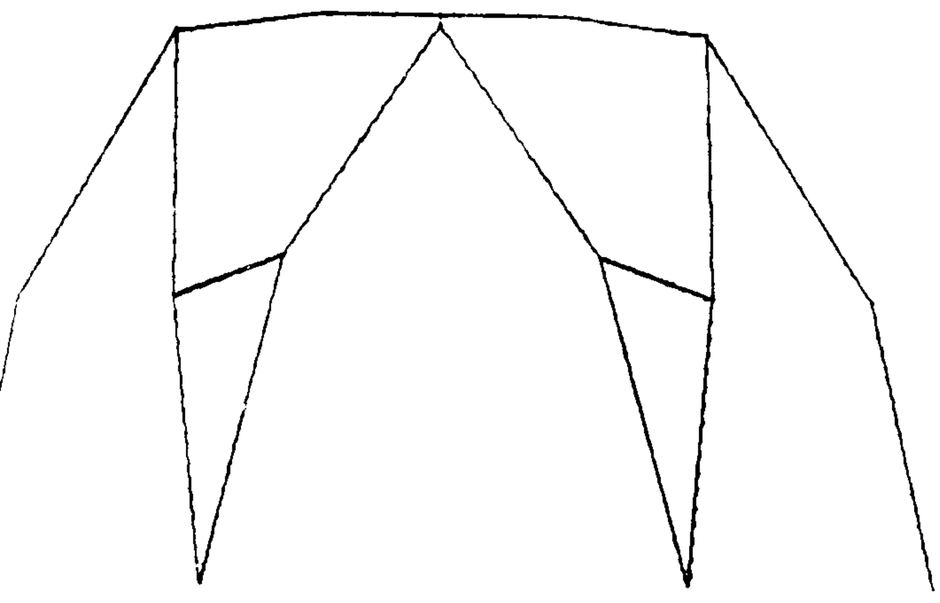

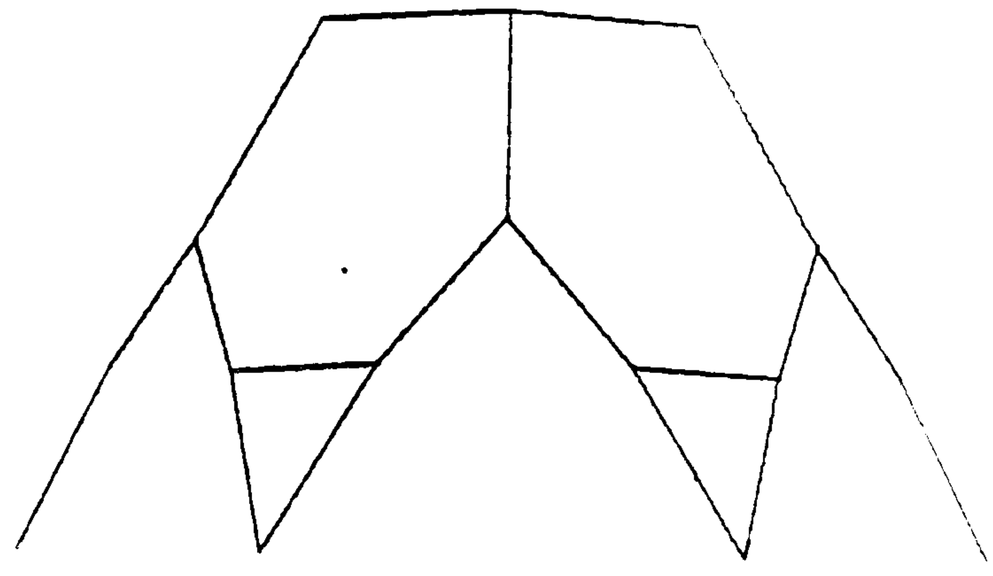

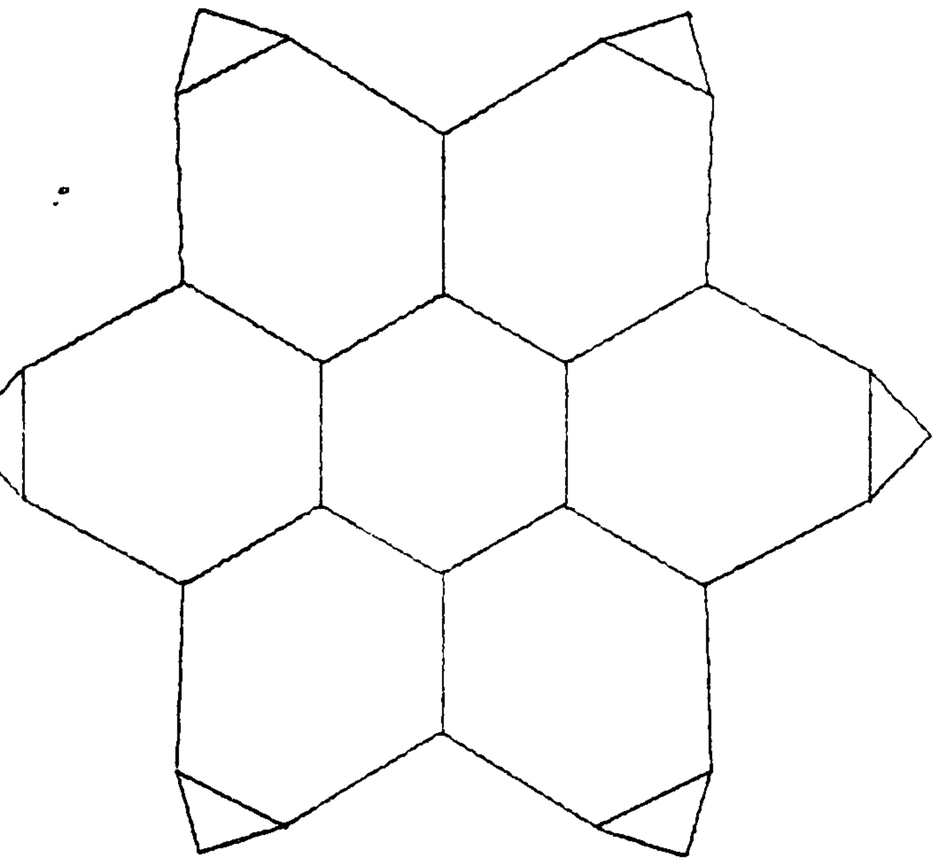

(a)

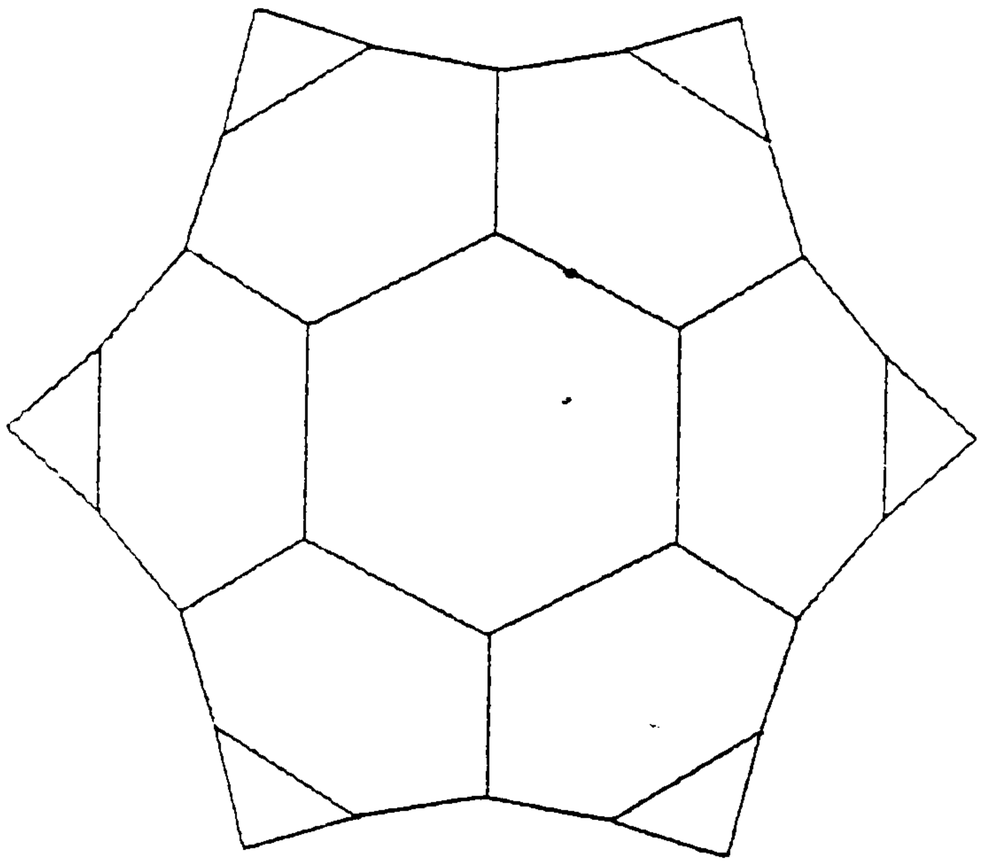

(b)

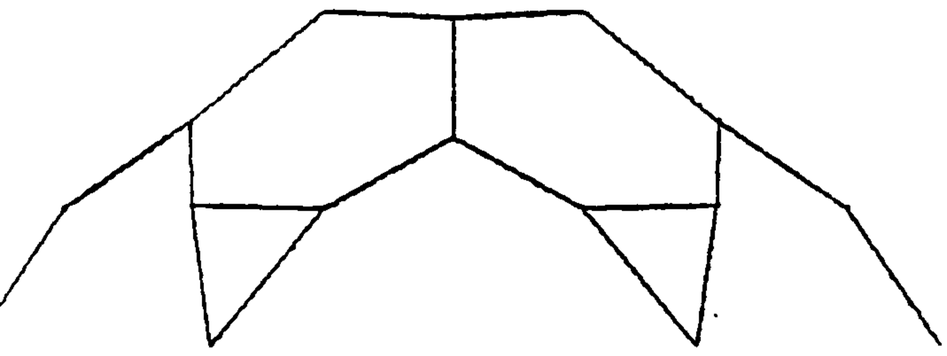

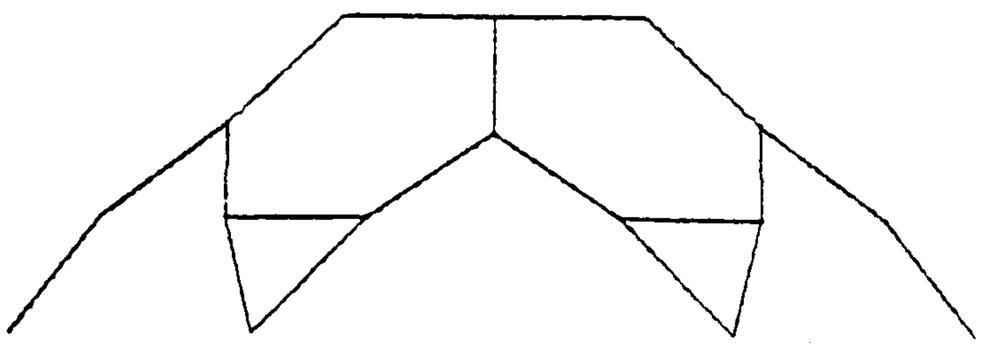

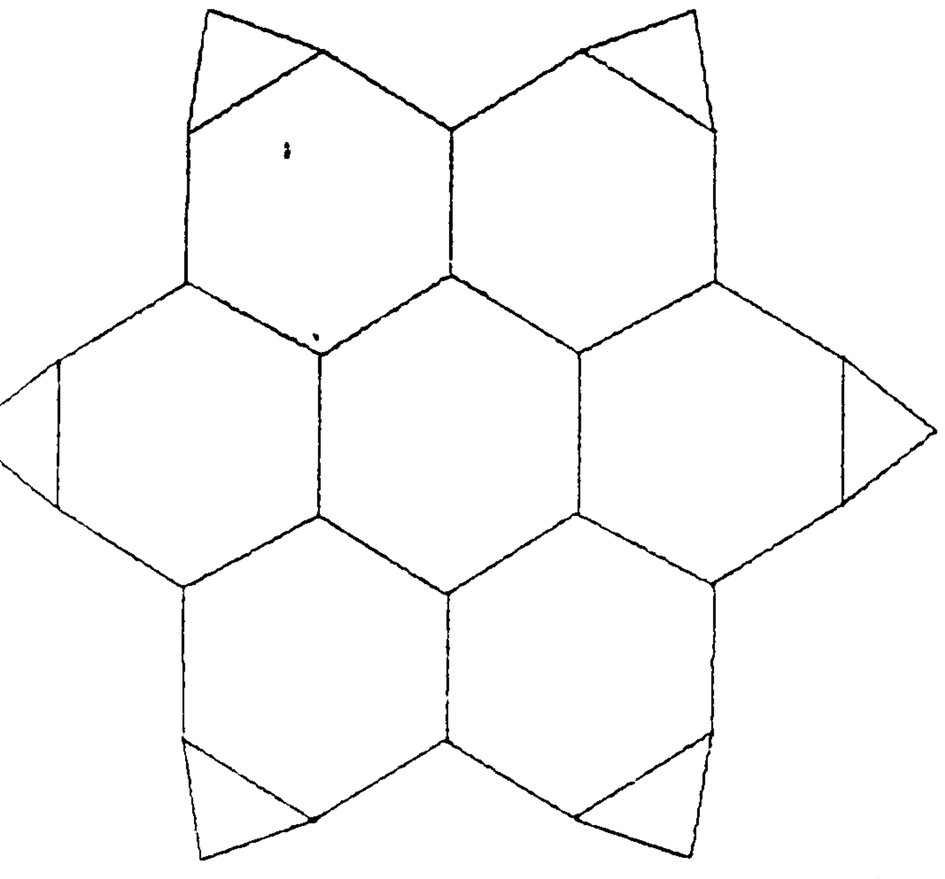

(c)

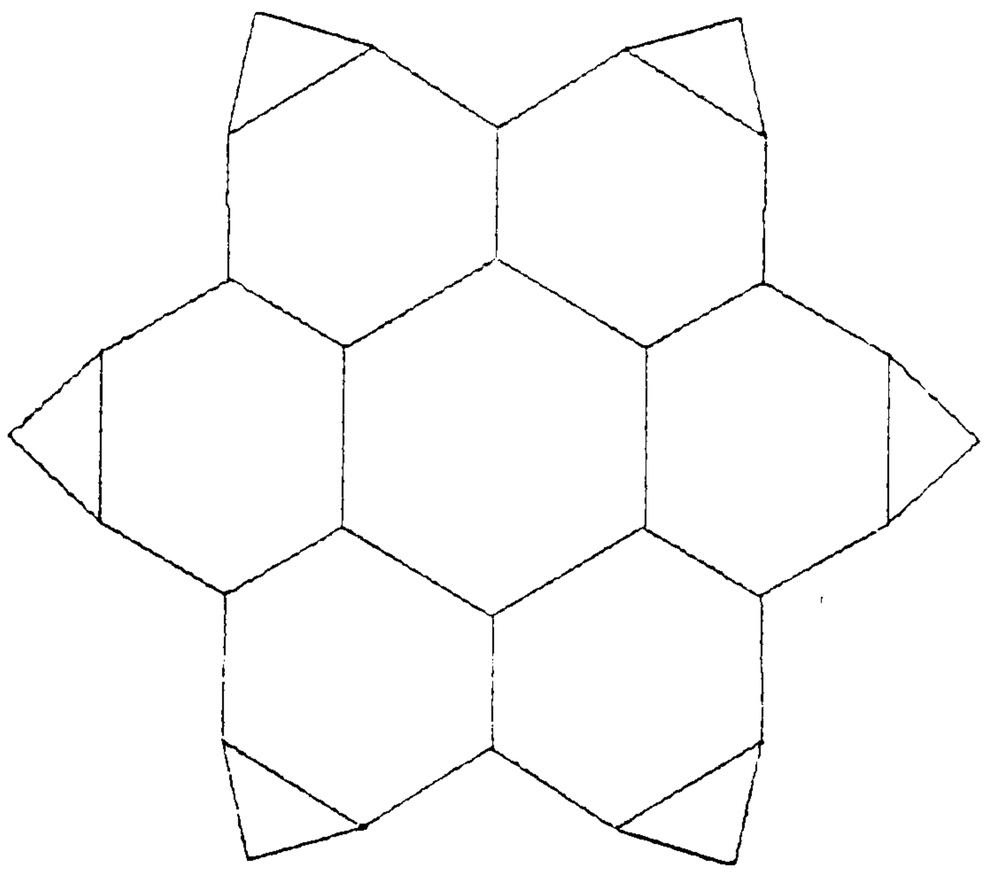

(d)

Figure 7.2

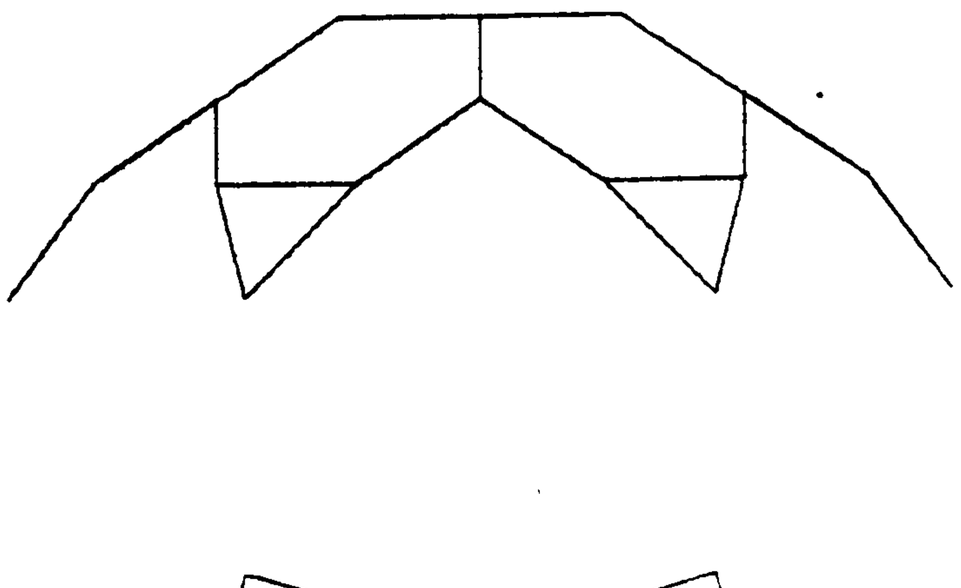

(e)

Figure 7.2

constant forces. The prime variables for formfinding, however, are those of force and length, with member properties frequently unknown at this stage.

Specified member lengths may be achieved by the use of a very high member stiffness, thus achieving a stressed length that is as close as desired to the required value. When the stiffness of such members is much greater than others in the structure, then the increased nodal masses necessary to ensure stability of the numerical integration for a given time interval will reduce the funadamental frequency of the overall structure and hence also the rate of convergence of the analysis. This problem may arise in both analysis (cable girders with short, rigid, struts) and formfinding to a required member length. Barnes (14) proposed a force transfer procedure for the treatment of stiff members, but this was limited in application by the need for over-critical viscous damping to ensure convergence.

A simple alternative approach may be considered for a line element, of slack length L^o, having current length L^t and force F^t defined by:

$$F^t = \frac{EA}{L^o} (L^t - L^o) \qquad (4.18)$$

Then if the required stressed length of the member is L^R, the slack length should be updated such that:

$$L^o \rightarrow L^o + L^R - L^t \qquad (4.19)$$

Any value of member elastic property EA may be employed, and for convenience this may be selected as approximately equal to the stiffness of adjacent elastically or geodesically controlled members, with the effect of reducing the convergence time of the analysis.

It then remains to determine the optimum frequency for the slack length reset of equation (4.19). Instability will occur if this reset occurs at every stage of the integration, and as final convergence is based upon the attainment of a specified maximum nodal residual, R_{max}, then it would seem logical to reset slack lengths when all residuals are less than $\gamma . R_{max}$, where $\gamma \geqslant 1.0$. Optimum values of γ between 1 and 50 have been obtained for differing problems. Table 7.2 shows the numbers of steps to final convergence for the formfinding of the hypar network described in figure 7.3. Although it is not possible to give a general rule as to the selection of the optimum γ factor, it has been found that $\gamma = 1.0$ gives consistently good solution times.

7.4 Formfinding and Compression Contours

The formfinding of purely tensile surface structures may readily be achieved by both physical and numerical modelling techniques. Physical methods are, however, less suitable when considering moment free compression contours, because of the inherently unstable nature of such structures. When derived under dead loading conditions, such contours provide the basic form for efficient rigid boundary structures.

γ FACTOR	ITERATION STEPS TO FINAL CONVERGENCE
1	151
5	164
10	196
20	131
25	131
50	214
100	NO CONVERENCE BY 500

Table 7.2 : Effect of Slack Length Reset Factor, γ, on Convergence of Hypar problem

HYPAR PROBLEM INITIAL DATA

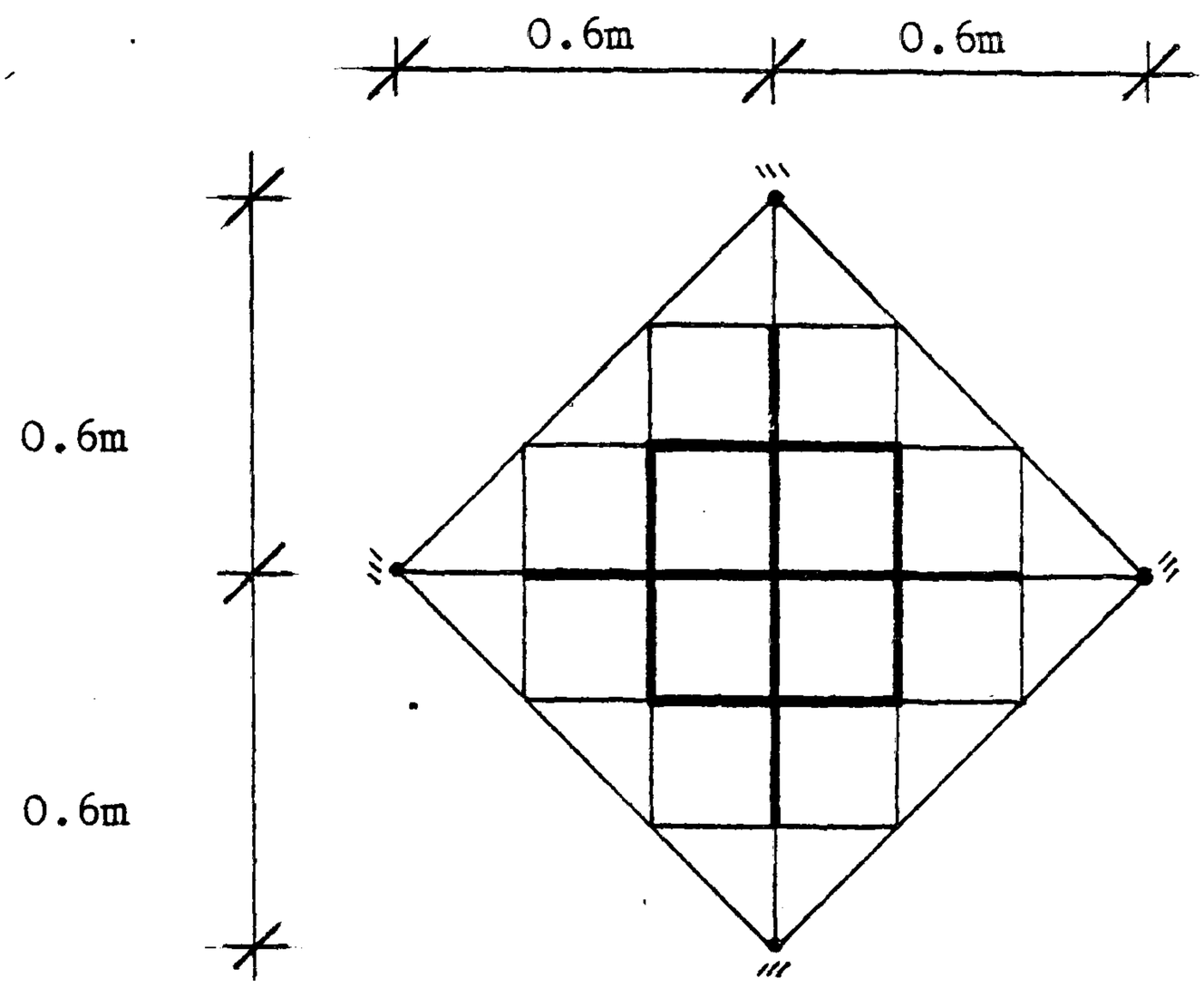

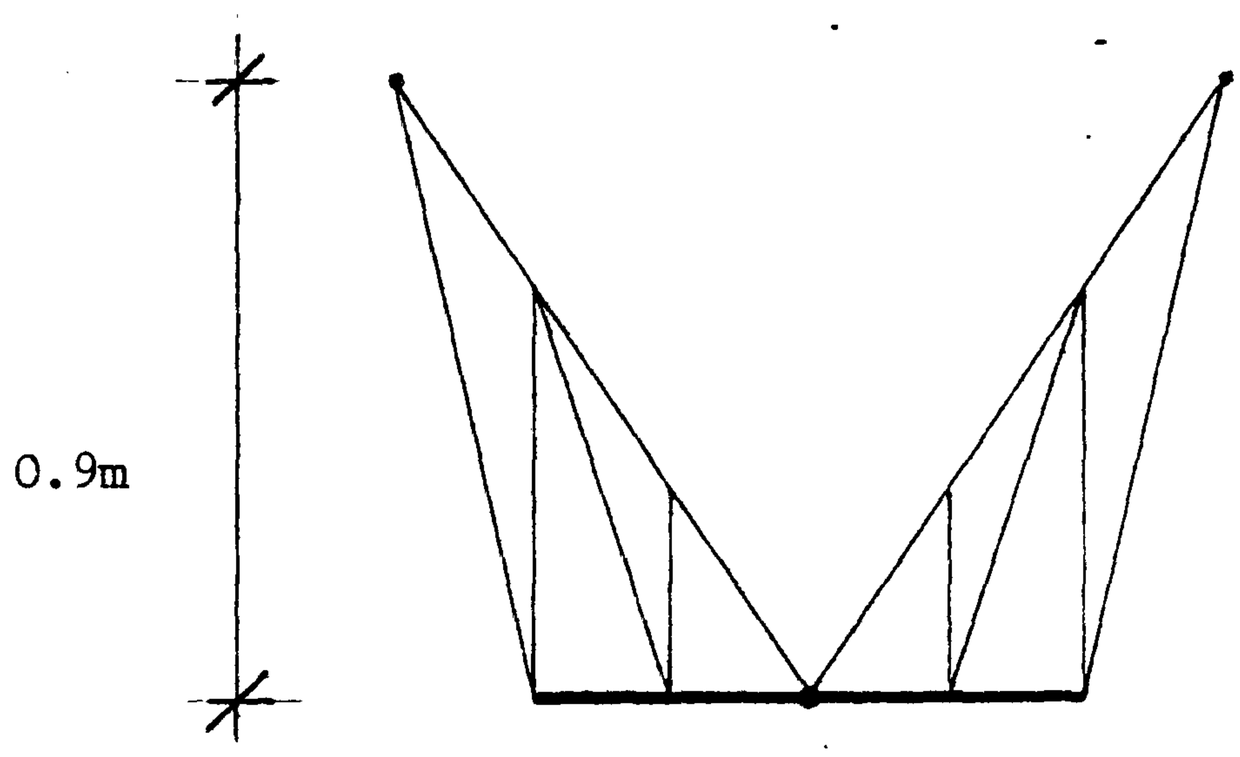

TIME INTERVAL: $\Delta t = .0014$

EDGE CABLES: EA = 0.2 MN

10 kN CONSTANT FORCE IN MIDDLE CABLE OF EACH EDGE

SURFACE CABLES: ——— CONSTANT LENGTH CABLES (0.2M)

REMAINING SURFACE CABLES HAVE CONSTANT FORCE OF 0.5 kN

NODAL MASSES: EDGE NODES - M_x, M_y, M_x = 1.0

SURFACE NODES - M_x, M_y = 0.6, M_z = 0.5

Figure 7.3

If, in the standard Dynamic Relaxation formfinding process, constant compressive forces are specified in edge links then the structural system will always become unstable. As a simple example of this instability consider the segment of a pin-jointed boundary structure shown in figure 7.4a, with specified compressive forces C_1 and C_2 and a tensile force T exerted by the surface structure upon the boundary node A. The equilibrium state is that shown in figure 7.4a, whilst figure 7.4b shows the boundary node A moved a distance δz from that state. This results in a nett out of balance force acting upon node A in the same direction as the movement δz, which in turn induces further motion in that direction. Convergence towards the equilibrium state is not, therefore, possible for such a system of specified forces as these.

Barnes (21) has shown that, in order to derive moment-free compression contours, the boundary must be determined as a tension funicular to the reflected image of the surface structure. This is achieved by assigning either negative stiffness or negative member force to the edge links, and by reversing the sign of boundary node residual forces at every stage of the analysis. As in the case of a tensile loop, a compressive outer boundary may only be controlled by specified compression forces provided that at least one element of that boundary is elastically controlled. The stable and convergent reflected equivalent of the example of figure 7.4b is shown in figure 7.4c. The treatment of specified length compression boundary members is identical to that outlined in the above section for tensile elements.

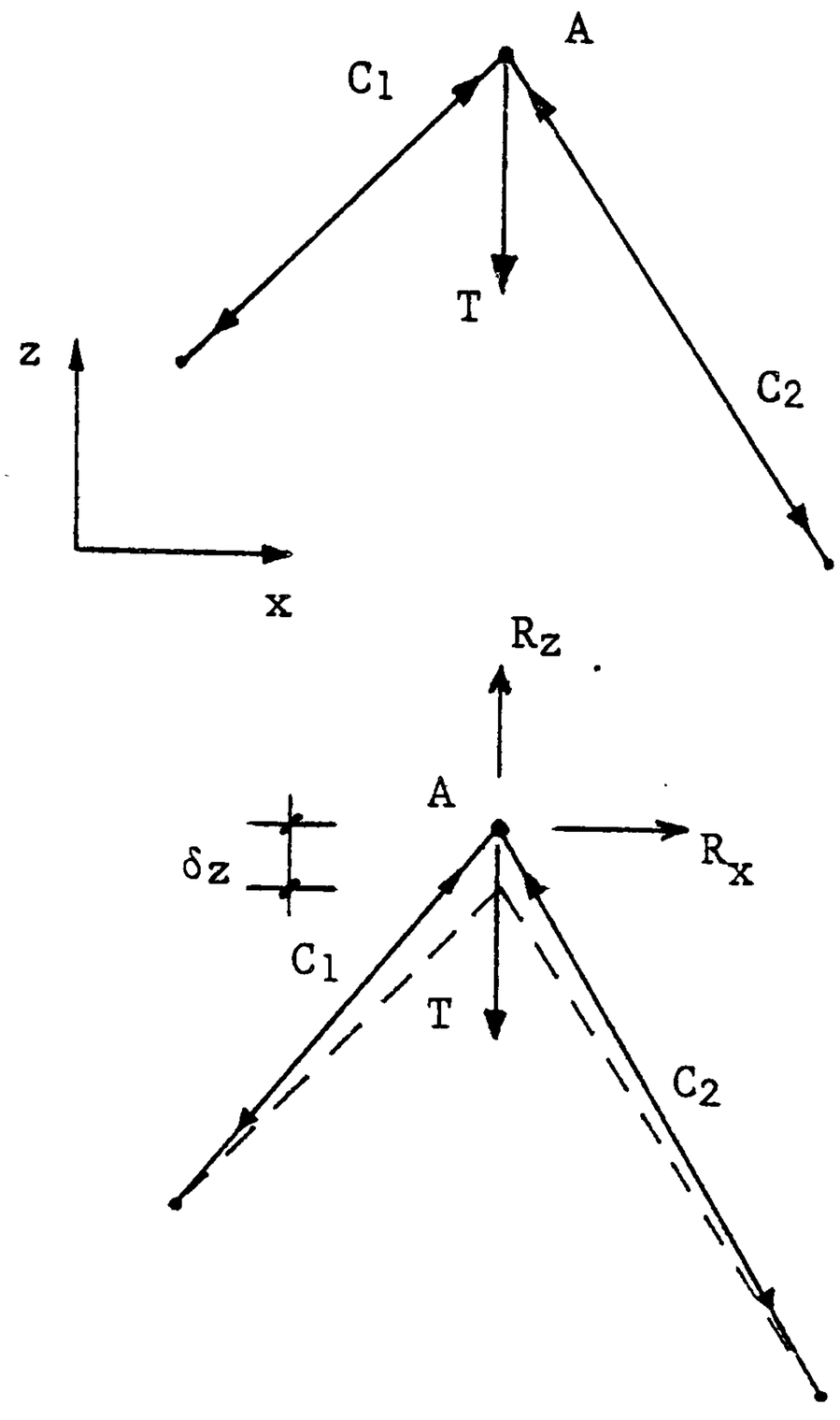

Figure 7.4

Planar and spatially curved moment free compression contours have been derived by Barnes (18) as external boundaries to surface structures defined by constant stress membrane elements. Variation in the radius of boundary curvature was achieved by the introduction of traction forces in order to generate a force gradient in edge links. In practice such traction forces might be resisted by shear walls following the boundary contour.

Figure 7.5 shows a mesh for the investigation of a compression arch within a diagonal pretensioned network. The mesh assumes an axis of symmetry along the arch members, numbered 1 to 12. The slack length of these arch members, having EA = 1000 000., are set equal to 5.5, and all cable elements have an assigned constant force = 100.. With all nodes having an initially zero vertical coordinate, the formfinding sequence depicted in figures 7.6a to 7.6d was initiated by resetting the vertical coordinate of the arch central node to 2.0. A moment-free compression arch stabilised within a pretensioned network results, and, utilising this as starting data, the effect of increasing the specified boundary element lengths may be seen in figures 7.7 and 7.8 .

By returning to the initially flat net, and then resetting two non-zero vertical coordinates (z_{25} = 2.0 and z_{29} = -2.0) an alternative equilibrium state is obtained, as shown in figure 7.9 . The basic structural data has not been changed, only the starting point of the analysis. Although the state shown has converged fully, the equilibrium state achieved is not stable and the application of any assymetric loading will precipitate a partial snapthrough to the more stable configuration derived initially.

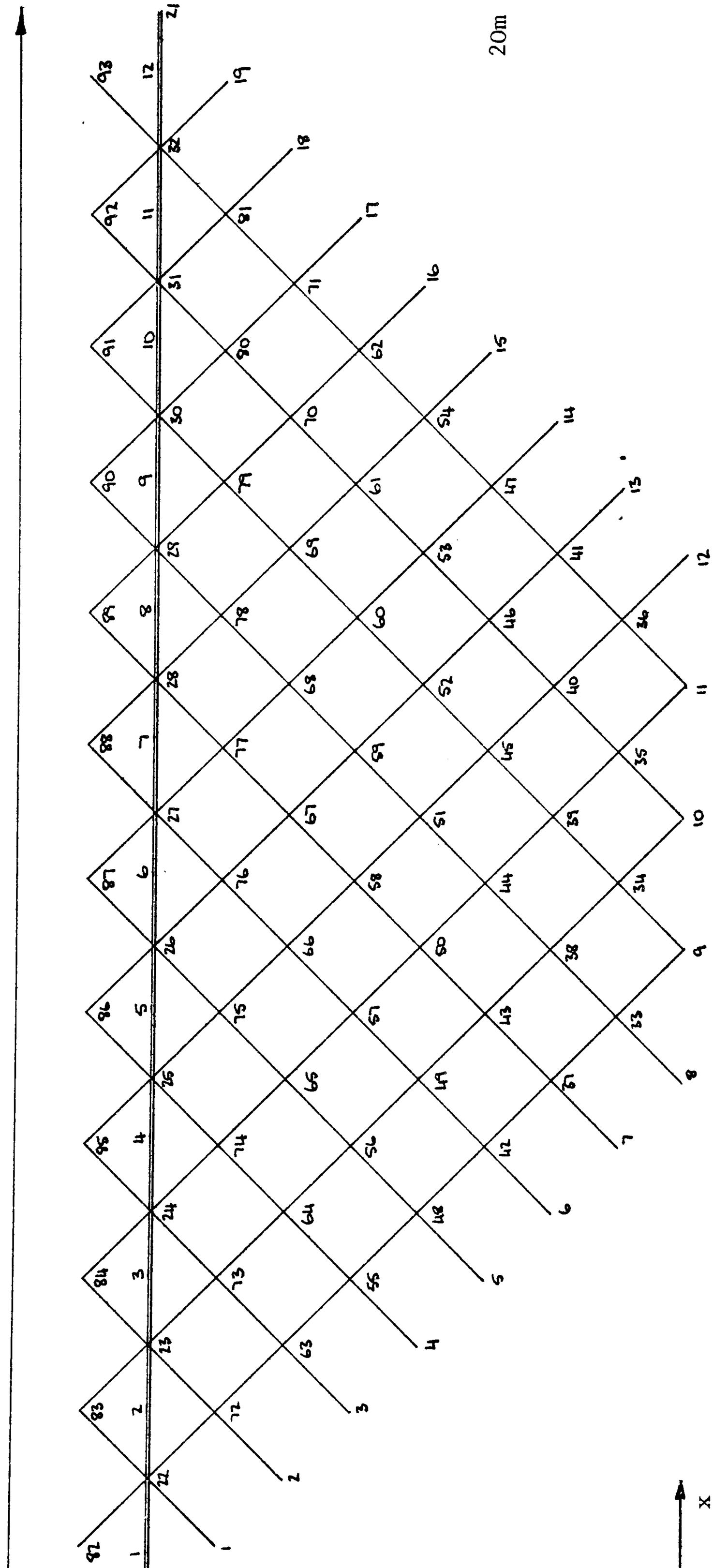

Figure 7.5

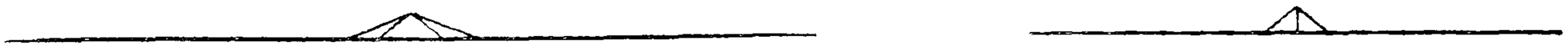

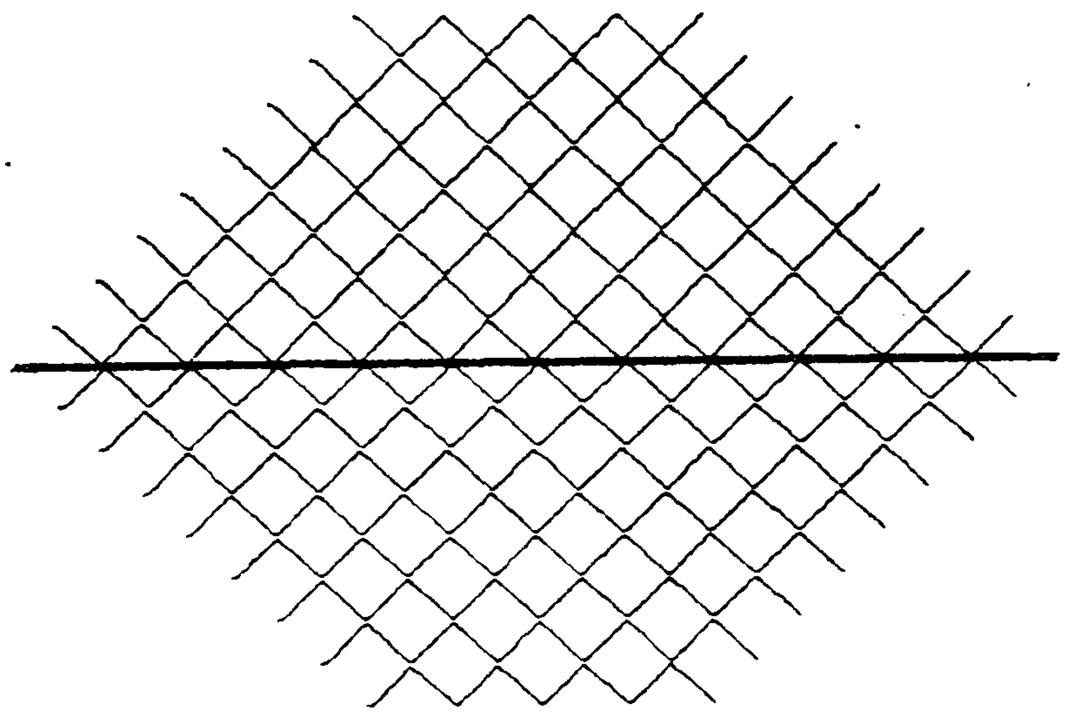

INITIAL STATE

Figure 7.6 (a)

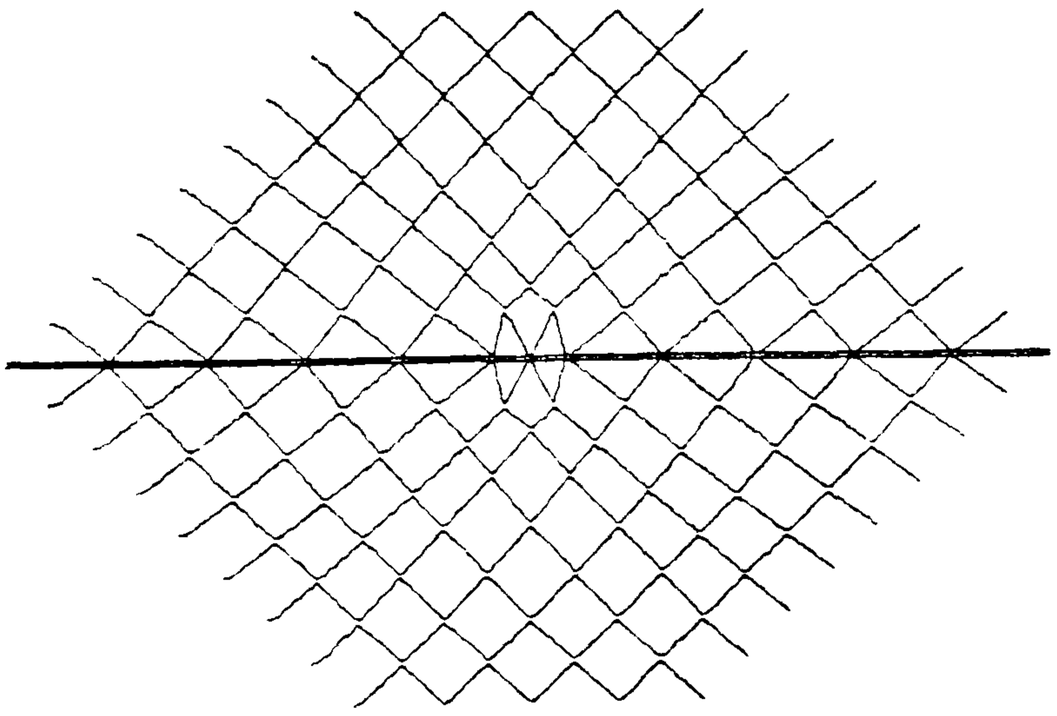

ENERGY RESET 1

Figure 7.6 (b)

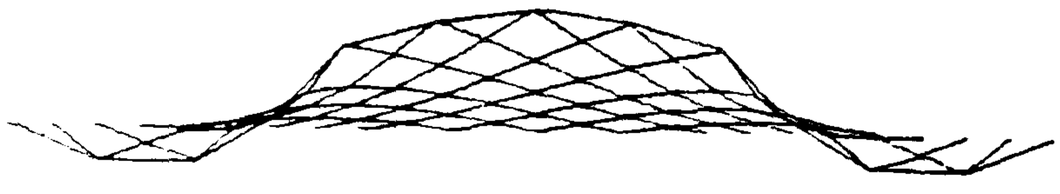

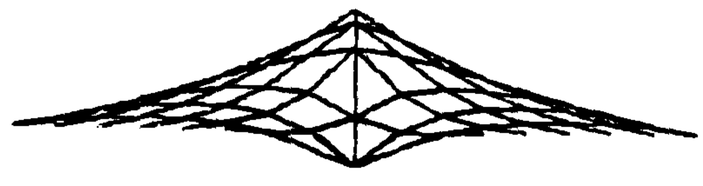

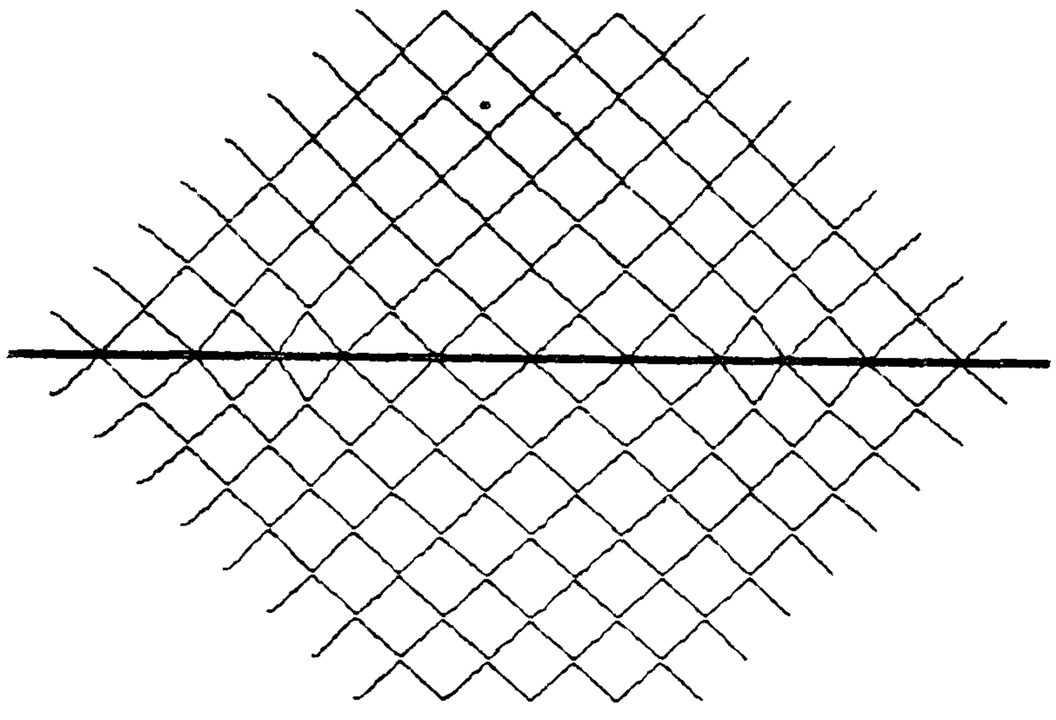

ENERGY RESET 3

Figure 7.6 (c)

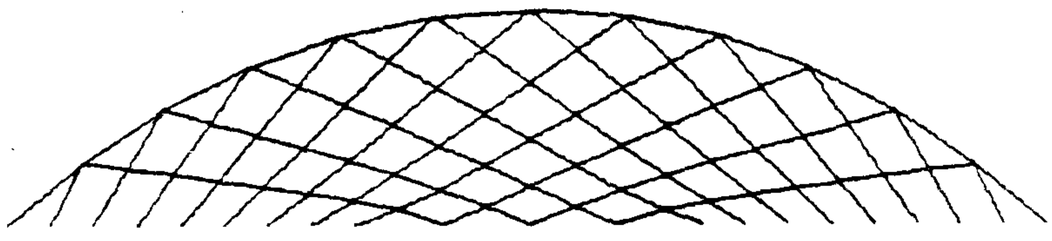

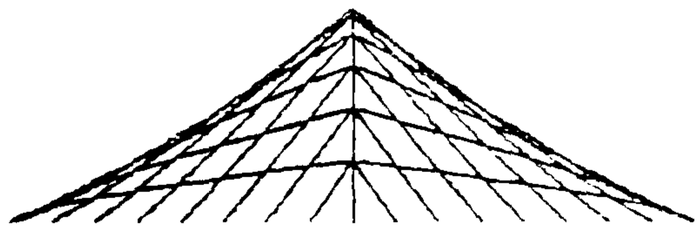

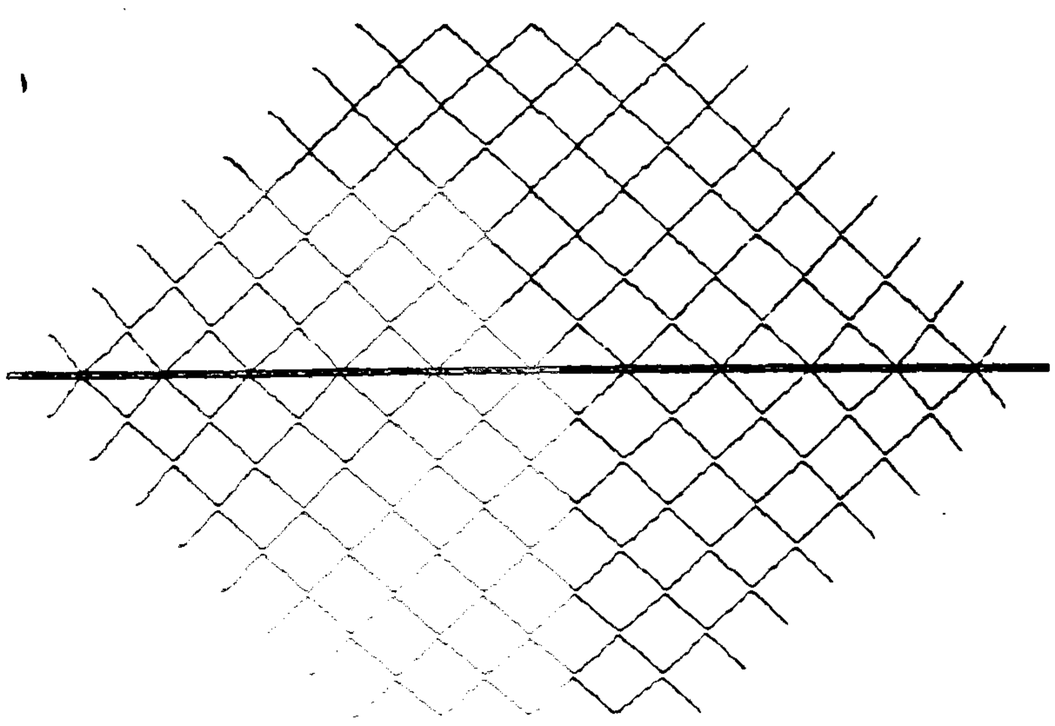

CONVERGED STATE

Figure 7.6 (d)

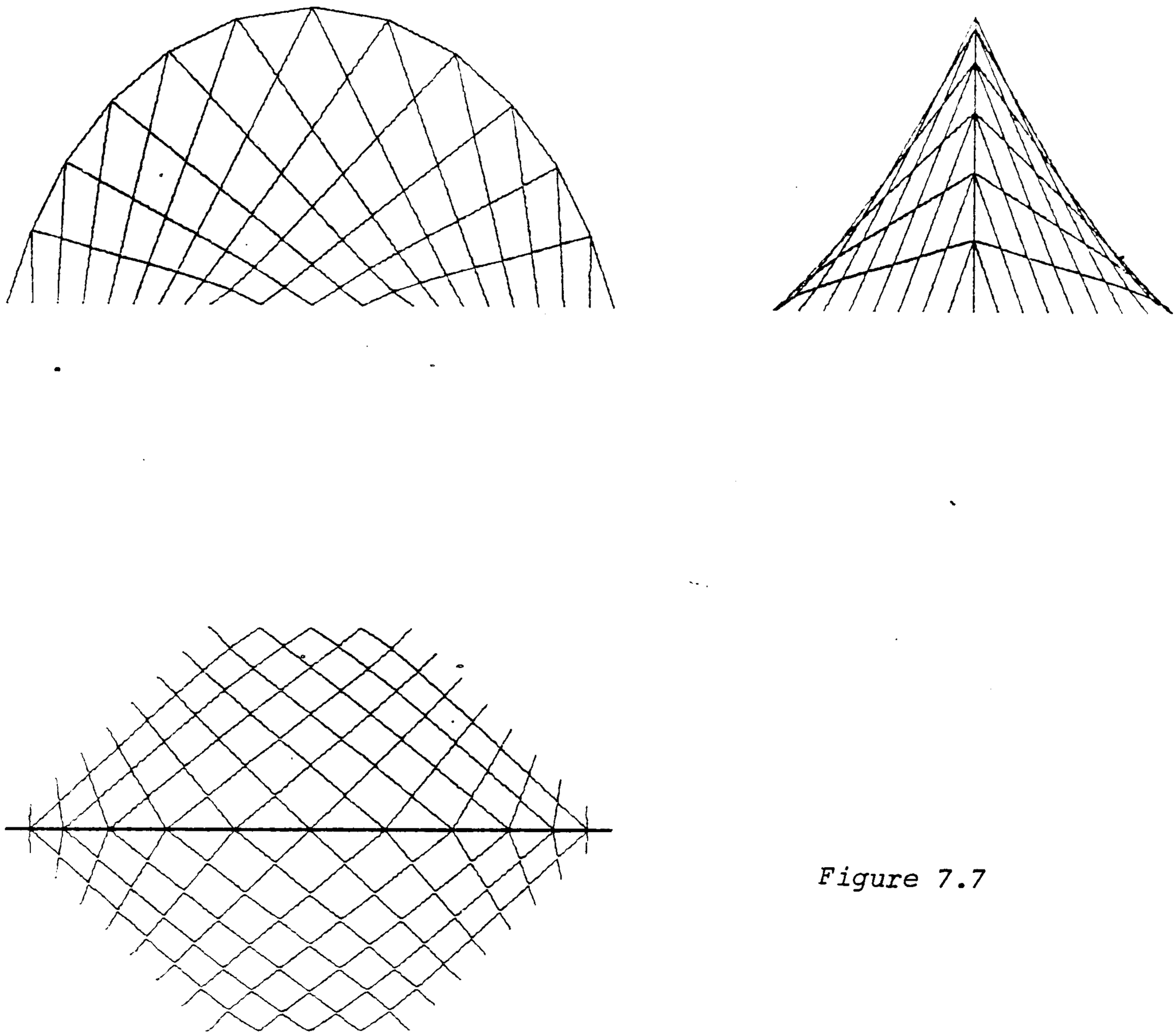

Figure 7.7

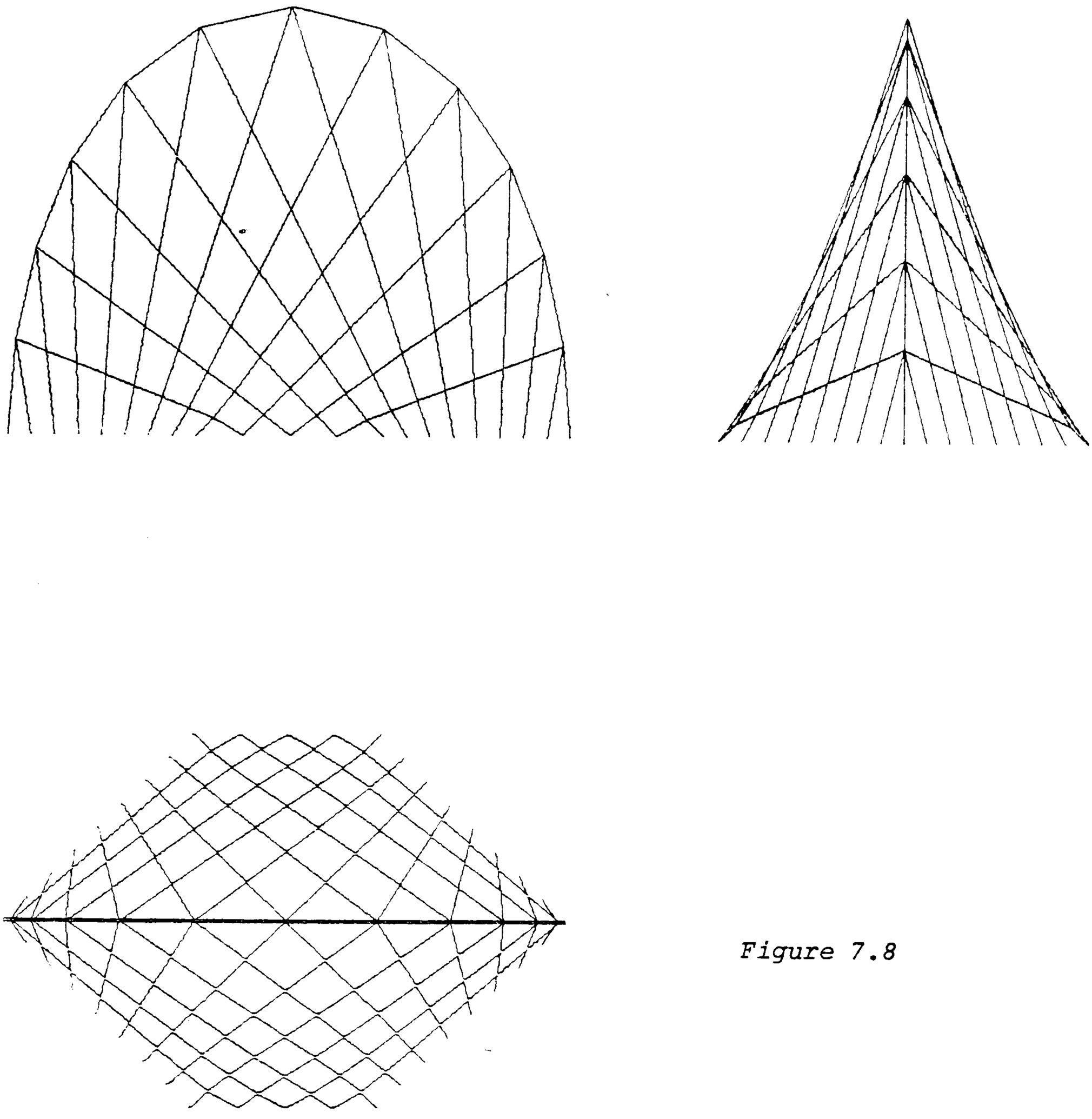

Figure 7.8

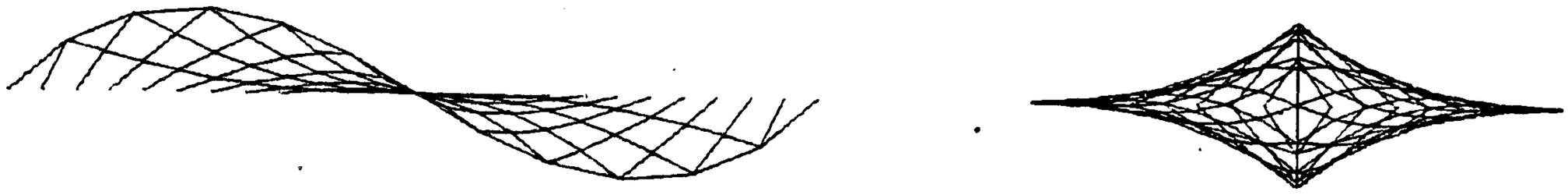

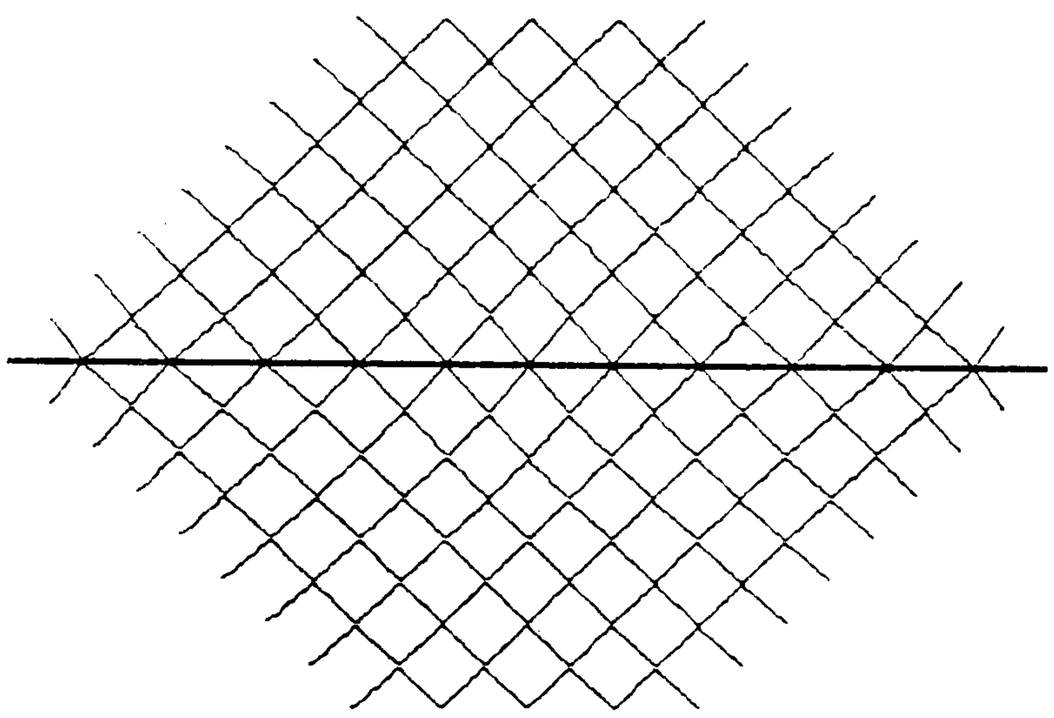

Figure 7.9

In addition to the formfinding investigations above, in which a moment-free contour has been derived, rigid jointed boundary elements may be specified for a compression contour of known geometry and properties and the pretension configuration determined for the complete structure. Again using the mesh outlined in figure 7.5 , with a 12.5m high parabolic arch idealised by spatial flexural elements, the initial data for such a problem is given in figure 7.10. For a 25 kN specified force in all cable elements, and all surface nodes initially flat, satisfactory and rapid convergence to the equilibrium position of figure 7.11 was achieved. A subsequent increase of pretension to 100 kN in all cables proved less straightforward. By energy reset number 11 the arch appears visually converged, and the kinetic energy value has fallen steadily to that stage. The number of steps to reset 12 is then greater than the total required to reach stage 11, and the kinetic energy shows an increase in value. After this stage the next energy peak has yet to be detected after 1500 iterations. The reason is illustrated by figures 7.12a to 7.12c which show the intermediate form at 500, 1000 and 1500 iterations respectively. Snapthrough buckling of the encastre arch has occured, and this collapse after apparent convergence illustrates the importance of utilising nodal residuals as the final proof of convergence.

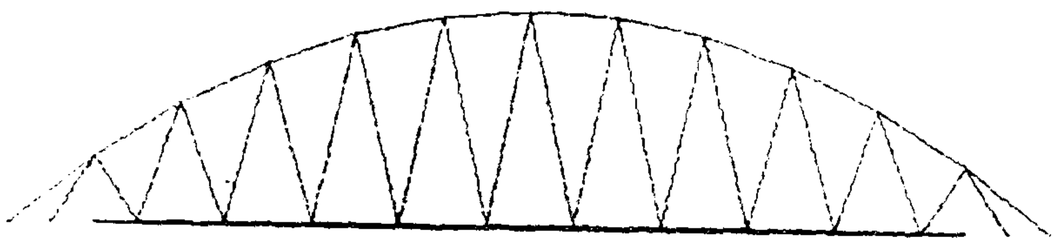

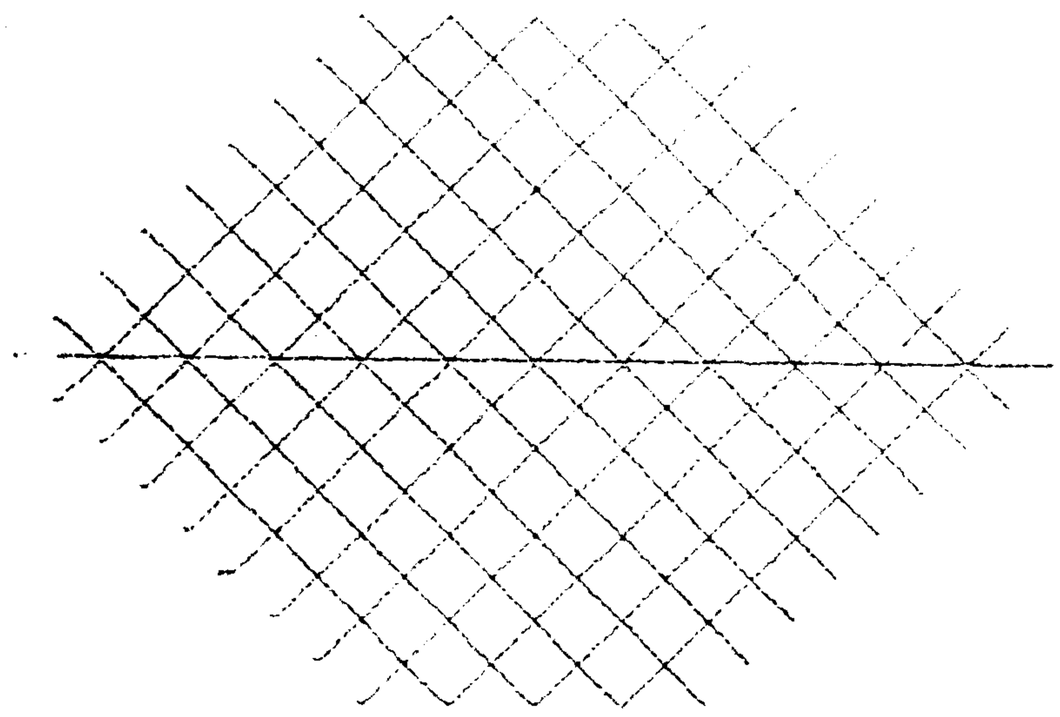

ARCH PROBLEM: INTIAL STATE

ARCH PROPERTIES: EA = 3 628 000

$EI_y' = EI_z' = 67\ 340$

GJ = 12 954

Figure 7.10

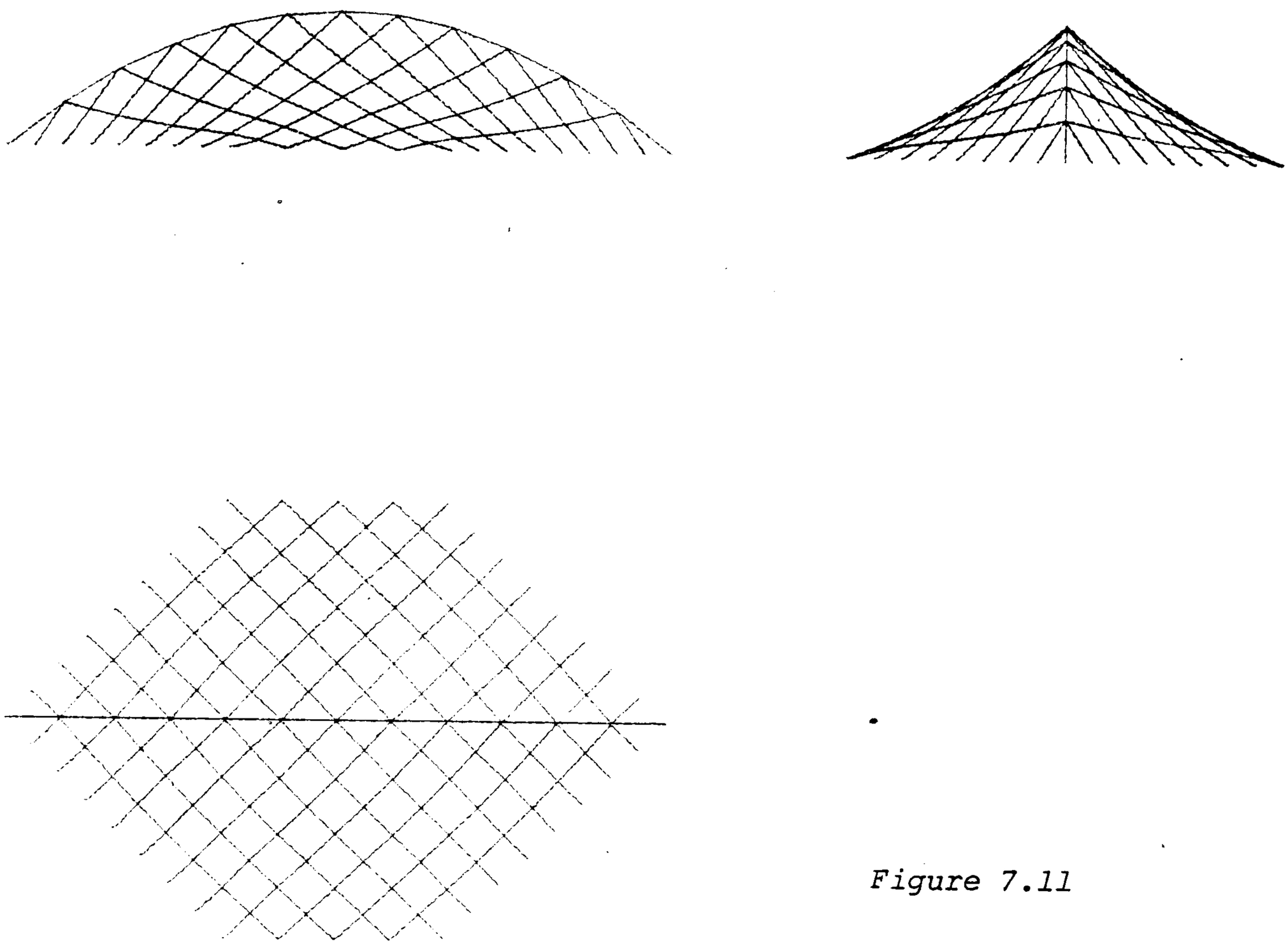

Figure 7.11

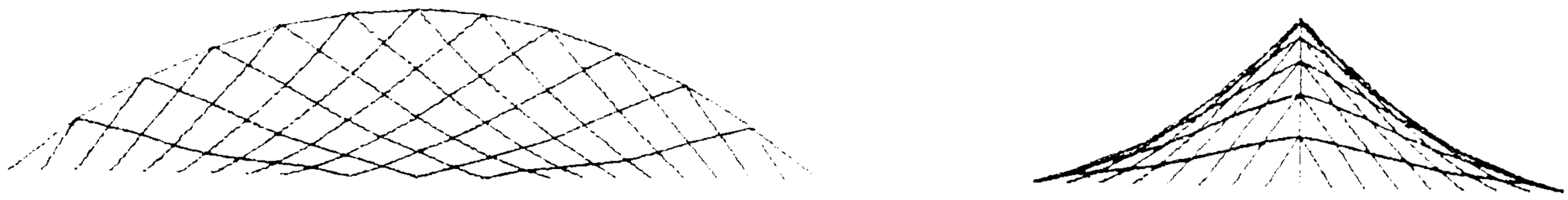

Figure 7.12 (a)

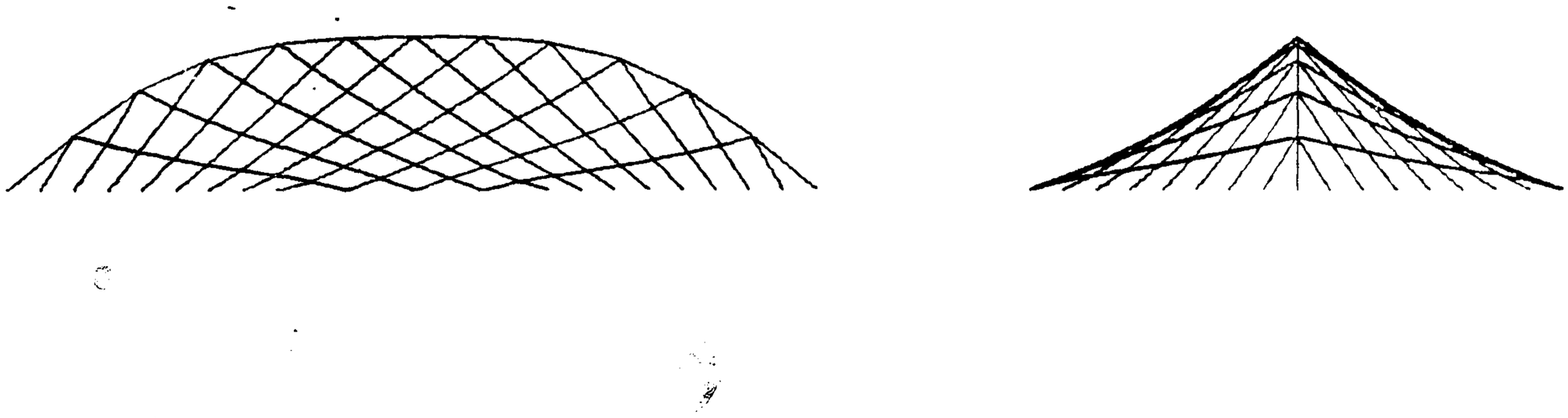

Figure 7.12 (b)

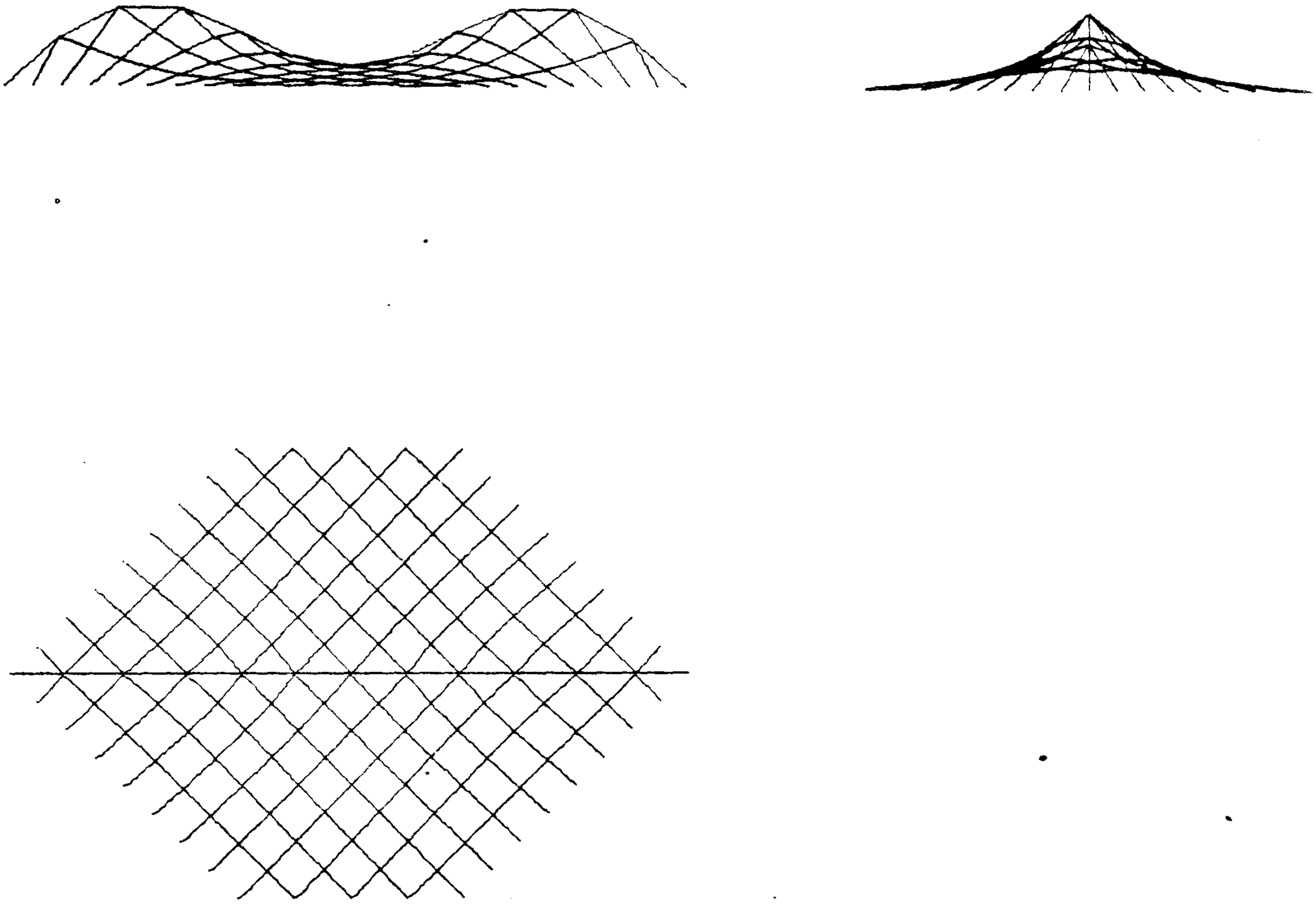

Figure 7.12 (c)

7.5 *Summary*

The first section of this chapter reviews the development of linear and non-linear techniques for numerical formfinding. Dynamic Relaxation with viscous nodal damping has been successfully applied by Barnes (21) to the formfinding of a wide range of problems. Conjugate gradient analysis, the other explicit integration method widely utilised for the analysis of network structures, is, however, fundamentally unsuited for formfinding because of its inability to cope with significant out of balance forces.

In section 7.2 an example is given of kinetic damping control of formfinding by DR for a hanging chain network whose form is dependent upon the funicular equilibrium of member forces and deadweight loading. In particular this analysis combination is shown to converge rapidly and satisfactorily when some initial member forces are of the order 10 greater than their final converged values. There appear to be no bounds on this ability to control out of balance forces.

The elastic and geodesic control of members is well established, and a simple technique for the treatment of specified length members is considered in section 7.3. This technique is equally applicable in increasing the rate of convergence of analyses involving members that are extremely stiff, such as struts in cable beams.

The generation of moment-free compression arches is demonstrated in section 7.4. Alternative, stable, forms are derived

from the same basic data by varying only the initial coordinates of the analysis. Formfinding of the pretension geometry is then illustrated with the boundary structure idealised by spatial flexural elements. In one example the collapse of an internal arch, idealised in this way, after apparent convergence emphasises the importance of utilising nodal residuals as the only reliable proof of convergence.

CHAPTER 8

ANALYSIS OF PRETENSIONED NETWORKS WITH FLEXIBLE BOUNDARIES

The Dynamic Relaxation analyses for network and rigid-jointed structures presented in preceeding chapters are here combined for the unified analysis of the complete structure. Previous approaches to this problem are reviewed and a generalisation of the gradient method to include non-linear boundary structures is outlined. The explicit Dynamic Relaxation and Scaled Conjugate Gradient methods are then applied to published planar and saddle-shaped network problems.

8.1 *Introduction*

The use of compression boundary structures to support pretensioned networks has become increasingly popular, enabling the construction of large span tensile structures without the need for tension anchorages. The spatially curved boundary structures, circular in plan, of the Scandinavium in Gothenburg (101), 108 m in diameter and the Milan Palasport (153), 130 m diameter, are examples of this trend.

Møllmann (122 and Samuelli-Ferretti (153) have noted that the flexibility of the support system must be taken into account in analysis of the structure, as the differences in results between flexible and rigid boundary analyses are sufficient to negate the use of the latter even for initial, approximate, calculations. The tension system provides elastic support to the boundary structure, enabling the use of slender compression members. Consequently the analysis of the complete structure should include the effects of both finite boundary displacements and non-linear moment-curvature relations for the boundary elements.

An implicit finite element displacement analysis for the complete structure has been proposed by Møllmann (122). The derivation of the stiffness relations for the flexural member in space was based upon the natural stiffness/basic strain expressions, which were subsequently transformed into the global coordinate system with the addition of sufficient degrees of freedom to define rigid-body movement. It was, however, assumed that boundary

displacements were small, and the effect of axial force on the bending stiffness was neglected. This latter assumption was made on the grounds that any improvement in accuracy was questionable because of approximations made in the treatment of torsion and the neglect of torsion/flexure interaction. Samuelli-Ferretti and Zingali (153) have, however, reported minimal effects of torsion on the analysis of structures of this class, and Møllmann himself noted the need for examination of the stability of the support structure.

A mixed method of analysis was also outlined by Møllmann (123), in which it was assumed that cable strains were small, as were the horizontal components of surface node displacements in comparison with their vertical counterparts. Good agreement was reported between the results of the finite element mixed and displacement formulations. A mixed finite element approach was also adopted by Kärrholm and Samuelsson (101), who considered the cables and their support system to be separate sub-structures which were analysed alternately.

Buchholdt, Das and Al-Hilli (42) extended the conjugate gradient method to include the analysis of linear boundary structures, and the details of this work are reviewed in Chapter 2. Scaling of the potential energy surface was introduced to facilitate convergence of this ill-conditioned problem, and favourable solution times were reported in comparison with the Newton-Raphson approach. Buchholdt (43) has used this method for a parametric study of the effect of the main design variables (curvature, ring-beam stiffness,

cable size and magnitude of pretension) on the behaviour of circular saddle-shaped nets with flexible boundaries. He concluded that economy in design and structural efficiency for this type of structure were achieved by shallow curvatures, slender ring beams and high pretension in the cables. Stability effect, however, clearly play an important role in the analysis of such structures.

8.2 Explicit Analysis of the Complete Structure

Analysis of the combined tensile system and rigid-jointed boundary structure may be readily achieved by Dynamic Relaxation. The full non-linear analysis of rigid jointed spatial structures presented in Chapter 6 requires minor modifications to permit the inclusion of cable elements. The principles of optimisation of nodal masses and application of kinetic damping remain unchanged. The developed program is equally applicable to formfinding, as discussed in the preceeding chapter.

In the conjugate gradient approach to the analysis of the complete structure (42) it was assumed that the behaviour of the boundary structure was linear. This assumption is not, however, essential, and details for the inclusion of non-linear boundary response are presented here.

The strain energy, U, of a structural element or assemblage of elements having a current displacement $\{\delta\}$ from a

reference state, and internal reactions $\{R\}$ to that displacement, is equal to the work done in moving from the reference to the current state and may be written:

$$U = -\int_{0}^{\{\delta\}} \{R\} \cdot d\{\delta\} \tag{8.1}$$

where the negative sign is due to the opposing sense of $\{R\}$ and $\{\delta\}$.

For a linear structure:

$$\{R\} = -[K]\{\delta\} \tag{8.2}$$

and, on substitution into equation (8.1) and integration, one obtains:

$$U = \frac{1}{2}\{\delta\}^T[K]\{\delta\} \tag{8.3}$$

For non-linear analysis by the conjugate gradient method it is assumed that the element tangential stiffness matrices of the assembly are updated periodically as the analysis proceeds in a series of linearised steps.

Consider then the current reaction $\{R\}$ due to displacements $\{\Delta\delta_j\}$ relative to the displacement state $\{\delta_j\}$ when the tangent stiffness was reset to $[K_j^*]$:

$$\{R\} = \{R_j\} - [K_j^*]\{\Delta\delta_j\} \tag{8.4}$$

where $\{R_j\}$ are the reactions associated with $\{\delta_j\}$. For the current strain energy, U, then:

$$U = U_{j-1} + \Delta U_j \tag{8.5}$$

and:

$$\Delta U_j = -\int_0^{\{\Delta\delta_j\}} \{R\} \; d\{\Delta\delta_j\}$$

$$= -\{R_j\}^T\{\Delta\delta_j\} + \frac{1}{2}\{\Delta\delta_j\}^T\left[K_j^*\right]\{\Delta\delta_j\} \tag{8.6}$$

The tangent stiffness matrix for a full non-linear analysis may be updated at each step of the gradient analysis, or less frequently. As is the case with the modified Newton-Raphson method, the latter will probably prove to be the more efficient approach.

Although there is apparently no inherent difficulty in including non-linear boundary response in a conjugate gradient analysis, the subsequent investigations presented in this chapter all assumed a linear response. The initial, unstressed, stiffness matrix was used throughout, with displacements $\{\delta\}$ measured from that unstressed state, although the pretension geometry was utilised to provide initial coordinate data for the load analyses. In this way it was intended that the numerical significance of the two alternatives be seen, and comparisons of computation times be made between the simplest conjugate gradient and most complex DR formulations.

8.3 Numerical Example: Planar Network

Figure 8.1 shows a flat rectangular network within a flexible boundary having full translational (but not rotational) restraints at the four corner nodes. This problem was investigated both numerically and experimentally by Al-Hilli (2). All cable elements are subject to a pretension of 889.6 N, with cable intersections clamped together after this initial tensioning. A uniform out of plane loading is then applied at these intersections.

The following analyses of this problem have been performed:

(i) Dynamic Relaxation formfinding analysis with non-linear beam element idealisation of the boundary and all cable forces held constant at 889.6 N (utilising the mesh of Figure 8.1),

(ii) Scaled Conjugate Gradient linear analysis of the boundary structure along, with nodal loads of 889.6 N applied in the direction of the cable members,

(iii) Dynamic Relaxation analyses of the pretensioned network subject first to 30 N and then 20 N loads applied at all network nodes (utilising the equilibrium state from state (i)) as initial data),

(iv) Scaled Conjugate Gradient analysis of the network as for (iii) above.

RECTANGULAR NETWORK PROBLEM

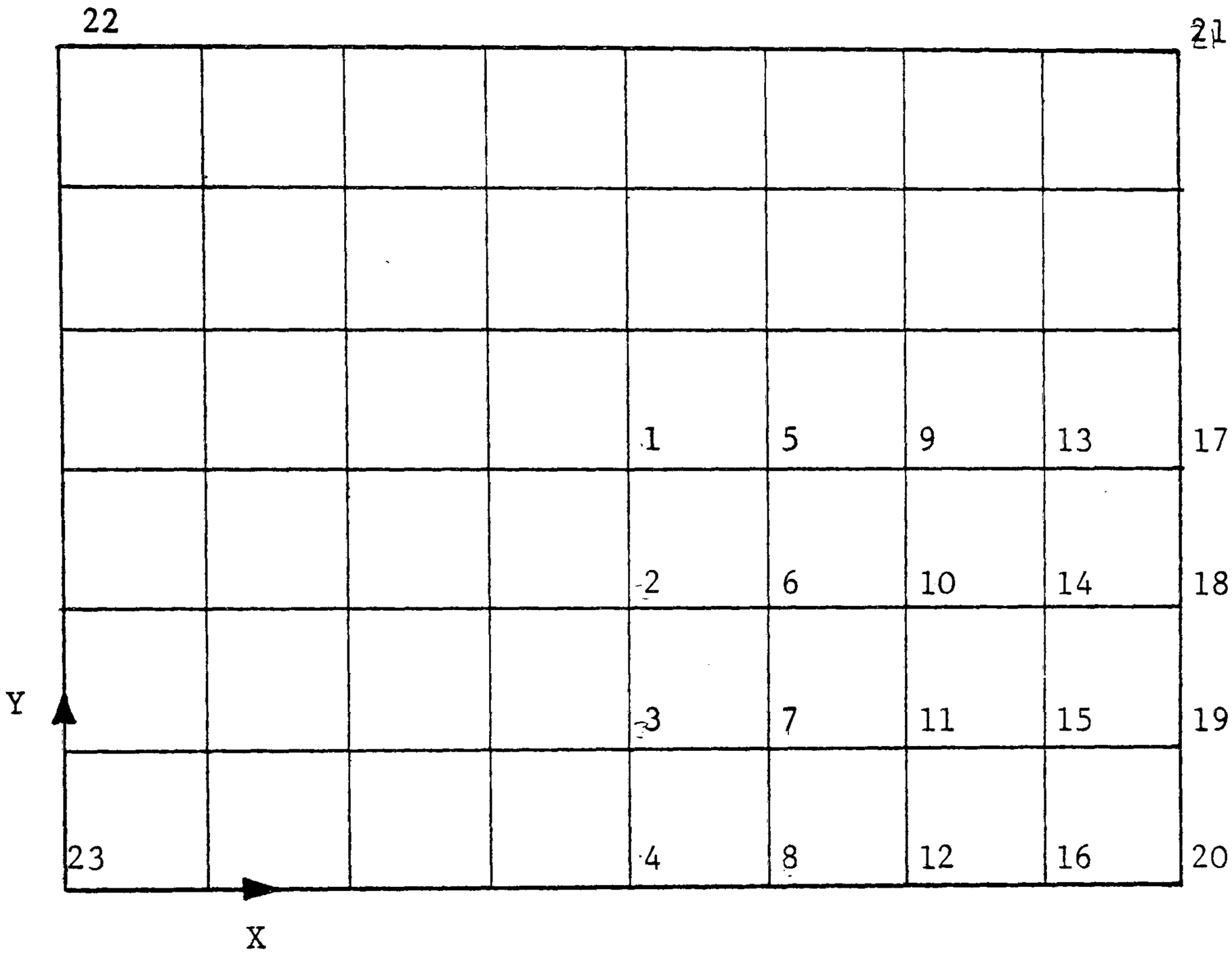

ALL MEMBER INITIAL LENGTHS = 0.5

MEMBER PROPERTIES:

EDGE BEAM:
$A = 17.06\ cm^2$
$E = 20.076 \times 10^6\ N/cm^2$
$I_{z'} = 50.37\ cm^4$
$I_{y'} = 477.0\ cm^4$
$J = 3.29\ cm^4$

CABLES:
$A = 3.243 \times 10^{-2}\ cm^2$
$E = 19.03 \times 10^6\ N/cm^2$

Figure 8.1

The Scaled Conjugate Gradient network analyses have all employed the modified polynomial coefficients derived in Chapter 4.
The analyses above have been compared with the published results of Al-Hilli:

(v) An experimental investigation of the full size structure,

(vi) Conjugate Gradient analysis, unscaled and employing Buchholdt's coefficients for the energy polynomial,

(vii) Newton-Raphson analysis.

Boundary node displacements due to pretension only in the plane of the net and normal to the edge beam are given in Table 8.1 for both the present and Al-Hilli analyses. The conjugate gradient analyses both assume a linear boundary structure, and the difference between the present SCG and Al-Hilli CG (scaled from results presented graphically) is probably due to the different degrees of convergence specified. The Al-Hilli results were deemed converged when the Euclidean norm of the residual had reduced to 1% of its value at commencement of the analysis. The present analysis, both DR and SCG, are presented for convergence of the residual force at every active degree of freedom to less than.1% of the minimum applied nodal load.

The difference in boundary displacements of up to 2 mm between the results of the present DR and SCG analyses are due entirely to the inclusion of finite boundary displacements in the inherently non-linear DR formulation, contrasting with linear boundary analysis of the SCG approach. In the latter, as the

BOUNDARY NODE	AL-HILLI		PRESENT INVESTIGATION			
	EXPT.	CG	SCG	DR	DR & REDUCED EA EA=1000	EA=10
4	1.96	1.98	2.05	1.80	2.05	2.05
8	1.76	1.79	1.85	1.63	1.85	1.85
12	1.23	1.27	1.32	1.15	1.32	1.32
16	.55	.58	.61	.53	.61	.61
17	.296	.276	.288	.181	.286	.289
18	.298	.280	.293	.197	.291	.294
19	.251	.243	.251	.192	.251	.252

Table 8.1 Boundary node displacement, in-plane and normal to the edge beam, for the pretension case. Displacements (cms) positive in the positive X and Y directions (Figure 8.1)

edge beams are initially straight, the effect of axial forces in the edge beams is ignored. For this problem, where the beam ends are restrained against translation, this catenary effect under normal loading is important, and as a consequence SCG deflections are overestimated relative to those of DR. This effect may be demonstrated by repeating the DR analyses with reduced axial stiffness (EA) values in order to simulate the SCG idealisation employed. As can be seen in table 8.1 the resultant displacements are then effectively identical. The present Dynamic Relaxation analysis predicts boundary displacements less than those reported by Al-Hilli from his experimental investigation. These latter are closer to the present SCG results, suggesting that the ball and socket arrangements used for the boundary corners in the experiments did not fully restrain the translational degrees of freedom at those nodes.

The full network structure with flexible boundary was then analysed subjected to a vertical loading of 30 N at each surface node. The results obtained for the deflection of the cable net, together with those obtained by Al-Hilli, are shown in table 8.2. The unloaded pretension form determined by DR was used for both of the present analyses.

Al-Hilli reported significant differences between his Newton-Raphson and Conjugate Gradient solutions, as may be seen from table 8.2. The present SCG analysis yields results which give very close agreement with the NR displacements of Al-Hilli. The difference between present and previous SCG analyses confirms

NODE NUMBER	AL-HILLI			PRESENT	
	EXPT.	NR	CG	SCG	DR
1	5.00	5.06	4.73	5.06	5.03
2	4.45	4.54	4.22	4.54	4.51
3	2.83	2.88	2.73	2.89	2.88
5	4.73	4.83	4.48	4.82	4.80
6	4.28	4.31	4.04	4.33	4.31
7	2.65	2.75	2.60	2.77	2.76
9	3.99	4.01	3.75	4.04	4.03
10	3.58	3.66	3.43	3.65	3.64
11	2.31	2.38	2.25	2.38	2.37
13	2.45	2.55	2.38	2.55	2.55
14	2.23	2.31	2.17	2.33	2.32
15	1.56	1.57	1.49	1.58	1.57

Table 8.2: Surface Node Displacements (cms)

- 30 N load on all surface nodes

that the utilisation of the revised polynomial coefficients presented in Chapter 4 rather than those due to Buchholdt (Chapter 2) enables full convergence to a true equilibrium solution when calbe elements are employed. The close agreement between present SCG and DR analyses suggests that the nonlinear response of the edge beam is not significant under this level of loading of the network. The catenary effect of edge beam axial forces is now included in the SCG boundary analysis as the initial beam profile is that from the pretension state. The results plotted in table 8.3 for a reduced surface load of 20 N per joint yield conclusions identical to those given above.

The in plane displacements of the boundary nodes, when all the surface nodes are subjected to the 30 N vertical load, are given in table 8.4. These displacements, normal to the edge beam, are quoted relative to the unloaded, pretensioned, state. There is close agreement between the present DR and SCG analyses and Al-Hilli's experimental results. This agreement between the former confirms the linear response of the boundary structure at this level of loading. The difference between the two Conjugate Gradient analyses again illustrates the effect of the modified energy poynomial coefficients.

NODE NUMBER	A1-HILLI			PRESENT	
	EXPT.	NR	CG	SCG	DR
1	3.50	3.54	3.33	3.54	3.53
2	3.12	3.18	2.97	3.17	3.16
3	1.97	2.02	1.90	2.01	2.01
5	3.31	3.40	3.18	3.37	3.36
6	2.98	3.02	2.84	3.02	3.02
7	1.82	1.95	1.81	1.93	1.93
9	2.81	2.84	2.68	2.83	2.83
10	2.49	2.56	2.43	2.55	2.55
11	1.60	1.68	1.58	1.66	1.66
13	1.72	1.80	1.71	1.79	1.79
14	1.59	1.65	1.55	1.63	1.63
15	1.13	1.13	1.04	1.10	1.10

Table 8.3: Surface Node Displacements (cms)

- 20 N load on all surface nodes

NODE NUMBER	AL-HILLI		PRESENT	
	EXPT.	CG	SCG	DR
4	0.10	0.07	0.10	0.10
8	0.09	0.06	0.09	0.08
12	0.06	0.04	0.05	0.06
16	0.03	0.02	0.02	0.02
17	0.039	0.022	0.045	0.045
18	0.030	0.020	0.035	0.035
19	0.011	0.013	0.011	0.012

Table 8.4: Boundary node displacements, in-plane and normal to the edge beam for 30 N vertical load at all surface nodes.
Displacements (cms) relative to the pretension state and positive in the positive X and Y directions.

8.4 Numerical Example: Saddle Shaped Structure

Figure 8.2 illustrates a pretensioned network within a spatially curved compression boundary. This problem configuration was utilised by Møllmann to demonstrate the application of the Newton-Raphson method to the analysis of the complete structure (123). A similar problem has been investigated by Buchholdt (43) who examined the effect of varying the principal design parameters on the performance and efficiency of the structure.

The reinforced concrete ringbeam is approximately circular in plan, comprising a combination of circular and parabolic segments as described in figure 8.3, with the aim of minimising boundary structure bending moments in the pretension state. The spatial coordinates of the boundary structure are defined by the intercept of a cylinder, having the plane of figure 8.3 as its section, and the surface of a hyperbolic paraboloid having a 14 m rise between its lowest and highest points. The full boundary coordinates are tabulated in table 8.5 for the unstressed state of the boundary structure. All of the 28 boundary nodes are restrained vertically, with lateral restraint imposed additionally at nodes 1 and 15 in the Y-direction and at node 22 in the X-direction. The section of reinforced concrete ringbeam twists about the perimeter such that all the beam element y -axes lie in the plane of the network surface (in its prestressed state) adjacent to that element.

The defined prestressed state is that in which all cable elements have a horizontal tension component of 260 t, whilst all

SADDLE SHAPED NETWORK

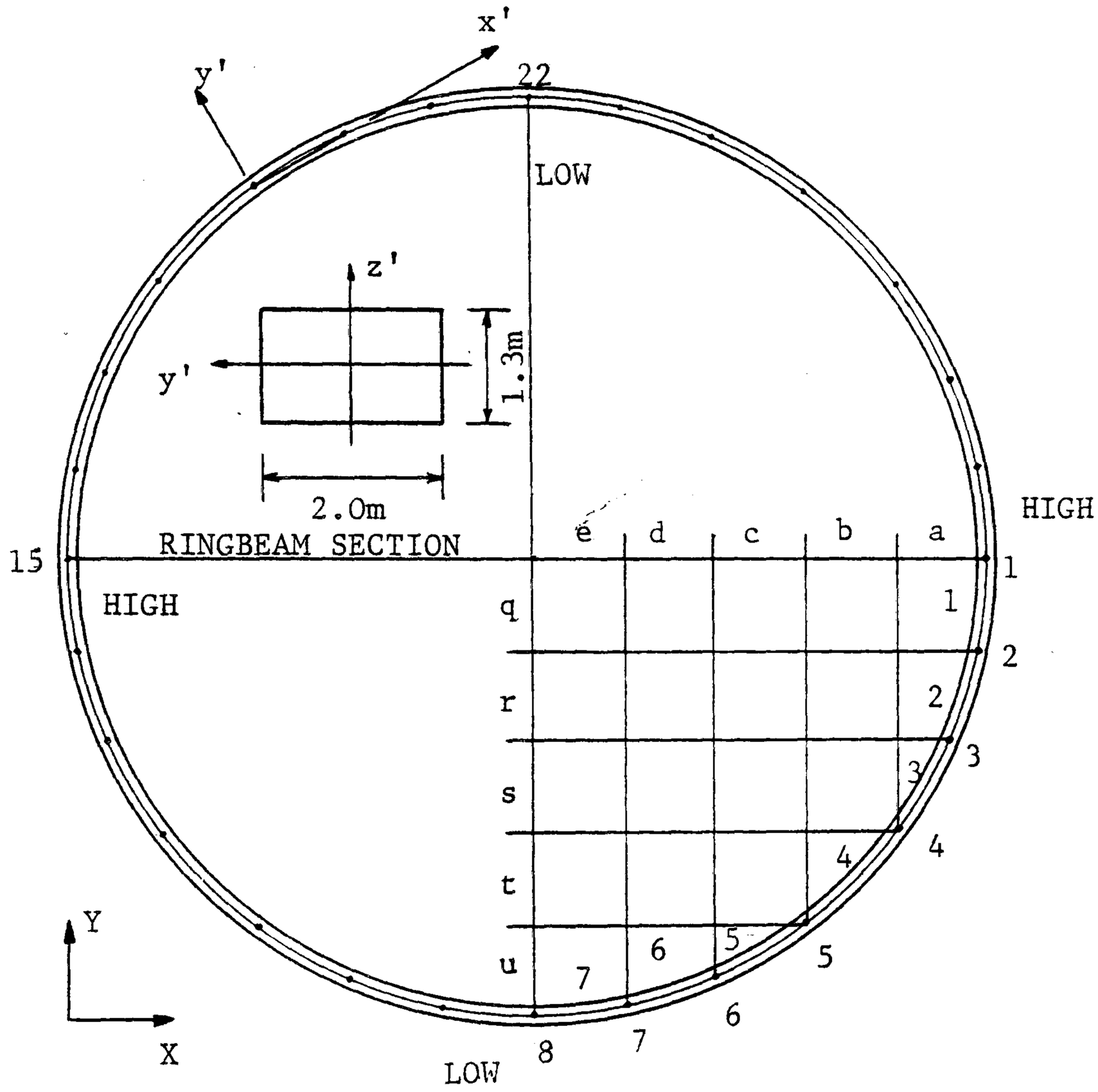

MEMBER PROPERTIES:

CABLES : EA = 83200 t

BEAMS : EA = 5200000 t

ν = 0

Figure 8.2

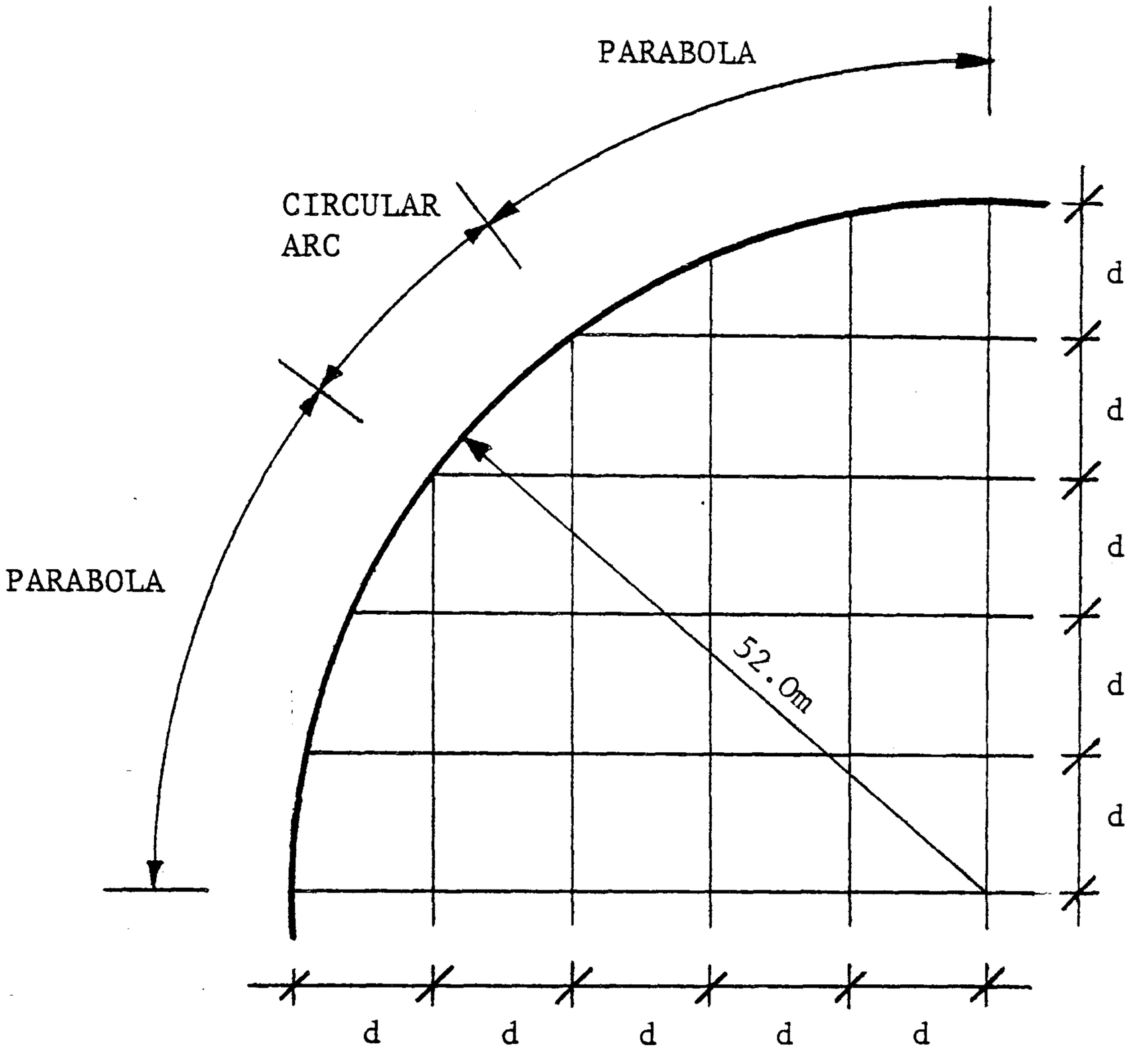

d = 10.4 m

SADDLE SHAPED NETWORK

RINGBEAM PLAN GEOMETRY

Figure 8.3

NODE NUMBER	COORDINATES (m) X	Y	Z
1	104.0	52.0	14.0
2	102.844	41.6	13.412
3	99.378	31.2	11.691
4	93.6	20.8	8.960
5	83.2	10.4	5.040
6	72.8	4.622	2.309
7	62.4	1.156	0.588
8	52.0	0.	0.

BOUNDARY NODE COORDINATES (INITIAL STATE PRIOR TO CABLE TENSIONING).

REMAINING BOUNDARY COORDINATES OBTAINED BY SYMMETRY.

Table 8.5

surface nodes are subject to a dead load of 6.49 t due to a cable and cladding selfweight of 60 kg/m . Møllmann (122) suggests that the selfweight of the ringbeam was also taken into account, but as all boundary nodes are restrained vertically it is not clear how this was achieved.

In the absence of specific data for the axial twist of the boundary elements, these were obtained from an initial computer analysis. The form of the network surface was determined assuming rigid boundary nodes, the Dynamic Relaxation program being simply modified to permit the inclusion of cable members having constant horizontal force components. From this generated surface the required boundary element twist was determined from the adjacent normal as outlined in Appendix D .

The Dynamic Relaxation formfinding was then repeated for the complete structure with elastic properties assigned to the spatial flexural elements idealising the boundary structure. The initial edge geometry was as defined above, whilst the network was assumed flat with surface nodes having a zero initial vertical coordinate. Thus the network prestressed configuration and boundary stresses were determined by a single DR analysis, an approach that compares favourably with the iterative process adopted by Møllmann (122) which entails successive separate analyses of the surface and boundary structures.

Having obtained the pretensioned state by DR, the problem was then analysed for its behaviour under load by both DR and the Scaled Conjugate Gradient method. For the latter approach the

linear boundary stiffness matrix was calculated from the unstressed configuration and held constant throughout the subsequent analysis. The pretensioned beam geometry was, however, utilised as starting data for the minimisation. The various loading cases considered are reviewed in figure 8.4. In the following comparison of results the tabulated values reported by Møllmann (122) have been scaled from small scale graphical plots.

When comparing the present DR formfinding results with those of Møllmann, significant differences are apparent in the ringbeam in plane bending moments and radial displacements. The maximum DR bending moment is 1.1 tm, whilst the maximum reported by Møllmann is 115 tm. This latter value represents approximately 25% of the maximum moment obtained during load analyses, and as such seems high for a boundary structure shape that has been deliberately adopted so as to minimise these moments at the pretension stage. The same DR program was used for both formfinding and load analyses, and the latter achieved results close to those of the SCG analyses, with any small differences being attributable to the assumption of linear boundary structure response in the SCG program. Thus an independent check had been made between the non-linear natural stiffness relations, held in separated form, of DR and the linear, assembled global stiffness relations of the SCG method. The level of agreement achieved indicates that the DR program utilised for both stages of the investigation of this problem is functioning satisfactorily.

The discrepancies between the results presented in table 8.6 may be due to the incorrect interpretation of the relatively

LOAD CASE	DESCRIPTION
I	SNOWLOAD ON WHOLE ROOF PLUS SELFWEIGHT
II	SNOWLOAD ON HALF ROOF (x>52) PLUS SELFWEIGHT
III	SNOWLOAD ON HALF ROOF (y>52) PLUS SELFWEIGHT
IV	WIND SUCTION ON WHOLE ROOF PLUS SELFWEIGHT
V	ZERO LOAD
VI	UDL = 200 kg/m^2 ON WHOLE ROOF
VII	UDL = 300 kg/m^2 ON WHOLE ROOF

SELFWEIGHT = 60 kg/m^2

SNOWLOAD = 75 kg/m^2

WIND SUCTION = -40 kg/m^2

ALL SURFACE NODES ASSUMED TO TAKE LOAD EQUIVALENT

TO 10.4 x 10.4 = 108.16 m^2 SURFACE AREA

Figure 8.4

NODE/ ELEMENT	NODAL IN-PLANE BENDING MOMENT		NODAL RADIAL DISPLACEMENT		ELEMENT AXIAL FORCE	
	MØLLMANN	DR	MØLLMANN	DR	MØLLMANN	DR
8	115	.031	-.11	-.0139	1180	1179
9	105	-.443	-.10	-.0138	1230	1248
10	65	.625	-.08	-.0134	1386	1373
11	40	.452	-.04	-.0132	1325	1332
12	-20	.671	.01	-.0130	1360	1373
13	-45	1.105	.05	-.0130	1230	1248
14	-85	.341	.07	-.0131	1177	1179
15	-77	.900	.08	-.0132	-	-

Table 8.6 Pretension Analysis for ringbeam bending moments (tm), radial displacements (m) and axial forces (t).

sparse structure setting-out information or the nodal fixity specification. It should, however, be noted that the ringbeam axial forces established by Møllmann and the present formfinding differ by a maximum of 1%.

The example structure has then been subjected to the various load analyses detailed in figure 8.4. Because of the apparent discrepancy in pretension state results discussed above, the boundary structure in-plane bending moment results quoted by Møllmann for Newton-Raphson implicit matrix analysis have been adjusted to values relative to the pretension state rather than the initial unstressed state. The Møllmann values for radial displacement have been similarly adjusted, and again both sets of results have been scaled from a graphical presentation.

In tables 8.7 to 8.10 the response of the boundary structure to load cases I to IV is tabulated for in-plane bending moments, radial displacement of the nodes and member compressive force. The results given for DR and SCG are relative to the initial state of the structure.

It may be observed that there is close agreement between the three methods considered when calculating the in-plane bending moments. This is as expected since the DR pretension moments are relatively very small. There is also close agreement between radial displacements. Although this is to be expected for the DR and SCG analyses, in which results are tabulated relative to the initial state, the Møllmann results (relative to the pretension state) also agree closely. In particular it may be noted that the

NODE/ ELEMENT	NODAL IN-PLANE BENDING MOMENT			NODAL RADIAL DISPLACEMENT			ELEMENT AXIAL FORCE		
	MØ*	DR	SCG	MØ*	DR	SCG	MØ	DR	SCG
8	-442	-443	-429	-.221	-.221	-.213	1480	1499	1484
9	-405	-401	-387	-.200	-.201	-.194	1570	1590	1576
10	-285	-251	-243	-.140	-.142	-.137	1759	1753	1741
11	15	17	9	-.055	-.051	-.049	1700	1721	1713
12	190	198	189	.060	.064	.062	1720	1760	1757
13	205	209	203	.130	.135	.131	1580	1596	1596
14	225	232	233	.175	.176	.171	1493	1507	1508
15	226	244	247	.188	.189	.184	-	-	-

Table 8.7 Load Case I - analysis for ringbeam bending moments (tm), radial displacements (m) and axial forces (t).

* - results of Møllmann analyses given relative to the pretension state, DR and SCG relative to the initial state

NODE/ ELEMENT	NODAL IN-PLANE BENDING MOMENT			NODAL RADIAL DISPLACEMENT			ELEMENT AXIAL FORCE		
	MØ*	DR	SCG	MØ*	DR	SCG	MØ	DR	SCG
8	-366	-367	-353	-.158	-.165	-.158	1336	1343	1332
9	-343	-329	-316	-.144	-.149	-.143	1410	1425	1414
10	-228	-200	-193	-.100	-.101	-.097	1560	1571	1561
11	-4	22	16	-.030	-.029	-.028	1525	1534	1528
12	233	237	227	.059	.059	.057	1576	1576	1574
13	327	311	301	.104	.105	.102	1420	1433	1433
14	289	295	290	.117	.119	.115	1350	1354	1354
15	138	148	149	.104	.106	.104	1350	1350	1350
16	-24	-23	-20	.078	.079	.077	1440	1430	1429
17	-87	-84	-80	.045	.045	.044	1570	1578	1576
18	-49	-33	-31	.014	.011	.011	1530	1541	1539
19	-33	-16	-16	-.028	-.029	-.028	1588	1581	1577
20	-84	-75	-74	-.050	-.057	-.055	1440	1436	1432
21	-119	-108	-107	-.072	-.074	-.072	1350	1356	1352
22	-112	-116	-115	-.078	-.079	-.078	-	-	-

Table 8.8 Load Case II - analysis for ringbeam bending moments (tm), radial displacements (m) and axial forces (t)

* - results of Møllmann analysis given relative to the pretension state, DR & SCG results relative to the initial state.

NODE/ ELEMENT	NODAL IN-PLANE BENDING MOMENT			NODAL RADIAL DISPLACEMENT			ELEMENT AXIAL FORCE		
	MØ*	DR	SCG	MØ*	DR	SCG	MØ	DR	SCG
1	-77	-77	-58	.031	.031	.034	1310	1331	1325
2	-54	-57	-41	.033	.032	.035	1321	1411	1405
3	16	14	18	.037	.036	.037	1550	1557	1549
4	143	147	136	.035	.035	.034	1500	1522	1515
5	245	243	221	.015	.014	.011	1540	1566	1559
6	188	197	179	-.025	-.026	-.027	1420	1426	1419
7	52	44	37	-.075	-.075	-.074	1340	1346	1339
8	-232	-234	-227	-.110	-.119	-.115	1330	1341	1333
9	-478	-471	-451	-.142	-.143	-.136	1400	1422	1414
10	-480	-472	-445	-.125	-.129	-.122	1550	1572	1566
11	-224	-236	-221	-.070	-.070	-.065	1540	1545	1543
12	64	62	64	.033	.034	.033	1593	1593	1595
13	215	217	206	.105	.111	.106	1440	1448	1453
14	297	314	298	.152	.159	.151	1365	1369	1374
15	330	348	331	.172	.175	.167	-	-	-

Table 8.9 Load Case III - analysis of ringbeam bending moments (tm), radial displacements (m) and axial forces (t)

* - results of Møllmann analyses given relative to the pretension state, DR & SCG results relative to the initial state.

NODE/ ELEMENT	NODAL IN-PLANE BENDING MOMENT			NODAL RADIAL DISPLACEMENT			ELEMENT AXIAL FORCES		
	MØ*	DR	SCG	MØ*	DR	SCG	MØ	DR	SCG
8	318	320	311	.176	.173	.167	1040	1045	1053
9	287	292	283	.158	.158	.153	1095	1104	1113
10	210	200	193	.115	.114	.110	1227	1212	1220
11	40	40	41	.054	.044	.043	1150	1167	1172
12	-120	-114	-110	-.045	-.050	-.047	1200	1209	1211
13	-180	-176	-170	-.110	-.112	-.108	1095	1100	1101
14	-232	-222	-217	-.145	-.149	-.144	1041	1038	1038
15	-224	-238	-234	-.164	-.161	-.155	-	-	-

Table 8.10 Load Case IV - analysis for ringbeam bending moments (tm), radial displacements (m) and axial forces (t).

* - results of Møllmann analyses given relative to the pretension state, DR and SCG results relative to the initial state.

small differences in these displacements as tabulated are significantly less than the displacement increment between initial and pretension configuration. Good correspondence is also achieved for the axial forces in the boundary members. For the levels of loading considered the effect of introducing non-linearity into the support structure response is not significant. It may be concluded that there is satisfactory agreement between the present DR and SCG load analyses for the ringbeam and those reported by Møllmann for the Newton Raphson method.

There remains, however, the discrepancies between the formfinding analyses. The close agreement between all load analyses and the fact that the present DR formfinding and analysis employ the same program suggests that incorrect results may have been presented by Møllmann for the formfinding. The fact that the discrepancies have been consistently summed into the load analysis results suggests that any error may have occurred at the transfer between the separate formfinding and analysis programs. The close agreement between load analysis results makes it less likely that the problem specification has been incorrectly interpreted in the present work. It also implies that the inclusion of non-linear terms in the bending elements is not significant at the level of loading involved in cases I to IV.

Table 8.11 gives the vertical displacement of the central node of the network surface when the whole of that surface is subjected to uniformly distributed loading. Close agreement at all levels of loading is noted for the SCG and Newton Raphson

UDL (kg/m^2)	LOAD CASE	DISPLACEMENT (m) MØ	DR	SCG
0	V	1.50	1.527	1.477
20	IV	.95	.950	.922
60	DL	.0	.0	.0
135	I	-1.15	-1.172	-1.143
200	VI	-1.85	-1.866	-1.820
300	VII	-2.60	-2.665	-2.598

Table 8.11 Network central node vertical displacement for uniformly distributed loading

analyses which both assume a linear boundary structure response. As the load is increased then the displacement calculated by the DR analysis becomes up to 2.5% greater than that of the other methods when the current u.d.l. is 5 times the magnitude of the dead load alone.

Comparitive cable forces for the DR and SCG analyses of load cases I and III are given in table 8.12 for both hanging and bracing cables. Again there is close agreement between the tabulated results, with the consistent small difference being due to the differing boundary displacements of the linear and non-linear discretisations. For comparison results are also presented for the analysis repeated assuming a rigid boundary with fully fixed boundary nodes, and the fact that this simplification grossly underestimates the forces in the bracing cables is clearly illustrated.

Computer program execution times on a CDC 7600 are presented in table 8.13 for the load cases I to IV which show a clear advantage in favour of Dynamic Relaxation. DR is here between 1.9 and 2.8 times faster than SCG, with the relative lack of efficiency of the latter primarily due to the complexity of the energy polynomial coefficient calculations for the boundary structure. The programs utilised for the comparison were as similar as possible, with identical input and output segments, and convergence deemed to have been achieved when all active nodal residuals were less than .1% of the maximum applied nodal load. The DR formulation utilised the purely diagonal stiffness derivation of mass components.

	ELEMENT	LOAD CASE I			LOAD CASE III		
		DR	SCG	RIGID BDY.	DR	SCG	RIGID BDY.
BRACING CABLES	A	336.3	333.4	207.3	302.2	300.5	236.3
	B	335.1	332.2	206.3	301.0	299.2	235.2
	C	334.1	331.1	205.4	299.9	298.1	234.4
	D	333.4	330.4	204.8	299.0	297.3	233.8
	E	333.1	330.1	204.5	298.3	296.6	233.5
HANGING CABLES	F	334.5	335.5	341.3	298.3	298.7	301.2
	G	336.4	337.4	342.8	299.8	300.2	302.5
	H	340.2	341.2	346.0	302.8	303.2	305.2
	J	345.8	346.8	350.7	307.3	307.6	309.2
	K	353.1	354.1	357.2	313.2	313.2	314.7

Table 8.12 Element axial forces (t) for Load Cases I and II

LOAD CASE	DYNAMIC RELAXATION STEPS	ENERGY RESETS	TIME	SCG STEPS	TIME
I	251	13	3.709	172	7.230
II	295	15	4.282	296	12.178
III	278	15	4.102	168	7.136
IV	190	12	2.944	164	6.939

Table 8.13 Comparitive CDC 7600 execution times (secs.) for the Møllmann problem.

8.5 Summary

This chapter opens with a brief review of published methods for the analysis of pretensioned networks with rigid-jointed boundary structures. Although the importance of including the support flexibility in an overall analysis has been clearly recognised, to date the full non-linear response of the boundary structure has been neglected. This has proved a reasonable approximation as the boundary contours utilised for these structures have traditionally been very stiff, especially when compared with the lightweight surface structures they support.

Dynamic relaxation may readily be applied to the full non-linear analysis of the complete structure by a combination of the network and rigid jointed space frame analyses outlined in previous chapters. A generalisation of the strain energy expression necessary for full non-linear analysis by the Conjugate Gradient methods is presented on the basis of periodic updates of the associated tangent stiffness matrix.

Two numerical investigations of previously studied problems are described, demonstrating the close agreement between explicit DR and SCG analyses and the implicit Newton-Raphson matrix approach for load analyses of this class of structure.

The suitability of Dynamic Relaxation for the unified formfinding and analysis of tension systems with flexible boundaries has been demonstrated, and significant improvements in convergence

time over SCG noted. For the latter analyses the revised energy polynomial coefficients were successfully employed. When Buchholdt's coefficients were utilised for the same problems in conjunction with exact calculation of nodal out-of-balance forces, convergence was not achieved.

A likely future development is the employment of more flexible compression contours which permit boundary displacements and utilise the stabilising effects of the tensile system. This will necessitate the full non-linear idealisation of the boundary structure. The Dynamic Relaxation approach presented here is well placed to fulfill this role, being simple to implement, having low computer storage requirements and proving here to be at least twice as fast as the Scaled Conjugate Gradient analysis with linear boundary response.

For problems where linear boundary analysis is adequate it is likely that the convergence rate of the Dynamic Relaxation method may be further improved by the adoption of a constant, linear, representation of the boundary structure.

CHAPTER 9

GENERAL SUMMARY AND CONCLUSIONS

This thesis is concerned with the application of direct integration methods, particularly Dynamic Relaxation, to the non-linear formfinding and analysis of pretensioned networks supported by compression arches.

The development, formulation and application of the Dynamic Relaxation and Scaled Conjugate Gradient methods are reviewed in Chapter 2. These are the two principal explicit integration techniques currently in use for the numerical investigation of tension structures.

In Chapter 3 the automated control of Dynamic Relaxation is considered, together with the efficient implementation of arbitrary element types. A modified kinetic damping procedure is shown to be an efficient alternative to viscous nodal damping that does not require prior determination of a damping constant. A generalised derivation of critical fictitious nodal mass components is presented as the basis for automatic establishment of either diagonal or square nodal mass matrices. In addition it is shown that Dynamic Relaxation with kinetic damping may be interpreted as a dynamic implementation of a first order gradient minimisation technique. The inherent simplicity of DR nonlinear analysis has been coupled with the automatic control characteristic of the gradient method to provide an effective analysis procedure that retains a clear physical interpretation.

The implementation of the Scaled Conjugate Gradient method due to Buchholdt is limited to cable elements exhibiting small strains. A modification of Buchholdt's approach which permits arbitrary member strains. A modification of Buchhholdt's approach which permits

arbitrary member strains is presented in Chapter 4, and utilised for subsequent comparisons with Dynamic Relaxation. Indeed convergence was not obtained for analyses of the complete structure including boundary arches unless the current modification was incorporated.

In Chapter 5 a generalised test problem is proposed for the comparative analysis of pretensioned networks with rigid boundaries. Dynamic Relaxation with kinetic damping is shown to converge more quickly than the Conjugate Gradient method in all cases for a range of network curvatures, pretension levels and loading patterns idealised by increasing mesh sizes up to 2523 degrees of freedom and 1860 elements. DR requires between 0.4 and 0.8 of the time to converge by SCG, with this advantage increasing with problem size.

As a precursor to the complete analysis of tension systems plus boundary structure, a strategy for the non-linear analysis of space frames by Dynamic Relaxation is outlined in Chapter 6. Rotational degrees of freedom are introduced, with rotations treated as displacements from the initial state. The implementation of both planar and spatial flexural elements is described, with natural treatment of finite and rigid-body motion and the effect of axial force on the moment-curvature relations included. The latter stability functions are conveniently updated at the energy peak stages of the kinetic damping procedure. A simplified constant moment bending element is also presented for planar analysis. Flexural members are idealised as a series of bar elements, which may deform axially, whilst flexural stiffness is lumped at the

inter-connecting nodes. Although a finer idealisation is necessary for a given accuracy compared with conventional cubic displacement elements, this element may still be of use where such an idealisation is a geometric or topographic requirement. Results of Dynamic Relaxation investigations are compared with published solutions to non-linear planar and spatial problems. The successful treatment of finite displacements through snap-through and into post-buckling response is demonstrated.

In the first section of Chapter 7 the development of linear and non-linear techniques for numerical formfinding is reviewed. In subsequent sections the suitability of kinetic damping for controlling Dynamic Relaxation formfinding is demonstrated, in particular its ability to cope with gross out of balance forces and with structural mechanisms. The generation of moment-free compression arches within tension networks is illustrated, and alternative, stable, boundary forms derived from the same basic data.

Chapter 8 opens with a summary of published methods for the analysis of pretensioned networks with rigid-jointed boundary structures. Although the importance of including support flexibility in an overall analysis has been clearly recognised, the full non-linear response of the boundary structure has not been included to date. The various elements of preceeding chapters are combined here to achieve such an analysis by Dynamic Relaxation. Two numerical investigations of previously reported problems are described, demonstrating close agreement between DR, SCG and Newton-Raphson analyses for working loads and relatively stiff boundary structures.

The Dynamic Relaxation method with non-linear boundary representation has proved to converge at least twice as fast as the SCG approach with linear boundary response.

It is concluded that Dynamic Relaxation is a simple and efficient analysis technique, retaining a clear physical analogy that facilitates the understanding, implementation and execution of non-linear response investigations. The numerical control parameters necessary for an optimised yet stable direct numerical integration have been fully automated, with consequent elimination of the need for trial analyses.

Dynamic Relaxation has proved equally suited to both the formfinding and analysis of the class of tension structures considered in detail in this thesis, with the explicit formation making is particularly suited to the interactive implementation of these processes. The generation of a wide range of moment-free compression contours may be readily achieved numerically using DR, and this is especially relevant in the light of the difficulty in physical investigation of this problem. When the complete structure is subsequently analysed under load the full non-linear DR idealisation of the boundary permits the investigation of the stabilising effects of the surface tensile system on that boundary. Thus the way is open to the future use of more flexible, and economic, compression contours that are more closely allied to the lightweight ideal of the surface structure.

APPENDIX A

PRINCIPAL STIFFNESS DIRECTIONS IN TWO AND THREE DIMENSIONS

A.1 Planar Case

Consider any node n having stiffness terms in the global coordinate system:

$$\begin{bmatrix} S_{xx} & S_{xy} \\ S_{yx} & S_{yy} \end{bmatrix} \tag{A.1}$$

The axis transformation angle ϕ_p that will maximise the transformed S_{xx} stiffness component such that the diagonal principal stiffness matrix $\left[S_p\right]$ is obtained:

$$\left[S_p \right] = \begin{bmatrix} S'_{xx} & 0 \\ 0 & S'_{yy} \end{bmatrix} \tag{A.2}$$

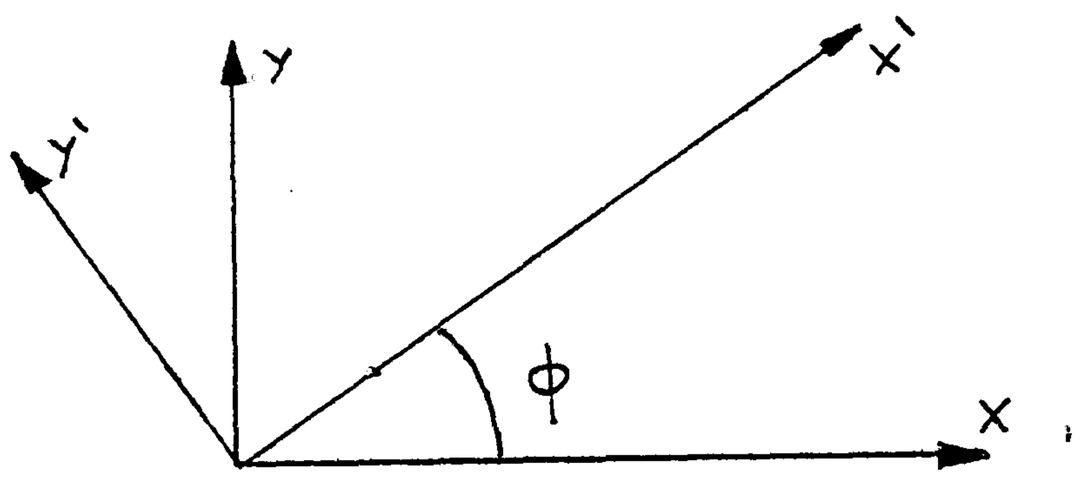

The full transformation of the nodal stiffness is given by:

$$\begin{bmatrix} \cos\phi & \sin\phi \\ -\sin\phi & \cos\phi \end{bmatrix}\begin{bmatrix} S_{xx} & S_{xy} \\ S_{yx} & S_{yy} \end{bmatrix}\begin{bmatrix} \cos\phi & -\sin\phi \\ \sin\phi & \cos\phi \end{bmatrix} = \begin{bmatrix} S'_{xx} & S'_{xy} \\ S'_{yx} & S'_{yy} \end{bmatrix} \tag{A.3}$$

thus $\hat{S}_{xx} = S_{xx} \cos^2\phi + S_{yy} \sin^2\phi + 2S_{xy} \sin\phi \cos\phi$

$$\frac{d\hat{S}_{xx}}{d\phi} = -S_{xx} \sin 2\phi + S_{yy} \sin 2\phi + 2S_{xy} \cos 2\phi \qquad (A.4)$$

Then for $\hat{S}_{xx}$ to be a maximum or minimum:

$$(S_{xx} - S_{yy}) \sin 2\phi_p = 2S_{xy} \cos 2\phi_p$$

$$\tan 2\phi_p = \frac{2S_{xy}}{(S_{xx} - S_{yy})}$$

A.2 Three Dimensional Case

It has been shown above that the derivation of principal stiffnesses for the planar case is analogous to a Mohr Circle for stiffness. The three dimensional case may then be investigated with this analogy in mind.

Consider the transformation of the nodal direct stiffness terms:

$$[S_p] = [T_p][S][T_p] \qquad (A.6)$$

where $[S] = \begin{bmatrix} S_{xx} & S_{xy} & S_{xz} \\ S_{yx} & S_{yy} & S_{yz} \\ S_{zx} & S_{zy} & S_{zz} \end{bmatrix}$ nodal direct stiffness in global coords.

$$[S_p] = \begin{bmatrix} S_1 & 0 & 0 \\ 0 & S_2 & 0 \\ 0 & 0 & S_3 \end{bmatrix}$$ nodal principal direct stiffness

$$\left[T_P \right] = \begin{bmatrix} \ell_1 & m_1 & n_1 \\ \ell_2 & m_2 & n_2 \\ \ell_3 & m_3 & n_3 \end{bmatrix} \text{ transformation matrix}$$

Premultiplication of equation (A.6) gives:

$$\left[T_P \right]^T \left[S_P \right] = \left[S \right] \left[T_P \right]^T \tag{A.7}$$

which may be written in full:

$$\begin{bmatrix} \ell_1 & \ell_2 & \ell_3 \\ m_1 & m_2 & m_3 \\ n_1 & n_2 & n_3 \end{bmatrix} \begin{bmatrix} S_1 & 0 & 0 \\ 0 & S_2 & 0 \\ 0 & 0 & S_3 \end{bmatrix} = \begin{bmatrix} S_{xx} & S_{xy} & S_{xz} \\ S_{yx} & S_{yy} & S_{yz} \\ S_{zx} & S_{zy} & S_{zz} \end{bmatrix} \begin{bmatrix} \ell_1 & \ell_2 & \ell_3 \\ m_1 & m_2 & m_3 \\ n_1 & n_2 & n_3 \end{bmatrix} \tag{A.8}$$

Then for the principal stiffness term S_i $(i = 1,2,3)$ having direction cosines ℓ_i, m_i, n_i, consider the individual coefficient equalities of equation (A.8):

$$\begin{aligned} \ell_i S_i &= \ell_i S_{xx} + m_i S_{xy} + n_i S_{xz} \\ m_i S_i &= \ell_i S_{xy} + m_i S_{yy} + n_i S_{zy} \\ n_i S_i &= \ell_i S_{xz} + m_i S_{yz} + n_i S_{zz} \end{aligned} \tag{A.9}$$

which yields three homogenous equations:

$$\begin{bmatrix} (S_{xx} - S_i) & S_{xy} & S_{xz} \\ S_{xy} & (S_{yy} - S_i) & S_{zy} \\ S_{xz} & S_{zy} & (S_{zz} - S_i) \end{bmatrix} \begin{Bmatrix} \ell_i \\ m_i \\ n_i \end{Bmatrix} = \begin{Bmatrix} 0 \\ 0 \\ 0 \end{Bmatrix}$$

$$\left[S_i'' \right] \left\{ \lambda_i \right\} = \left\{ 0 \right\} \tag{A.10}$$

These equations will give a non-trivial solution provided that the determinant of coefficients is zero:

$$\left| S''_{\lambda} \right| = 0 \qquad \text{(A.11)}$$

Expansion of this determinant results in the following cubic equation whose three real roots are the principal stiffness components:

$$S_{\lambda}^3 + \alpha S_{\lambda}^2 + \beta S_{\lambda} + \jmath = 0 \qquad \text{(A.12)}$$

where $\alpha = -(S_{xx} + S_{yy} + S_{zz})$

$$\beta = S_{xx}S_{yy} + S_{xx}S_{zz} + S_{yy}S_{zz} - S_{xy}^2 - S_{xz}^2 - S_{zy}^2$$

$$\jmath = S_{xy}^2 S_{zz} + S_{xz}^2 S_{yy} + S_{yz}^2 S_{xx} - 2S_{xz}S_{xy}S_{zy} - S_{xx}S_{yy}S_{zz}$$

Solution of this cubic equation may be achieved by the following standard method:

put: $S_{\lambda} = x - \alpha/3$

giving: $x^3 + (\beta - \frac{\alpha^2}{3})\, x + (\jmath - \frac{\alpha\beta}{3} + \frac{2}{27}\alpha^3) = 0$

or: $x^3 - qx - r = 0$

For three real roots ($27r^2 < 4q^3$) this equation has the solution:

$$\phi = \cos^{-1}\left[\left(\frac{3}{q}\right)^{\frac{3}{2}} \frac{r}{2} \right]$$

$$x_1 = \frac{2}{\sqrt{3}}\, q^{1/2} \cos \phi/3$$

$$x_2 = \frac{-2}{\sqrt{3}}\, q^{1/2} \cos (\pi-\phi)/3$$

$$x_3 = \frac{-2}{\sqrt{3}}\, q^{1/2} \cos (\pi+\phi)/3$$

and hence $S_i = x_i - \frac{\alpha}{3}$ for $i = 1,2,3$.

If, in the solution of the cubic equation (A.12), $j = 0$ then one of the principal stiffnesses is zero and the problem reduces to that of soliving a quadratic for the non-zero components:

$$S_i^2 + \alpha S_i + \beta = 0 \qquad \text{(A.13)}$$

Similarly if both j and β are zero there are two zero principal stiffnesses, and $S_i = -\alpha$ yields the non-zero value. In this case one of the principal stiffness directions associated with a zero value must be assigned aribrarily in order to ensure a unique coordinate system.

The principal stiffness direction is generally obtained by backsubstituting for S_i into equation (A.10) and using the additional relation:

$$\ell_i^2 + m_i^2 + n_i^2 = 1 \qquad \text{(A.14)}$$

which results in the equations:

$$n_i = \sqrt{\left\{1/(1 + a^2 + b^2)\right\}}$$

$$a = \left\{ \frac{S''_{21}}{S''_{22}} \frac{S''_{13}}{S''_{11}} - \frac{S''_{23}}{S''_{22}} \right\} \Big/ \left\{ 1 - \frac{S''_{21}}{S''_{22}} \frac{S''_{12}}{S''_{11}} \right\}$$

$$b = \frac{-S_{12}}{S''_{11}} a - \frac{S_{13}}{S''_{11}}$$

$$\ell_i = b\, n_i \quad \text{and} \quad m_i = a\, n_i \qquad \text{(A.15)}$$

where S''_{jk} are coefficients of equation (A.10).

In practice only the directions of S_1 and S_2 need be found in this way, with the third set of direction cosines then determined from the vector cross-product.

It is, however, possible for n_i to be zero in the above equations when the principal stiffness direction does not follow one of the global axes if:

$$\frac{S''_{12} \quad S''_{21}}{S''_{11} \quad S''_{22}} = 1$$

and no solution is obtained for a. As only the directions of S_1 and S_2 are determined in this manner, then, if on checking the above factor n_j (j = 1 or 2) is zero, a simple expedient is to exchange the principal stiffness values S_j and S_3. As the principal stiffness directions are mutually perpendicular the revised n_j cannot be zero and the process continues satisfactorily.

APPENDIX B

CORRECTIONS FOR BOWING OF SPATIAL FLEXURAL ELEMENTS

Saafan (151) has derived a correction factor for the effect of bowing on the axial displacement of a planar member. For the member illustrated in figure B.1, the axial displacement may be defined as:

$$\delta L = L - L_c$$

$$= \frac{PL}{EA} + \delta_B \qquad \text{(B.1)}$$

where δ_B is the difference between the arc length L_A and the chord length L_c

$$\delta_B = \int_0^{L_c} (ds - dx) \qquad \text{(B.2)}$$

where $ds = \sqrt{(dy^2 + dx^2)}$

$$\text{therefore } \delta_B = \int_0^{L_c} \left[\sqrt{\left(1 + \left(\frac{dy}{dx}\right)^2\right)} - 1 \right] dx \qquad \text{(B.3)}$$

On binomial expansion of equation (B.3), neglecting 4th and higher order terms, one obtains:

$$\delta_B = \int_0^{L_c} \frac{1}{2} \left(\frac{dy}{dx}\right)^2 dx \qquad \text{(B.4)}$$

Solution of this equation (reference (151)) yields:

$$\delta_B = L_c \left[b_1 (\Theta_1 + \Theta_2)^2 + b_2 (\Theta_1 - \Theta_2)^2 \right]$$

$$b_1 = \frac{s(1 + c)(sc - 2)}{8\Pi}$$

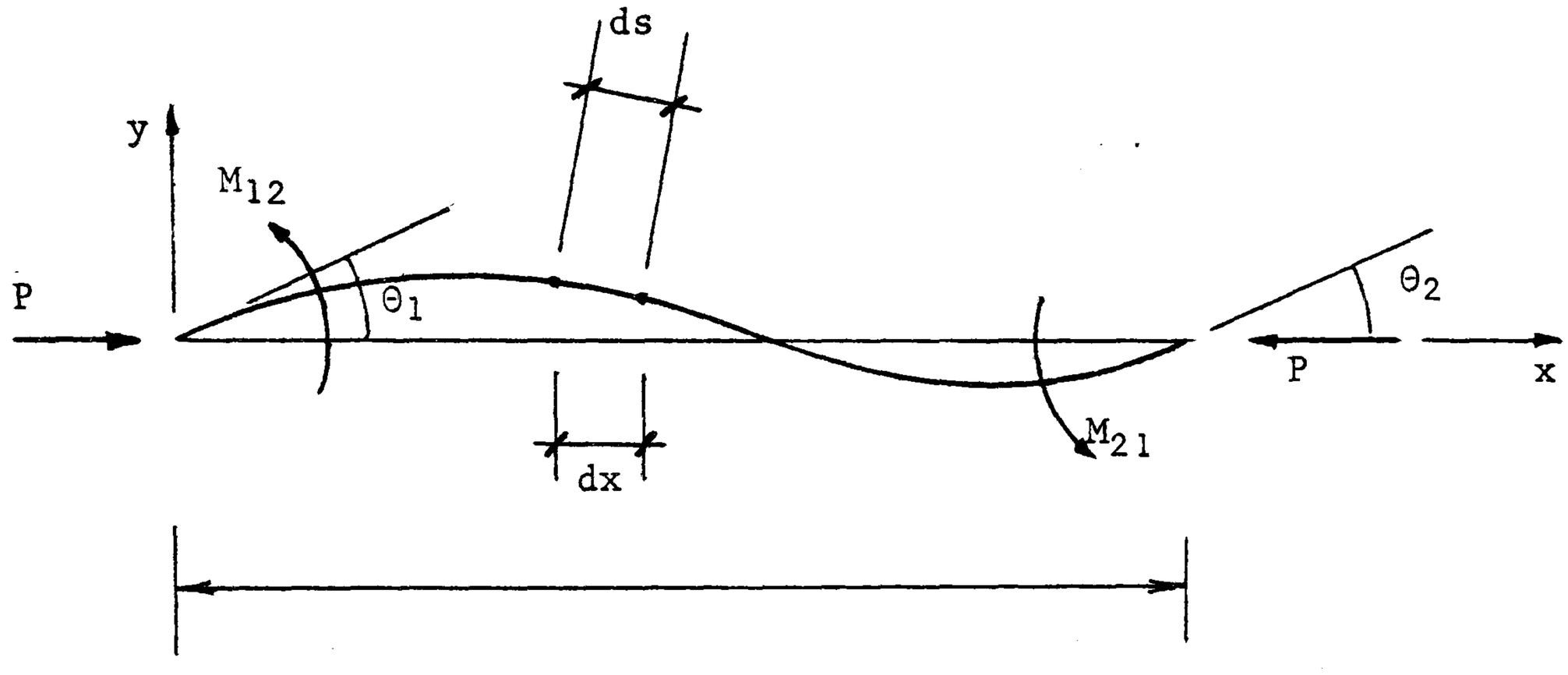

Figure B.1

$$b_2 = \frac{c}{8(1 + c)} \tag{B.5}$$

When the three dimensional case is considered:

$$\delta_B = \int_0^{L_c} (ds - dx)$$

where dx is again a small increment along the member chord

$$ds = \sqrt{(dx^2 + dy^2 + dz^2)}$$

$$\text{therefore} \quad \delta_B = \int_0^{L_c} \left\{ \left[1 + \left(\frac{dy}{dx}\right)^2 + \left(\frac{dz}{dx}\right)^2 \right]^{1/2} - 1 \right\} dx \tag{B.6}$$

and approximating as before:

$$\delta_B = \int_0^{L_c} \frac{1}{2} \left\{ \left(\frac{dy}{dx}\right)^2 + \left(\frac{dz}{dx}\right)^2 \right\} dx \tag{B.7}$$

Bowing of spatial members may therefore be incorporated by considering two in-plane effects separately (for the local $\grave{x}\,\grave{z}$ and $\grave{x}\,\grave{y}$ planes) and summing the results to obtain δ_B. The member axial force may then be obtained from equations (B.1).

APPENDIX C

COORDINATE TRANSFORMATIONS IN THREE DIMENSIONS

Consider the coordinate transformation necessary for the arbitrary orientation of a flexural element in space. The coordinate axes are as shown in figure C.1, with initial transformation for global axes $\{x\}$ to intermediate stage $\{\grave{x}\}$ and subsequent rotation through angle β to the final $\{\acute{x}\}$ state.

The global coordinate system is denoted $\{x \quad y \quad z\}$, and the intermediate stage, $\{\grave{x} \quad \grave{y} \quad \grave{z}\}$, defined such that $\grave{x}$ lies in the line of the member chord and $\grave{z}$ lies in the plane defined by $\grave{x}$ and the global z-axis. The transformation between the two systems is given by:

$$\{\grave{x}\} = [\grave{L}]\{x\} = \begin{bmatrix} \lambda_{\grave{x}x} & \lambda_{\grave{x}y} & \lambda_{\grave{x}z} \\ \lambda_{\grave{y}x} & \lambda_{\grave{y}y} & \lambda_{\grave{y}z} \\ \lambda_{\grave{z}x} & \lambda_{\grave{z}y} & \lambda_{\grave{z}z} \end{bmatrix} \begin{Bmatrix} x \\ y \\ z \end{Bmatrix} \qquad (C.1)$$

Let the unit vector along the $\grave{x}$ axis, in global terms, be:

$$\begin{Bmatrix} \ell \\ m \\ n \end{Bmatrix} = \begin{Bmatrix} \lambda_{\grave{x}x} \\ \lambda_{\grave{x}y} \\ \lambda_{\grave{x}z} \end{Bmatrix} \qquad (C.2)$$

A vector in the $\grave{y}$-direction may be erected by considering the cross product of the $\grave{x}$ unit vector and a unit vector in the global z direction:

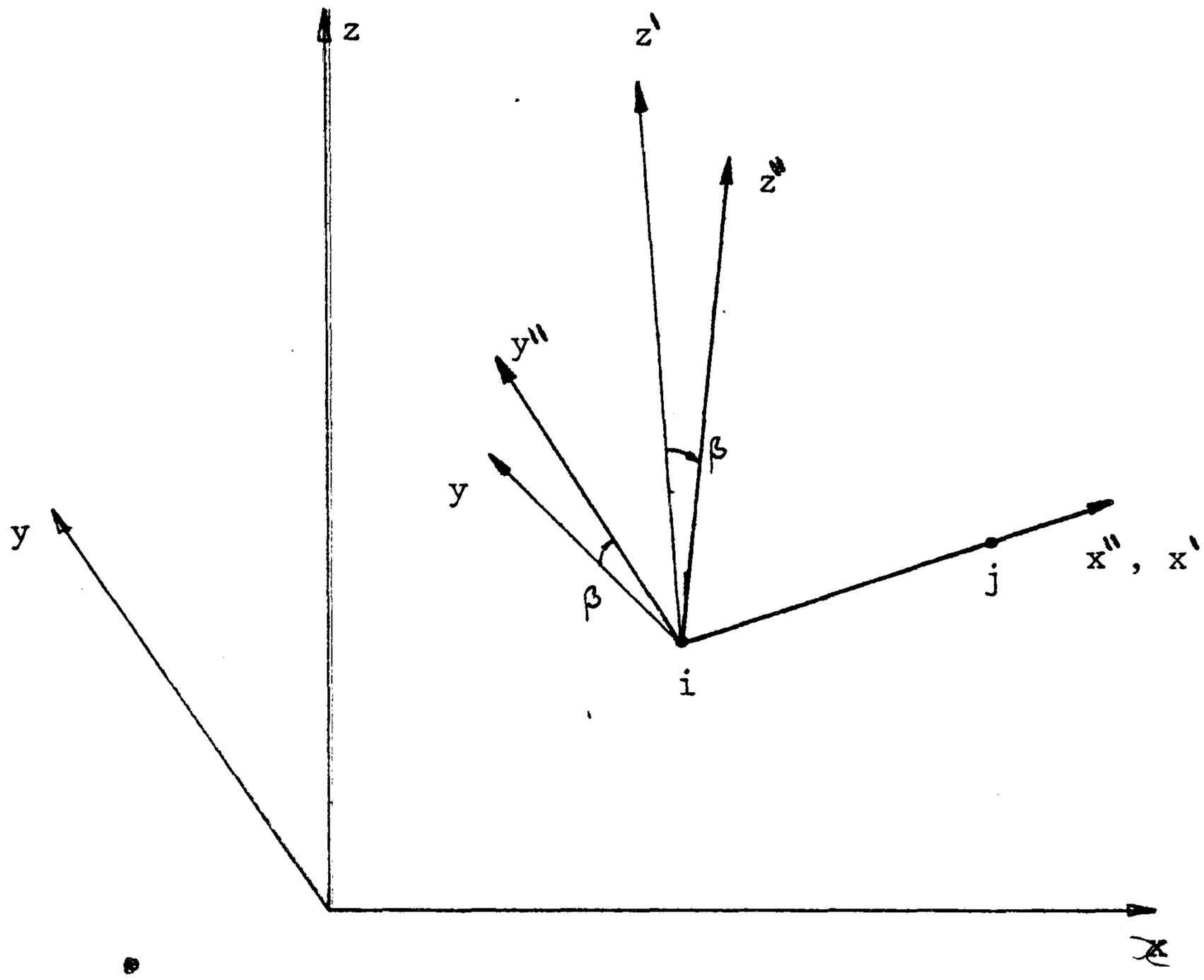

Figure C.1

$$y` = \begin{Bmatrix} 0 \\ 0 \\ 1 \end{Bmatrix} \times \begin{Bmatrix} \ell \\ m \\ n \end{Bmatrix} = \begin{Bmatrix} -m \\ \ell \\ 0 \end{Bmatrix} \qquad (C.3)$$

thus: $$\begin{Bmatrix} \lambda_{y'x} \\ \lambda_{y'y} \\ \lambda_{y'z} \end{Bmatrix} = \frac{1}{\sqrt{(\ell^2 + m^2)}} \begin{Bmatrix} -m \\ \ell \\ 0 \end{Bmatrix} \qquad (C.4)$$

Similarly for a vector in the $z`$ direction:

$$\begin{Bmatrix} \ell \\ m \\ n \end{Bmatrix} \times \begin{Bmatrix} -m \\ \ell \\ 0 \end{Bmatrix} = \begin{Bmatrix} -n\ \ell \\ -n\ m \\ \ell^2 + m^2 \end{Bmatrix} \qquad (C.5)$$

and again vector length $= \sqrt{(\ell^2 + m^2)} = \sqrt{(1 - n^2)}$, giving:

$$\begin{Bmatrix} \lambda_{z'x} \\ \lambda_{z'y} \\ \lambda_{z'z} \end{Bmatrix} = \frac{1}{\sqrt{(1 - n^2)}} \begin{Bmatrix} -n\ \ell \\ -n\ m \\ 1 - n^2 \end{Bmatrix} \qquad (C.6)$$

Thus the intermediate transformation matrix of equation (C.1) may be written:

$$[L`] = \frac{1}{a} \begin{bmatrix} a\ \ell & a\ m & a\ n \\ -m & \ell & 0 \\ -n\ \ell & -n\ m & 1-n^2 \end{bmatrix} \qquad (C.7)$$

$$a = \left| \sqrt{(1 - n^2)} \right|$$

where ℓ, m and n are the direction cosines of the member.

The second stage of the transformation represents the rotation through angle β about the common $\grave{x}/\grave{\grave{x}}$ axis of the true local coordinate system $\left\{ \grave{\grave{x}}, \grave{\grave{y}}, \grave{\grave{z}} \right\}$ from $\left\{ \grave{x}, \grave{y}, \grave{z} \right\}$:

$$\left\{ \grave{\grave{x}} \right\} = \left[\grave{\grave{L}} \right] \left\{ \grave{x} \right\} = \begin{bmatrix} 1 & 0 & 0 \\ 0 & \cos\beta & \sin\beta \\ 0 & -\sin\beta & \cos\beta \end{bmatrix} \left\{ \begin{matrix} \grave{x} \\ \grave{y} \\ \grave{z} \end{matrix} \right\} \qquad (C.8)$$

The complete transformation is then:

$$\left\{ \grave{\grave{x}} \right\} = \left[\grave{\grave{L}} \right] \left[\grave{L} \right] \left\{ x \right\} \qquad (C.9)$$

which may be written in full:

$$\left\{ \chi'' \right\} = \begin{bmatrix} 1 & 0 & 0 \\ 0 & \cos\beta & \sin\beta \\ 0 & -\sin\beta & \cos\beta \end{bmatrix} \begin{bmatrix} \ell & m & n \\ -\frac{m}{a} & \frac{\ell}{a} & 0 \\ -\frac{n\ell}{a} & -\frac{nm}{a} & a \end{bmatrix} \left\{ x \right\} \qquad (C.10)$$

$$a = \left| \sqrt{(1 - n^2)} \right|$$

Some modification is necessary for members with $\ell = m = 0$ and $n = \overset{+}{-}1$, as the general divisor a becomes zero. For the angles β as defined in figure C.2, then:

$$\left\{ \grave{\grave{x}} \right\} = \begin{bmatrix} 1 & 0 & 0 \\ 0 & \cos\beta & \sin\beta \\ 0 & -\sin\beta & \cos\beta \end{bmatrix} \begin{bmatrix} 0 & 0 & n \\ 0 & 1 & 0 \\ -n & 0 & 0 \end{bmatrix} \left\{ x \right\}$$

$$\left\{ \grave{\grave{x}} \right\} = \begin{bmatrix} 0 & 0 & n \\ -n\sin\beta & \cos\beta & 0 \\ -n\cos\beta & -\sin\beta & 0 \end{bmatrix} \left\{ x \right\} \qquad (C.11)$$

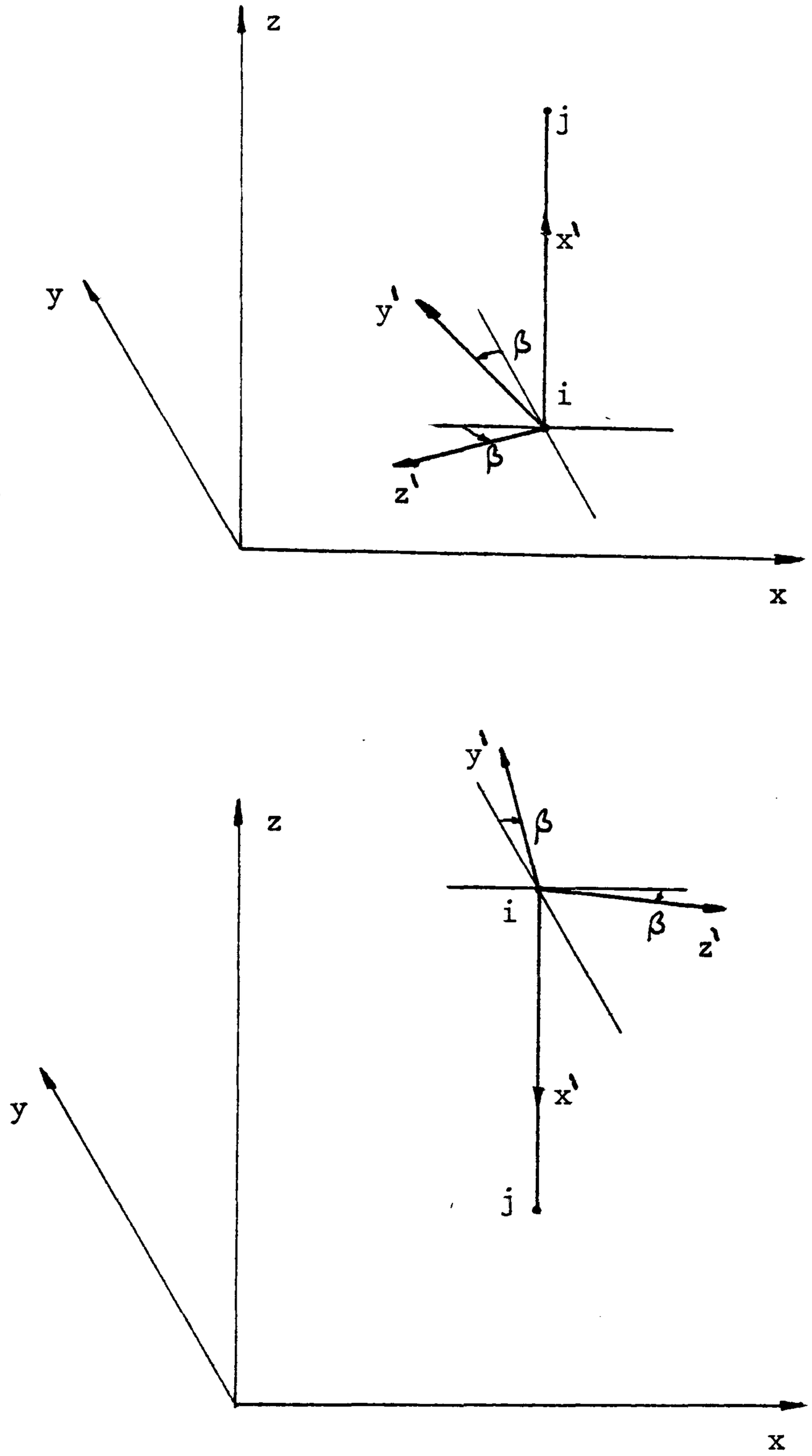

Figure C.2

APPENDIX D

BOUNDARY STRUCTURE CURVATURE FOR SADDLE-SHAPED NETWORKS

Consider an automated procedure for determining the angle of twist, β, of boundary elements when one of their principal cross-sectional axes is parallel to the adjacent surface of the tension network.

Figure D.1 shows a section through such a boundary element, with s an adjacent surface node. The vector $\{z''\}$ is perpendicular to the boundary element vector $\{b\}$, connecting nodes i and j, and lies in the plane formed by $\{b\}$ and the global z-axis (figure D.2).

$$\{y''\} = \{b\} \times \begin{Bmatrix} 0 \\ 0 \\ 1 \end{Bmatrix} = \begin{Bmatrix} b_y \\ -b_x \\ 0 \end{Bmatrix}$$

$$\{z''\} = \{y''\} \times \{b\} = \begin{Bmatrix} -b_x b_z \\ -b_y b_z \\ b_y^2 + b_x^2 \end{Bmatrix} \qquad (D.1)$$

Hence the direction cosines of $\{z''\}$:

$$\{\lambda_{z''}\} = \frac{1}{\ell_b} \{z''\} \qquad (D.2)$$

Then from figures D.3 and D.4:

$$\delta_{z''} = \{\lambda_{z''}\}^T \{v_{is}\}$$

$$= \{\lambda_{z''}\}^T \begin{Bmatrix} x_s - x_i \\ y_s - y_i \\ z_s - z_i \end{Bmatrix} \qquad (D.3)$$

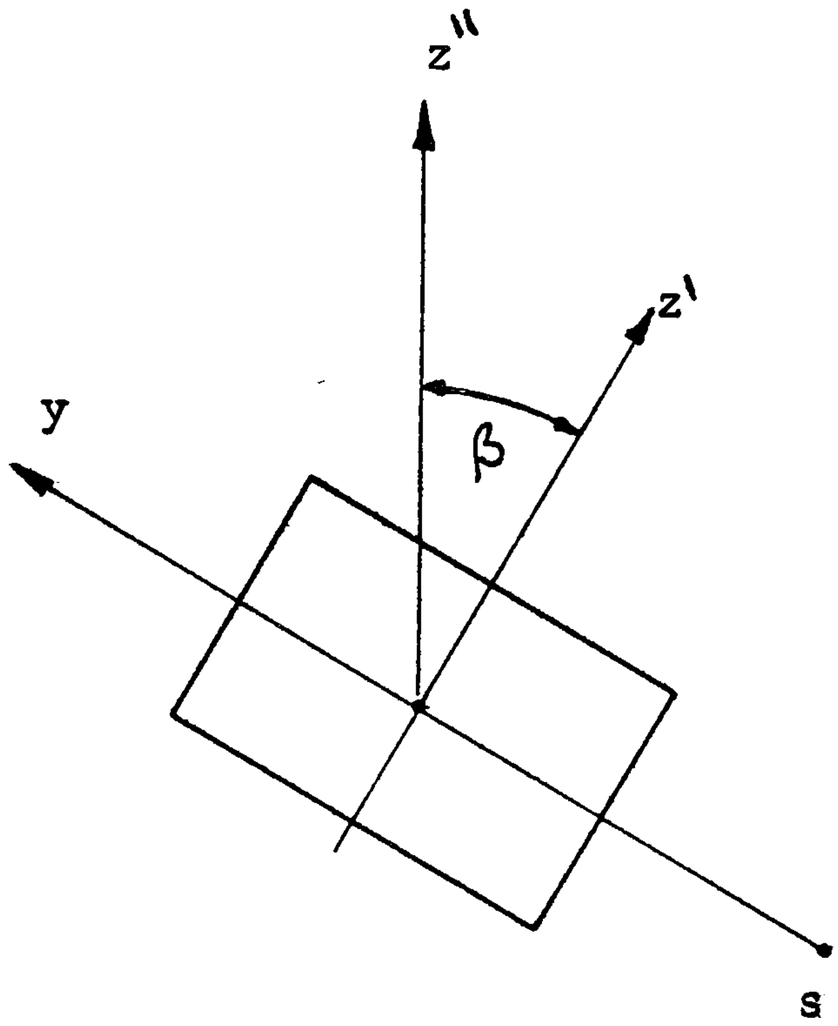

Figure D.1

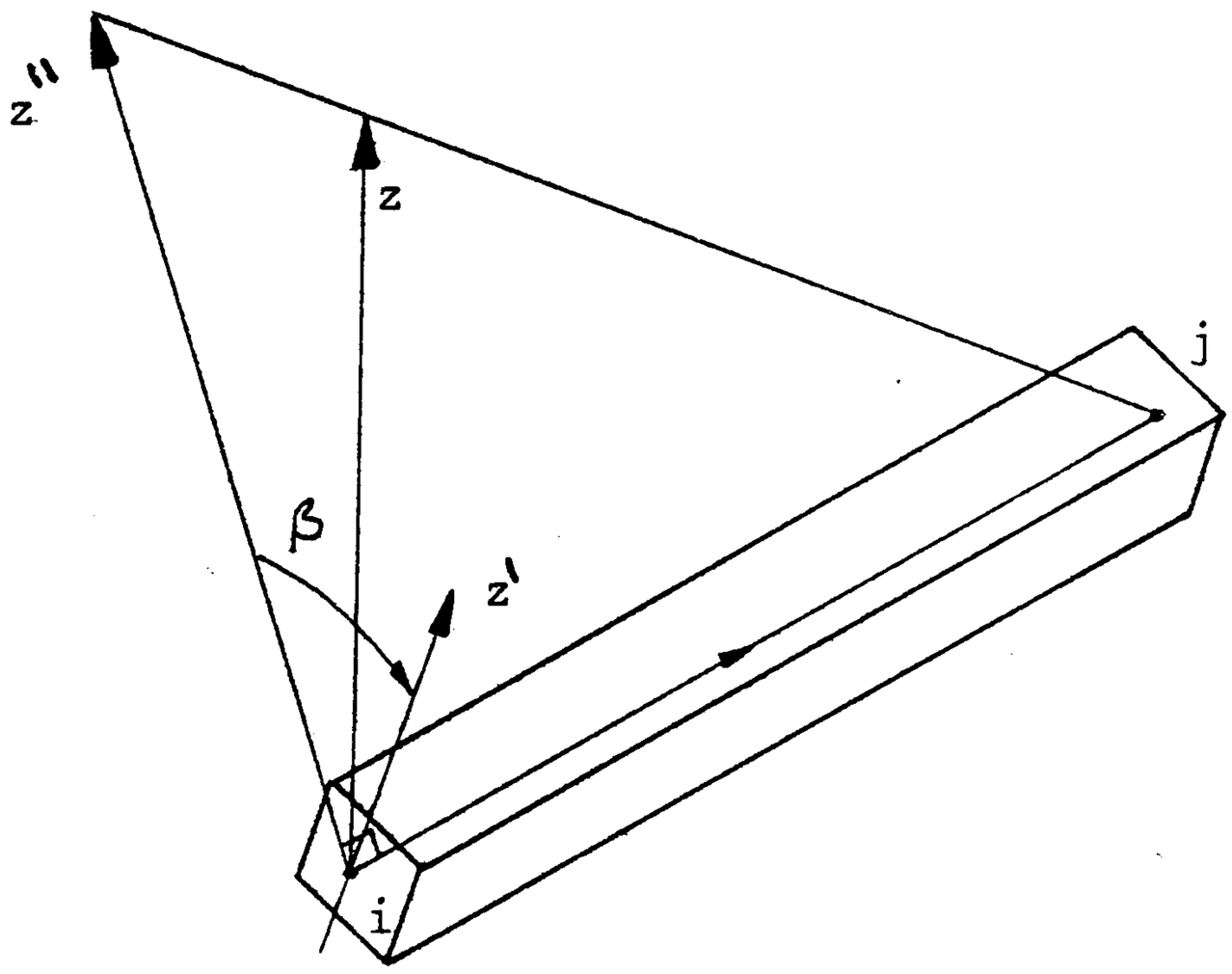

Figure D.2

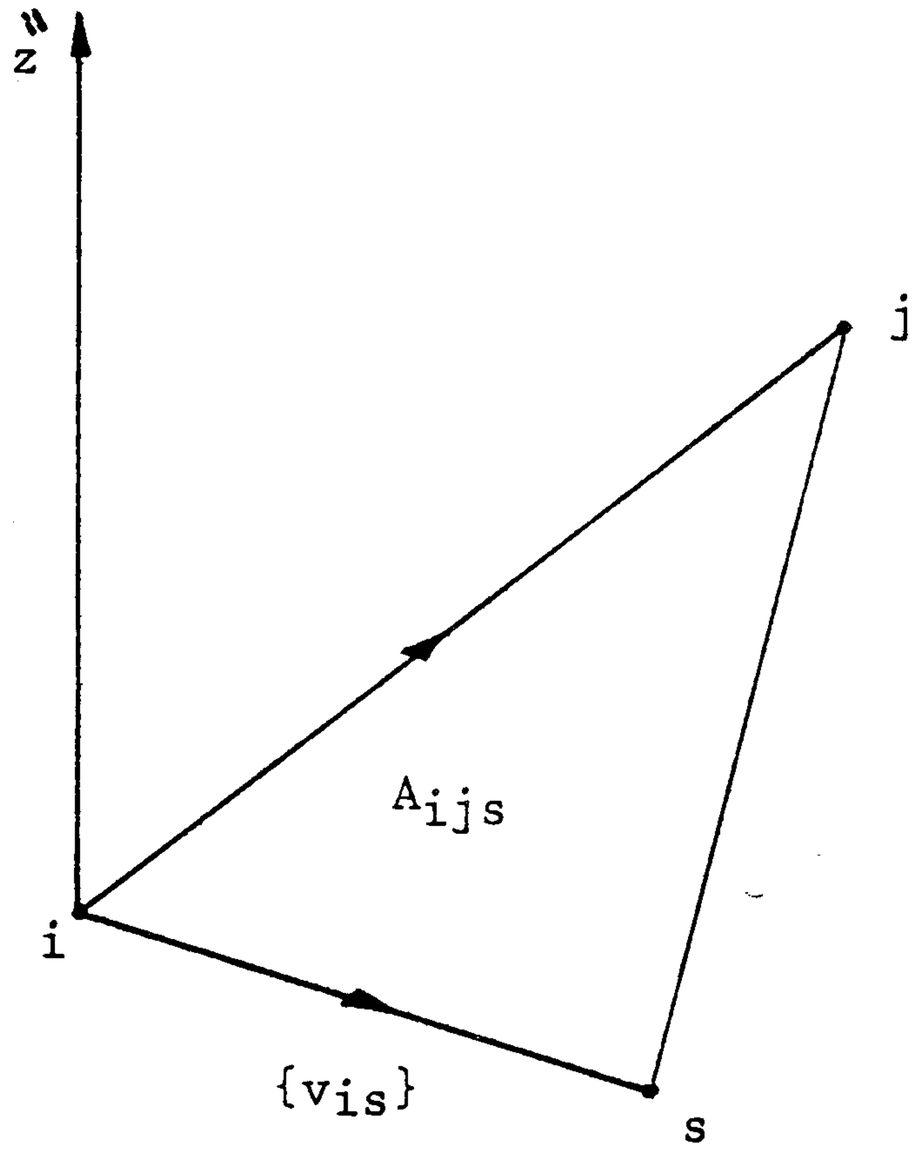

Figure D.3

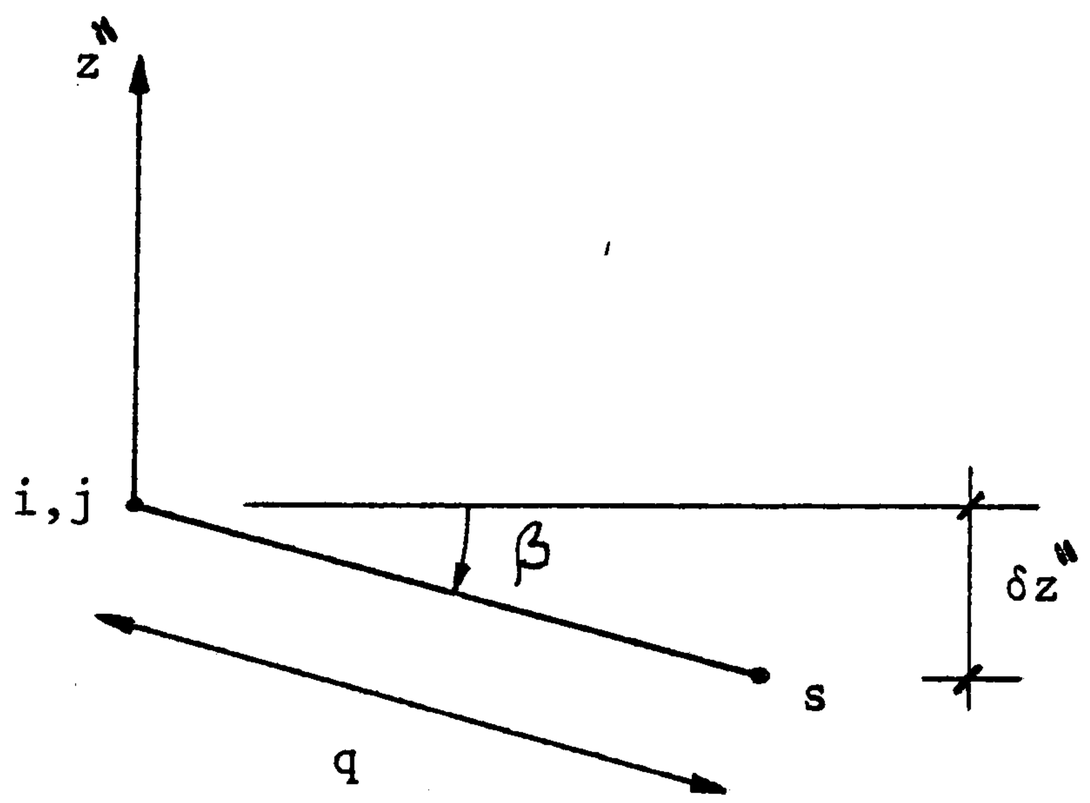

Figure D.4

$$\sin \beta = \frac{\delta z''}{q}$$

$$q = \frac{2A_{ijs}}{\ell_b} \qquad \text{(D.4)}$$

where A_{ijs} is the area of the triangle formed by nodes i, j and s.

Summarising:

$$\beta = \sin^{-1}\left[- \frac{\ell}{2A_{ijs}} \left\{ \lambda_{z''} \right\}^T \left\{ v_{ijs} \right\} \right] \qquad \text{(D.5)}$$

This procedure may readily be automated on assignation of local nodes s adjacent to each boundary member ij.

REFERENCES

1. Aalami, B., "Large Deflection of Elastic Plates under Patch Loading", J. Struct. Div. ASCE, 98, 2567-2585, 1972.

2. Al-Hilli, A., "Theoretical and Experimental Investigation into Flat Cable Nets with Elastic Boundaries", Ph.D. Thesis, CNAA, 1974.

3. Alwar, R.S. and Ramachandra Rao, N., "Nonlinear Analysis of Orthotropic Skew Plates", J.AIAA, 11, 495-498, 1973.

4. Alwar, R.S. and Rao, N.R., "Large Elastic Deformations of Clamped Skewed Plates by Dynamic Relaxation", Comp. Struct., 4, 381-398, 1974.

5. Argyris, J.H. and Scharpf, D.W., "Finite Elements in Time and Space", Nucl. Eng. Des., 10, 456-464, 1969.

6. Argyris, J.H. and Scharpf, D.W., "Some General Considerations on the Natural Mode Technique", J.R.Ae.S., 73, 218-226 and 361-368, 1969.

7. Argyris, J.H. and Chan, A.S.L., "Applications of Finite Elements in Space and Time", Ingenieur-Archiv, 41, 235-257, 1972.

8. Argyris, J.H. and Scharpf, D.W., "Large Deflection Analysis of Prestressed Networks", J. Struct. Div. ASCE, 98, 633-654, 1972.

9. Argyris, J.H., Dunne, P.C., and Angelopoulos, T., "Nonlinear Oscillations using the Finite Element Technique", Comp. Meth. Appl. Mech. Eng., 2, 203-250, 1973.

10. Argyris, J., Angelopolous, T., and Bichat B., "A General Method for the Shape Finding of Lightweight Tension Structures", Proc. Int. Conf. Tension Structures, London, April 1974.

11. Bandel, H.K., "Das Orthogonale Seilnetz Hyperbolisch-parabolischer Form unter Vertikalen Lastzuständen und Temperaturänderungein", Der Bauingenieur, 34, 394-401, 1959.

12. Barnes, M.R., "Pretensioned Cable Networks", CONRAD, 3, April, 1971.

13. Barnes, M.R., "Dynamic Relaxation Analysis of Tension Structures", Proc. Int. Conf. Tension Structures, London, April 1974.

14. Barnes, M.R., "Application of Dynamic Relaxation to the Design and Analysis of Cable, Membrane and Pneumatic Structures", Proc. Int. Conf. Space Structures, Guildford, September, 1975.

15. Barnes, M.R., "Formfinding of Minimum Surface Membranes", Proc. World Conf. on Space Enclosures, Montreal, July, 1976.

16. Barnes, M.R., "Explicit Dynamic Analysis and Model Correlation of Tension Structures", Proc. Int. Symp. Wide Span Surface Structures, Stuttgart, April 1976.

17. Barnes, M.R., "An Investigation of Vibration Decay in a Model Pneumatic Dome", Proc. Int. Symp. Wide Span Surface Structures, Stuttgart, April 1976.

18. Barnes, M.R., "Interactive Graphical Design of Tension Surface Structures", Proc. Int. Symp. Wide Span Surface Structures, Stuttgart, April 1976.

19. Barnes, M.R., "Form-matching of Cable Net Models", Unpublished Report, 1977.

20. Barnes, M.R., Topping, B.H.V., and Wakefield, D.S., "Some Aspects of Form-Finding by Dynamic Relaxation", Int. Conf. Slender Structures, London, September 1977.

21. Barnes, M.R., "Form-Finding and Analysis of Tension Space Structures by Dynamic Relaxation", Ph.D. Thesis, The City University, Oct. 1977.

22. Baron, F., and Venkatesan, M.S., "Nonlinear Analysis of Cable and Truss Structures", J. Struct. Div. ASCE, 97, 679-710, 1971.

23. Basu, A.K. and Dawson, J.M., "Orthotropic Sandwich Plates", Proc. ICE, 45, Supp. Paper 7275S, 1970.

24. Bathe, K.J., and Wilson, E.L., "Stability and Accuracy Analysis of Direct Integration Methods", I J Earthquake Eng. Struct. Dyn., 1, 1973.

25. Bathe, K.J., Ramm, E., and Wilson, E.L., "Finite Element Formulations for Large Deformation Dynamic Analysis", IJNME, 9, 353-386, 1975.

26. Belytschiko, T. and Hsieh, B.J., "Non-linear Transient Finite Element Analysis with Convected Coordinates", IJNME, 7, 255-271, 1973.

27. Belytschko, T., and Hsieh, B.J., "Nonlinear Transient Analysis by Convected Elements", Proc. AIAA/ASME/SAE, Conf. Williamsburg, Va., March 1973.

28. Belytschko, T., Chiappetta, R.L., and Bartel, H.D., "Efficient Large Scale Nonlinear Transient Analysis by Finite Element", IJNME, 10, 579-596, 1976.

29. Bergan, P.G., and Søreide, T., "A Comparative Study of Different Numerical Solution Techniques as Applied to a Nonlinear Structural Problem", Comp. Meth. Appl. Mech. Eng., 2, 185-201, 1973.

30. Biggs, J.M., "Introduction to Structural Dynamics" McGraw-Hill, 1964.

31. Bogner, F.K., Mallett, R.H., Minich, M.D., and Schmit, L.A., "Development and Evaluation of Energy Search Methods of Non-Linear Structural Analysis", AFFDL-TR-65-113, 1965.

32. Brew, J., "The Application of Dynamic Relaxation to the Solution of Nonlinear Structural Plane Frames", M.Sc. Thesis, UMIST, Manchester, 1968.

33. Brew, J.S., and Brotton, D.M., "Nonlinear Structural Analysis by Dynamic Relaxation", IJNME, e, 463-483, 1971.

34. Buchholdt, H.A., "Prestressed Cable Nets with Finite Displacements", Ph.D. Thesis, Univ. of London, 1967.

35. Buchholdt, H.A., "The Configuration of Prestressed Cable Nets", Acta Polytechnica Scandinavica, Ci54, Trondheim, 1968.

36. Buchholdt, H.A. Davies, M., and Hussey, M.J.L., "The Analysis of Cable Nets", J. Inst. Math. Appl, 4, 339-358, 1968.

37. Buchholdt, H.A., "A Nonlinear Deformation Theory Applied to Two-Dimensional Pretensioned Cable Assemblies", Proc. ICE, 42, 129-141, 1969.

38. Buchholdt,H.A., "Tension Structures", The Structural Engineer, February, 1970.

39. Buchholdt, H.A., and McMillan, B., "Iterative Methods for the Solution of Pretension Cable Structures and Pinjointed Assemblies Having Significant Geometrical Displacements", Proc. IASS Pacific Symp. II, Tension Structures and Space Frames, Tokyo and Kyoto, 1971.

40. Buchholdt, H.A., "The Newton-Raphson Approach to Skeletal Assemblies having Significant Displacements", Acta Plytechnica Scandinavica, Ci72, Trondheim, 1971.

41. Buchholdt, H.A., and McMillan, B., "A Non-linear Vector Method for the Analysis of Vertically and Laterally Loaded Cable Assemblies", Proc. ICE, 55, 211-228, 1973.

42. Buchholdt, H.A., Das, N.K., and Al-Hilli, A., "A Gradient Method for the Analysis of Cable Structures with Flexible Boundaries", Inf. Conf. Tension Structures, London, April, 1974.

43. Buchholdt, H.A., "The Behaviour of Circular Saddle Shaped Nets with Flexible Boundaries", Int. Symp. Wide Span Surface Structures, Stuttgart, 1976.

44. Bunce, J.W., "A Note on the Estimation of Critical Damping in Dynamic Relaxation" IJNME, 4, 301-304, 1972.

45. Bunce, J.W., and Brown, E.H., "The Finite Deflection of Plane Frames", I J Mech. Sci, 15, 189-198, 1973.

46. Burke, B.G. and Tighe, J.T., "A Time Series Model for Dynamic Behaviour of Off-Shore Structures", J. Soc. Petroleum Eng., 253, 1972.

47. Cassell, A.C., "Shells of Revolution under Arbitrary Loading and the use of Fictitious Densities in Dynamic Relaxation", Proc. ICE, 45, 65-78, 1970.

48. Cassell, A.C., Kinsey, P.J., and Sefton, D.J., "Cylindrical Shell Analysis by Dynamic Relaxation", Proc. ICE, 39, 75-84, 1968.

49. Cassell, A.C., and Hobbs, R.E., "Dynamic Relaxation". Proc. IUTAM Sump. 'High Speed Computing of Elastic Structures', Univ. of Liege, 1970.

50. Cassell, A.C. and Hobbs, R.E., "Numerical Stability of Dynamic Relaxation Analysis of Non-linear Structures", IJNME, 10, 1407-10, 1976.

51. Chaplin, T.K., "Metadynamic Relaxation Applied to Automatic Analyses of Slabs, Plates and Beams on Elastic Foundations", Proc. Symp. Interaction of Structure and Foundation, Univ. of Birmingham, July, 1971.

52. Chaplin, T.K., Discussion of "Large Elastic Deformations ..." by Alwar, R.S. and Rao, N.R., Comp. and Struc., 8, 257, 1978.

53. Chaudhury, N.K., Brotton, D.M., and Merchant, W., "A Numerical Method for Dynamic Analysis of Structural Frameworks", I.J. Mech. Sci., 8, 149-162, 1966.

54. Clough, R.W., "Analysis of Structural Vibrations and Dynamic Response", Proc. 1st US-Japan Seminar, Tokyo, 1969.

55. Clough, R.W. and Bathe, K.J., "Finite Element Analysis of Dynamic Response", Proc. 2nd US-Japan Seminar, Compn. Meth. Struct. Mech. Des., Berkeley, Ca., August, 1972.

56. Clough, R.W., and Wilson, E.L., "Dynamic Finite Element Analysis of Arbitrary Thin Shells", Comp. Struct., 1, 33-55, 1972.

57. Contro, R., and Zavelani-Rossi, A., "Creep Analysis of Pretensioned Cable Systems", Proc. IASS Symp. II, Tension Structures and Spaceframes, Tokyo and Kyoto, 1971.

58. Cundall, P., "Explicit Finite-Difference Methods in Geomechanics", Proc. Conf. Numerical Methods in Geomechanics, Blacksburg, Va., June 1976.

59. Davidson, I., "The Analysis of Cracked Structures", Trans. 3rd Int. Conf. Struct. Mech. and Reactor Tech., 3, 1975.

60. Day, A.S., "An Introduction to Dynamic Relaxation", The Engineer, January 29th 1965.

61. Day, A.S., "Analysis of Plates by Dynamic Relaxation with Special Reference to Boundary Conditions", Proc. Int. Symp. Comp. Struct. Analysis, Newcastle-upon-Tyne, 1966.

62. Day, A.S., and Bunce, J., "The Analysis of Hanging Roofs", Arup Journal, Sept. 1969, 30-31.

63. Day, A.S., and Bunche, J.W., "Analysis of Cable Networks by Dynamic Relaxation", Civ. Eng. Pub. Wks. Rev., April, 1970.

64. Dean, D.L., and Ugarte, C.P., "Analysis of Structural Nets", IABSE Publications, 23, 71-90, 1963.

65. Dickie, J.F., and Broughton, P., "Stability Criteria for Shallow Arches", J. Eng. Mech. Div. ASCE, 97, 951-965, 1971.

66. Dickie, J.F., and Broughton, P., "Geometric Nonlinearity", J. Struc. Mech., 1, 249-266, 1972.

67. Dowling, P.J., and Bawa, A.S., "Influence Surfaces for Orthotropic Steel Bridge Decks", Proc. ICE II, 59, 149-168, 1975.

68. Felippa, C.A., "Finite Element Analysis of Three-Dimensional Cable Structures", Proc. Int. Conf. Comp. Meth. in Nonlinear Mech., Austin, Texas, Sept. 1974.

69. Fletcher, R., and Reeves, C.M., "Function Minimisation by Conjugate Gradients", Computer Journal, 7, 149-154, 1964.

70. Forsythe, G.E., and Wasow, W.R., "Finite Difference Methods for Partial Differential Equations", J. Wiley, 1960.

71. Frieze, P.A., Hobbs, R.E., and Dowling, P.J., "Application of Dynamic Relaxation to the Large Deflection Elasto-Plastic Analysis of Plates", Comp. Struct., 8, 301-310, 1978½

72. Frieze, P.A., "Elasto-Plastic Buckling in Short Thin-Walled Beams and Columns", Proc. ICE, 65, 857-874, 1978.

73. Galletly, G.D., and Tuma, F.Y., "Large Deflection Analysis of Plates using Dynamic Relaxation", Proc. 4th Canadian Cong. Appl. Mech., Montreal, May 1973.

74. Gallo-Curcio, A., and Piccarreta, F., "Experimental Tests on a Hanging Roof Model of the new Palasport in Milan", Proc. Int. Conf. Tension Structures, London, April 1974.

75. Greenberg, D.P., "Inelastic Analysis of Suspension Roof Structures", J. Struct. Div. ASCE, 96, 905-930, 1970.

76. Gruendig, L., and Schek, H.J., "Analytical Formfinding and Analysis of Prestressed Cable Networks", Proc. Int. Conf. Tension Structures, London, April 1974.

77. Haisler, W.E., and Stricklin, J.A., "Computational Structural Mechanics Problems", Proc. Int. Conf. Comp. Methods in Nonlinear Mech., Austin, Texas, Sept. 1974.

78. Hangleiter, V., "Problems of Accuracy with Prestressed Cable Net Structures", Proc. Int. Conf. Tension Structures, London, April 1974.

79. Happold, E., and Liddell, W.I., "Timber Lattice Roof for the Mannheim Bundesgartenschan", The Structural Engineer, 53,. 99-135, 1975.

80. Happold, E., and Liddell, W.I., "Timber Lattice Roof for the Mannheim Bundesgartenschan", Discussion: The Structural Engineer, 54, 247-257, 1976.

81. Harding, J.E., Hobbs, R.E., and Neal, B.G., "The Elasto-Plastic Nalysis of Imperfect Square Plates under In-Plane Loading", Proc. ICE II, 63, 137-158, 1977.

82. Hashmi, S.J., Al-Hassani, S.T.S., and Johnson, W., "Large Deflection Elastic-Plastic Response of Certain Structures to Impulsive Load", I.J. Mech. Sci., 14, 843-860, 1972.

83. Haug, E., and Powell, G.H., "Analytical Shape Finding for Cable Nets", Proc. IASS Pacific Symposium II, Tension Structures and Space Frames, Tokyo and Kyoto, 1971.

84. Haug, E., "Remarks on Unsymmetric Coefficient Matrices in Implicit Non-Linear Finite Element Membrane and Cable Analyses", Proc. Int. Symp. Wide Span Surface Structures, Stuttgart, April 1976.

85. Hennicke, J., "Building with Gridshells - Comments on the Load Bearing Behaviour, the Construction and the Utilization of a new Lightweight Structure", Proc. Int. Symp. Wide Span Surface Structures, Stuttgart, April 1976.

86. Hestenes, M.R., and Stiefel, E., "Methods of Conjugate Gradients for Solving Linear Systems", J. Res. Nat. Bur. St., 49, 409-436, 1952.

87. Hinton, E., Owen, D.R.J., and Shantaram, D., "Dynamic Transient Linear and Nonlinear Behaviour of Thick and Thin Plates", Proc. Conf. Mathematics of Finite Elements, Brunel Univ., 1976.

88. Hodgkins, W.R., "On the Relation between Dynamic Relaxation and Semi-Iterative Matrix Methods", Numerische Mathematik, 9, 446-451, 1967.

89. Holland, J.A., "Dynamic Relaxation Applied to Local Effects", Proc. Conf. Prestressed Conc. Pressure Vessels", ICE, March 1967.

90. Hook, P.M., "The Application of Dynamic Relaxation to Non-Linear Structural Problems" Ph.D. Thesis, Univ. of Birmingham, 1973.

91. Houbolt, J.C., "A Recurrence Matrix Solution for the Dynamic Response of Elastic Aircraft", J. Aero. Sci., 17, 540-450, 1950.

92. Iwegbue, I.E., and Brotton, D.M., "A Numerical Integration Method for Computing the Flutter Speeds of Suspension Bridges in Erection Conditions", Proc. ICE II, 63, 785-802, 1977.

93. Jennings, A., "The Elastic Stability of Rigidly Jointed Frames", I.J. Mech. Sci., 5, 99-113, 1963.

94. Jennings, A., and Majid, K., "An Elastic-Plastic Analysis by Computer for Framed Structures Loaded up to Collapse", The Structural Engineer, 43, 407-412, 1965.

95. Jennings, A., "Frame Analysis Including Change of Geometry", J. Struct. Div. ASCE, 94, 627-644, 1968.

96. Jensen, J.J., "An Investigation of the Static and Dynamic Behaviour of Suspension Structures", Proc. IASS Pacific Symp. II, Tension Structures and Spaceframes, Tokyo and Kyoto, 1971.

97. Jensen, J.J., "Dynamics of Tension Roof Structures", Proc. Int. Conf. Tension Structures", London, April 1974.

98. Johnson, D., and Brotton, D.M., "A Finite Deflection Analysis for Space Structures", Proc. Int. Conf. on Space Structures, Univ. of Surrey, September 1966.

99. Jonatowski, J., and Birnstiel, C., "Inelastic Analysis of Suspension Structures", J. Struc. Div. ASCE, 96, 1143-1166, 1970.

100. Jonatowski, J., "Tension Roof Structures: An Inelastic Analysis", Proc. Int. Conf. Tension Structures, London, April 1974.

101. Karrholm, G., and Samuelsson, A., "Analysis of a Prestressed Cable Curved Ring Beam", Prelim. Report 9th IABSE Congress, Amsterdam.

102. Knudson, W.C., "Static and Dynamic Analysis of Cable Net Structures", Ph.D. Thesis, Univ. of California, Berkeley, 1971.

103. Knudson, W.C.,"Response of Cable Net Structures Under Dynamic Loads", Proc. IASS Pacific Symp. II, Tension Structures and Space Frames, Tokyo and Kyoto, 1971.

104. Knudson, W.C., and Scordelis, A.C., "Cable Forces for Desired Shapes in Cable Net Structures", Proc. IASS Pacific Symposium II, Tension Structure and Space Frames, Tokyo and Kyoto, 1971.

105. Knudson, W., and Nagy, D., "Spline Interpolation and Automatic Generation of Initial Geometry for Cable Net Structures", Proc. Int. Conf. Tension Structures, London, April 1974.

106. Koenig, H.A., and Davids, N., "Dynamical Finite Element Analysis for Elastic Waves in Beams and Plates", I J Solids Struct., 4, 643-660, 1968.

107. Koenig, H.A., and Davids, N., "The Damped Transient Behaviour of Finite Beams and Plates", IJNME, 1, 151-162, 1969.

108. Krieg, R.D., "Unconditional Stability in Numerical Time Integration Methods", J. Appl. Mech. ASME, June, 1973.

109. Krieg, R.D., and Key, S.W., "Transient Shell Response by Numerical Time Integration", IJNME, 7, 273-286, 1973.

110. Levy, S., and Kroll, W.D., "Errors Introduced by Finite Space and Time Increments in Dynamic Response Computation", J. Res. Nat. Bur. Stds., 51, 57-68, 1953.

111. Linkwitz, K., "New Methods for the Determination of Cutting Patterns of Prestressed Cable Nets and their Application to the Olympic Roofs, Munich", Proc. IASS Pacific Symposium II, Tension Structures and Space Frames, Tokyo and Kyoto, 1971.

112. Linkwitz, K., "Combined Use of Computation Techniques and Models for the process of Formfinding for Prestressed Nets, Gridshells and Membranes", Proc. Int. Symp. Wide Span Surface Structures, Stuttgart, April 1976.

113. Liudkovsky, I.M., "Optimum Types of Suspended Roofs and their Bearing Contours", Proc. IASS Colloq. Hanging Roofs, Paris, 1962.

114. Livesley, R.K., and Chandler, D.B., "Stability Functions for Structural Frameworks", Manchester, 1956.

115. Lowe, P.A., and Flint, A.R., "Prediction of Collapse Loadings for Composite Highway Bridges", Proc. ICE, 48, 645-659, 1971.

116. Lynch, R.D., Kelsey, S., and Saxe, H.C., "The Application of Dynamic Relaxation to the Finite Element Method of Structural Analysis", Tech. Rep. THEMIS-UND-68-1, Univ. of Notre Dame, Sept. 1968.

117. Malone, D.W., and Connor, J.J., "Transient Dynamic Response of Linearly Viscoelastic Structures and Continua", Proc. ASME/AIAA Conf., New Orleans, 1969.

118. Martin, H.C., "On the Derivation of Stiffness Matrices for the Analysis of Large Deflection and Stability Problems", Proc. Conf. Matrix Meth. Struct. Mech., Wright-Patterson, AFB, Ohio, 1965.

119. Møllmann, H., "A Study in the Theory of Suspension Structures", Akademisk Forlag, 1965.

120. Møllmann, H., and Lundus Mortensen, P., "The Analysis of Prestressed Suspended Roofs", Space Structures, Oxford 1976.

121. Møllmann, H., "Analytical Solution for a Cable Net over a Rectangular Plan", Proc. IASS Pacific Symposium II, Tension Structures and Spaceframes, Tokyo and Kyoto, 1971.

122. Møllmann, H., "Analysis of Hanging Roofs by means of the Displacement Method", Polyteknisk Forlag, Lyngby, Denmark, 1974.

123. Møllmann, H., "Analysis of prestressed cable systems supported by elastic boundary structures", Proc. Int. Conf. Tension Structures, London, April 1974.

124. Murthy, S.D.N., and Sherbourne, A.N., "Nonlinear Bending of Elastic Plates of Variable Profile", J. Eng. Mech. Div. ASCE, 100, 251-265, 1974.

125. Myklestad, N.O., and Lawrence, K.L.,"Transient Beam Response Calculations Using Euler's Method", J. AIAA, 5, 376-378, 1967.

126. Namita, Y., and Nakanishi, H., "A Method of Computation for Determining the Shape of Cable Structures", Proc. Int. Conf. Tension Structures, London, April 1974.

127. Nakanishi, H., and Namita, Y., "Shape Determination Analysis of Cable Structures by Means of the Methods for Optimisation Problems", Proc. Int. Symp. Wide Span Surface Structures, Stuttgart, April 1976.

128. Newmark, N, M., "A Method of Computation for Structural Dynamics", Trans. ASCE, 127, 1406-1435, 1962.

129. Ni, C.M., "A Numerical Method for Nonlinear Impact Analysis of Planar Frames", Proc. Int. Conf. Comp. Meth. in Nonlinear Mechanics, Austin, Texas, Sept. 1974.

130. Nickell, R.E., "On the Stability of Approximation Operators in Problems of Structural Dynamics", I J Solids Struct., 7, 301-319, 1971.

131. Oden, J.T., Key, J.E., and Fost, R.B., "A Note on the Analysis of Nonlinear Dynamics of Elastic Membranes by the Finite Element Method", Comp. Struct., 4, 445-452, 1974.

132. Otter, J.R.H., "Computations for Prestressed Concrete Reactor Pressure Vessels using Dynamic Relaxation", Nucl. Struct. Eng., 1, 61-75, 1965.

133. Otter, J.R.H., "Dynamic Relaxation Compared with other Iterative Finite Difference Methods", Nucl. Eng. Des., 3, 183-185, 1966.

134. Otter, J.R.H., Cassell, A.C. and Hobbs, R.E., "Dynamic Relaxation,"Proc. ICE, 35, 633-656, 1966.

135. Otter, J.R.H., Cassell, A.C., and Hobbs, R.E., Discussion on "Dynamic Relaxation" , Proc. ICE, 36, 723-750, 1967.

136. Otto,F., and Trostel, R., "Tensile Structures: Vol. I", MIT Press, Cambridge, Mass., 1967.

137. Otto, F., and Schleyer, F.K., "Tensile Structures: Vol. II", MIT Press, Cambridge, Mass., 1969.

138. Perrone, N., Kao, R., "A General Non-Linear Relaxation Iteration Technique for Solving Non-Linear Problems in Mechanics", J. Appl. Mech., 38, June 1971.

139. Peters, H.L., "Zur Berechnung allgemeiner Flächentragwerke mit Hilfe der Dynamischen Relaxation", Ingenieur-Archiv, 42, 42-57, 1972.

140. Pian, T.H.H., Balmer, H.A., and Bucciarelli, L.L., "Dynamic Buckling of a Circular Ring Constrained in a Rigid Circular Surface", Proc. Int. Conf. Dyn. Stability Struct., Illinois 1965.

141. Poskitt, T.J., "Numerical Solution of Nonlinear Structures", J. Struct. Div. ASCE, 93, 69-94, 1967.

142. Przemieniecki, J.S., "Theory of Matrix Structural Analysis", New York, 1968.

143. Roland, C.,"Frei Otto : Tension Structures", Praeger, New York, 1970.

144. Rushton, K.R., "Dynamic Relaxation Solutions of Elastic Plate Problems", J. Strain Analysis, 3, 23-32, 1968.

145. Ruston, K.R., "The Dynamic Relaxation Method used for Stress Analysis", Royal Aero. Soc. Conf. Stress Analysis, March 1968.

146. Rushton, K.R., "Large Deflection of Variable-Thickness Plates", I J Mech. Sci., 10. 723-735, 1968.

147. Rushton, K.R., "Dynamic Relaxation Solution for the Large Deflection of Plates with Specified Boundary Stresses", J. Strain Analysis, 4, 75-80, 1969.

148. Rushton, K.R., "Postbuckling of Tapered Plates", I J Mech. Sci., 11, 461-480, 1969.

149. Rushton, K.R., and Hook, P.M., "Large Deflection of Plates and Beams Obeying Non-linear Stress-Strain Laws", J. Strain Analysis, 9, 178-184, 1974.

150. Riyadh Sports Centre - White, Young & Partners, New Civil Engineer, 30 September 1976.

151. Saafan, S.A., "Nonlinear Behaviour of Structural Plane Frames", J. Struct. Div. ASCE, 89, 557-579, 1963.

152. Saafan, S.A., "Theoretical Analysis of Suspension Roofs", J. Struct. Div. ASCE, 96, 393-405, 1970.

153. Samuelli Ferretti, A., and Zingali, A., "A Large Span Hanging Roof : The Palasport in Milan", Prelim. Report 9th IABSE Congress, Amsterdam, 1972.

154. Schek, H.J., "The Force Density Method for Form-Finding and Computation of General Networks", Comp. Meth. Appl. Mech. Eng., 3, 1974.

155. Shantaram, D., Owen, D.R.J., and Zienkiewicz, O.C., "Dynamic Transient Behaviour of Two- and Three-Dimensional Structures Including Plasticity, Large Deformation Effects and Fluid Interaction", Earthquake Eng. Struc. Dyn., 4, 561-578, 1976.

156. Siev, A., "Stability of Prestressed Suspended Roofs", Thesis, Technion, Haifa, 1961.

157. Siev, A., and Eidelman, J., "Shapes of Suspended Roofs", Proc. IASS Colloq., Paris, 1962.

158. Siev A., "A General Analysis of Prestressed Nets", IABSE Publications, 23, 283-292, 1963.

159. Siev, A., and Eidelman, J., "Stress Analysis of Prestressed Suspended Roofs", J. Struct. Div. ASCE, 90, 103-121, 1964.

160. Stricklin, J.A. and Haisler, W.E., "Evaluation of Solution Procedures for Material and/or Geometrically Nonlinear Structural Analysis", J. AIAA, 11, 292-297, 1973.

161. Tezcan, S.S., "Computer Analysis of Plane and Space Structures", J. Struct. Div. ASCE, 92, 143-173, 1966.

162. Tezcan, S.S. and Mahapatra, B.C., "Tangent Stiffness Matrix for Space Frame Members", J. Struct. Div. ASCE, 95, 1257-1270, 1969.

163. Thornton, C.H. and Birnstiel, C., "Three-Dimensional Suspension Structures", J. Struct. Div. ASCE, 93, 247-270, 1967.

164. Torbe, I., "A Cruciform Element for the Analysis of Fabric Structures", Proc. Conf. Math. Finite Elements and Appl., April 1976.

165. Turner, J.J., Dill, E.H., Martin, H.C., and Melosh, R.J., "Heating and External Loads", J.Aero. Sci., 27, 99-106, 1960.

166. Turvey, G.J., and Wittrick, W.H., "The Large Deflection and Post-Buckling Behaviour of Some Laminated Plates", Aero. Quart., , 77-86, 1973

167. Turvey, G.J., "Large Deflection of Tapered Annular Plates by Dynamic Relaxation", J. Eng. Mech. Div. ASCE, 104, 351-366, 1978.

168. Tveit, P., "The Design of Network Arches", The Structural Engineer, July 1966.

169. Virdi, K.S., and Dowling, P.J., "A General Formulation of the Nonlinear Analysis and Stability of Space Frames", Proc. Int. Conf. Space Structures, Guildford, September 1975.

170. Williams, F.W., "An Approach to the Non-Linear Behaviour of the Members of a Rigid Jointed Plane Framework with Finite Deflections", Q.J. Mech. Appl. Math., XVII, 451-469, 1964.

171. Wilson, E.L., Farhoomand, I., and Bathe, K.J., "Nonlinear Dynamic Analysis of Complex Structures", I.J. Earthquake Eng., Struct. Dyn., 1, 241-252, 1973.

172. Witmer, E.A., Balmer, H.A., Leech, J.W., and Pian, T.H.H., "Large Dynamic Deformations of Beams, Rings, Plates and Shells", J. AIAA, 1, 1848-1857, 1963.

173. Wood, W.L., "Comparison of Dynamic Relaxation with Three Other Iterative Methods", The Engineer, Nov. 24th, 1967.

174. Wood, W.L., "Note on Dynamic Relaxation", IJNME, 3, 145-147, 1971.

175. Wright, D.T., "Membrane Forces and Buckling in Reticulated Shells", J. Struct. Div. ASCE, 91, 173-201, 1965.

176. Wu, R.W.H., and Witmer, E.A., "Finite Element Analysis of Large Elastic-Plastic Transient Deformations of Simple Structures", J.AIAA, 9, 1719-1724, 1971.

177. Wu, R.W.H., and Witmer, E.A., "Nonlinear Transient Responses of Structures by the Spatial Finite Element Method", J. AIAA, 11, 1110-1117, 1973.

178. Zienkiewicz, O.C., "The Finite Element Method in Engineering Science", McGraw-Hill, London, 1971.

179. Zienkiewicz, O.C., "A New Look at the Newmark, Houbolt and other Time-Stepping Formulae - a Weighted Residual Approach", Earthquake Eng. Struct. Dyn., 5, 413-418, 1977.

180. Otter, J.R.M., and Day, A.S., "Tidal Computations", The Engineer, January, 1960.

181. Frankel, S.P., "Convergence Rates of Iterative Treatments of Partial Differential Equations", Mathematical Tables, 4, 72-73, 1950.

182. Turvey, G.J., "Axisymmetric elasto-plastic flexure of circular plates in the large deflection regime", Proc. ICE, II, 67, 81-92, 1979.

183. Papadrakakis, M., "Gradient and Relaxation Nonlinear Techniques for the Analysis of Cable Supported Structures", Ph.D. Thesis, The City University, July 1978.

184. Welch, A.K., Ph.D. Thesis, University of Southampton, 1969.

185. Orr, R.S., and Holland, J.A., "Theoretical Analysis of a Model Spherical Vessel", Proc. Conf. Prestressed Concrete Vessels, ICE, London 1967.

186. Malvick, A.J., and Pearson, E.T., "Theoretical Elastic Deformations of a 4 meter Optical Mirror using Dynamic Relaxation", Applied Optics, 7, 1207-1202, 1968.

187. Malvick, A.J., "Dynamic Relaxation: A General Method for Determination of Elastic Deformation of Mirrors", Applied Optics, 7, 2117-2121, 1968.

188. Topping, B.H.V., "The Application of Dynamic Relaxation to the Design of Modular Space Structures", Ph.D. Thesis, The City University, October 1968.

189. Mallett, R.H., and Schmidt, L.A., "Non-linear Structural Analysis by Energy Search", J. Struct. Div., ASCE, 93, 1967.

190. Davidon, W.C., "Variable Metric Method for Minimisation", A.E.C., R. and D. Report ANL-5990.

191. Das, N.K., "The Analysis of Cable Structures with Fixed and Flexible Boundaries", Ph.D. Thesis, University of London, 1974.